Geometric characterization and comparison of subsurface structures, and data requirement assessment for geological modeling

Von der Fakultät für Georessourcen und Materialtechnik der Rheinisch-Westfälischen Technischen Hochschule Aachen

zur Erlangung des akademischen Grades eines

Doktors der Naturwissenschaften

genehmigte Dissertation

vorgelegt von

Friedrich Carl, M.Sc.

Berichter: Univ.-Prof. Dr. rer. nat. Florian Amann
Univ.-Prof. Florian Wellmann, Ph.D.

Tag der mündlichen Prüfung: 29.06.2026

Diese Dissertation ist auf den Internetseiten der Universitätsbibliothek online verfügbar

Prüfungskommission:

Prof. Dr. Florian Amann, Berichter
Prof. Dr. Florian Wellmann, Berichter
Prof. Dr. Stefan Back, Vorsitz

Betreuer:

Prof. Dr. Florian Amann, Betreuer
Dr. Peter Achtziger-zupančič, Co-Betreuer
Dr. Mohammadreza Jalali, Co-Betreuer

RWTH Aachen Universität
Lehrstuhl für Ingenieurgeologie und Hydrogeologie
Aachen, Deutschland

Abstract

Structural geological modeling is essential for the description of the subsurface. This is relevant, for instance, for the planning of the storage of highly radioactive waste, where the long-term safety of a disposal site is strongly dependent on the characterizability of the surrounding rock mass, that shall serve as a thermal and physical buffer. Therefore, it is essential to analyze the statistical uncertainties in geological models, that can arise in every modeling step. This has been done in the GeoBlocks project, in whose context this work has been conducted. A substantial factor contributing to statistical uncertainties in geomodels is the geometric complexity of the subsurface, that can only be reproduced insufficiently in geomodeling. A common approach to nevertheless approximate the geometric uncertainty is to create large numbers of probabilistic model realizations. In order to geometrically characterize these sets, and to compare individual models, quantitative comparison methods are required. One of such comparison methods has been created in the context of this thesis. It is based on the measurement of geometric parameters on two-dimensional cross sections in three-dimensional objects. The horizontal and vertical extents of a structure are determined perpendicular to the two horizontal main axes of the object. Furthermore, gradient and curvature data are measured. The data analysis provides insight into the geometric characteristics of structures. The extensional data inform about the anisotropy of a structure, indicate the existence of overhang configurations and reveal the character of the top surface. Gradient and curvature data provide insight into the steepness of the lateral walls of a structure, its sphericity and its top surface. The Kullback-Leibler divergence allows for the quantitative comparison of data distributions of individual geometric parameters. Furthermore, a dimensionally reduced cluster analysis based on the geometric parameters is conducted for the grouping and systematization of structures. The methodology is applied to a set of synthetic, regular "standard geometries", developed to act as benchmark models in modeling workflows. With the cluster analysis, the benchmark models are evaluated regarding their geometric dis-/similarity, which allows the quantitative reduction of the set to obtain geometrically dissimilar structures. It is anticipated that the quantification method and the benchmark models aid in different stages of a geomodeling workflow.

Geometric quantification methods in geomodeling should be capable of investigating the full range of structural complexity. In the context of the German site selection, this range is covered by intrusive salt structures and crystalline bodies. Thus, the

method is applied to 239 geomodels of intrusive salt bodies, and to 67 models of crystalline intrusives. In the dimensionally reduced cluster analysis, the subsurface models are assigned to the respective benchmark model of highest geometric similarity. Subsequently, the results of the cluster analysis are contextualized in the respective regional geology. The application to a database covering the full range of geometric complexity of isolated geological structures illustrates the efficiency of the approach in the geometric analysis of a large number of geological models.

The potential input data for geological modeling is diverse, but commonly of sparse availability. This is due to the high costs and the large time investment of data acquisition. Thus, it is of interest to assess, how much input data is required to create realistic geomodels. This objective is approached with two quantitative metrics for the determination of minimum data requirements: the mean averaged Kullback-Leibler divergence – based on the similarity of parameter distributions – and the mean Euclidean distance in principal component space, based on dimensionally reduced parameter data, determined respectively between condensed probabilistic model realizations and a reference. The database consists of two models of intrusive salt structures and a sphere model. The choice of the real models is based on the cluster analysis of the second study and guarantees, that the bodies cover a large range of geometric complexity. Synthetic datasets in 15 data configurations are randomly extracted from the input meshes and modeled in 3D. Thereby, 1500 model realizations per structure are created as the basis for the following analyses. Subsequently, the model realizations are condensed into five percentile threshold models per data configuration, and these models as well as the references are characterized with the quantification method established in this thesis. The geometric data constitute the basis for the application of the developed metrics. For both metrics, intermediate results are analyzed for every single combination of data configuration and threshold model. Subsequently, the values of the five threshold models per data configuration are averaged respectively, to obtain the final metrics. In the metrics, it is analyzed which increases of data quantity coincide with considerable improvements of model similarity. Minimum data requirements are derived for all three test cases, with the required quantities being higher, the larger the structural complexity.

This thesis has contributed in various ways to the overall project goal of developing methods to quantify and visualize geological uncertainties. The quantification method is expected to aid in geomodeling workflows with sparse data in several steps: it is utilizable in the conceptualization of a model, the parametrization of the interpolation method, evaluation of reasonableness of model realizations, and the quantified geometric description, systematization and comparison of models. Furthermore, the metrics for the assessment of minimum data quantity requirements for realistic geomodeling can be considered in evaluations whether a database is sufficient to model a given structure.

Kurzfassung

Strukturelle geologische Modellierung ist zur Beschreibung des Untergrundes essentiell. Diese ist beispielsweise relevant für die Planung der unterirdischen Lagerung hochradioaktiver Abfälle, wobei die Langzeitsicherheit eines Endlagers maßgeblich von der Charakterisierbarkeit des Umgebungsgesteins abhängt, das als stofflicher und thermischer Puffer dienen soll. Daher ist es wichtig, statistische Ungewissheiten in geologischen Modellen zu untersuchen, die in jedem Schritt der Modellierung auftreten können. Dies wurde im GeoBlocks-Projekt getan, in dessen Rahmen diese Arbeit entstand. Ein wesentlicher Faktor, der zu statistischen Ungewissheiten in Geomodellen beiträgt, ist die geometrische Komplexität des Untergrundes, die bei der Geomodellierung nur unzureichend reproduziert werden kann. Ein gängiger Weg, die geometrische Variabilität trotzdem zu approximieren, ist die Erstellung großer Mengen probabilistischer Modellrealisationen. Um diese Sets geometrisch zu charakterisieren und einzelne Modelle zu vergleichen, bedarf es jedoch quantitativer Vergleichsmethoden. Eine solche Methode wurde im Rahmen dieser Arbeit entwickelt. Sie beruht auf der Messung geometrischer Parameter an zweidimensionalen Schnitten aus dreidimensionalen Körpern. Die horizontalen und vertikalen Ausdehnungen einer Struktur werden orthogonal zu den horizontalen Hauptachsen des Körpers erfasst. Zudem werden Gradienten- und Krümmungsdaten gemessen. Die Datenanalyse gibt Einblick in geometrische Eigenschaften von Strukturen. Die Ausdehnungsdaten spiegeln die Anisotropie einer Struktur wider, belegen die Existenz von Überhangskonfigurationen und offenbaren den Charakter der Top-Fläche. Die Gradienten- und Krümmungsdaten gewähren Einblick in die Steilheit der lateralen Wände eines Körpers, seiner Sphärizität und der Top-Fläche. Die Kullback-Leibler Divergenz ermöglicht den quantitativen Vergleich der Datenverteilungen individueller geometrischer Parameter. Des Weiteren wird eine dimensionsreduzierte Clusteranalyse auf Basis der geometrischen Parameter zur Gruppierung und Systematisierung von Körpern durchgeführt. Die Methodik wird an einem Set synthetischer, regelmäßiger "Standardgeometrien" angewandt, die als Benchmarkmodelle in Workflows für die Modellierung dienen sollen. Durch die Clusteranalyse können die Benchmarkmodelle auf geometrische Ähnlichkeit untersucht werden, was die quantitative Reduzierung des Sets auf geometrisch unterschiedliche Strukturen erlaubt. Es wird erwartet, dass die Quantifizierungsmethode und die Benchmarkmodelle verschiedene Phasen eines Geomodellierungsworkflows unterstützen.

Geometrische Quantifizierungsmethoden in der Geomodellierung sollten die volle Bandbreite struktureller Komplexität abbilden können. Im Kontext der deutschen Standortsuche kann diese Bandbreite durch intrusive Salzstrukturen und kristalline Körper

abgedeckt werden. Daher wird die Methode auf 239 Geomodelle intrusiver Salzkörper sowie auf 67 Modelle kristalliner Intrusionen angewandt. In der dimensionsreduzierten Clusteranalyse werden die Untergrundmodelle dem Benchmarkmodell mit der jeweils größten geometrischen Ähnlichkeit zugewiesen. Anschließend werden die Resultate der Clusteranalyse im Kontext der jeweiligen regionalen Geologie verortet. Die Anwendung der Methodik auf eine Datenbasis, die die volle Bandbreite geometrischer Komplexität isolierter geologischer Strukturen abbildet, verdeutlicht die Effizienz des Ansatzes in der geometrischen Analyse einer großen Anzahl geologischer Modelle.

Mögliche Eingangsdaten für die Geomodellierung sind divers, jedoch meist nur spärlich verfügbar. Dies liegt an den hohen Akquisitionskosten und dem großen zeitlichen Aufwand der Datenerhebung. Daher ist es von Interesse, zu ergründen, wie viele Eingangsdaten zur Erstellung realistischer Geomodelle benötigt werden. Diese Zielsetzung wird mit zwei quantitativen Metriken zur Bestimmung minimal benötigter Eingangsdatenmengen angegangen: Die mittlere gemittelte Kullback-Leibler Divergenz – basierend auf der Ähnlichkeit von Parameterverteilungen – und die mittlere euklidische Distanz im Hauptkomponenten-Raum, basierend auf dimensionsreduzierten Parameterdaten, jeweils erfasst zwischen zusammengefassten probabilistischen Modellrealisationen und einer Referenz. Die Datenbasis umfasst zwei Modelle intrusiver Salzstrukturen und ein Kugelmodell. Die Wahl der Realmodelle basiert auf der Clusteranalyse der zweiten Studie und garantiert, dass die Körper eine große Bandbreite geometrischer Komplexität abdecken. Synthetische Datensätze in 15 Datenkonfigurationen werden randomisiert aus den Eingangsmodellen extrahiert, und in 3D modelliert. Dadurch werden 1500 Modellrealisationen pro Struktur als Basis für die weiteren Analysen geschaffen. Die Modellrealisationen werden anschließend in fünf Perzentil-Schwellenwertsmodellen pro Datenkonfiguration kondensiert, die ebenso wie die Referenzmodelle mit der in der Arbeit entwickelten Quantifizierungsmethode charakterisiert werden. Die geometrischen Daten bilden die Basis für die folgende Anwendung der entwickelten Metriken. Für beide Metriken werden Zwischenergebnisse für jede Kombination aus Datenkonfiguration und Schwellenwertsmodell analysiert. Anschließend werden die Werte der fünf Schwellenwertsmodelle pro Datenkonfiguration jeweils gemittelt, um die finalen Metriken zu erhalten. Bei diesen wird geprüft, wann eine Zunahme der Datenquantität mit großen Verbesserungen der Modellähnlichkeit einhergeht. Minimal benötigte Datenmengen können für alle drei Testmodelle abgeleitet werden, wobei die erforderlichen Mengen größer sind, desto höher die strukturelle Komplexität ist.

Diese Thesis hat in mehrfacher Hinsicht zum übergeordneten Projektziel der Methodenentwicklung zur Quantifizierung und Visualisierung geologischer Ungewissheiten beigetragen. Die Quantifizierungsmethode kann Workflows zur Geomodellierung mit spärlichen Daten verschiedenartig unterstützen: sie kann in der Konzeptualisierung eines Modells angewandt werden, sowie für die Parametrisierung der Interpolationsmethode, Untersuchung der Plausibilität von Modellrealisationen und für die quantitative geometrische Beschreibung, Systematisierung und den Vergleich von Modellen. Die Metriken zur Untersuchung minimal benötigter Datenmengen für realistische geologische Modellierung können des Weiteren zur individuellen Evaluierung herangezogen werden, ob eine Datenbasis zur Modellierung einer bestimmten Struktur ausreicht.

Acknowledgements

I can hardly believe that, after three and a half years, this work is finally complete. The process of method development, data measurements and analyses was marked by setbacks until the very end. However, thanks to my willpower and perseverance, as well as the support of many people, I was able to prevail.

First, I would like to express my deepest gratitude to Florian Amann, Florian Wellmann und Peter Achtziger-Zupančič. I am very grateful to Florian A., for your ever-helpful prompt support whenever it was needed, and your words of encouragement when things did not go as planned. Special thanks to Florian W., for all the scientific guidance, helpful feedback on my work and the management of the GeoBlocks team. I am especially indebted to Peter. You have spent so much time and energy on my supervision, provided me with feedback countless times and guided me towards the successful completion of this thesis. Many thanks for that!

The German Federal Company for Radioactive Waste Disposal (BGE) is gratefully acknowledged for the financial funding of this project.

My gratitude goes to Stefan for serving as chair of my PhD defense and for providing us with data in the GeoBlocks project.

I would also like to thank Reza for the administrative support at the LIH and your genuine interest in my work in our meetings.

I am grateful to the GeoBlocks team for our successful collaboration and the many hours we spent together.

Many thanks to all my friends and colleagues from LIH, CG3 and NUG, for the enjoyable time we shared.

Finally, I would like to thank my family and friends, especially my parents and my best friend Tom, for their never-ending support throughout these past years.

Contents

List of Figures **xi**
List of Tables **xv**
1 Introduction **1**
1.1 Background: Radioactive waste disposal and the challenges of geological modeling in the site selection . . . 1
1.2 Literature review . . . 3
1.2.1 Overview of a general workflow for structural geological modeling and comparison of explicit vs. implicit geomodeling methods . . 3
1.2.2 Classification of uncertainties in geological models . . . 4
1.2.3 Uncertainty quantification approaches and the effect of data integration on uncertainties . . . 5
1.2.4 Structural-geometric complexity and the necessity of model generalization and benchmarking . . . 7
1.2.5 Quantitative methods for the comparison of 3D objects in geomodeling . . . 8
1.2.5.1 Direct shape comparison through distance functions . . 8
1.2.5.2 Additional dissimilarity metrics applied in geomodeling 10
1.3 Methods . . . 11
1.3.1 Segmentation and measurement algorithm . . . 11
1.3.2 Data analysis . . . 13
1.4 Motivation and problem definition . . . 15
1.5 Synopsis of the research situation and unresolved questions . . . 17
1.6 Outline of this thesis . . . 19
References . . . 20
2 Quantitative comparison of three-dimensional bodies using geometrical properties to validate the dissimilarity of a standard collection of 3D geomodels **29**
Abstract . . . 29
2.1 Introduction . . . 30
2.1.1 Shape quantification and comparison – previous studies and gaps in current research . . . 30

2.1.2 Geological description of the example model "Altenbruch-Beverstedt" . . . 35
2.1.3 Content, motivation and distinction of this study . . . 37
2.2 Methods . . . 39
2.2.1 Segmentation and measurement algorithm . . . 39
2.2.2 Data analysis . . . 42
2.3 Results . . . 42
2.3.1 Segmentation and measurement algorithm . . . 43
2.3.2 Data analysis . . . 43
2.3.3 Cluster analysis . . . 50
2.4 Discussion . . . 55
2.4.1 Comparison of existing methods for 3D shape characterization with the proposed workflow . . . 56
2.4.2 Assumptions and compromises of the algorithm ensuring its universal applicability . . . 57
2.4.3 Intended direct application and potential further usage of the quantification method and the standard geometries . . . 58
2.5 Conclusion . . . 59
References . . . 61
3 Quantitative comparison of subsurface structures: an application to salt domes and crystalline bodies 65
Abstract . . . 65
3.1 Introduction . . . 66
3.1.1 Previous studies . . . 66
3.1.2 Brief introduction to the case study . . . 68
3.1.2.1 Database: subsurface datasets and benchmark models 68
3.1.2.2 Geological overview and location of case study regions 71
3.1.3 Content and motivation of this study . . . 74
3.2 Methods . . . 75
3.2.1 Measurement of geometric parameters . . . 75
3.2.2 Data analysis . . . 76
3.3 Results . . . 78
3.3.1 Analysis of histograms and data distributions of the geometric data . . . 79
3.3.2 Cluster analysis after normalization and dimensional reduction . 84
3.3.2.1 Mean-centering for all parameters . . . 84
3.3.2.2 Gradient data aligned with normalized 0 . . . 88
3.3.3 Cluster results in the context of the regional geology . . . 95
3.4 Discussion . . . 98

3.4.1 Implications from the method application to irregular meshes . 99
3.4.2 Influence of input model construction on study results 100
3.4.3 Cluster results in the context of the regional geology – implications 100
3.4.4 Contribution of this study to the initial quantification method . 101
3.5 Conclusion 102
References 103
4 Minimum data quantity requirements for structural geological modeling 111
Abstract 111
4.1 Introduction 112
4.1.1 Previous studies 112
4.1.2 Database 115
4.1.3 Content and aims of this study 116
4.2 Methods 117
4.2.1 Generation of synthetic datasets, model realizations and threshold models 117
4.2.2 Measurement of geometric data 119
4.2.3 Data analysis 121
4.3 Results 122
4.3.1 Geometric characteristics of the reference models 122
4.3.2 (Mean) averaged Kullback-Leibler divergences 123
4.3.2.1 Sphere 124
4.3.2.2 Gielow 125
4.3.2.3 Juliusburg_Koestorf-Rosenthal 126
4.3.3 (Mean) Euclidean distances in principal component space 129
4.3.3.1 Sphere 129
4.3.3.2 Gielow 130
4.3.3.3 Juliusburg_Koestorf-Rosenthal 131
4.3.4 Comparison of the results of both metrics between the structures 134
4.3.5 Assessment of minimum data requirements 134
4.4 Discussion 139
4.4.1 Methodology – data and model generation and setup of metrics 139
4.4.2 Comparison between both metrics 141
4.4.3 Further considerations on minimum data requirements 142
4.4.4 Comparison of the workflow to previously proposed approaches . 143
4.4.5 Implications of the study results 145
4.5 Conclusion 145
References 148

5 Concluding remarks **151**
5.1 Synopsis and conclusions 151
5.2 Recommendations for future research 155
References 156
Appendix **159**
Chap. 2 - Supplementary Material 159
Chap. 3 - Supplementary Material 161
Scientific contributions **163**

List of Figures

Chapter 2 **29**

2.1 Geometrical systematization of the rock types for the catalogue of benchmark models ("standard geometries") 35
2.2 Overview of regular synthetic models ("standard geometries") used in this study 36
2.3 3D model of Altenbruch-Beverstedt, taken from BGR et al. (2022) . . . 37
2.4 Pseudocode of the segmentation and measurement algorithm 41
2.5 Visual representation of the segmentation and measurement algorithm . 44
2.6 Data distributions and cumulative distribution functions (CDF's) for the extensional parameters 47
2.7 Gradient and curvature data for the two example cases 48
2.8 Analysis of data distributions to reproduce geometric characteristics of input models 49
2.9 Visualized Kullback-Leibler divergences 51
2.10 Calculated supplementary information for the setup and interpretation of the cluster analysis after principal component analysis 53
2.11 Matrix plot of principal components (PC's) 53
2.12 Condensed collection of standard geometries after application of the quantification method 55

Chapter 3 **65**

3.1 Geometrical systematization of the rock types covered by our database 70
3.2 Example models from the database of the present study 70
3.3 Set of benchmark models ("standard geometries") employed in this study 72
3.4 Location of the subsurface structures assessed with our method 73
3.5 Pseudocode of the segmentation and measurement algorithm 77
3.6 Visual representation of the segmentation and measurement algorithm for the intrusive salt structure Altenbruch-Beverstedt 78
3.7 Range of parameter measurements for all irregular input meshes of the database 80

3.8 Combined cumulative distribution functions of all irregular input meshes of the database . . . 81
3.9 Example cases for the variability of data distributions (blue) along the corresponding CDF's (red) among dimensional parameters . . . 83
3.10 Example of a subsurface structure showing overhang configurations ("Neuenhuntorf") . . . 84
3.11 Example cases of gradient and curvature data . . . 85
3.12 Calculated supplementary graphs for the setup and interpretation of the first cluster analysis . . . 86
3.13 Matrix plot of principal components (PC's) for the first cluster analysis 87
3.14 Variance per feature (percentiles of the PDF's of the input parameters) in the cluster analyses . . . 88
3.15 Calculated supplementary graphs for the setup and interpretation of the second cluster analysis . . . 90
3.16 Matrix plot of principal components (PC's) for the second cluster analysis aligning gradients = 0 with normalized 0 . . . 91
3.17 Combined cumulative distribution functions of all irregular input meshes of the database colorized according to the results of the second cluster approach . . . 92
3.18 Distance histograms of datasets to the respective cluster centroid . . . 93
3.19 Cluster results from the second approach (see also Fig. 3.16) translated onto the 3D models from BGR et al. (2022) and LfULG . . . 97

Chapter 4 **111**

4.1 3D models of the three tested structures . . . 115
4.2 Exemplary visualization of the synthetic datasets extracted from the input meshes of the test structures . . . 118
4.3 Exemplary visualization of the threshold models measured and compared in the present study, alongside the respective reference mesh . . . 120
4.4 Data distributions of the geometric parameters for the three tested reference structures . . . 123
4.5 Averaged Kullback-Leibler divergence (avKLD) values between threshold models and the reference model for the sphere; and condensed mean avKLD plot . . . 125
4.6 Averaged Kullback-Leibler divergence (avKLD) values between threshold models and the reference model for Gielow; and condensed mean avKLD plot . . . 127

4.7 Averaged Kullback-Leibler divergence (avKLD) values between threshold models and the reference model for Juliusburg_Koestorf-Rosenthal; and condensed mean avKLD plot 128
4.8 Euclidean distance values in principal component (PC) space between threshold models and the reference model for the sphere; and condensed mean PC space distance plot 130
4.9 Euclidean distance values in principal component (PC) space between threshold models and the reference model for Gielow; and condensed mean PC space distance plot 132
4.10 Euclidean distance values in principal component (PC) space between threshold models and the reference model for Juliusburg_Koestorf-Rosenthal; and condensed mean PC space distance plot 133
4.11 Exemplary visualization of the effect of data integration on threshold models for the sphere 136
4.12 Visualization of the threshold models of the configuration "3 sections 3 boreholes" for Gielow 138
4.13 Visualization of the threshold models of the configuration "8 sections 8 boreholes" for Juliusburg_Koestorf-Rosenthal 138
4.14 Visualization of the Kullback-Leibler divergence calculation and mismatches of data maxima 142

Appendix **159**

A2.1 Visualization of the advantages of measuring the extents of input meshes on sections normal to their horizontal main axes 159
A2.2 Matrix plot for the angles between feature axes in PC space 160
A3.1 Combined cumulative distribution functions of all irregular input meshes, separated per cluster 162

List of Tables

Chapter 2 **29**

2.1 First three statistical moments, standard deviation and median per parameter for the two example cases 45
2.2 Comparison of KL divergences with and without the usage of a 95th percentile overflow bin for the curvature distributions 50

Chapter 3 **65**

3.1 Averaged statistical moments, median and standard deviation for the four dimensional parameters measured for all input meshes of the database 80
3.2 Color-coded PC scores of cluster centroids and assigned standard geometries of the second cluster approach 95

Chapter 4 **111**

4.1 Overview of the 15 data configurations tested in this study, ranging from very sparse to extensive data situations 117

Appendix **159**

A3.1 PC scores of cluster centroids and standard geometries in the second cluster analysis 161

CHAPTER

ONE

INTRODUCTION

1.1 Background: Radioactive waste disposal and the challenges of geological modeling in the site selection

Radioactive material is produced in various industries and in scientific research. Most waste accumulates in the operation and decommissioning of nuclear power plants (Lersow and Waggitt 2020). Although several countries, including Germany in 2023, have executed the nuclear power phase-out, the waste that has been produced thus far and the continuously produced radioactive material from other sources require a disposal that protects the living organisms from adverse radiation effects. For the integrity of a disposal site, the heat emission originating during the radioactive decay is of importance as well. Thus, two common classification schemes for nuclear waste exist. Internationally, radioactive waste is classified into low-level waste (LLW), intermediate-level waste (ILW) and high-level waste (HLW) (IAEA 2009). In Germany, where all waste is set to be disposed in deep subsurface repositories, the material is distinguished into heat-generating waste that comprises the HLW and parts of the ILW, and radioactive waste with negligible heat generation, encompassing the remaining waste (BMU 2010). Nuclear waste disposal is a national task. Several European countries have already selected their waste disposal site and are in different stages of construction planning. While Sweden and Finland plan to store their high-level waste in crystalline host rock, in France and Switzerland, claystone formations have been chosen (Neeft et al. 2025).

In the German site selection, halite is additionally considered as a third potential host rock type. In addition to the host rock representing the geological barrier, geotechnical sealing barriers and the waste containers keep the radioactive material contained.

The German site selection is conducted by the Federal Company for Radioactive Waste Disposal (BGE). The process has been subdivided into three phases and is currently being estimated to potentially take until 2074 (Krohn et al. 2024). Until 2020, the BGE excluded areas definitely unsuitable to host a waste disposal site, using minimum requirements, exclusion criteria and geoscientific consideration criteria, such as the minimum thickness and depth of the isolating host rock zone, volcanism, influences from current or past mining activities or active fault zones (BGE 2020a). Since then, the BGE has been working on further limiting the considered areas to the so-called "siting regions" that will be explored from the surface in the next step of the site selection process. In the current step two of phase one of their action plan, the suitability of the remaining areas is assessed in the "representative preliminary safety analyses" ("rvSU"). Properties like the thickness of potential host rock bodies, the depth of their upper and lower contacts, their areal extent and potential tectonic overprint are being (re-)evaluated at this stage (see repository of rvSU-documents at BGE 2024). This is done based only on existing data as prescribed by the federal law. However, these data were acquired initially throughout several decades and partially by private companies. Thus, data quality and quantity vary strongly between federal states and regions. In the rvSUs, this varying quality of existing data requires time-consuming data reprocessing and integration, including digitization of data and editing of old geomodels (merging and/or slicing), or complete remodeling (see BGE 2020b). Furthermore, data is reported to be partially incomplete (for instance, depth information is partially missing on analogue geological profiles; BGE 2020b). Regarding data quantity, statewide 3D structural models are only available for parts of Germany (BGE 2020a; BGE 2020b). Heterogeneous data availability is also driven by economic factors, as data is often concentrated in small areas of former resource exploration and production.

Even after entering the phase 2 of the site selection, where BGE will be able to use new data from surveys above ground to create new geomodels and update existing ones (BGE 2019), most data-related challenges will remain. And as few companies are capable of extensive acquisition campaigns (Krohn et al. 2024), and with the acquisition being both expensive and time consuming, the data situation for some of the future siting regions will remain suboptimal for some time. Thus, to potentially save time and budget, the questions arise 1) how much data is required to produce realistic geomodels in varying regimes of geological and structural complexity, and 2) whether one is able to estimate models from little data early on.

Given the overall data situation, many uncertainties have to be considered that are difficult to quantify and even more difficult to compare across potential sites. In addition to these data-related uncertainties, methodological uncertainties and subjective bias are commonly present in geomodeling and subsurface characterization, as described in Subsect. 1.2.2 (see also Wellmann and Caumon 2018). Consequently, to analyze the various sources of uncertainty and to optimize and integrate the geomodeling workflow, the GeoBlocks project, under which this thesis has been conducted, was initiated.

1.2 Literature review

1.2.1 Overview of a general workflow for structural geological modeling and comparison of explicit vs. implicit geomodeling methods

The visualized characterization of the subsurface can be approached by the measurement, processing and interpretation of geophysical data, or be based to a larger extent on geological data and principles to create structural geological models (Wellmann and Caumon 2018). After the input data for geomodeling has been acquired, the first step of a workflow for structural geological modeling is the combination of said data with geological knowledge and universal principles to inform a conceptual model (Wellmann and Caumon 2018). This conceptualization is frequently rather qualitative and depends on subjective expertise (Bond et al. 2007). The conceptual model represents the foundation for the mathematical model, hence the spatial interpolation algorithm. Interpolation in the geomodeling context uses explicit or implicit methods, both having advantages as well as disadvantages, depending on model aim, data and complexity (see Caumon et al. 2009; Wellmann and Caumon 2018). In explicit interpolation methods, every model element is explicitly defined by a mesh whose nodes are either exactly or approximately tied to the input data. Thus, geological interfaces between objects are directly built. Explicit algorithms have been developed for decades (e.g., Fisher and Wales 1992; de Kemp 1998; Mallet 1992) and rely on techniques such as direct mesh triangulation, kriging or spline interpolation (Caumon et al. 2009; Sprague and Kemp 2005). However, as explicit modeling requires considerable manual input from the user to create a single model representation, the application of implicit methods has advanced lately, as reflected in the relative volume of research in this millennium (see Wellmann and Caumon 2018). In implicit interpolation algorithms (e.g., Calcagno et al. 2008; Caumon et al. 2007; Caumon et al. 2012; Lajaunie et al. 1997), the geological boundaries of an object are represented as an isosurface within a volumetric scalar field, i.e., the surface of a model element has a constant scalar value (Wellmann

and Caumon 2018). However, while the input data (interface points and partially orientation data) inform the scalar field, conformable packages of strata are defined by the same scalar field. Thus, frequently less data and less manipulation is required to model a subsurface configuration implicitly, than explicitly. The general choice of an interpolation method for the mathematical model is not only dependent on personal preferences though but also dictated by the assumed structural complexity and the available input data that define the appearance and relationship of model elements (Wellmann and Caumon 2018). In addition, the conceptual knowledge and the input data also inform the parameters of the interpolation function like for instance a variogram model. After the setup of the interpolation method and the parametrization is completed, geometric model realizations are obtained as possible representations of the true subsurface conditions. Subsequently, the consistency and realism of these models is investigated in the given context, before model realizations are applied as the foundation of further modeling, simulation or decision-making.

1.2.2 Classification of uncertainties in geological models

In the applied field of structural geological modeling, uncertainties have to be considered at every step of model construction. As reflected by Wellmann and Caumon (2018), the types and sources of uncertainties in geological models have been studied intensively, yet, no particular definition has been found to be conclusive. Some approaches shall still be reviewed below, considering the background of the GeoBlocks project and focusing on aspects relevant to this thesis. A detailed review and discussion of all uncertainties, however, is beyond the scope of this thesis. For a broader overview the reader is referred to Wellmann and Caumon (2018).

Wellmann and Caumon (2018) describe that in all stages of a geomodeling workflow reviewed above, uncertainties are introduced. At the stage of conceptualization, lack of knowledge and personal biases are major sources of uncertainties (see also Alcalde et al. 2019; Bond et al. 2007). However, also when defining and parametrizing the mathematical model, uncertainties arise, just as when defining the location of input data in the model for the interpolation. An earlier approach on uncertainty classification in the context of geomodel construction has been proposed by Wellmann et al. (2010). The authors adapt a classification of Mann (1993), systematizing uncertainties into three types. Type 1 uncertainties concern any introduced error or present imprecision during the initial acquisition of data, type 2 refers to uncertainties related to interpolation and extrapolation from/of this input, and type 3 arise from incomplete knowledge about the structural configurations in the subsurface and from the need for conceptual simplifications. In another classification approach, Pérez-Díaz et al. (2020) describe the distinction between objective and subjective uncertainty. Objective uncertainty is

present in data acquisition, processing and analysis, while subjective uncertainty results from personal biases and missing or flawed knowledge of individuals or groups of people. In all of these comprehensive classification approaches, uncertainties in input data are clearly recognized. Their appearance and impact in data acquisition, processing and integration have been studied extensively (e.g., Abellan and Noetinger 2010; Barbosa et al. 2020; Bodur and Rey 2019; Høyer et al. 2024; Jones et al. 2004; Mern and Caers 2023). In all of the three steps related to the handling of data, subjective uncertainties based on knowledge, experience and "beliefs" (Zimmermann 2000) are introduced. Especially the interpretative part of data integration is an ever-present source of uncertainty and thus subject of many studies (e.g., Bond et al. 2007; Bond et al. 2012; Bond et al. 2015; Causer et al. 2020; Jacoby and Smilde 2009). Similarly, decision-making after modeling is prone to personal biases (e.g., Wilson et al. 2019).

While the GeoBlocks project as a whole is also concerned with uncertainties in interpretation and in input data quality, this thesis focusses on aspects related to quantified geometric variability, model generalization and benchmarking as well as the role of data density in geomodels.

1.2.3 Uncertainty quantification approaches and the effect of data integration on uncertainties

Given the wide array of potentially present uncertainties, a lot of research on uncertainty quantification and reduction has been conducted in the past decades. A common way to represent existing uncertainties is by creating sets of probabilistic model realizations (Wellmann and Caumon 2018). For the setup of these realizations, specific interpolation algorithms like for instance sequential Gaussian simulation (see Deutsch and Journel 1992) or sequential indicator simulation (Journel and Alabert 1990) can be used, or initial models or input data are randomized. Stochastic perturbation of initial models can be approached differently based on the chosen modeling method. In research, perturbation of explicit models has been performed for instance by Wang et al. (2023) and Suzuki et al. (2008) who apply stochastic perturbation fields to faults (both studies) and horizons (Suzuki et al. 2008); and Li et al. (2024) who perturb initial models by adding spatially uncorrelated random noise to a subset of randomly selected coordinates in a grid. In implicit approaches, the scalar field can be perturbed directly, in areas without input data (e.g., Caumon 2010; Cherpeau and Caumon 2015). However, input data perturbations are more common. Usually, parameters are coupled with probability distributions, and samples are drawn from these distributions to obtain perturbed datasets for modeling. Orientation data has been perturbed this way (e.g., Krajnovich et al. 2020; Li et al. 2021; Lindsay et al. 2012; Lv and Liu 2026; Wellmann et al. 2010), just as interface point data (e.g., Thiele et al. 2016b; Well-

mann and Regenauer-Lieb 2012; Wellmann et al. 2010). While most of these studies apply measures for uncertainty quantification, Wellmann and Regenauer-Lieb (2012) stand out as their work has been the basis for uncertainty quantification in several of the more recent publications. The authors describe the concepts of information entropy (Shannon 1948), fuzzy set entropy (Luca and Termini 1993) and total model entropy/mean entropy in the geomodeling context, as cell/voxel-based measures for uncertainty description, communication and comparison. The entropy essentially captures the amount of missing information with respect to the position of a geological unit. Additional measures from information theory in the geomodeling context have been explored by Wellmann (2013): Joint entropy is applied for the quantified evaluation of the combined uncertainty at two positions in space. Mutual information is used as a measure for shared information between two locations. Conditional entropy indicates where, and how additional information at a single position reduces uncertainties elsewhere, and multivariate conditional entropy enhances this measure to information at multiple locations.

Beyond the objective of uncertainty quantification, many geoscientific studies have been concerned with uncertainty reduction, given the commonly sparse data available for subsurface modeling. While many types of input data can be obtained in theory (surface data, 2D maps and cross sections, borehole data and different geophysical data; see Wellmann and Caumon 2018), the high acquisition costs of most data types (Bjørlykke 2015) have a major influence on data density. Thus, data is mainly concentrated in areas of economic interest. Another factor is the age of the datasets. As legacy data have been obtained with outdated methods and/or equipment in many cases (see e.g., BGE 2021), compatibility of data from different sources and integrability is not guaranteed, even after (re-)processing. Given the high costs of new data, a lot of emphasis in research has been put on the evaluation of uncertainty reduction through data integration to assess, in which locations within a model, additional data has the most influence on geomodeling results. This optimized positioning of additional data is the main objective of optimal experimental design, that has been studied extensively across geoscientific disciplines, for instance for geothermal exploration (e.g., Seidler et al. 2016), in hydrogeological considerations (e.g., Nowak and Guthke 2016) and hydrocarbon exploration (e.g., Eide et al. 2017; White and Royer 2003). In the context of structural geomodeling, the effect of data integration on model realizations has been evaluated for instance by Wellmann and Regenauer-Lieb (2012), Lindsay et al. (2012), Schweizer et al. (2017) and Wang et al. (2022). Among these studies, data integration has been mainly found to reduce uncertainties in geomodels in areas of lower geological complexity. However, observation/introduction of more complex model elements like faults has been identified to increase uncertainties proximally as well. An inverse approach to the evaluation of the influence of data quantities on model

results has been followed by Putz et al. (2006). However, their assessment of the effects of stepwise reduction of input data on modeling results has only been qualitative and visually. In contrast, Carmichael and Ailleres (2016) address the influence of varying orientation data densities on geomodels quantitatively, evaluating the performance of different upscaling methods in reproducing the main geological trends in an input dataset. Weighted upscaling methods outperform stochastic removal approaches, and models based on sparse data represent statistical outliers. Equally important as quantifying the effects of data integration/removal is the assessment of model reliability. Especially under sparse data, a fraction of probabilistic model realizations is likely to be implausible, not respecting geological principles, knowledge about the local geology or even the input data. An approach for the automatic checking of reliability and consistency of model realizations that applies to geomodels consisting of several stratigraphic units has recently been presented by Parquer et al. (2025). Furthermore, Wei et al. (2026) have investigated the falsification of implausible geological hypotheses by data.

1.2.4 Structural-geometric complexity and the necessity of model generalization and benchmarking

The configuration of geological bodies in the subsurface results from a long geological history, creating structural complexity on all observable scales (Fossen 2016). In a geometric and topological context, increasing complexity correlates with the number of geological features in the system and the present relations between these features (Pellerin et al. 2015; Thiele et al. 2016a; Thiele et al. 2016b). Common features particularly increasing complexity are for instance faults, creating geometric discontinuities that need to be modeled. As the overall geological complexity cannot possibly be fully resolved by subsurface investigations like drilling and geophysics, every attempt to model the subsurface is inherently an approximation of reality, informed by and (ideally) coherent with all available measurements, observations, and a-priori knowledge (Wellmann and Caumon 2018). Given this constraint, geomodels are purposely built to focus on specific elements of the subsurface or (geo-)physical aspects, acknowledging that the model represents a single potential realization of the true conditions. Within these levels of abstraction, complexity is addressed more easily. Often, this is only done qualitatively, introducing a bias dependent on the experience, knowledge, viewpoint and means of the geoscientist (Pellerin et al. 2015). However, as complexity is often important for economic considerations, influencing directly the costs and risks of exploration and exploitation endeavors, approaches of complexity quantification have been developed (e.g., Dromgoole and Speers 1997; Ford and Blenkinsop 2008; Ford and McCuaig 2010; Trubetskoy et al. 2012; Zhao et al. 2011). Quantifica-

tion of structural complexity is also important for landslide risk assessment, as different spatial configurations of stratigraphic elements in a slope are associated with varying risks of mass wasting events (Esposito et al. 2021; Zhang et al. 2025). In the field of structural geomodeling, complexity measures have been proposed for instance by Lindsay et al. (2013a) and Pellerin et al. (2015), identifying both global (system-wide) measures as well as local measures based on adjacent model elements. An alternative to addressing structural complexity in geomodels through direct quantification are comparative analyses to benchmarks of defined spatial characteristics. Although benchmarks in geosciences are more often established for reservoir and petrophysical modeling (e.g., Correia et al. 2015; Karmakar et al. 2022; Kolditz et al. 2012; Nordbotten et al. 2022; Zhu et al. 2015) or thermo-hydro-mechanical modeling (e.g., Alonso et al. 2005; Rutqvist et al. 2006; Simo et al. 2025), structural benchmarks have been suggested by Pellerin et al. (2015) as well. These aim at models consisting of a number of stratigraphic elements. In some geological contexts like the site selection for nuclear waste disposal, however, intrusive structures are also assessed as isolated geometries. To enable quantitative comparison of models of these structures, respective benchmark models are thus required.

1.2.5 Quantitative methods for the comparison of 3D objects in geomodeling

Dis-/similarity metrics for quantitative shape comparison originate from mathematics, computer sciences and engineering, among others (Webb and Copsey 2003). In the context of structural geomodeling, shape quantification and comparison can be approached with two types of metrics (Wellmann and Caumon 2018): 1) misfit functions that assess the dis-/similarity of a model realization to an external reference model or information, and 2) distance metrics that evaluate the dis-/similarity between model realizations. As the algorithms and methods described in this thesis fit into both categories, both misfit and distance metrics applied in geoscientific studies are reviewed.

1.2.5.1 Direct shape comparison through distance functions

The **Jaccard distance** d_{JAC} (see Webb and Copsey 2003) is defined as 1 minus the Jaccard similarity, s_{JAC}. The Jaccard similarity is set as the size of the intersection divided by the size of the union of two sample sets M:

$$s_{JAC} = \frac{\left|Q^t_{M_1} \cap Q^t_{M_2}\right|}{\left|Q^t_{M_1} \cup Q^t_{M_2}\right|} \tag{1.1}$$

With the threshold value t, and Q_M^t representing the locations where the probability $P_x(U)$ of belonging to a specific geological unit U exceeds the threshold t:

$$Q_M^t = \{x\}_{P_x(U)>t} \tag{1.2}$$

As s_{JAC} translates to the similarity in position of the geological unit U between two geological models, $d_{JAC} = 1$ would indicate that at no location in the two models, unit U could be observed simultaneously. Thus, the Jaccard distance is essentially a binary metric (Schweizer et al. 2017). The Jaccard distance as a dis-/similarity metric in geomodeling has been applied for instance by Giraud et al. (2021), Llanes et al. (2022), Schaaf et al. (2021), Schweizer et al. (2017) and Zhang et al. (2026).

The **normalized city-block distance** (see Paul and Maji 2013; Webb and Copsey 2003) has been applied in the geomodeling context by Schweizer et al. (2017) and Zhang et al. (2026). It captures the fuzziness (see e.g., Yager 1995) of geological boundaries and is defined as:

$$d_{\mathrm{NCB}} = \frac{1}{N} \sum_{x=1}^{N} \left| P_x^{M_1}(U) - P_x^{M_2}(U) \right| \tag{1.3}$$

Where $P_x^{M_1}(U)$ and $P_x^{M_2}(U)$ represent the respective lithology probability of unit U at grid cell x in the models M, and N is the total number of cells in the models. The distance is largest with $d_{NCB} = 1$.

The **Hausdorff distance** has been applied as a dis-/similarity distance for instance in reservoir modeling (Lee et al. 2013; Suzuki et al. 2008; Zhang et al. 2019), structural geomodeling (Lindsay et al. 2013b) and CO_2 plume monitoring (Jeong and Srinivasan 2017). Two structures have to be represented as point sets $A = \{a_1, \ldots, a_n\}$ and $B = \{b_1, \ldots, b_n\}$ (see also Huttenlocher et al. 1993). The locations of points a_n and b_n are defined as u^{a_n} and u^{b_n}, and the Euclidean distance between the locations of a_n and b_n is set as $||u^{a_n} - u^{b_n}||$. The spatial distance from a point a_n to the point set B is then defined as:

$$h(a_n, B) = \min_{b_n \in B} ||u^{a_n} - u^{b_n}|| \tag{1.4}$$

And the distance from A to B is:

$$h(A, B) = \max_{a_n \in A} h(a_n, B) \tag{1.5}$$

Thus, the point a_n that is farthest from any point in B is determined, and the distance from a_n to the nearest neighbor in B is measured. $h(A, B)$ effectively ranks each point of A based on its distance to the nearest point of B and then recognizes the largest ranked point as the distance. The calculation is then repeated vice versa. The Hausdorff distance is thus defined as:

$$H(A, B) = \max \{h(A, B), h(B, A)\} \tag{1.6}$$

This factors in that the Hausdorff distance is oriented, i.e., $h(A, B)$ is not necessarily equal to $h(B, A)$. In essence, the Hausdorff distance quantifies the overlap of two geometries, focusing on the point in an object that is most deviated from the other object (the larger the deviation, the larger the Hausdorff distance).

1.2.5.2 Additional dissimilarity metrics applied in geomodeling

In addition to the dissimilarity distances described above, a variety of metrics has been proposed for the quantitative assessment of model/object differences in the context of structural geomodeling. The geodiversity metrics established by Lindsay et al. (2013a) evaluate the depth, volume, contact surface area, curvature and geological complexity of/between stratigraphic units within model realizations. Principal component analysis is employed to analyze the contribution of the geodiversity metrics to the geometric variability and to quantify geometric dis-/similarities between assessed geomodels. The concept of the geodiversity metrics has been applied by Carmichael and Ailleres (2016), and Thiele et al. (2016b) propose topological differences between model realizations as an additional geodiversity metric, clustered in dendrograms. Similarly to the dissimilarity distances described above, Wellmann and Regenauer-Lieb (2012) present metrics that are single values between model realizations or stratigraphic units: the application of the mean entropy (one value per model) and fuzziness entropy (one value per stratigraphic unit) as metrics for model comparison is proposed. These measures have been applied by Schweizer et al. (2017) in addition to the Jaccard distance and city-block distance as described above. For implicit geomodels, quantitative comparison is also achievable using the cosine similarity of gradients (Caumon 2022), being a continuous dis-/similarity measure for scalar fields. In a reservoir modeling context, distances between model realizations are furthermore definable based on flow simulations as a function of time (e.g., Park et al. 2013; Scheidt and Caers 2009). Misfit functions calculated between model realizations and a reference are described by Jessell et al. (2010). Structural, lithological, gravity and magnetic misfits are considered.

Besides the dissimilarity metrics proposed or explored in geoscientific contexts, there is a computer-scientific approach relevant for this thesis due to some similarities. The method of Celenk (1995) is based on the matching of cross sections between geometries.

The centroids of the sections are determined using the first order moments. The second order moments are computed to determine the straight, unsegmented main axes of the sections. Cross sections of two objects are aligned along their straight main axes, also corresponding to the direction of the gradient vector given by:

$$\nabla I(x,y) = \frac{\partial I}{\partial x}\, i + \frac{\partial I}{\partial y}\, j \tag{1.7}$$

Shape differences d_i are determined at the $M = 4$ polygon shape boundary points along the aligned axes in all N cross-sectional planes to obtain the average shape difference S between two objects:

$$S = \frac{1}{NM} \sum_{i=1}^{N} \sum_{j=1}^{M} d_j \tag{1.8}$$

1.3 Methods

1.3.1 Segmentation and measurement algorithm

Calculation of the polygon area of cross sections

In the methodology for the quantitative characterization and comparison of 3D structures, the parameters are measured on cross sections perpendicular to the horizontal main axes (see e.g., chapter 2). Thus, two sets of cross sections have to be created. The respective correct orientation of the sections of the first set has been determined by progressively rotating each section, calculating the area of the rotation steps and selecting the one per section with the smallest area. The area of the polygons has been calculated using the shoelace formula that involves cross-multiplying the coordinates of the different vertices of a polygon (adapted after Braden 1986):

$$\text{area} = \frac{1}{2} \left| \sum_{i=1}^{n-1} y_i z_{i+1} + y_n z_1 - \sum_{i=1}^{n-1} y_{i+1} z_i - y_1 z_n \right| \tag{1.9}$$

With the y-coordinate chosen given that the sections have been rotated parallel to the y-axis and projected on that axis for area calculation (see chapter 2).

Interquartile range method

The interquartile range method (IQR; e.g., Upton and Cook 1996) has been used in chapter 3 to determine whether the individual open cross-sectional polygons of a structure need to be levelled to allow for comparable vertical measurements. The IQR has been calculated on the z-coordinate of the last vertex of each section, which is located at the shallower end of the open polygon line (see e.g., Fig. 3.6b). The IQR is defined as the difference between the 75th and 25th percentiles of the z-coordinate of

the last vertex of the cross sections, so:

$$\mathrm{IQR} = Q_3 - Q_1 \tag{1.10}$$

Sections below the upper bound (= third quartile + $1.5 \cdot$ interquartile range) in terms of z-values are cropped at the constant base level per structure, that is defined as the median of the z-coordinate of the last vertex of the cross sections. Outlier sections which are not cropped to create a levelled lower base are defined as being above the upper bound.

Gradient calculation

The gradient data has been calculated on the polygons of the cross sections, between two consecutive vertices. Depending on whether the sections have been rotated parallel to the x- or y-axis and projected on this axis before the measurements (see chapter 2), x- or y-coordinates have been used in the following equation:

$$\text{gradient} = \frac{z_2 - z_1}{x_2 - x_1 \text{ or } y_2 - y_1} \tag{1.11}$$

Curvature calculation

Curvature calculation has been done between three consecutive vertices of a polygon. In 3D, the mean curvature and/or the Gaussian curvature is/are usually being determined, as described in detail for example by Chen and Schmitt (1992), Lisle and Toimil (2007) and Mynatt et al. (2007). For irregular surface meshes, curvatures can only be calculated approximately, with different approaches being in use (e.g., Chen and Schmitt 1992; Dong and Wang 2005). As we determine the curvature on the 2D cross sections, however, the computation can be simplified, making use of the curvature in 2D being defined as the reciprocal of the circumradius of a triangle. It is thus computed between three consecutive vertices in either the xz- or yz-plane. First, the side lengths (a, b and c) of the triangle between the points are calculated. Given the three vertices $V_0 = (x_0, z_0)$, $V_1 = (x_1, z_1)$ and $V_2 = (x_2, z_2)$, the side lengths are:

$$a = \sqrt{(x_1 - x_0)^2 + (z_1 - z_0)^2} \tag{1.12}$$

$$b = \sqrt{(x_2 - x_1)^2 + (z_2 - z_1)^2} \tag{1.13}$$

$$c = \sqrt{(x_2 - x_0)^2 + (z_2 - z_0)^2} \tag{1.14}$$

With x being interchangeable with y depending on the plane. Next, the semiperimeter of the triangle is determined as:

$$s = \frac{(a+b+c)}{2} \tag{1.15}$$

before the area through Heron's formula is computed:

$$\text{area} = \sqrt{s \cdot (s-a) \cdot (s-b) \cdot (s-c)} \tag{1.16}$$

At last, the curvature is calculated through:

$$\text{curvature} = \frac{4 \cdot \text{area}}{a \cdot b \cdot c} \tag{1.17}$$

1.3.2 Data analysis

Kullback-Leibler divergence

The Kullback-Leibler divergence (Kullback and Leibler 1951) is a measure from information theory used in chapters 2 and 4 to quantify the similarity of two probability distributions p and q. It is defined (after Kullback 1959) as:

$$\text{KLD}(p \parallel q) = \sum_{x \in \mathcal{X}} p(x) \log \left(\frac{p(x)}{q(x)} \right) \tag{1.18}$$

The Kullback-Leibler divergence is restricted to positive values. The smaller the value, the larger the similarity between both distributions, with a value of 0 indicating equality. In this thesis, the Kullback-Leibler divergence is computed between data distributions of individual geometric parameters measured for objects.

Principal component analysis and K-means clustering algorithm

In the studies of chapters 2 and 3, cluster analysis has been carried out, following data normalization to a range of -1 to 1 and principal component analysis (PCA; see Jolliffe 2002). In addition, PCA without clustering has been performed in chapter 4. PCA aims to reduce the number of variables in a dataset that contains many interrelated measures, while preserving as much of the original variance as possible. This is accomplished by transforming the original variables into a new set of uncorrelated variables, the principal components (PCs), that explain a progressively lower degree of variance in the data from the first to the final PC. Therefore, each PC comprises a combination of variability across all input parameters, instead of only one parameter. Principal components are calculated as follows:

1. Definition of input data: in the studies of this thesis, 20 percentiles of the probability density functions (PDFs) of statistical parameters (combined horizontal data, vertical data, gradients and partially curvatures) have been chosen as variables ("features"), resulting in 60–80 input features
2. Standardization of each feature, so that every feature has a mean = 0
3. Calculation of the covariance matrix
4. Computation of eigenvectors (giving the direction of a PC) and eigenvalues (the variance explained by a PC)
5. Sorting of eigenvectors of the covariance matrix by eigenvalues in descending order
6. Projection of datasets onto the principal components

Automatic clustering has been conducted using the K-means algorithm (see MacQueen 1967). Starting from an initial random assignment of data points to K clusters, each data point is reassigned to the nearest cluster center. Then, cluster centers are relocated by computing the mean of all data points of respective clusters. This process is repeated for a fixed number of iterations or until convergence. Repeating the procedure with different random initializations helps to assess the stability and robustness of the clustering results. The ideal number of clusters is determined by the semi-quantitative evaluation of the elbow plot (e.g., Ashari et al. 2023) and by the quantitative silhouette score (e.g., Shahapure and Nicholas 2020). In the former, the inertia that measures how tightly data points are clustered together is plotted against the number of clusters. The "elbow" is defined as the point where the typically rapid decline of inertia tapers off, indicating the optimal number of clusters (see e.g., Fig. 3.12b). In contrast, the silhouette score is a quantitative measure using the mean intra-cluster distance a and the mean nearest-cluster distance b for each datapoint:

$$\text{silhouette score} = \frac{b - a}{\max(a, b)} \tag{1.19}$$

The score is determined for all data points and then averaged. The averaged value is plotted against the number of clusters. The highest averaged silhouette score represents the optimal number of clusters (see e.g., Fig. 3.12b).

Visual analysis of cluster results can be cautiously approached by evaluating which features show the highest positive and negative contributions to a PC in the feature contribution matrix. These features explain the highest amount of variance across all features. Knowing what distributional shapes in the PDFs are associated with which kind of structural property ((an-)isotropy, the roundness of top surfaces etc.; see Subsect. 2.3.2), we assess the feature contribution matrix to interpret the structural

appearance of models within clusters from the features showing the highest contributions to the PCs. However, the positions of datasets in a principal component diagram (the PC scores) cannot be derived and interpreted exactly from a few features showing the highest positive and negative loadings: PC scores for a dataset are computed as the weighted sum of all the original feature values, where the weights are given by the loadings:

$$\text{PC score} = \sum_{i=1}^{n} L_i \cdot x_i \tag{1.20}$$

Where n is the number of features, L_i is the loading for the i-th bin (from the contribution matrix) and x_i is the corresponding probability of that bin in the dataset (equation adapted after Jolliffe 2002). As PCs are linear combinations of the mean probability of all features from the PDFs, all bins contribute to the position of a dataset: although a high loading of a bin indicates that differences in that bin's value among datasets are highly influential in defining that PC, the other non-zero bins are also contributing according to their positive or negative weight. Thus, analyzing the highest loadings can only give a general idea of the characteristics of a dataset.

1.4 Motivation and problem definition

In the German site selection, the importance of uncertainty analysis in regional subsurface characterization is recognized (StandAG 2017). Still, distinct gaps remain, considering the inhomogeneous data situation and the complex and equally heterogeneous geology. To study the different sources of uncertainty in the context of the site selection and to develop approaches to quantify, visualize and communicate them, GeoBlocks has been subdivided into several work packages, addressing the following aspects:

1. a systematic analysis of the uncertainties in the geological and geophysical input data
2. the quantitative description of the geometric variability of the potential host rocks
3. the development of methods for the comparison of regions showing different data sparsity situations from different acquisition sources
4. the development of methods for uncertainty reduction through techniques of optimal experimental design

The results of these analyses and method developments will be integrated to form a workflow for structural geological modeling with uncertainty quantification, comprising all relevant workflow phases. To reiterate, this includes: 1) data integration, 2)

the setup of a conceptual model, 3) the definition of the mathematical model, 4) its parametrization, 5) the creation of geometric model realizations and 6) the assessment of their plausibility, i.e., the falsification of unrealistic models.

In the context of the German site selection, the modeling workflow shall be tailored for the different potential host rock types and their geometric variability, that is large, encompassing a wide range of geological-tectonic settings and both concordant and discordant geometries (BGE 2020b). For an efficient consideration of this variability in the conceptualization of a model, the systematization of the geometries relevant for the site selection is only feasible establishing a limited set of end member geometries. These end members may act as initial approximations of host rock configurations, but only if they are geometrically dissimilar, to avoid ambiguities in their selection. At the same time, it has to be evaluated whether some end members across rock types are represented by the same 3D geometry to avoid redundancy. Since regions in the German site selection will be compared in their suitability to host a waste disposal site, quantitative comparability of the structural geomodels characterizing these locations is vital. Thus, for the underlying geomodeling workflow, every consideration and process step should be approached as quantitatively as possible. Regarding the conceptualization using the geometric end members, the assessment of their suitability to approximate a certain subsurface configuration should be based on the quantitative analysis of the available input data. However, based on the present research, there is no dedicated approach or recommended practice to characterize input data geometrically, to infer the potential suitability of geometric end members, i.e., geometric benchmarks for conceptualization. Provided a suitable approach is creatable, the quantitative assessment of the input data situation in combination with the geometric end members should also be capable of answering the fundamental question whether the available input data in a location is sufficient to construct reasonably uncertain ("good enough") structural geomodels. This is especially relevant in the context of the German site selection, as a sparse data situation is not a valid reason to exclude a region from the process (BGE 2023).

Considering the aim of a quantified model conceptualization, a quantitative method for the geometric characterization and comparison of unmodeled datasets and conceptual models is thus required. The reviewed methods for object comparison from previous research provide information on the dis-/similarity of two isolated geo-objects but are incapable to indicate where the shape of models differs spatially. Given the structural diversity especially of intrusive rock types relevant in the site selection (see Hudec and Jackson 2007; Philpotts and Ague 2009), and considering the quantitative decision criteria in the search for a nuclear waste disposal site (see BGE 2023; BGE 2024), both information on size and shape differences between objects need to be quantifiable

in the context of the site selection though. Therefore, there is a need for a quantitative comparison method for models and unmodeled datasets focusing on geometric properties. When the conceptualization has been completed, the quantitatively established conceptual model informs the interpolation method that is used to generate the model realizations. In the latter step, the geometric uncertainty is represented best by constructing a large set of probabilistic realizations. Thus, geometric variability is reproduced, that is quantifiable with the same comparison method as already employed. Furthermore, the conceptual model is utilizable as a reference to assist in the geometric falsification of the realizations, given that according to the reviewed literature, no dedicated method has been established for the plausibility assessment of isolated geoobjects. Thus, the ensemble set is reduced to realistic models. In the context of the site selection, different regions are likely to be represented by one or few respective models only, on which comparative assessments between regions will be conducted. It is thus also important to consider approaches to communicate and visualize the resulting uncertainties. Here, comparative metrics based on geometric properties may represent the basis for a communication approach that is accessible to a broader audience than (geo-)statistical concepts being the foundation of many established methods.

1.5 Synopsis of the research situation and unresolved questions

Many approaches for uncertainty quantification in geomodels have been proposed especially throughout the past two decades. As the acquisition of input data for geomodeling is expensive, the data situation is commonly sparse and regionally heterogeneous, as seen for instance for the German subsurface. Thus, various studies have focused on the influence of data density on modeling results, either by assessing the effect of data integration on uncertainties or the result of data removal. However, given the structurally complex subsurface, uncertainties are never addressed entirely and conclusively. Every geological model is a single possible approximation of the subsurface conditions; thus, probabilistic model realizations are often produced to visualize the range of uncertainties. To assess the differences of model realizations and of geological models between various locations, quantitative methods for the comparison and structural characterization of geomodels have been proposed.

Even though there have been significant advances in these research fields over the past years and decades, relevant research questions are concluded given the site selection-context of the present thesis, and will be addressed in the following chapters:

1. Previously established metrics for the quantitative comparison of geological models tend to be hardly accessible without much geological and statistical expertise. Furthermore, many methods like the three reviewed distance functions have in common, that they indicate the dissimilarity of two datasets, but are unsuitable to provide any information on where the compared entities differ spatially. Can an approach based on geometric parameters measured on cross sections perpendicular to the horizontal main axes of a structure reproduce the main geometric characteristics of input datasets and quantify their dis-/similarities? Is it capable of showing where structures differ spatially? Can the method be designed in a way, that it is utilizable at different stages of a geomodeling workflow, from structural conceptualization to the falsification of model realizations by data?

2. The current state of research reveals a lack of benchmark models for structural geomodeling, especially for isolated geometries. Such benchmarks are required to establish and apply misfit functions for geometric dis-/similarity, and are applicable at several stages of a geomodeling workflow. Can the geometric dis-/similarity of a set of benchmark models be quantified with the established quantification approach? How many benchmark models are required to approximate the structural variability of the potential host rocks for nuclear waste disposal considered in Germany? Do different rock types exhibit vastly different geometric ranges or can they partially be approximated by the same benchmark models?

3. A quantification method to assess geomodel dis-/similarity has to be applicable to the full range of real structural complexity. Most existing methods are presented on a limited number of input datasets and/or on synthetically perturbed data. Can the established quantification method and the benchmarks be utilized to cover and analyze the full geometric complexity of the structures in the German subsurface? Is it possible to relate the geometric properties from the quantification method to the geological processes shaping the geo-bodies? Does the quantification algorithm allow for the interpretation of geometric patterns without visual examination of the geological models and without the need to run a full-scale implicit comparison of these models?

4. While uncertainty reduction in geological models and the effect of data integration is a research objective of many studies, there is a lack of specific investigations on how much data is required at minimum for sufficiently certain structural geomodeling. Is it possible to define metrics for this objective based on the geometric parameters assessed throughout the thesis? How high are the requirements according to the chosen approach? Can uniform minimum requirements be derived for different structures, or is this aspect dependent on structural complexity?

1.6 Outline of this thesis

The thesis is organized into 5 chapters. In chapter 1, the topic of the thesis is outlined and the literature is reviewed that constitutes the theoretical basis of the research. Furthermore, methods employed in the studies of the thesis are reviewed. Subsequently, the motivation of the work is presented, and the state of the research is summarized briefly, followed by the deduction of the research questions addressed in the main part of this thesis. Furthermore, the structure of the thesis is shown. The main body consists of two peer-reviewed articles and the manuscript of a third study, arranged as individual chapters:

Chapter 2 Quantitative comparison of three-dimensional bodies using geometrical properties to validate the dissimilarity of a standard collection of 3D geomodels (Carl et al., 2026a)

This chapter establishes a methodology for the quantitative characterization and comparison of 3D geological objects based on the measurement of geometric parameters on 2D sections that are oriented perpendicular to the horizontal main axes of the structure. Furthermore, a set of regular 3D geometries serving as benchmark models in 3D structural geomodeling is developed, and a geometric systematization of the potential host rock types for nuclear waste disposal is reviewed. The proposed quantification method is demonstrated on the benchmarks and additional simple geometric bodies to evaluate their geometric dis-/similarity. The horizontal and vertical extents, gradients and curvatures are measured on the cross sections. The subsequent data analysis provides information on the (an-)isotropy, surface morphology and sphericity of the tested models and visualizes geometric dis-/similarities. The Kullback-Leibler divergence and a dimensionally reduced cluster analysis serve for the quantitative geometric systematization of the structures, leading to the exclusion of models from the set of benchmarks due to high geometric similarity.

Chapter 3 Quantitative comparison of subsurface structures: an application to salt domes and crystalline bodies (Carl et al., 2026b)

This study applies the method of the preceding chapter, adapting it to open meshes of irregular input structures. 306 datasets of intrusive salt structures from the North German Basin and crystalline geo-objects from Saxony (Germany) are quantified with the algorithm alongside the benchmark models from the previous chapter, revealing the geometric dis/-similarities between the subsurface structures and their dis/-similarities to the set of benchmarks. The cluster results are put into the context of the regional geology of the two case study regions. The study demonstrates the universal applicability of the quantification algorithm,

representing an efficient way for the geometric analysis of subsurface structures without visual expert assessment and without the requirement for a full-scale comparative analysis of implicit model realizations.

Chapter 4 Minimum data quantity requirements for structural geological modeling (the draft of a manuscript)

This chapter covers the setup of two metrics to assess minimum data quantities required to construct realistic geological models. The mean averaged Kullback-Leibler divergence – based on the similarity of parameter distributions – and the mean Euclidean distance in principal component space – based on dimensionally reduced parameter data – are established and their performance is assessed. Existing 3D models of two subsurface structures and a sphere are taken as input and reference, as datasets in 15 data configurations are extracted randomly from the meshes and interpolated implicitly to create model realizations covering geometric uncertainty. Model realizations are condensed into threshold models, and these models and the references are quantified with the shape quantification method established earlier. The resulting geometric data is the input for the two metrics, assessing which data configurations are sufficient to model the structures realistically. Minimum data requirements can be derived for all three test cases.

In the final chapter 5, the main points of this thesis are summarized and the results are evaluated given the initial aims of the research within the GeoBlocks project. Moreover, recommendations for further research are presented.

References

Abellan, A. and Noetinger, B. (2010). "Optimizing Subsurface Field Data Acquisition Using Information Theory". en. In: *Mathematical Geosciences* 42.6, pp. 603–630. ISSN: 1874-8953. DOI: 10.1007/s11004-010-9285-6. URL: https://doi.org/10.1007/s11004-010-9285-6 (visited on 03/11/2026).

Alcalde, J., Bond, C. E., Johnson, G., Kloppenburg, A., Ferrer, O., Bell, R., and Ayarza, P. (2019). "Fault interpretation in seismic reflection data: an experiment analysing the impact of conceptual model anchoring and vertical exaggeration". English. In: *Solid Earth* 10.5, pp. 1651–1662. ISSN: 1869-9510. DOI: 10.5194/se-10-1651-2019. URL: https://se.copernicus.org/articles/10/1651/2019/ (visited on 03/11/2026).

Alonso, E. E., Alcoverro, J., Coste, F., Malinsky, L., Merrien-Soukatchoff, V., Kadiri, I., Nowak, T., Shao, H., Nguyen, T. S., Selvadurai, A. P. S., Armand, G., Sobolik, S. R., Itamura, M., Stone, C. M., Webb, S. W., Rejeb, A., Tijani, M., Maouche, Z., Kobayashi, A., Kurikami, H., Ito, A., Sugita, Y., Chijimatsu, M., Börgesson, L., Hernelind, J., Rutqvist, J., Tsang, C. .-., and Jussila, P. (2005). "The FEBEX benchmark test: case definition and comparison of modelling approaches". In: *International Journal of Rock Mechanics and Mining Sciences*. Research results from the Decovalex III & Benchpar projects 42.5, pp. 611–638. ISSN: 1365-1609. DOI: 10.1016/j.ijrmms.2005.03.004. URL: https://www.sciencedirect.com/science/article/pii/S1365160905000316 (visited on 08/11/2025).

Ashari, I. F., Nugroho, E. D., Baraku, R., Yanda, I. N., and Liwardana, R. (2023). "Analysis of Elbow, Silhouette, Davies-Bouldin, Calinski-Harabasz, and Rand-Index Evaluation on K-Means Algorithm for Classifying Flood-Affected Areas in Jakarta". en. In: *Journal of Applied Informatics and Computing* 7.1, pp. 95–103. ISSN: 2548-6861. DOI: 10.30871/jaic.v7i1.4947. URL: https://jurnal.polibatam.ac.id/index.php/JAIC/article/view/4947 (visited on 03/16/2026).

Barbosa, C. H. S., Kunstmann, L. N. O., Silva, R. M., Alves, C. D. S., Silva, B. S., Filho, D. M. S., Mattoso, M., Rochinha, F. A., and Coutinho, A. L. G. A. (2020). "A workflow for seismic imaging with quantified uncertainty". In: *Computers & Geosciences* 145, p. 104615. ISSN: 0098-3004. DOI: 10.1016/j.cageo.2020.104615. URL: https://www.sciencedirect.com/science/article/pii/S0098300420305951 (visited on 08/06/2025).

BGE (2019). *Umsetzungsstrategie für ein lernendes Verfahren in der Standortauswahl*. Tech. rep. URL: https://www.bge.de/fileadmin/user_upload/Standortsuche/Wesentliche_Unterlagen/Methodik/Umsetzungsstrategie_lernendes_Verfahren_-_Endfassung.pdf (visited on 04/04/2026).

— (2020a). *Mindestanforderungen gemäß § 23 StandAG und geowissenschaftlichen Abwägungskriterien gemäß § 24 StandAG*. Tech. rep. URL: https://www.bge.de/fileadmin/user_upload/Standortsuche/Wesentliche_Unterlagen/Zwischenbericht_Teilgebiete/Datenbericht_Teil_2_von_4_MA_und_geoWK_barrierefrei.pdf (visited on 04/04/2026).

— (2020b). *Zwischenbericht Teilgebiete gemäß § 13 StandAG*. Tech. rep. URL: https://www.bge.de/fileadmin/user_upload/Standortsuche/Wesentliche_Unterlagen/Zwischenbericht_Teilgebiete/Zwischenbericht_Teilgebiete_barrierefrei.pdf (visited on 04/04/2026).

— (2021). *Arbeitsgruppe K 3 – Geodaten: Datenverfügbarkeit und Tranparenz*. URL: https://www.bge.de/fileadmin/user_upload/Standortsuche/Wesentliche_Unterlagen/Zwischenbericht_Teilgebiete/Vortraege_Fachkonferenz/Zweiter_Beratungstermin/20210612_3_AG_K-3_Impulsvortrag_barrierefrei.pdf (visited on 04/04/2026).

— (2023). *Vorgehen zur Ermittlung von Standortregionen aus den Teilgebieten*. Tech. rep. URL: https://www.bge.de/fileadmin/user_%20upload/Standortsuche/Wesentliche_Unterlagen/Methodik/%20Phase_I_Schritt_2/20231004_Vorgehen_zur_Ermittlung_von_%20Standortregionen_aus_den_Teilgebieten_barrierefrei.pdf (visited on 01/22/2026).

— (2024). *Dokumente zu rvSU-Kriterien*. URL: https://www.bge.de/de/endlagersuche/unterlagen/arbeitsstaende-standortregionen/ (visited on 04/04/2026).

Bjørlykke, K., ed. (2015). *Petroleum Geoscience: From Sedimentary Environments to Rock Physics*. en. Berlin, Heidelberg: Springer. ISBN: 978-3-642-34131-1 978-3-642-34132-8. DOI: 10.1007/978-3-642-34132-8. URL: https://link.springer.com/10.1007/978-3-642-34132-8 (visited on 10/13/2025).

BMU (2010). *Sicherheitsanforderungen an die Endlagerung wärmeentwickelnder radioaktiver Abfälle (Stand: 30. September 2010)*. Tech. rep. URL: https://www.bundestag.de/resource/blob/329904/91e0daa80e9a895923c6f250f1071dca/kmat_10-data.pdf (visited on 04/04/2026).

Bodur, Ö. F. and Rey, P. F. (2019). "The impact of rheological uncertainty on dynamic topography predictions". English. In: *Solid Earth* 10.6, pp. 2167–2178. ISSN: 1869-9510. DOI: 10.5194/se-10-2167-2019. URL: https://se.copernicus.org/articles/10/2167/2019/ (visited on 03/11/2026).

Bond, C. E., Johnson, G., and Ellis, J. F. (2015). "Structural model creation: the impact of data type and creative space on geological reasoning and interpretation". English. In: *Special Publication - Geological Society of London* 421, pp. 83–97. ISSN: 0375-6440. DOI: 10.1144/SP421.4. URL: https://abdn.elsevierpure.com/en/publications/structural-model-creation-the-impact-of-data-type-and-creative-sp (visited on 08/06/2025).

Bond, C. E., Lunn, R. J., Shipton, Z. K., and Lunn, A. D. (2012). "What makes an expert effective at interpreting seismic images?" English. In: *Geology* 40.1, pp. 75–78. ISSN: 0091-7613. DOI: 10.1130/G32375.1. URL: https://abdn.elsevierpure.com/en/publications/what-makes-an-expert-effective-at-interpreting-seismic-images (visited on 08/06/2025).

Bond, C. E., Gibbs, A. D., Shipton, Z. K., and Jones, S. (2007). "What do you think this is?: "Conceptual uncertainty" In geoscience interpretation". English. In: *GSA Today* 17.11, pp. 4–10. ISSN: 1052-5173. DOI: 10.1130/GSAT01711A.1. URL: https://abdn.elsevierpure.com/en/publications/what-do-you-think-this-is-conceptual-uncertainty-in-geoscience-in (visited on 08/06/2025).

Braden, B. (1986). "The Surveyor's Area Formula". In: *The College Mathematics Journal* 17.4, pp. 326–337. ISSN: 0746-8342.

DOI: 10.1080/07468342.1986.11972974. URL: https://doi.org/10.1080/07468342.1986.11972974 (visited on 07/25/2025).

Calcagno, P., Chilès, J.-P., Courrioux, G., and Guillen, A. (2008). "Geological modelling from field data and geological knowledge: Part I. Modelling method coupling 3D potential-field interpolation and geological rules". In: *Physics of the earth and planetary interiors* 171.1-4, pp. 147–157. (Visited on 03/04/2026).

Carmichael, T. and Ailleres, L. (2016). "Method and analysis for the upscaling of structural data". In: *Journal of Structural Geology* 83, pp. 121–133. ISSN: 0191-8141. DOI: 10.1016/j.jsg.2015.09.002. URL: https://www.sciencedirect.com/science/article/pii/S0191814115300353 (visited on 03/11/2026).

Caumon, G., Antoine, C., and Tertois, A. (2007). "Building 3D geological surfaces from field data using implicit surfaces". In: *Proceedings of the 27th Gocad Meeting, Nancy*. Vol. 6. (Visited on 04/04/2026).

Caumon, G. (2022). "On some comparison metrics between 3D implicit structural models." In: Nancy, France: IAMG 21st annual conference. (Visited on 04/04/2026).

Caumon, G., Collon-Drouaillet, P., Le Carlier de Veslud, C., Viseur, S., and Sausse, J. (2009). "Surface-Based 3D Modeling of Geological Structures". en. In: *Mathematical Geosciences* 41.8, pp. 927–945. ISSN: 1874-8953. DOI: 10.1007/s11004-009-9244-2. URL: https://doi.org/10.1007/s11004-009-9244-2 (visited on 02/26/2026).

Caumon, G. (2010). "Towards Stochastic Time-Varying Geological Modeling". en. In: *Mathematical Geosciences* 42.5, pp. 555–569. ISSN: 1874-8953. DOI: 10.1007/s11004-010-9280-y. URL: https://doi.org/10.1007/s11004-010-9280-y (visited on 02/27/2026).

Caumon, G., Gray, G., Antoine, C., and Titeux, M.-O. (2012). "Three-dimensional implicit stratigraphic model building from remote sensing data on tetrahedral meshes: theory and application to a regional model of La Popa Basin, NE Mexico". In: *IEEE Transactions on Geoscience and Remote Sensing* 51.3, pp. 1613–1621. (Visited on 04/04/2026).

Causer, A., Pérez-Díaz, L., Adam, J., and Eagles, G. (2020). "Uncertainties in break-up markers along the Iberia–Newfoundland margins illustrated by new seismic data". In: *Solid Earth* 11.2, pp. 397–417. ISSN: 1869-9510. DOI: 10.5194/se-11-397-2020. URL: https://se.copernicus.org/articles/11/397/2020/ (visited on 03/11/2026).

Celenk, M. (1995). "Three-dimensional object recognition using cross-sections". In: *Proceedings of the Twenty-Seventh Southeastern Symposium on System Theory.* Starkville, MS, USA: IEEE Comput. Soc. Press, pp. 92–96. ISBN: 978-0-8186-6985-9. DOI: 10.1109/SSST.1995.390611. URL: http://ieeexplore.ieee.org/document/390611/ (visited on 02/12/2025).

Chen, X. and Schmitt, F. (1992). "Intrinsic surface properties from surface triangulation". en. In: *Computer Vision — ECCV'92*. Ed. by G. Sandini. Berlin, Heidelberg: Springer, pp. 739–743. ISBN: 978-3-540-47069-4. DOI: 10.1007/3-540-55426-2_83. (Visited on 04/04/2026).

Cherpeau, N. and Caumon, G. (2015). "Stochastic structural modelling in sparse data situations". In: *Petroleum Geoscience* 21.4, pp. 233–247. ISSN: 1354-0793. DOI: 10.1144/petgeo2013-030. URL: https://doi.org/10.1144/petgeo2013-030 (visited on 02/27/2026).

Correia, M., Hohendorff, J., Gaspar, A. T., and Schiozer, D. (2015). "UNISIM-II-D: Benchmark Case Proposal Based on a Carbonate Reservoir". en. In: OnePetro. DOI: 10.2118/177140-MS. URL: https://dx.doi.org/10.2118/177140-MS (visited on 08/11/2025).

de Kemp, E. A. (1998). "Three-dimensional projection of curvilinear geological features through direction cosine interpolation of structural field observations". In: *Computers & Geosciences* 24.3, pp. 269–284. ISSN: 0098-3004. DOI: https://doi.org/10.1016/S0098-3004(97)00066-6. URL: https://www.sciencedirect.com/science/article/pii/S0098300497000666 (visited on 04/04/2026).

Deutsch, C. V. and Journel, A. G. (1992). "GSLIB: Geostatistical Software Library and User's Guide". In: URL: https://claytonvdeutsch.com/wp-content/uploads/2019/03/GSLIB-Book-Second-Edition.pdf (visited on 04/04/2026).

Dong, C. and Wang, G. (2005). "Curvatures estimation on triangular mesh". In: *Journal of Zhejiang University: Science* A6, pp. 128–136. (Visited on 04/04/2026).

Dromgoole, P. and Speers, R. (1997). "Geoscore; a method for quantifying uncertainty in field reserve estimates". In: *Petroleum Geoscience* 3.1, pp. 1–12. DOI: 10.1144/petgeo.3.1.1. URL: https://www.lyellcollection.org/doi/abs/10.1144/petgeo.3.1.1 (visited on 02/26/2026).

Eide, C. H., Schofield, N., Jerram, D. A., and Howell, J. A. (2017). "Basin-scale architecture of deeply emplaced sill complexes: Jameson Land, East Greenland". In: *Journal of the Geological Society* 174.1, pp. 23–40. DOI: 10.1144/jgs2016-018. URL: https://www.lyellcollection.org/doi/full/10.1144/jgs2016-018 (visited on 09/03/2025).

Esposito, G., Carabella, C., Paglia, G., and Miccadei, E. (2021). "Relationships between Morphostructural/Geological Framework and Landslide Types: Historical Landslides in the Hilly Piedmont Area of Abruzzo Region (Central Italy)". en. In: *Land* 10.3, p. 287. ISSN: 2073-445X. DOI: 10.3390/land10030287. URL: https://www.mdpi.com/2073-445X/10/3/287 (visited on 03/12/2026).

Fisher, T. R. and Wales, R. Q. (1992). "Three Dimensional Solid Modeling of Geo-Objects Using Non-Uniform Rational B-Splines (NURBS)". In: *Three-Dimensional Modeling with Geoscientific Information Systems*. Ed. by A. K. Turner. Dordrecht: Springer Netherlands, pp. 85–105. ISBN: 978-94-011-2556-7. DOI: 10.1007/978-94-011-2556-7_9. URL: https://doi.org/10.1007/978-94-011-2556-7_9 (visited on 04/04/2026).

Ford, A. and Blenkinsop, T. G. (2008). "Evaluating geological complexity and complexity gradients as controls on copper mineralisation, Mt Isa Inlier". In: *Australian Journal of Earth Sciences* 55.1, pp. 13–23. ISSN: 0812-0099. DOI: 10.1080/08120090701581364. URL: https://doi.org/10.1080/08120090701581364 (visited on 03/12/2026).

Ford, A. and McCuaig, T. C. (2010). "The effect of map scale on geological complexity for computer-aided exploration targeting". In: *Ore Geology Reviews*. Mineral Prospectivity Analysis and Quantitative Resource Estimation 38.3, pp. 156–167. ISSN: 0169-1368. DOI: 10.1016/j.oregeorev.2010.03.008. URL: https://www.sciencedirect.com/science/article/pii/S0169136810000405 (visited on 02/26/2026).

Fossen, H. (2016). *Structural Geology*. en. Cambridge University Press. ISBN: 978-1-107-41509-6. DOI: 10.1017/9781107415096. (Visited on 04/04/2026).

Giraud, J., Lindsay, M. D., and Jessell, M. (2021). "Generalization of level-set inversion to an arbitrary number of geologic units in a regularized least-squares framework". In: *Geophysics* 86.4, R623–R637. ISSN: 0016-8033. DOI: 10.1190/geo2020-0263.1. URL: https://doi.org/10.1190/geo2020-0263.1 (visited on 03/12/2026).

Høyer, A. S., Sandersen, P. B. E., Andersen, L. T., Madsen, R. B., Mortensen, M. H., and Møller, I. (2024). "Evaluating the chain of uncertainties in the 3D geological modelling workflow". In: *Engineering Geology* 343, p. 107792. ISSN: 0013-7952. DOI: 10.1016/j.enggeo.2024.107792. URL: https://www.sciencedirect.com/science/article/pii/S0013795224003922 (visited on 08/06/2025).

Hudec, M. R. and Jackson, M. P. A. (2007). "Terra infirma: Understanding salt tectonics". In: *Earth-Science Reviews* 82.1, pp. 1–28. ISSN: 0012-8252. DOI: 10.1016/j.earscirev.2007.01.001. URL: https://www.sciencedirect.com/science/article/pii/S0012825207000025 (visited on 11/30/2024).

Huttenlocher, D., Klanderman, G., and Rucklidge, W. (1993). "Comparing images using the Hausdorff distance". In: *IEEE Transactions on Pattern Analysis and Machine Intelligence* 15.9, pp. 850–863. ISSN: 0162-8828. DOI: 10.1109/34.232073. URL: http://ieeexplore.ieee.org/document/232073/ (visited on 07/24/2025).

IAEA (2009). *Classification of radioactive waste—general safety guide*. Tech. rep. GSG-1. URL: https://www-pub.iaea.org/MTCD/Publications/PDF/Pub1419_web.pdf? (visited on 04/04/2026).

Jacoby, W. and Smilde, P. L. (2009). *Gravity Interpretation: Fundamentals and Application of Gravity Inversion and Geological Interpretation*. en. Berlin, Heidelberg: Springer. ISBN: 978-3-540-85328-2 978-3-540-85329-9. DOI: 10.1007/978-3-540-85329-9. URL: http://link.springer.com/10.1007/978-3-540-85329-9 (visited on 08/06/2025).

Jeong, H. and Srinivasan, S. (2017). "Fast selection of geologic models honoring CO2 plume monitoring data using Hausdorff distance and scaled connectivity analysis". In: *International Journal of Greenhouse Gas Control* 59, pp. 40–57. ISSN: 1750-5836. DOI: 10.1016/j.ijggc.2017.02.005. URL: https://www.sciencedirect.com/science/article/pii/S1750583616305291 (visited on 03/13/2026).

Jessell, M. W., Ailleres, L., and Kemp, E. A. de (2010). "Towards an integrated inversion of geoscientific data: What price of geology?" In: *Tectonophysics* 490.3, pp. 294–306. ISSN: 0040-1951. DOI: 10.1016/j.tecto.2010.05.020. URL: https:

/ / www . sciencedirect . com / science / article / pii / S0040195110002246 (visited on 02/18/2026).

Jolliffe, I. T. (2002). *Principal Component Analysis*. en. Springer Series in Statistics. New York: Springer-Verlag. ISBN: 978-0-387-95442-4. DOI: 10.1007/b98835. URL: http://link.springer.com/10.1007/b98835 (visited on 04/23/2025).

Jones, R. R., McCaffrey, K. J. W., Wilson, R. W., and Holdsworth, R. E. (2004). "Digital field data acquisition: towards increased quantification of uncertainty during geological mapping". In: *Geological Prior Information: Informing Science and Engineering*. Ed. by A. Curtis and R. Wood. Vol. 239. Geological Society of London, pp. 43–56. ISBN: 978-1-86239-171-0. DOI: 10.1144/GSL.SP.2004.239.01.04. URL: https://doi.org/10.1144/GSL.SP.2004.239.01.04 (visited on 03/11/2026).

Journel, A. G. and Alabert, G. (1990). "New Method for Reservoir Mapping". en. In: DOI: https://doi.org/10.2118/18324-PA. (Visited on 04/04/2026).

Karmakar, S., Tatomir, A., Oehlmann, S., Giese, M., and Sauter, M. (2022). "Numerical Benchmark Studies on Flow and Solute Transport in Geological Reservoirs". en. In: *Water* 14.8, p. 1310. ISSN: 2073-4441. DOI: 10.3390/w14081310. URL: https://www.mdpi.com/2073-4441/14/8/1310 (visited on 08/11/2025).

Kolditz, O., Bauer, S., Beyer, C., Böttcher, N., Dietrich, P., Görke, U.-J., Kalbacher, T., Park, C.-H., Sauer, U., Schütze, C., Shao, H., Singh, A., Taron, J., Wang, W., and Watanabe, N. (2012). "A systematic benchmarking approach for geologic CO2 injection and storage". en. In: *Environmental Earth Sciences* 67.2, pp. 613–632. ISSN: 1866-6299. DOI: 10.1007/s12665-012-1656-5. URL: https://doi.org/10.1007/s12665-012-1656-5 (visited on 08/11/2025).

Krajnovich, A., Zhou, W., and Gutierrez, M. (2020). "Uncertainty assessment for 3D geologic modeling of fault zones based on geologic inputs and prior knowledge". English. In: *Solid Earth* 11.4, pp. 1457–1474. ISSN: 1869-9510. DOI: 10.5194/se-11-1457-2020. URL: https://se.copernicus.org/articles/11/1457/2020/ (visited on 02/27/2026).

Krohn, J., Spieth-Achtnich, A., Schütte, S., Mbah, M., Lampke, A., Hünecke, K., Fouquet, D., Kuhbier, J., and Reinhardt, T. (2024). *Unterstützung des BASE bei der Prozessanalyse des Standortauswahlverfahrens (PaSta)*. Tech. rep. URL: https://www.base.bund.de/shareddocs/downloads/de/fachinfo/fa/pasta_abschlussbericht.pdf?__blob=publicationFile&v=3 (visited on 04/04/2026).

Kullback, S. (1959). *Information Theory*. New York: Wiley. URL: https://theswissbay.ch/pdf/Gentoomen%20Library/Information%20Theory/Information%20Theory/Information%20theory%20and%20statistics%20-%20Solomon%20Kullback.pdf (visited on 04/04/2026).

Kullback, S. and Leibler, R. A. (1951). "On Information and Sufficiency". en. In: *The Annals of Mathematical Statistics* 22.1, pp. 79–86. ISSN: 0003-4851. DOI: 10.1214/aoms/1177729694. URL: http://projecteuclid.org/euclid.aoms/1177729694 (visited on 12/01/2024).

Lajaunie, C., Courrioux, G., and Manuel, L. (1997). "Foliation fields and 3D cartography in geology: Principles of a method based on potential interpolation". en. In: *Mathematical Geology* 29.4, pp. 571–584. ISSN: 1573-8868. DOI: 10.1007/BF02775087. URL: https://doi.org/10.1007/BF02775087 (visited on 03/16/2026).

Lee, K., Jeong, H., Jung, S., and Choe, J. (2013). "Characterization of Channelized Reservoir Using Ensemble Kalman Filter with Clustered Covariance". EN. In: *Energy Exploration & Exploitation* 31.1, pp. 17–29. ISSN: 0144-5987. DOI: 10.1260/0144-5987.31.1.17. URL: https://doi.org/10.1260/0144-5987.31.1.17 (visited on 03/13/2026).

Lersow, M. and Waggitt, P. (2020). *Disposal of All Forms of Radioactive Waste and Residues: Long-Term Stable and Safe Storage in Geotechnical Environmental Structures*. en. Cham: Springer International Publishing. ISBN: 978-3-030-32909-9 978-3-030-32910-5. DOI: 10.1007/978-3-030-32910-5. URL: http://link.springer.com/10.1007/978-3-030-32910-5 (visited on 07/18/2025).

Li, A., Grana, D., Parsekian, A. D., and Carr, B. (2024). "Uncertainty Quantification in Tomographic Inversion of Near-Surface Seismic Refraction Data". en. In: *Mathematical Geosciences* 56.1, pp. 77–101. ISSN: 1874-8953. DOI: 10.1007/s11004-023-10083-9. URL: https://doi.org/10.1007/s11004-023-10083-9 (visited on 02/27/2026).

Li, N., Li, C., Chu, W., Xiao, K., Tao, W., Song, X., Cao, R., Xu, Y., and Fan, M. (2021). "Uncertainty Visualisation of a 3D Geological Geometry Model and Its Application in GIS-Based Mineral Resource

Assessment: A Case Study in Huayuan District, Northwestern Hunan Province, China". en. In: *Journal of Earth Science* 32.2, pp. 358–369. ISSN: 1867-111X. DOI: 10.1007/s12583-021-1434-y. URL: https://doi.org/10.1007/s12583-021-1434-y (visited on 02/27/2026).

Lindsay, M. D., Jessell, M. W., Ailleres, L., Perrouty, S., Kemp, E. de, and Betts, P. G. (2013a). "Geodiversity: Exploration of 3D geological model space". In: *Tectonophysics* 594, pp. 27–37. ISSN: 0040-1951. DOI: 10.1016/j.tecto.2013.03.013. URL: https://www.sciencedirect.com/science/article/pii/S004019511300187X (visited on 04/04/2025).

Lindsay, M. D., Aillères, L., Jessell, M. W., Kemp, E. A. de, and Betts, P. G. (2012). "Locating and quantifying geological uncertainty in three-dimensional models: Analysis of the Gippsland Basin, southeastern Australia". In: *Tectonophysics* 546-547, pp. 10–27. ISSN: 0040-1951. DOI: 10.1016/j.tecto.2012.04.007. URL: https://www.sciencedirect.com/science/article/pii/S0040195112002004 (visited on 07/31/2025).

Lindsay, M. D., Perrouty, S., Jessell, M. W., and Aillères, L. (2013b). "Making the link between geological and geophysical uncertainty: geodiversity in the Ashanti Greenstone Belt". en. In: *Geophysical Journal International* 195.2, pp. 903–922. ISSN: 0956-540X. DOI: 10.1093/gji/ggt311. URL: https://dx.doi.org/10.1093/gji/ggt311 (visited on 03/13/2026).

Lisle, R. J. and Toimil, N. C. (2007). "Defining folds on three-dimensional surfaces". In: *Geology* 35.6, pp. 519–522. ISSN: 0091-7613. DOI: 10.1130/G23207A.1. URL: https://doi.org/10.1130/G23207A.1 (visited on 04/07/2025).

Llanes, J. D., Viñales, A., and Juri, J. (2022). "Assisted 3D Model Construction and Facies Propagation in Golfo San Jorge Basin Reservoirs for Modelling EOR". en. In: OnePetro. DOI: 10.2118/209400-MS. URL: https://dx.doi.org/10.2118/209400-MS (visited on 03/12/2026).

Luca, A. de and Termini, S. (1993). "A Definition of a Nonprobabilistic Entropy in the Setting of Fuzzy Sets Theory". en-US. In: *Readings in Fuzzy Sets for Intelligent Systems*. Morgan Kaufmann, pp. 197–202. DOI: 10.1016/B978-1-4832-1450-4.50020-1. URL: https://www.sciencedirect.com/science/chapter/edited-volume/abs/pii/B9781483214504500201 (visited on 02/23/2026).

Lv, W. and Liu, X. (2026). "Three-dimensional bedrock implicit modeling and uncertainty quantification from sparse geological map data". In: *Journal of Structural Geology* 204, p. 105627. ISSN: 0191-8141. DOI: 10.1016/j.jsg.2026.105627. URL: https://www.sciencedirect.com/science/article/pii/S0191814126000131 (visited on 02/27/2026).

MacQueen, J. B. (1967). "Some methods for classification and analysis of multivariate observations." In: *Proceedings of the fifth Berkeley symposium on mathematical statistics and probability*. Vol. Vol. 1. Berkeley: University of California Press, pp. 281–297. URL: https://www.cs.cmu.edu/~bhiksha/courses/mlsp.fall2010/class14/macqueen.pdf (visited on 04/04/2026).

Mallet, J. L. (1992). "GOCAD: A Computer Aided Design Program for Geological Applications". In: *Three-Dimensional Modeling with Geoscientific Information Systems*. Ed. by A. K. Turner. Dordrecht: Springer Netherlands, pp. 123–141. ISBN: 978-94-011-2556-7. DOI: 10.1007/978-94-011-2556-7_11. URL: https://doi.org/10.1007/978-94-011-2556-7_11.

Mann, J. C. (1993). "Uncertainty in geology". In: *Computers in geology|25 years of progress*. Oxford University Press, pp. 241–254.

Mern, J. and Caers, J. (2023). "The Intelligent Prospector v1.0: geoscientific model development and prediction by sequential data acquisition planning with application to mineral exploration". English. In: *Geoscientific Model Development* 16.1, pp. 289–313. ISSN: 1991-959X. DOI: 10.5194/gmd-16-289-2023. URL: https://gmd.copernicus.org/articles/16/289/2023/ (visited on 03/11/2026).

Mynatt, I., Bergbauer, S., and Pollard, D. D. (2007). "Using differential geometry to describe 3-D folds". In: *Journal of Structural Geology* 29.7, pp. 1256–1266. ISSN: 0191-8141. DOI: 10.1016/j.jsg.2007.02.006. URL: https://www.sciencedirect.com/science/article/pii/S0191814107000193 (visited on 04/07/2025).

Neeft, E., Bartol, J., Vuorio, M., and Vis, G.-J. (2025). "Geological disposal of radioactive waste". In: *Geology of the Netherlands*. Ed. by G.-J. Vis, J. H. t. Veen, J. de Jager, and T. E. Wong. Second Edition. Amsterdam University Press, pp. 769–791. ISBN: 978-94-6372-836-2. URL: https://www.jstor.org/stable/jj.27435714.25 (visited on 07/18/2025).

Nordbotten, J. M., Fernø, M., Flemisch, B., Juanes, R., and Jørgensen, M. (2022). "Final Benchmark Description: FluidFlower

International Benchmark Study". In: URL: https://zenodo.org/records/6807102 (visited on 08/11/2025).

Nowak, W. and Guthke, A. (2016). "Entropy-Based Experimental Design for Optimal Model Discrimination in the Geosciences". en. In: *Entropy* 18.11, p. 409. ISSN: 1099-4300. DOI: 10.3390/e18110409. URL: https://www.mdpi.com/1099-4300/18/11/409 (visited on 03/06/2026).

Park, H., Scheidt, C., Fenwick, D., Boucher, A., and Caers, J. (2013). "History matching and uncertainty quantification of facies models with multiple geological interpretations". en. In: *Computational Geosciences* 17.4, pp. 609–621. ISSN: 1573-1499. DOI: 10.1007/s10596-013-9343-5. URL: https://doi.org/10.1007/s10596-013-9343-5 (visited on 03/14/2026).

Parquer, M. N., Kemp, E. A. de, Brodaric, B., and Hillier, M. J. (2025). "Checking the consistency of 3D geological models". English. In: *Geoscientific Model Development* 18.1, pp. 71–100. ISSN: 1991-959X. DOI: 10.5194/gmd-18-71-2025. URL: https://gmd.copernicus.org/articles/18/71/2025/ (visited on 10/24/2025).

Paul, S. and Maji, P. (2013). "City Block Distance for Identification of Co-expressed MicroRNAs". en. In: *Swarm, Evolutionary, and Memetic Computing*. Ed. by B. K. Panigrahi, P. N. Suganthan, S. Das, and S. S. Dash. Cham: Springer International Publishing, pp. 387–396. ISBN: 978-3-319-03756-1. DOI: 10.1007/978-3-319-03756-1_35.

Pellerin, J., Caumon, G., Julio, C., Mejia-Herrera, P., and Botella, A. (2015). "Elements for measuring the complexity of 3D structural models: Connectivity and geometry". In: *Computers & Geosciences* 76, pp. 130–140. ISSN: 0098-3004. DOI: 10.1016/j.cageo.2015.01.002. URL: https://www.sciencedirect.com/science/article/pii/S0098300415000035 (visited on 08/12/2025).

Pérez-Díaz, L., Alcalde, J., and Bond, C. E. (2020). "Introduction: Handling uncertainty in the geosciences: identification, mitigation and communication". English. In: *Solid Earth* 11.3, pp. 889–897. ISSN: 1869-9510. DOI: 10.5194/se-11-889-2020. URL: https://se.copernicus.org/articles/11/889/2020/ (visited on 03/11/2026).

Philpotts, A. and Ague, J. (2009). *Principles of Igneous and Metamorphic Petrology*. 2nd ed. Cambridge: Cambridge University Press. DOI: 10.1017/CBO9780511813429. (Visited on 06/04/2025).

Putz, M., Stüwe, K., Jessell, M., and Calcagno, P. (2006). "Three-dimensional model and late stage warping of the Plattengneis Shear Zone in the Eastern Alps". In: *Tectonophysics* 412.1, pp. 87–103. ISSN: 0040-1951. DOI: 10.1016/j.tecto.2005.10.003. URL: https://www.sciencedirect.com/science/article/pii/S0040195105004531 (visited on 02/18/2026).

Rutqvist, J., Feng, X.-T., Hudson, J., Jing, L., Kobayashi, A., Koyama, T., Pan, P.-Z., Lee, H.-S., Rinne, M., Sonnenthal, E., and Yamamoto, Y. (2006). "Multiple-code benchmark simulation study of coupled THMC processes in the excavation disturbed zone associated with geological nuclear waste repositories". en. In: URL: https://escholarship.org/uc/item/4g154293 (visited on 08/11/2025).

Schaaf, A., Varga, M. de la, Wellmann, F., and Bond, C. E. (2021). "Constraining stochastic 3-D structural geological models with topology information using approximate Bayesian computation in GemPy 2.1". English. In: *Geoscientific Model Development* 14.6, pp. 3899–3913. ISSN: 1991-959X. DOI: 10.5194/gmd-14-3899-2021. URL: https://gmd.copernicus.org/articles/14/3899/2021/ (visited on 03/12/2026).

Scheidt, C. and Caers, J. (2009). "Representing Spatial Uncertainty Using Distances and Kernels". en. In: *Mathematical Geosciences* 41.4, pp. 397–419. ISSN: 1874-8953. DOI: 10.1007/s11004-008-9186-0. URL: https://doi.org/10.1007/s11004-008-9186-0 (visited on 03/14/2026).

Schweizer, D., Blum, P., and Butscher, C. (2017). "Uncertainty assessment in 3-D geological models of increasing complexity". English. In: *Solid Earth* 8.2, pp. 515–530. ISSN: 1869-9510. DOI: 10.5194/se-8-515-2017. URL: https://se.copernicus.org/articles/8/515/2017/ (visited on 04/04/2025).

Seidler, R., Padalkina, K., Bücker, H. M., Ebigbo, A., Herty, M., Marquart, G., and Niederau, J. (2016). "Optimal experimental design for reservoir property estimates in geothermal exploration". en. In: *Computational Geosciences* 20.2, pp. 375–383. ISSN: 1573-1499. DOI: 10.1007/s10596-016-9565-4. URL: https://doi.org/10.1007/s10596-016-9565-4 (visited on 03/06/2026).

Shahapure, K. R. and Nicholas, C. (2020). "Cluster Quality Analysis Using Silhouette Score". In: *2020 IEEE 7th International Conference on Data Science and Advanced Analytics (DSAA)*, pp. 747–748. DOI: 10.1109/DSAA49011.2020.00096. URL: https://ieeexplore.ieee.org/abstract/document/9260048 (visited on 03/16/2026).

Shannon, C. E. (1948). "A mathematical theory of communication". In: *The Bell System Technical Journal* 27.3, pp. 379–423. ISSN: 0005-8580. DOI: 10.1002/j.1538-7305.1948.tb01338.x. URL: https://ieeexplore.ieee.org/document/6773024 (visited on 06/11/2025).

Simo, E., Lesquen, C. de, Vu, M.-n., Raude, S., El Tabbal, G., Narkuniene, A., Poskas, P., Collin, F., Abhishek, R., Song, H., Gens, A., Song, F., Leon-Vargas, R. P., Tatomir, A.-B., Mánica, M., Nagel, T., and Buchwald, J. (2025). "Benchmarking thermo-hydro-mechanical models for geological barrier integrity in clay-based repositories". In: *Acta Geotechnica*. ISSN: 1861-1133. DOI: 10.1007/s11440-025-02683-y. URL: https://doi.org/10.1007/s11440-025-02683-y.

Sprague, K. B. and Kemp, E. A. de (2005). "Interpretive tools for 3-D structural geological modelling part II: Surface design from sparse spatial data". In: *GeoInformatica* 9.1, pp. 5–32. URL: https://link.springer.com/article/10.1007/s10707-004-5620-8 (visited on 04/04/2026).

StandAG (2017). *StandAG - Gesetz zur Suche und Auswahl eines Standortes für ein Endlager für hochradioaktive Abfälle*. URL: https://www.gesetze-im-internet.de/standag_2017/BJNR107410017.html (visited on 07/21/2025).

Suzuki, S., Caumon, G., and Caers, J. (2008). "Dynamic data integration for structural modeling: model screening approach using a distance-based model parameterization". en. In: *Computational Geosciences* 12.1, pp. 105–119. ISSN: 1573-1499. DOI: 10.1007/s10596-007-9063-9. URL: https://doi.org/10.1007/s10596-007-9063-9 (visited on 06/10/2025).

Thiele, S. T., Jessell, M. W., Lindsay, M., Ogarko, V., Wellmann, J. F., and Pakyuz-Charrier, E. (2016a). "The topology of geology 1: Topological analysis". In: *Journal of Structural Geology* 91, pp. 27–38. ISSN: 0191-8141. DOI: 10.1016/j.jsg.2016.08.009. URL: https://www.sciencedirect.com/science/article/pii/S0191814116301110 (visited on 12/01/2024).

Thiele, S. T., Jessell, M. W., Lindsay, M. D., Wellmann, J. F., and Pakyuz-Charrier, E. (2016b). "The topology of geology 2: Topological uncertainty". In: *Journal of Structural Geology* 91, pp. 74–87. ISSN: 0191-8141. DOI: 10.1016/j.jsg.2016.08.010. URL: https://www.sciencedirect.com/science/article/pii/S0191814116301122 (visited on 07/24/2025).

Trubetskoy, K. N., Galchenko, Y. P., and Sabyanin, G. V. (2012). "Evaluation methodology for structural complexity of ore deposits as development targets". en. In: *Journal of Mining Science* 48.6, pp. 1006–1015. ISSN: 1573-8736. DOI: 10.1134/S1062739148060081. URL: https://doi.org/10.1134/S1062739148060081 (visited on 02/26/2026).

Upton, G. and Cook, I. (1996). *Understanding Statistics*. en. OUP Oxford. ISBN: 978-0-19-914391-7. URL: https://books.google.de/books?id=vXzWG09_SzAC&printsec=frontcover&hl=de&source=gbs_ge_summary_r&cad=0#v=onepage&q&f=false (visited on 04/04/2026).

Wang, S., Cai, Z., Si, X., and Cui, Y. (2023). "A Three-Dimensional Geological Structure Modeling Framework and Its Application in Machine Learning". en. In: *Mathematical Geosciences* 55.2, pp. 163–200. ISSN: 1874-8953. DOI: 10.1007/s11004-022-10027-9. URL: https://doi.org/10.1007/s11004-022-10027-9 (visited on 02/27/2026).

Wang, S.-J., Nguyen, Q. C., Lu, Y.-C., Doyoro, Y. G., and Tran, D.-H. (2022). "Evaluation of geological model uncertainty caused by data sufficiency using groundwater flow and land subsidence modeling as example". en. In: *Bulletin of Engineering Geology and the Environment* 81.8, p. 331. ISSN: 1435-9537. DOI: 10.1007/s10064-022-02832-7. URL: https://doi.org/10.1007/s10064-022-02832-7 (visited on 02/19/2026).

Webb, A. R. and Copsey, K. D. (2003). *Statistical pattern recognition*. Chichester Weinheim: Wiley. ISBN: 978-0-470-84513-4 978-0-470-84514-1. URL: https://theswissbay.ch/pdf/Gentoomen%20Library/Artificial%20Intelligence/Pattern%20recognition/Statistical%20Pattern%20Recognition%202nd%20Ed%20-%20Andrew%20R.%20Webb.pdf (visited on 04/04/2026).

Wei, X., Yin, Z., Bonner, W., and Caers, J. (2026). "Falsification of Geological Hypotheses Using Drillholes and Geophysics". en. In: *Surveys in Geophysics*. ISSN: 1573-0956. DOI: 10.1007/s10712-026-09936-9. URL: https://doi.org/10.1007/s10712-026-09936-9 (visited on 03/03/2026).

Wellmann, F. and Regenauer-Lieb, K. (2012). "Uncertainties have a meaning: Information entropy as a quality measure for 3-D geological models". In: *Tectonophysics*. Modelling in Geosciences 526-529, pp. 207–216. ISSN: 0040-1951. DOI: 10.1016/j.tecto.2011.05.001. URL:

https://www.sciencedirect.com/science/article/pii/S0040195111001788 (visited on 07/24/2025).

Wellmann, J. F. (2013). "Information Theory for Correlation Analysis and Estimation of Uncertainty Reduction in Maps and Models". en. In: *Entropy* 15.4, pp. 1464–1485. ISSN: 1099-4300. DOI: 10.3390/e15041464. URL: https://www.mdpi.com/1099-4300/15/4/1464 (visited on 08/08/2025).

Wellmann, J. F., Horowitz, F. G., Schill, E., and Regenauer-Lieb, K. (2010). "Towards incorporating uncertainty of structural data in 3D geological inversion". In: *Tectonophysics* 490.3, pp. 141–151. ISSN: 0040-1951. DOI: 10.1016/j.tecto.2010.04.022. URL: https://www.sciencedirect.com/science/article/pii/S0040195110001691 (visited on 07/31/2025).

Wellmann, J. F. and Caumon, G. (2018). "3-D Structural Geological Models: Concepts, Methods, and Uncertainties". English. In: *Advances in Geophysics*. 59. Elsevier, pp. 1–121. DOI: https://doi.org/10.1016/bs.agph.2018.09.001. (Visited on 04/04/2026).

White, C. D. and Royer, S. A. (2003). "Experimental Design as a Framework for Reservoir Studies". en. In: OnePetro. DOI: 10.2118/79676-MS. URL: https://dx.doi.org/10.2118/79676-MS (visited on 03/06/2026).

Wilson, C. G., Bond, C. E., and Shipley, T. F. (2019). "How can geologic decision-making under uncertainty be improved?" English. In: *Solid Earth* 10.5, pp. 1469–1488. ISSN: 1869-9510. DOI: 10.5194/se-10-1469-2019. URL: https://se.copernicus.org/articles/10/1469/2019/ (visited on 03/11/2026).

Yager, R. R. (1995). "Measures of entropy and fuzziness related to aggregation operators". In: *Information Sciences* 82.3, pp. 147–166. ISSN: 0020-0255. DOI: 10.1016/0020-0255(94)00030-F. URL: https://www.sciencedirect.com/science/article/pii/002002559400030F (visited on 07/31/2025).

Zhang, Q., Chassagne, R., and MacBeth, C. (2019). "4D Seismic and Production History Matching, a Combined Formulation Using Hausdorff and FréChet Metric". en. In: OnePetro. DOI: 10.2118/195542-MS. URL: https://dx.doi.org/10.2118/195542-MS (visited on 03/13/2026).

Zhang, R., Taherdangkoo, R., and Butscher, C. (2026). "Quantitative evaluation of borehole density impact on 3D geological modeling of quaternary structures". en. In: *Environmental Earth Sciences* 85.4, p. 107. ISSN: 1866-6299. DOI: 10.1007/s12665-026-12843-2. URL: https://doi.org/10.1007/s12665-026-12843-2 (visited on 03/12/2026).

Zhang, Y., Wu, C., Cui, P., Yi, S., Yuan, R., Jiang, Z., Li, Y., and Kong, W. (2025). "Geological Complexity: a novel index for measuring the relationship between landslide occurrences and geological conditions". en. In: *Bulletin of Engineering Geology and the Environment* 84.6, p. 301. ISSN: 1435-9537. DOI: 10.1007/s10064-025-04333-9. URL: https://doi.org/10.1007/s10064-025-04333-9 (visited on 02/26/2026).

Zhao, J., Chen, S., Zuo, R., and Carranza, E. J. M. (2011). "Mapping complexity of spatial distribution of faults using fractal and multifractal models: vectoring towards exploration targets". In: *Computers & Geosciences*. Geocomputation of Mineral Exploration Targets 37.12, pp. 1958–1966. ISSN: 0098-3004. DOI: 10.1016/j.cageo.2011.04.007. URL: https://www.sciencedirect.com/science/article/pii/S0098300411001397 (visited on 03/12/2026).

Zhu, C., Zhang, G., Lu, P., Meng, L., and Ji, X. (2015). "Benchmark modeling of the Sleipner CO2 plume: Calibration to seismic data for the uppermost layer and model sensitivity analysis". In: *International Journal of Greenhouse Gas Control* 43, pp. 233–246. ISSN: 1750-5836. DOI: 10.1016/j.ijggc.2014.12.016. URL: https://www.sciencedirect.com/science/article/pii/S1750583614003958 (visited on 08/11/2025).

Zimmermann, H. .-. (2000). "An application-oriented view of modeling uncertainty". In: *European Journal of Operational Research* 122.2, pp. 190–198. ISSN: 0377-2217. DOI: 10.1016/S0377-2217(99)00228-3. URL: https://www.sciencedirect.com/science/article/pii/S0377221799002283 (visited on 08/06/2025).

CHAPTER

TWO

QUANTITATIVE COMPARISON OF THREE-DIMENSIONAL BODIES USING GEOMETRICAL PROPERTIES TO VALIDATE THE DISSIMILARITY OF A STANDARD COLLECTION OF 3D GEOMODELS

This chapter was published as a peer-reviewed article:

Carl, F., Yang, J., Colling Cassel, M., Wellmann, F., Achtziger-Zupančič, P., 2026a. Quantitative comparison of three-dimensional bodies using geometrical properties to validate the dissimilarity of a standard collection of 3D geomodels, Solid Earth, 17, 155-178, https://doi.org/10.5194/se-17-155-2026.

Abstract

The quantification of 3D structural shapes is a central goal across multiple scientific disciplines, serving purposes such as image analysis and the precise geometric characterization of objects. This study proposes a methodology for the shape quantification based on a set of geometrical parameters in 2D sections of 3D geological shapes and establishes a set of synthetic regular geometries as benchmark models in 3D geomodeling approaches. The proposed methodology is demonstrated on a number of simple geometric bodies and the benchmark models to assess their geometrical dis-/similarity. The dimensions of the structures are measured perpendicular and vertically to their horizontal main axes on a fixed amount of cross sections. Furthermore, gradient and

curvature measurements on these cross sections are conducted. A subsequent multi-step data analysis provides insight into the main geometrical characteristics of the structures and visualizes differences between various datasets: Analysis of extension measurements reveals the anisotropy of structures, the existence of overhangs and the character of the top surface of an investigated structure. Analyzing the gradients and curvatures offers information on the slopes of the lateral walls of the structure and its sphericity as well as top surface. Kullback-Leibler divergence is utilized to quantitatively compare individual parameter distributions. Dimensionally reduced cluster analysis groups and systematizes input structures based on the combined statistical parameters and serves for the identification of benchmark models showing large geometrical similarity. It is expected that the methodology and set of benchmark models will aid in advances to model, analyse and compare subsurface structures based on sparse data, as our framework can be used for an initial structural approximation prior to modeling, for the setup of the interpolation method and for the falsification of probabilistic model realizations after interpolation.

2.1 Introduction

2.1.1 Shape quantification and comparison – previous studies and gaps in current research

The quantitative comparison of three-dimensional (3D) objects plays a crucial role in various scientific fields, including geology, computer science and engineering (see e.g., Cardone et al. 2003; Celenk 1995; Wellmann and Caumon 2018). Shape quantification aims at the numerical characterization of the geometry of objects, with their dis-/similarity not solely being a mathematical metric but also being dependent on the specific context (Laga et al. 2019). Accurate shape quantification independent of the objects' orientation is essential for applications such as geological modeling, resource management and structural analysis, where understanding the geometric properties of objects can inform decision making and enhance predictive capabilities.

Shape quantification can be complex when dealing with static 2D images of 3D bodies (see Laga et al. 2019), but when rotatable objects in 2D or 3D are available, basic geometrical parameters can be applied. This is commonly proposed in material science, where studies often focus on sand grain analysis. In these studies, the range of shape parameters in 2D and 3D include (but are not restricted to) principal dimensions, volumes, aspect ratios, radii, sphericities, convexity, circularity, roundness and compactness (Altuhafi et al. 2013; Cox and Budhu 2008; Zhao and Wang 2016), that partially describe similar structural characteristics. Furthermore, the shapes of aggre-

gate particles in building materials have been analyzed using parameters like sphericity, angularity, aspect ratios, gradients and radius indices (Al Rousan et al. 2007), and volcanic cinders have been assessed looking at elongation, roundness, and roughness (Nie et al. 2023). Similar analytical approaches can be valuable to study the geometry of subsurface structures, although at much larger scales and a higher structural complexity: The shape of individual geo-bodies can be of interest for resource exploration and storage of materials like for instance nuclear waste. However, geoscientific studies applying similar parameters as used in the mentioned material-scientific studies are rare: Gardoll et al. (2000), for instance, determine the aspect ratio, blockiness, elongation, compactness, complexity, roundness, spreadness and squareness of geological bodies from map data to assess the exploration potential for orogenic ore deposits. This is a highly specialized application though, usable for shallow horizontal data, but being inapplicable to (sub-)vertical input data. Instead of relying on geometrical parameters for the shape quantification of a single geo-object, in geosciences advances for the shape comparison of structural models are more common. These are mainly related to uncertainty assessment and quantification within geological models and often approached with distance metrics. For instance, Schweizer et al. (2017) apply the Jaccard distance and the normalized city-block distance as measures for model dissimilarity, while Suzuki et al. (2008) propose the usage of the Hausdorff distance for the same purpose. In contrast, Lindsay et al. (2013) developed an approach for model comparison not relying on such distance metrics: To determine the similarities between 101 realizations of a 3D composite geomodel based on the same perturbed input dataset, a set of geometrical "geodiversity" parameters (e.g., formation depth, volume, contact surface curvature) are calculated on all stratigraphic units. The resulting datasets are analyzed in their ranges to determine endmember model realizations. Furthermore, principal component analysis is employed to determine which geometrical characteristics contribute most to spatial uncertainty and to detect realization outliers for the combined geodiversity metrics. Despite the lack of geoscientific studies approaching shape quantification with simple geometrical parameters, the necessity of basic shape assessment in geomodeling is recognized as most commonly used geomodeling software are capable of obtaining simple geometrical properties like surface areas, aspect ratios and volumes from modeled 3D elements. However, these functionalities are error-prone determining basic geometrical properties in varying directions, like the extent along the horizontal main axes of a given irregular structure – a property of interest for the exploration of geo-bodies for storage purposes. An example of such an application can be found in the storage of high-level nuclear waste: In Germany, currently, intrusive salt bodies with varying internal structures as well as crystalline intrusives potentially exhibiting lateral zonation are considered as potential storage sites (BGE 2020).

In addition to these limitations in the analysis of 3D geo-bodies, geometrical characteristics of structures are hard to quantify prior to geomodelling as well, when input data is most commonly available in 1D (i.e., boreholes) and/or 2D (e.g., seismic sections). At this early stage within a modeling workflow, conceptual models are established based on sparse data, local geological knowledge like the regional geological history and universal geological knowledge such as common laws and principles (Parquer et al. 2025) but also defined spatial factors known to be related to certain variables of interest like resources (Gardoll et al. 2000). The identification of important geometrical features and the establishment or selection of an appropriate conceptual model can have a considerable impact on how realistic/reasonable model realizations are, thus influencing decision-making and the accuracy of predictions (Bond et al. 2007). Therefore, approaches to geometrically quantify available input data and to compare datasets to established conceptual models are valuable.

Given this identified current lack of analytical capabilities for the geometrical assessment of both unmodelled input data as well as modeled structures whose evaluation shall be direction-dependent, this study proposes a novel methodology for the quantitative description, comparison and systematization of datasets using a set of geometrical parameters. While the method development will be visualized based on explicitly modelled 3D geometries, it can be applied to lower dimensional data as well. In the present study, the algorithm is applied to a set of 36 3D geometries approximating subsurface structures of varying rock types, intended to act as benchmark "standard geometries", their geometrical dis-/similarity is analyzed. Furthermore, the methodology has been applied to a small set of basic 3D geometries (a cube, an ellipsoid, a prism, a pyramid and a sphere) with distinctive and expected divergence of geometrical properties. In what follows, the concept of "standard geometries" initially described by Carl et al. (2023) as a geometrical systematization to collect and catalogue subsurface geometries of the potential host rocks in the German site selection for a nuclear waste repository (halite rock, claystone and crystalline rocks) is reviewed, adapted and extended. Please note that the classification is purely geometric, even though the terminology of subdividing categories can also be found in topological considerations (see for instance Thiele et al. 2016a; Thiele et al. 2016b). For more details on the classification, please refer to Carl et al. (2023). For real word examples of the standardized geometries, we refer to the publications mentioned in the respective parts of the following paragraph.

Claystones and shales are clastic sedimentary rocks which are commonly deposited conformably onto the underlying strata (Selley 2000; see also Fig. 2.1, upper section). The appearance of these conformable layers can vary considerably: tilting and folding of a flat-lying structure can result in a range of geometries varying from a flat layered appearance that remain generally conformable (see Fig. 2.2, 4th and 9th row for

potential visual representation). By contrast, faulting, erosion and folding can produce unconformable geometries (see Fig. 2.2, 3rd and 4th row). Lateral stratigraphic pinchout is conformable proximally but results in an unconformity at its tip (see Fig. 2.2, 4th row). Salt rock (i.e., halite) is initially deposited conformably as an evaporitic sediment. Beyond the undeformed, concordant, flat-layer geometry, halite structures are mainly categorized according to two principles: The most common classification is based on the question whether a structure remained concordant in respect to its overlying rocks or intruded into its overburden (Hudec and Jackson 2007; see Fig. 2.1, middle section). Following this systematization, salt anticlines, pillows and rollers are categorized as concordant (see Fig. 2.2, 1st, 5th and 6th row), while salt stocks, sheets and walls are intrusive bodies (see Fig. 2.2, 7th to 11th row). In addition, a supplementary subdivision based on the length-to-width ratio of salt bodies is discussed by some authors (e.g., Hudec et al. 2011): Structures showing a length-to-width ratio higher than 2 in map view (thus being considerably anisotropic) are being defined as anticlines or walls, respectively. In contrast, rather isotropic geometries with a length-to-width ratio smaller than 2 are the pillows, stocks and, at least in their early evolutionary stages, sheets. An additional aspect to consider when classifying salt structures is whether the halite is allochthonous or autochthonous. Sheets are the only structural type categorizable as the former: If the bulb of a stock or wall is subhorizontally oriented or moderately dipping above the autochthonous salt source layer, this rock body can be defined as a salt sheet (Hudec and Jackson 2006). Crystalline rocks considered in the context of the German site selection are plutonic rocks as well as high-grade metamorphic rocks (migmatites and gneisses). As the high-grade metamorphic rocks originate from a wide array of protoliths, resulting in diverse geometries, the establishment of a single, coherent classification for both groups is difficult. For instance, orthogneisses and some migmatites originate from plutonic protoliths such as granitoids and exhibit structural characteristics similar to their igneous predecessors. By contrast, paragneisses and the remaining migmatites derive from various sedimentary sources. Their current shape depends not only on the geometry of the original rock body but also on the specific deformation history experienced during metamorphism. Overall, most high-grade metamorphic rock bodies in the German subsurface are laterally bounded by either plutonic intrusions or fault zones and their top is either bound by unconformities or represents the present-day topography in most cases. Consequently, for the purposes of our geometric approximation, we treat them as discordant rock volumes of varying shape and size (see Fig. 2.1, lower section and Fig. 2.2, 2nd, 6th and 8th to 9th row). For plutonic rocks, our classification combines the shape of the bodies with their relationship to the overlying strata (concordance or discordance) (Philpotts and Ague 2009; see Fig. 2.1, lower section). Among discordant bodies with varying shape, two size-based categories are distinguished (Fig. 2.2, 2nd, 6th and 8th to 9th

row): batholiths (exceeding 100 km^2 in areal extent) and stocks (smaller than 100 km^2). Additionally, cylindrical discordant bodies, mainly representing feeder pipes for ascending magma, are recognized (Fig. 2.2, 10th row). Moreover, two kinds of tabular geometries can be distinguished: discordant dikes and predominantly concordant sills (Fig. 2.2, 3rd and 8th row). Beyond these, three concordant geometries are noted: laccoliths (characterized by a roughly flat base and a convex roof), lopoliths (defined by a roughly flat top and a shallow convex base), and phacoliths (lens-shaped bodies lacking any flat boundaries; Fig. 2.2, 5th row).

Building on these classifications, a collection of geometrical end members (standard geometries) that approximate the shape variations of the rock types was set up by Carl et al. (2023). The geometries are intended to act as open source benchmark models for structural geomodeling, as realistic geological models depend on a clear definition of the rock type and the 3D geometries of evaluated rocks. In its initial form, each of the geometrical end members per potential host rock type was represented by a single version of a 3D body. However, as a large share of these initial end members can be represented by a multitude of possible regular geometrical representations, we designed alternative realizations after reviewing literature: Subsurface salt structures have been created after Hudec and Jackson (2007), Hudec et al. (2011) and Jackson and Talbot (1991), claystone geometries have been inspired by Selley (2000) and Nichols (2009), and crystalline rock geometries are based on Markl (2015) and Winter (2013). Additional inspiration was drawn from studying open source 3D models of real subsurface structures (Dutch subsurface models from TNO, available at https://www.dinoloket.nl/en/subsurface-models/map, last access: 21.4.25, and Australian subsurface models from Geoscience Australia, available at https://portal.ga.gov.au/3d, last access: 21.4.25. The standard geometries were created in blender (https://www.blender.org/, last access: 16.3.25, and are visible in Fig. 2.2. Some standard geometries are non-unique for rock types but can be used in different environments, e.g., stocks/batholiths for salt and crystalline intrusions. This is indicated in the model titles, as in these cases, the names of different structures are separated by an underscore. Blanks in model names are replaced with a period, and in brackets, additional geometrical information are given in some cases, such as the lateral character of the top of a structure (e.g., hourglass-shape) or the roundness of the top surface (rounded or flattened).

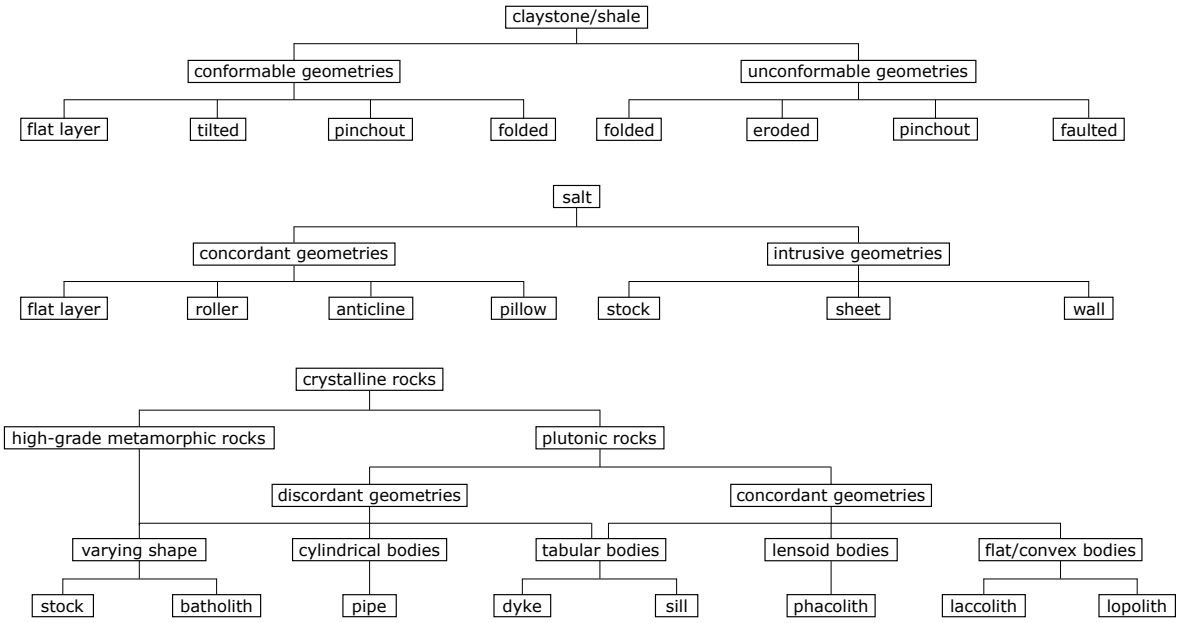


Figure 2.1: Geometrical systematization of the rock types considered for the establishment of the catalogue of benchmark models ("standard geometries"). Adapted after Carl et al. (2023)

2.1.2 Geological description of the example model "Altenbruch-Beverstedt"

The methodology presented herein is illustrated exemplarily on the mesh of the intrusive salt structure Altenbruch-Beverstedt (Lower Saxony, Germany; see Fig. 2.3). Tectonically, it is located within the roughly N-S striking Glückstadt Graben, developing since the Triassic (Scheck-Wenderoth et al. 2008). The considerably anisotropic salt wall is the result of a complex evolutionary history especially throughout the Mesozoic, as variations in the tectonic regime repeatedly led to shifts from subsidence to uplift in the sub-basins and grabens of the North German Basin (Maystrenko et al. 2008; Scheck-Wenderoth et al. 2008; Stollhofen et al. 2008). Within the Glückstadt Graben, the largest salt walls of the German subsurface can be found (Scheck-Wenderoth et al. 2008). The structure Altenbruch-Beverstedt represents a fitting example model for the methodology presented herein, due to its anisotropic, yet complex shape. The anisotropy visualizes well the cross sections created in the first part of the segmentation approach, while the sinusoidal shape illustrates well the segmented nature of the second set of sections (see Subsect. 2.2.1).

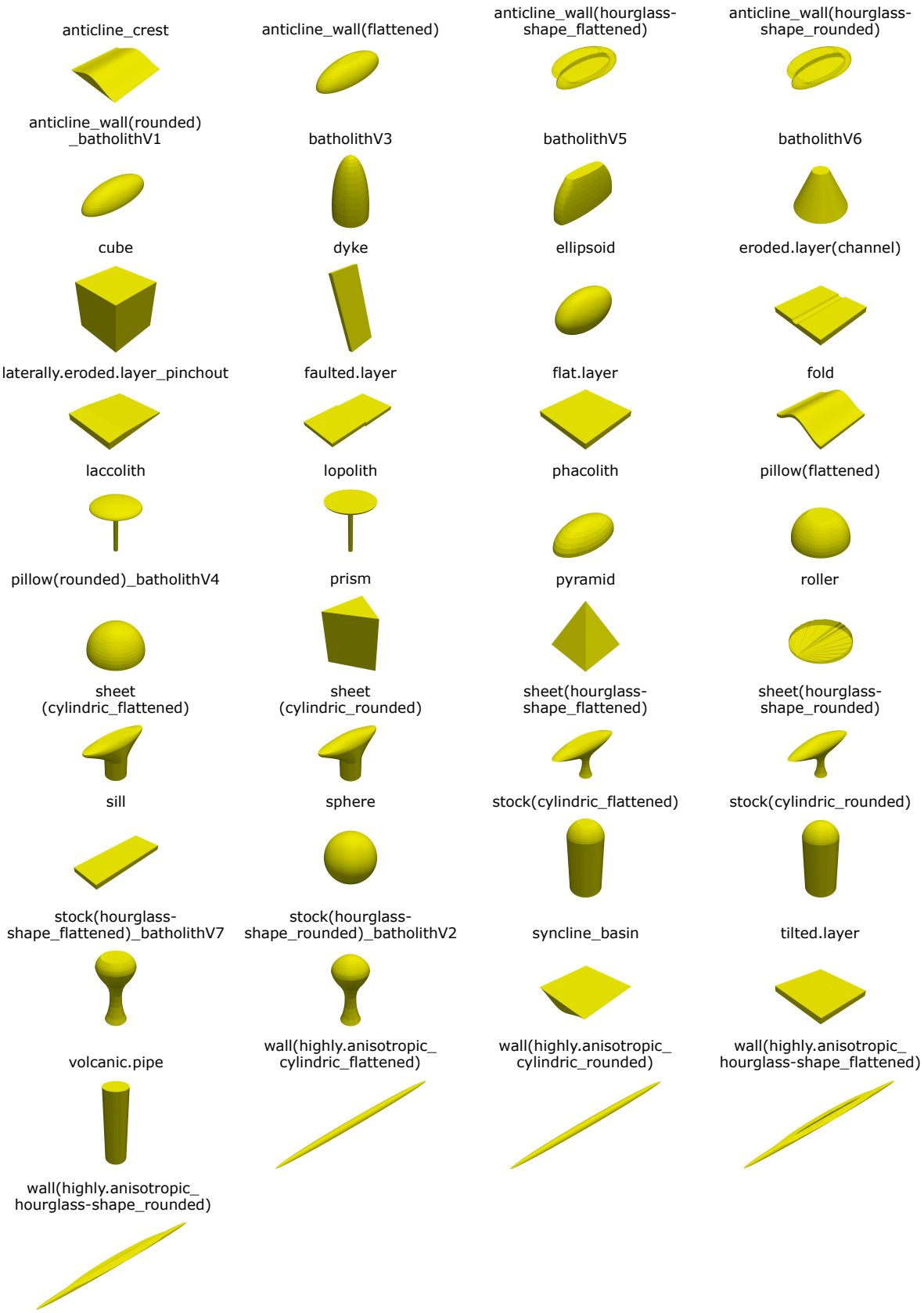


Figure 2.2: Overview of regular synthetic models used in this study. The structures (apart from the cube, ellipsoid, prism, pyramid and sphere) are meant to represent geometrical end members of different rock types ("standard geometries"). For information on the naming convention, please refer to the end of Subsect. 2.1.1. The size of the models was chosen arbitrarily

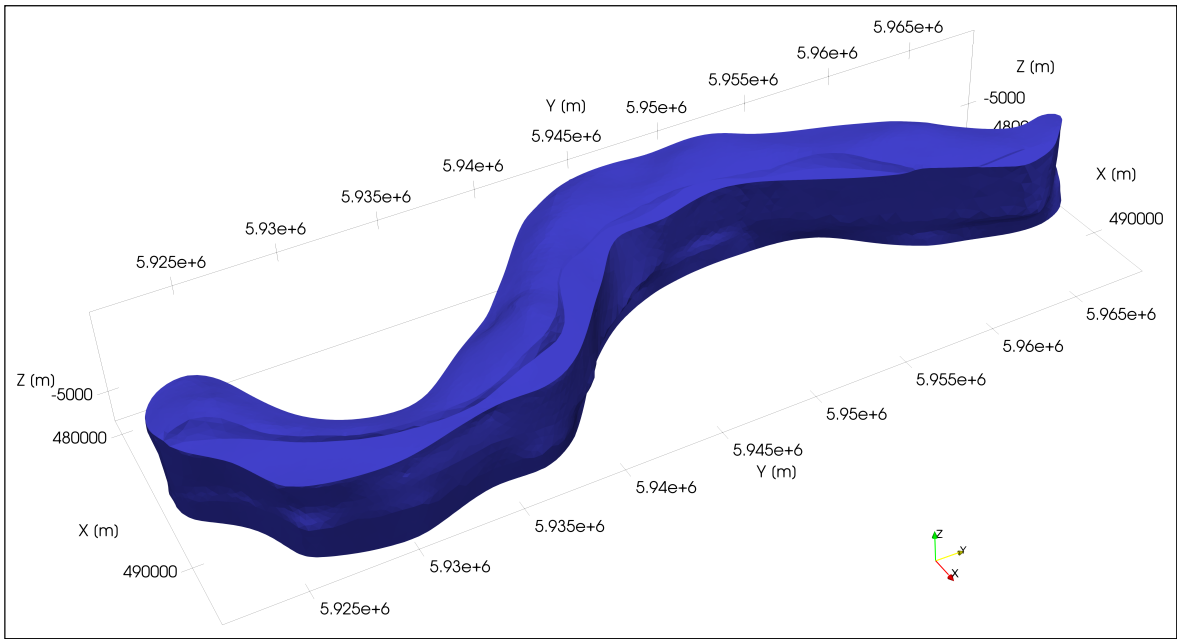


Figure 2.3: 3D model of Altenbruch-Beverstedt, taken from BGR et al. (2022). Coordinate system: EPSG:4647

2.1.3 Content, motivation and distinction of this study

The proposed methodology allows for the quantitative description, comparison and systematization of explicitly modelled structures and lower dimensional input data using a set of geometrical parameters. The horizontal and vertical dimensions as well as gradients and curvatures of 3D geometries are measured on vertical cross sections oriented perpendicular to the two horizontal main axes of the structures. For 2D inputs (such as 2D geophysical cross sections), alignment of sections is omitted. The resulting datasets are analyzed statistically, providing insight into the main geometrical characteristics of the input structures: the data analysis yields information about the anisotropy of structures, the potential existence of overhangs, the sphericity and the character of the lateral walls as well as top surface of evaluated structures. Furthermore, K-means clustering is used to systematize the datasets based on the measured parameters. Given 3D input, the setup of cross sections perpendicular to the main axes ensures, that the input structures are covered thoroughly with regular-spaced measurements that follow the 3D contours of the respective geometry. The method is applied to the standard geometries serving as benchmark geometries for structural modeling of geo-bodies. Applying the method to these models serves two purposes: While the functionality of the approach is validated, we also assess quantitatively, whether the developed benchmark models are geometrically dissimilar or whether some of them can be consolidated for their purpose. Our quantification method represents a rather simplistic approximation approach for the quantitative comparison of 3D structures and lower dimensional datasets that can reproduce the main geometrical characteristics of

input datasets fast but also enhances the interpretability of results, making them accessible to a broader audience. Our method cannot be used to quantitatively compare implicit representations of structures directly from a scalar field, though.

As recognized in Subsect. 2.1.1, similar approaches are rare in general and particularly in geosciences as quantitative approaches commonly aim at uncertainty assessment. In computer sciences, however, Celenk (1995) describes a method involving the alignment of equally-spaced cross sections in two objects via the computation of their respective horizontal main axes and subsequent section comparison. However, this method is more approximating compared to the proposed approach, as sections are not segmented to align with the contours of the structures.

The proposed method is intended to be utilized in a geomodeling workflow at different stages. 1) Given a sparse dataset including for instance borehole data and 2D seismics of limited quantity, the method can be initially used for a first structural approximation of a targeted geo-body. In the specific example of the German site selection, where most structurally complex bodies have already been excluded from the considerations (BGE 2020), this approximation can be achieved using the set of standard geometries that is established in this study. 2) Structural conceptualization and model approximation can also facilitate hyper parameter selection for subsequent interpolation (Wellmann and Caumon 2018). 3) After the creation of a set of stochastic model realizations, our quantification method and the benchmark models can be applied again in combination with the input data to limit the realizations to the geometrically reasonable ones. However, it has to be noted that this step would be rather time-consuming for large amounts of realizations. Here, the framework for automatic consistency checking of 3D geological models recently introduced by Parquer et al. (2025) represents a more sophisticated approach. Still, the proposed framework could reveal model realizations not respecting the conceptual model, which could prompt questions about the assumed geological situation and/or subjective bias, as studied for instance by Bond et al. (2007) and Bond et al. (2015). 4) Lastly, the proposed framework can be used for the direction-dependent quantification of modeled structures to assess their potential capacity for material storage (BGE 2023).

The paper is structured as follows: Sect. 2.2 outlines the methodology employed in this study, detailing the developed segmentation and measurement algorithm. Sect. 2.3 presents the results of applying the methodology to the benchmark models and a single subsurface dataset, while Sect. 2.4 discusses the implications of these findings in the context of existing research. Finally, Sect. 2.5 concludes with future research directions.

2.2 Methods

2.2.1 Segmentation and measurement algorithm

For our approach, we aimed at a high grade of automation and easy integration in a model analysis process. The method requires the dataset to either be a mesh with extractable vertices or a data frame of vertex coordinates themselves (the system currently only supports .vtk file formats). In what follows, the functionality of the method is explained given a 3D input mesh, but skipping the cross section generation, the algorithm is also usable for existing cross-sectional data (e.g., geophysical data).

To retrieve characteristic statistics, a geometrical segmentation algorithm (see e.g., Shamir 2008) has been established, which first discretizes the 3D model into 22 equidistant cross sections with the normal direction parallel to the longer horizontal axis of the mesh's bounding box. As measurements are conducted perpendicular to the two horizontal main axes of the structures, two sets of cross sections need to be determined separately. Orientation of sections normal to the longitudinal axis of the structure (first direction) have been determined by a minimization of the cross-sectional area, as sections are sequentially rotated (Stephenson 2018; Fig. 2.4, Part 1). The cross sections normal to the first set are set up by discretizing the established sections vertically, then first connecting raster lines of consecutive sections and lastly the resulting segments (Fig. 2.4, Part 3). After their respective setup, the cross sections of both directions are corrected automatically and/or manually for artifacts (Fig. 2.4, Part 2). Extensional measurements are conducted on each cross section at 5 equidistant transects (Fig. 2.4, Part 4). Since the very first and last cross section of both directions are excluded from the measurements as they would (undesirably) slice irregular polygons several times, 20 intervals are considered for every input structure. This results in 100 measurements being conducted respectively for each of the two horizontal parameters as well as 200 values for the vertical extent. Please note, that the assumption that a cross section of the first set is perpendicular to the longitudinal horizontal main axis only applies to the center point of the given section. The same limitation applies to a given cross sectional segment (trapezoidal segment) of an orthogonal section and the secondary horizontal main axis.

In addition to the extensional measurements, gradient and curvature calculations are carried out (see Fig. 2.4, Part 4). Both parameters are determined on all cross sections between consecutive vertices of a cross section. The curvature in 2D is defined as the reciprocal of the circumradius of a triangle. Therefore, it is calculated between three consecutive vertices in either the xz- or yz-plane, by first determining the side

lengths (a, b and c) of the triangle between the points, then the semi-perimeter of the triangle and the area through Heron's formula, before calculating the curvature as the reciprocal of the circumradius of the triangle through:

$$\text{curvature} = \frac{4 \cdot \text{area}}{a \cdot b \cdot c} \tag{2.1}$$

The selected method measuring the lateral extents of input meshes normal to their horizontal main axes (see Fig. A2.1a in appendix) is advantageous over approaches analyzing an input body using parallel sections as applied in various medical imaging techniques like for instance MRI (see e.g., Meyer-Baese and Schmid 2014). Such an approach would have resulted in a dissimilar amount of output measurements for the two horizontal extents for many input structures as well as for different structures overall, both in case of a uniform regular grid for all datasets (Fig. A2.1b & e) as well as an individual regular grid per dataset (Fig. A2.1c & f). Only the usage of an anisotropic grid, depending on the bounds of the input mesh, would have resulted in an equal amount of measurements per horizontal direction (Fig. A2.1d & g). However, using a supplementary grid would have generally resulted in the problem, that irregular structures would have often been cut several times along a horizontal measuring line. This would have created subordinate polygons that are completely disconnected from each other (see red lines in Fig. A2.1b).

In contrast, covering every input structure with a constant number of measurements as also applied similarly by Celenk (1995) comes with an advantage and a disadvantage: while it ensures that the quantification of input datasets with our method is scale-independent as datasets of different structures have the same amount of data, the geometrical spatial variability of larger bodies might not be captured equally well as the shape of smaller ones. The potential impact of this matter is currently being analyzed in a follow-up study that applies the methodology to a database of over 300 structural models of subsurface structures from various geological settings. The question whether structures shall be represented by equal or dissimilar data quantities also concerns the gradient and curvature data: Orthogonal sections are created from a set of 19 trapezoidal segments (i.e., 40 vertices), while cross sections in the first direction are based on a varying, most often higher number of vertices. As gradients and curvatures are being calculated between neighboring vertices, the potentially larger edges between vertices in the orthogonal sections lead to a less-rounded appearance of the cross sections, directly affecting the values of both parameters.

```
Part 1:
Input: initial cross sections
Output: cross sections rotated perpendicular to longer horizontal main axis by minimization of cross section area
for each initial section do
    for each of 38 rotation steps (0° to 180° in 5° increments) do
        Compute rotation angle (theta)
        Apply rotation matrix to original normal ([1,0,0] or [0,1,0]) to get rotated normal
    end for
    for each rotated normal do
        Slice mesh using rotated normal and center point of section
        Retrieve vertices from rotated slice
        Project cross section into YZ plane to calculate area
        Compute centroid of this projected section
        Sort points by angle relative to centroid
        Compute area of polygon using sorted points and shoelace formula
    end for
end for

Part 2:
Input: rotated cross sections
Output: rotated cross sections after artifact correction
Step 1:
for each rotated cross section do
    set vertex with lowest z-value as vertex index=0
    perform normalized nearest neighbour algorithm
end for

Step 2:
for each section after normalized nearest neighbour algorithm do
    apply correction criterion
    if correction criterion = True then
        initialize manual vertex order correction in plotly.dash
        for each section with artifacts do
            correct vertex order by clicking on previous (correct) vertex then incorrect vertex
        end for
    end if
end for

Part 3:
Input: corrected cross sections of 1st direction
Output: corrected cross sections of orthogonal direction
for each section of 1st direction do
    raster section vertically into 22 vertical lines
    for each vertical line do
        retrieve X, Y and Zmin+Zmax - coordinates
    end for
end for

for 2 consecutive sections of 1st direction do
    for all vertical lines in both sections do
        extract X, Y and Zmin+Zmax (=2 points per section)
        combine 4 points into trapezoidal segment
    end for
end for

for every index of vertical lines do
    combine trapezoidal segments to assemble uncorrected orthogonal section
end for

for uncorrected cross sections of orthogonal direction
    repeat Part 2

Part 4:
Input: all cross sections
Output: horizontal and vertical dimensional measurements
for each cross section of 1st direction except index 0 & 21 do
    rotate & project section onto YZ plane
    create 5 horizontal and vertical measurement transects
    measure horizontal and vertical dimensions between intersections of transect and polygon
end for

for each cross section of orthogonal direction except index 0 & 21 do
    rescale sections (corresponds to rotation & projection onto YZ plane)
    create 5 horizontal and vertical measurement transects
    measure horizontal and vertical dimensions between intersections of transect and polygon
end for

for all cross sections do
    compute gradients
    compute curvatures
end for
```

Figure 2.4: Pseudocode of the algorithm that creates the cross sections of both directions and measures the dimensional extents, gradients and curvatures on these sections. For further information, see Sect. 2.2

2.2.2 Data analysis

The geometrical measurements were combined into a database, analyzed by the first three statistical moments, standard deviation and median and visualized as histograms and cumulative distribution functions (CDF's). Comparative analyses of data distributions and a cluster analysis were carried out on the measured data, to demonstrate that the tested 3D bodies can be quantitatively compared based on the statistical distributions of geometrical properties and to assess their dis-/similarity.

Semi-quantitative comparison of histograms was done for the statistical data, analyzing the vertical extension measures, combined horizontal extension measurements, the gradients and curvatures. For gradient data, the frequency of infinite values was counted separately, since they represent vertical segments between two consecutive vertices. As those values cannot be plotted together with the remaining data as a separate bin, their frequency was visualized as a horizontal line. For gradients and curvatures, overflow bins were established: for the gradient data at the 5th and 95th percentile and for the curvatures only at the 95th percentile. This aimed at facilitating the interpretability of the histograms, since for most datasets, a small percentage of values (<5%) was considerably larger than the rest, thereby spreading the measurements to a large number of additional histogram bins. The Kullback-Leibler divergence (Kullback and Leibler 1951) was calculated on normalized data between the individual distributions of the geometrical parameters of the input models, for quantification of the similarity between the structures. Cluster analysis followed data normalization to a range of -1 to 1 and principal component analysis (PCA; see Jolliffe 2002). As variables ("features") for PCA, 20 percentiles of the probability density functions (PDF's) of the combined horizontal data, vertical data, gradients and curvatures were chosen. As the first two principle components only explained 40% of the variance, a matrix plot for the principal components 1 to 12 was assessed initially, to cover 90% of the variance. A feature angle matrix was then used to reduce the number of principal components in the cluster matrix plot. The number of clusters used in the K-means clustering algorithm was determined using an elbow plot and the silhouette score.

2.3 Results

Results of the segmentation and measurement algorithm as well as the data analysis are demonstrated using a sphere and the intrusive structure "Altenbruch-Beverstedt" (model taken from BGR et al. 2022). Subsequently, the results of the cluster analysis are presented.

2.3.1 Segmentation and measurement algorithm

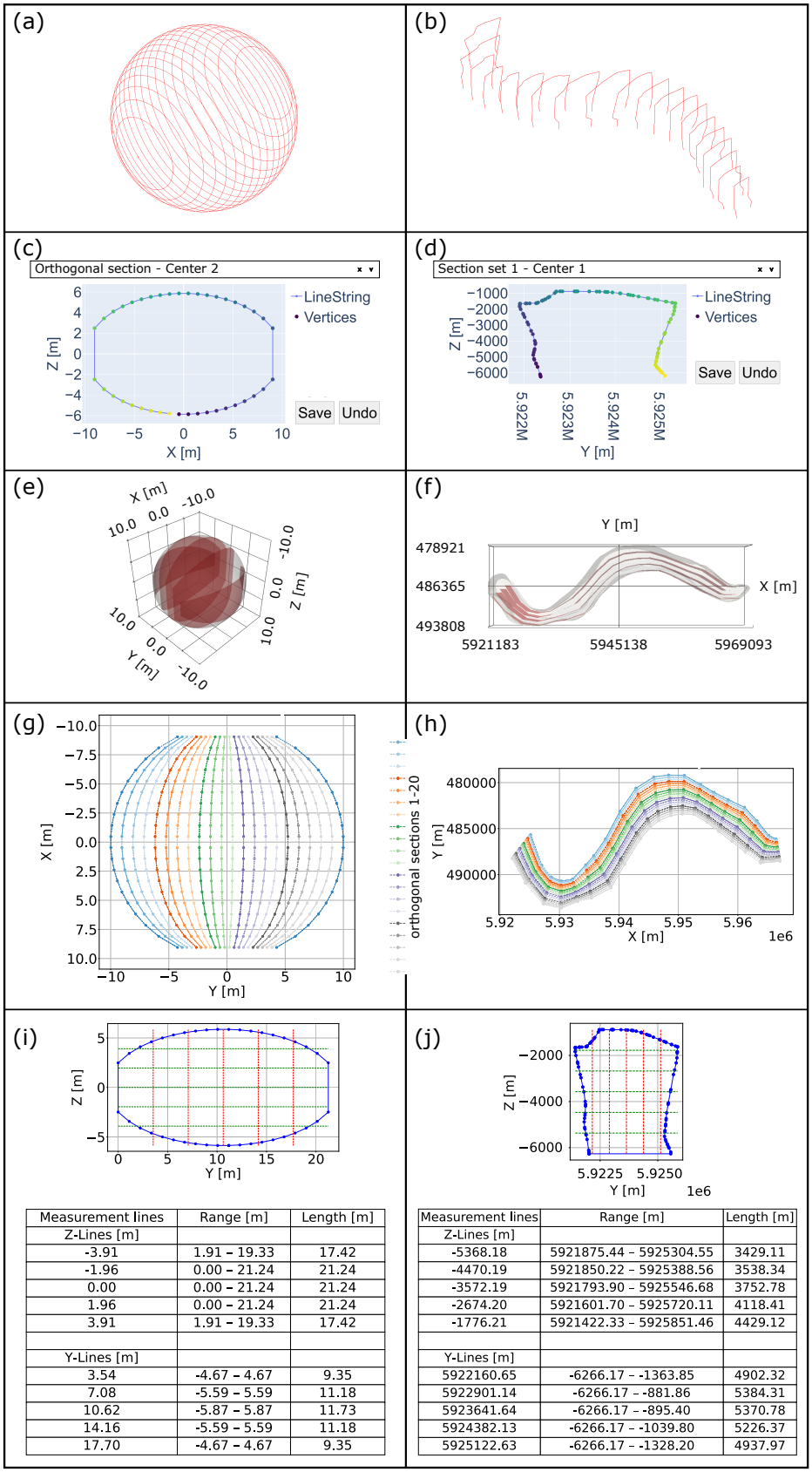
The initial subdivision of the input mesh (Fig. 2.5a & b) is followed by the stepwise rotation of the initial cross sections. The respective rotation step showing the minimal cross-sectional area is optimally oriented normal to the longitudinal main axis of the structure (first direction). Optimal orientation of all sections of the first direction of the sphere corresponds to 0° rotation, unlike when running the algorithm on an irregular mesh like Altenbruch-Beverstedt. This is the case due to the regularity and symmetry of all test models of this study. After subsequent artifact correction (Fig. 2.5c & d), the second set of cross sections is assembled from trapezoidal segments (for illustration, a subset of sections is shown in Fig. 2.5e & f).

Following potential artifact corrections of the orthogonal sections, both sets of cross sections are finalized (Fig. 2.5g & h) and extensional measurements as well as gradient and curvature calculations are carried out (Fig. 2.5i & j). The computational power required by the algorithm is low (runtime without varying artifact corrections: ca 60 s, using as the CPU an AMD Ryzen 7 PRO 5850U at max. 50% capacity at 3.5 GHz speed and the integrated GPU at 0.6 GB usage).

2.3.2 Data analysis

The results of the first analysis step, the first three statistical moments, standard deviation and median per parameter and the data visualized as histograms and CDF's, are seen in Table 2.1 and Fig. 2.6, respectively. The size of the sphere was chosen arbitrarily, as the subsequent Kullback-Leibler divergence and cluster analysis are based on normalized data. Both the statistical moments for the sphere and the distributions in Fig. 2.6 (left column) reveal differences for the three parameters, although individual extents should be the same in all three dimensions, if a sphere would be measured equally in all directions. This is due to compromises of the algorithm ensuring its universal applicability. For Altenbruch-Beverstedt, the large variance and standard deviation of the combined horizontal data and the difference between the mean values of both individual horizontal parameters reflect the strong anisotropy of the structure, while the statistics for the vertical data indicate a moderate variation in vertical measurements.

Gradient and curvature histograms of the example cases are visible in Fig. 2.7. For the sphere, the distribution of the gradient histogram is symmetric (Fig. 2.7a). The curvature histogram (Fig. 2.7c) shows a prevalence of very small values and subordinate maxima around 0.1, 0.2 and in the overflow bin that contains 394 values (5% of all data) above 0.37. For Altenbruch-Beverstedt, the gradient distribution is asymmetric and



Measurement lines	Range [m]	Length [m]
Z-Lines [m]		
-3.91	1.91 – 19.33	17.42
-1.96	0.00 – 21.24	21.24
0.00	0.00 – 21.24	21.24
1.96	0.00 – 21.24	21.24
3.91	1.91 – 19.33	17.42
Y-Lines [m]		
3.54	-4.67 – 4.67	9.35
7.08	-5.59 – 5.59	11.18
10.62	-5.87 – 5.87	11.73
14.16	-5.59 – 5.59	11.18
17.70	-4.67 – 4.67	9.35

Measurement lines	Range [m]	Length [m]
Z-Lines [m]		
-5368.18	5921875.44 – 5925304.55	3429.11
-4470.19	5921850.22 – 5925388.56	3538.34
-3572.19	5921793.90 – 5925546.68	3752.78
-2674.20	5921601.70 – 5925720.11	4118.41
-1776.21	5921422.33 – 5925851.46	4429.12
Y-Lines [m]		
5922160.65	-6266.17 – -1363.85	4902.32
5922901.14	-6266.17 – -881.86	5384.31
5923641.64	-6266.17 – -895.40	5370.78
5924382.13	-6266.17 – -1039.80	5226.37
5925122.63	-6266.17 – -1328.20	4937.97

Figure 2.5: Visual representation of the segmentation and measurement algorithm for a sphere model (left column) and the German intrusive salt structure "Altenbruch-Beverstedt" (right). a & b) initial segmentation of the input meshes. c & d) Plotly.dash app for vertex-order correction. e & f) Subset of orthogonal cross sections. g & h) Coverage of input structure with cross sections (top view). i & j) Example of extensional measurement results

Table 2.1: a) First three statistical moments, standard deviation and median per parameter for the sphere model (note: the dimensions of the sphere are chosen arbitrarily). b) First three statistical moments, standard deviation and median per parameter for the model of the real subsurface structure (Altenbruch-Beverstedt). Statistics for Altenbruch-Beverstedt reflect the strong anisotropy of the structure

(a) sphere	mean [m]	variance [m^2]	std. dev. [m]	skew	median [m]
Horizontal length	14	13	4	-0.4	14
Horizontal length orthogonal	18	4	2	0	18
Vertical length	14	13	4	-0.5	15
Horizontal data combined	16	13	4	-0.8	17

(b) Altenbruch-Beverstedt	mean [m]	variance [m^2]	std. dev. [m]	skew	median [m]
Horizontal length	3825	635352	797	-0.2	3795
Horizontal length orthogonal	48644	8956682	2993	-2.2	49845
Vertical length	4766	486158	697	-2.9	4856
Horizontal data combined	26235	5.07E+08	22516	0.02	21696

the number of infinite gradients is higher (Fig. 2.7b). In comparison to the curvature distribution of the sphere, the curvature data (Fig. 2.7d) is monomodal apart from the overflow bin.

In general, analyzing the data distributions of a structure visually already reproduces distinct geometrical characteristics of an input dataset. The distribution of the combined horizontal data indicates whether a pronounced anisotropy is present for an analyzed structure: if the data is separated into two clearly distinguishable subordinate distributions (see Fig. 2.8a), the geometry is considerably anisotropic (the farther apart the two maxima, the more anisotropic a body is). Caution is advised for a distribution with two close maxima (Fig. 2.8b): this could be the consequence of the inflated extent in the orthogonal direction (see Subsect. 2.4.2). Analyzing the combined horizontal data and the vertical data together reveals whether a structure shows substantial variations in its horizontal extent over its vertical range. Such a shape, in the subsurface more often present as overhangs rather than as upward tapering, is indicated by the simultaneous presence of multimodal distributions for both parameters (Fig. 2.8c & d). The vertical data distribution also characterizes the top surface of a geometry: if the distribution is monomodal, with a) the maximum being the bin representing the highest measurements, and b) the frequency in lower bins being substantially smaller, then the presence of a flat top surface is indicated. The existence of a flat top surface can be verified by analyzing the gradient and curvature data: a high

frequency of very small measurements for both parameters supports such an analysis (Fig. 2.8e - g). Gradient data also indicates the steepness of lateral surfaces of a body: as high and infinite gradient data stem from steep to vertical faces of a structure, the presence of steep-dipping lateral surfaces can be recognized (Fig. 2.8h). Combining the inferences from analyzing top and lateral surfaces therefore provides insight into the overall sphericity of an input dataset: a more spherical structure is represented by larger quantities of intermediate gradient measurements and of moderate to high curvature data (Fig. 2.8i & j).

The Kullback-Leibler (KL-)divergence (Kullback and Leibler 1951) was calculated to quantitatively determine the similarity between the tested geometries. The distributions of the six parameters (the individual horizontal extents along both horizontal main axes, the combined horizontal data, the vertical data, gradients and curvatures) were compared between the models. The similarity of two distributions is larger, the smaller the KL divergence is, with a value of 0 indicating equality of the distributions (obtained for instance when comparing a structure with itself). The result of the calculation of the individual KL divergences for the example cases is visualized in Fig. 2.9. For the sphere, the most similar models regarding the respective distributions of the six parameters are the "sheet(cylindric_rounded)" for the horizontal data of the first direction, the "prism" for the orthogonal horizontal data, the "batholithV3" for the combined horizontal data, the "anticline_wall(rounded)_batholithV1" for the vertical data, the "phacolith" model for the gradients and the "ellipsoid" for the curvatures (compare Fig. 2.2 for the model appearances). For Altenbruch-Beverstedt, "batholithV6" is most similar regarding the horizontal data of the first direction, "roller" for the orthogonal horizontal data, "wall(highly.anisotropic_hourglass-shape_flattened)" for the combined horizontal data, "wall(highly.anisotropic_hourglass-shape_rounded)" for the vertical data, "pillow_flattened" for the gradients and "roller" for the curvatures. In addition to KL divergences of individual parameters, an averaged KL divergence was calculated: by taking the mean of the values between two models, the overall dis-/similarity between models was assessed. According to the averaged KL divergence, the sphere is closest to the standard geometry "pillow(rounded)_batholithV4", while Altenbruch-Beverstedt is best approximated by the "wall(highly.anisotropic_hourglass-shape_rounded)". However, informational content of this parameter is limited, as there is no indication regarding which parameters two compared structures are most similar or differ more. Therefore, principal component analysis and K-means clustering have been employed as well, providing this information based on all combined parameters.

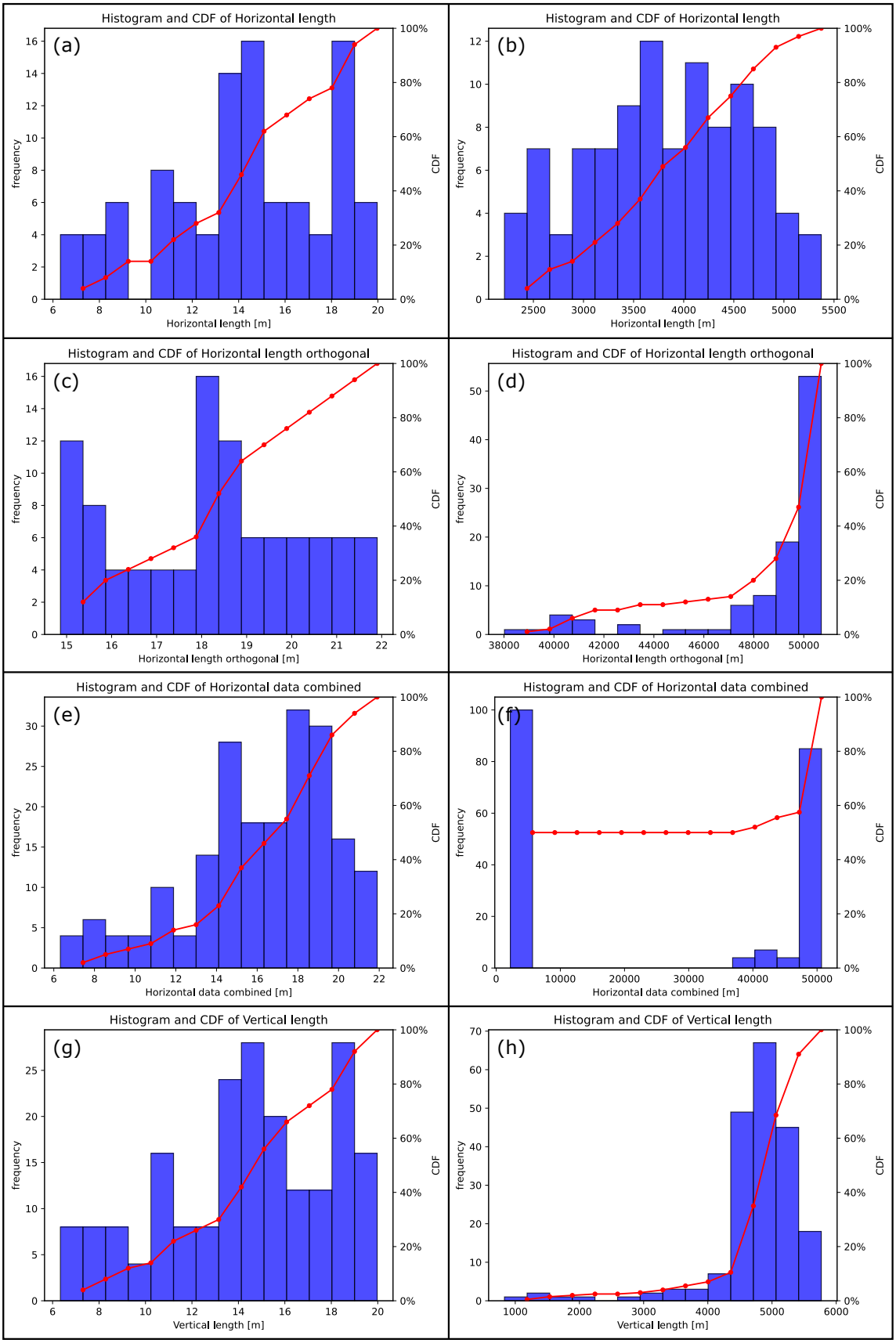


Figure 2.6: Data distributions and cumulative distribution functions (CDF's) for the extensional parameters. Left column: sphere, right column: Altenbruch-Beverstedt. a & b) Horizontal data from the first direction. c & d) Horizontal data from the orthogonal direction. e & f) Combined horizontal data. g & h) Vertical data

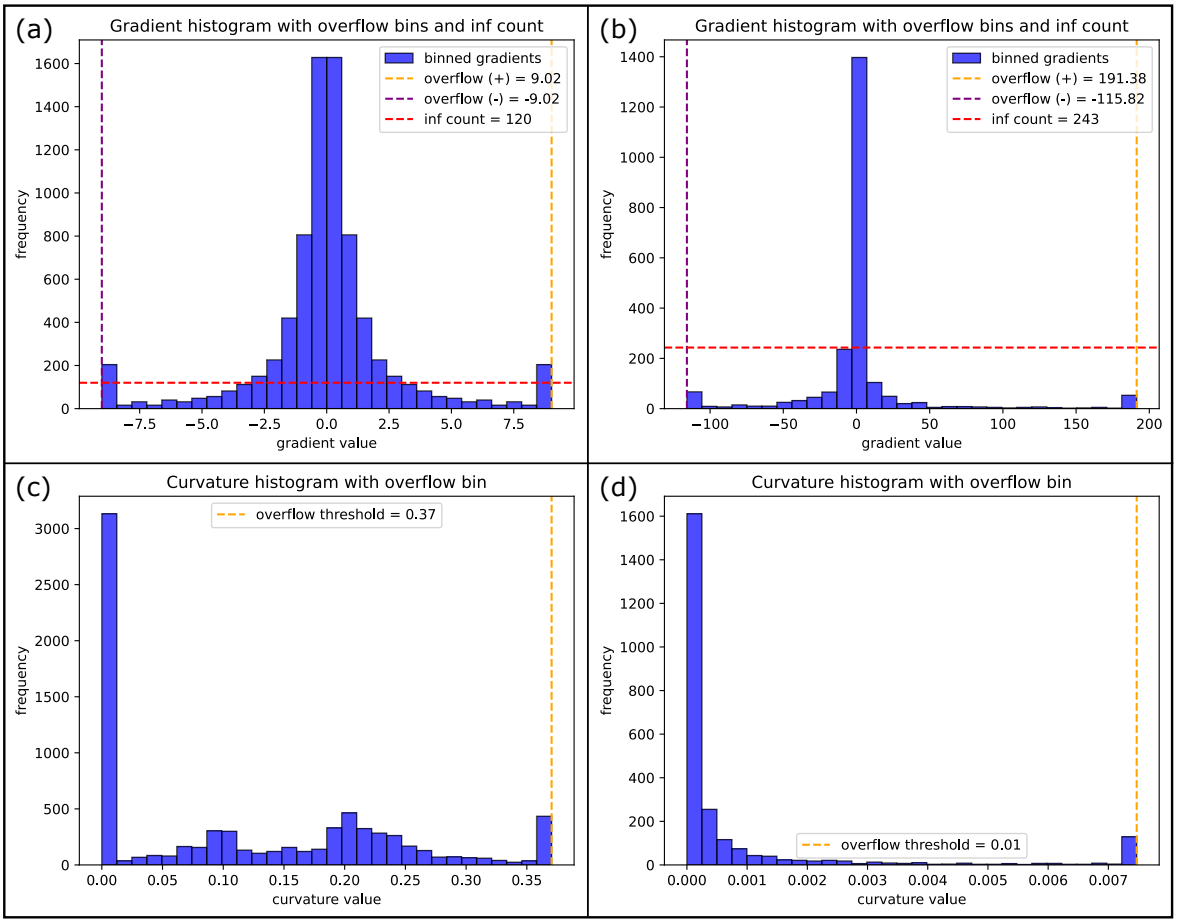


Figure 2.7: Gradient and curvature data for the sphere (a & c) and Altenbruch-Beverstedt (b & d). Amount of data in overflow bins: Gradient diagram (sphere) 384 values (4.8% of all data), Curvature diagram (sphere) 394 values (5%); Gradient diagram (Altenbruch-Beverstedt) 112 values (4.6%); Curvature diagram 101 values (4.1%)

In general, values of KL divergence show an error for the gradient distributions: infinite values had to be converted to the highest finite gradient value of a given dataset to enable the computation, inflating the highest bin. Furthermore, the large variance of curvature data for most input models (see for example Fig. 2.9f & l and Subsect. 2.4.2) decreases the applicability of the KL divergence for that parameter, as most models show very similar normalized distributions. To assess the impact of the large variance on individual KL divergences of curvature data and smallest averaged KL divergences, they were also calculated using a 95th percentile overflow bin (see Table 2.2). Smallest KL divergences for the curvatures of the two example models are notably higher, especially for the sphere, reflecting the dissimilarity of data distributions when applying the filter (column 1 & 2). The impact on the smallest averaged KL divergence (column 3 & 4) is smaller, yet still considerable.

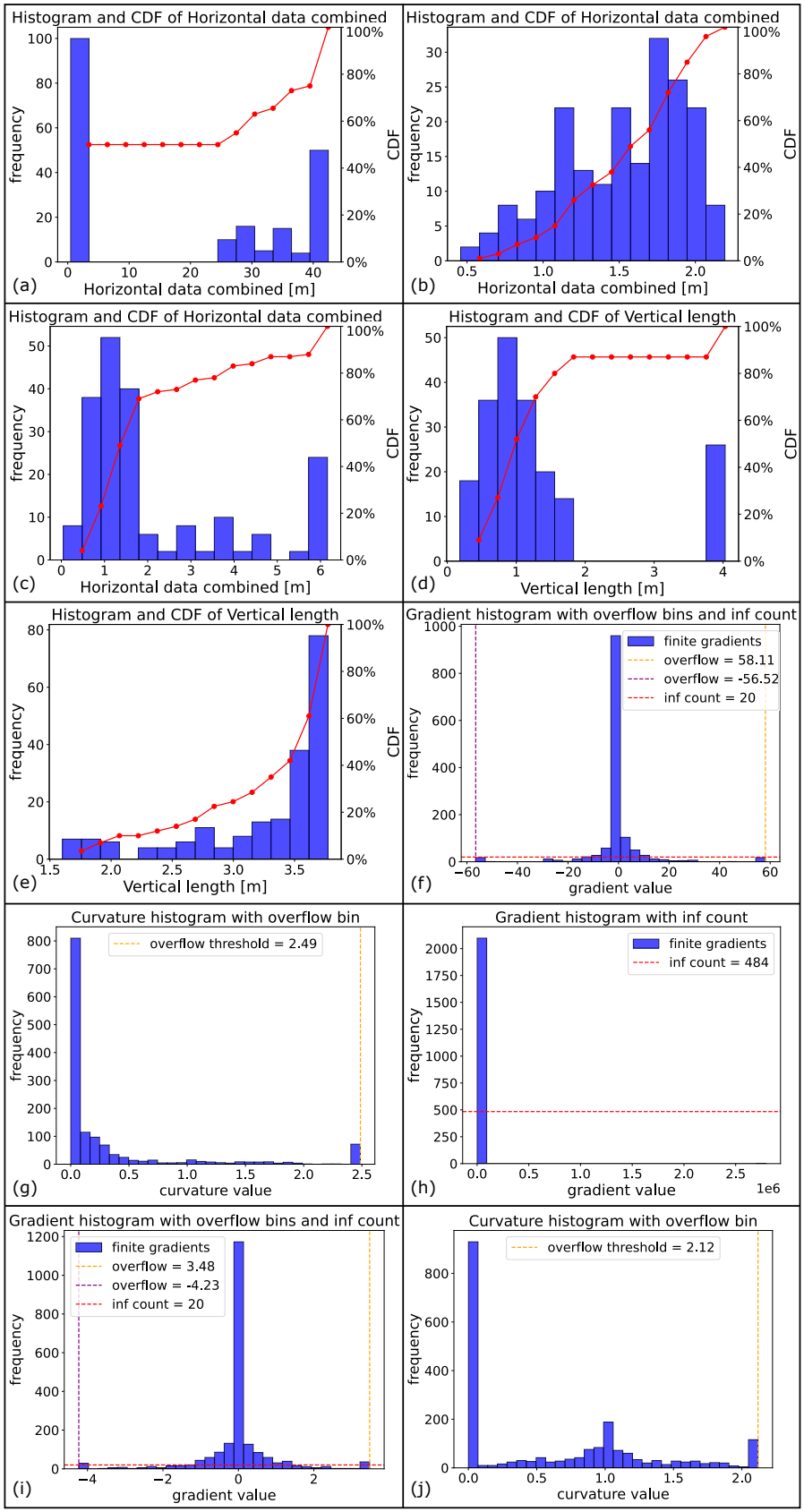


Figure 2.8: Analysis of data distributions to reproduce geometric characteristics of input models. Please compare with model appearances in Fig. 2.2.
a) Combined horizontal data of "wall(highly.anisotropic_hourglass-shape_-rounded)", reflecting strong anisotropy.
b) Combined horizontal data of "batholithV3", incorrectly indicating slight anisotropy.
c) & d) Combined horizontal data and vertical data of "sheet(hourglass-shape_rounded)", indicating presence of overhangs.
e) - g) Vertical data, gradients and curvatures of "batholithV5", revealing the presence of a flat top surface
h) Gradient data of "volcanic.pipe", reflecting the prominence of vertical lateral walls
i) & j) Gradient and curvature data of "pillow(rounded)_-batholithV4", showing the spherical character of the input model

Table 2.2: Comparison of KL divergences with and without the usage of a 95th percentile overflow bin for the curvature distributions.

Structure	Smallest KL divergence for curvature without overflow bin	Smallest KL divergence for curvature with overflow bin	Smallest averaged KL divergence for all properties without overflow in curvature	Smallest averaged KL divergence for all properties with overflow in curvature
sphere	0.0054 ("ellipsoid")	0.16 ("wall(highly. anisotropic_-cylindric_-rounded)")	0.45 ("pillow(rounded)_-batholithV4")	0.56 ("batholithV3")
Altenbruch-Beverstedt	0.036 ("roller")	0.05 ("batholithV5")	1.2 ("wall(highly. anisotropic_-hourglass-shape_-rounded)")	1.3 ("wall(highly. anisotropic_-hourglass-shape_-rounded)")

2.3.3 Cluster analysis

Cluster analysis on all measured data of the regular geometries resulted in 7 clusters considering the combined analysis of the elbow plot and silhouette score (Fig. 2.10b). With the first two principle components (PC's) only explaining 40% of the variance (see Fig. 2.10a), the number of PC's necessary to cover more than 90% of the variance was determined to be 12. A feature angle matrix (Fig. A2.2) was computed to check the dependencies between the percentiles of the PDF's. As a strong dependency was identified within several groups of features, the principal component matrix plot (Fig. 2.11) was limited to the first six PC's. The feature contribution matrix (Fig. 2.10c) reveals the contribution ("loadings") of the binned PDF's to the principal components, with bright yellowish colors indicating a strong positive contribution and dark blue colors a substantial negative contribution. In the contribution matrix, percentiles 0 to 19 represent the PDF of the combined horizontal data, followed by the vertical data (20 to 39), gradients (40 to 59) and curvatures (60 to 79).

The PC1 vs. PC2 cluster plot is visible in Fig. 2.11a. Positive contributions to PC1 are dominated by the 50 to 55% bins of the vertical data and gradient data, while there is no percentile with a strong negative contribution to PC1. This effectively separates the bluish-green cluster at high positive PC1 scores from the rest of the data. All four models ("flat.layer", "sill", "cube" and "prism"), share a distinct geometrical similarity:

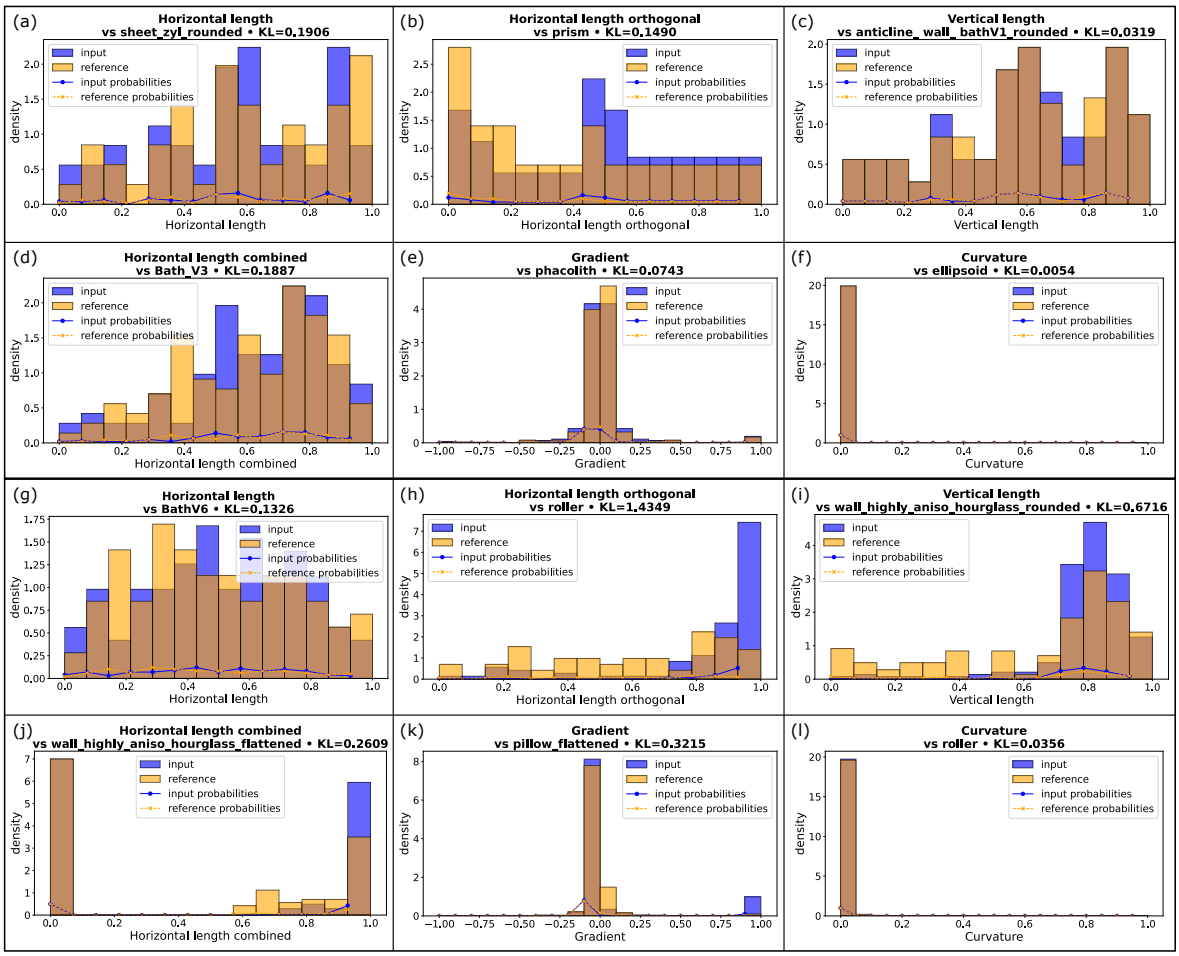


Figure 2.9: Visualized Kullback-Leibler divergences. a) - f): sphere, g) - l): Altenbruch-Beverstedt. Visualized is the most similar data distribution (orange) compared to the respective distribution of the two example models (blue). The calculated Kullback-Leibler divergences are noted in the headlines of individual figures

When segmenting them with our algorithm, cross sections are always flat at the top and of exactly the same vertical extent throughout the entire structure. This results in a step-wise appearance of the respective PDF's, with the step being in the middle of the functions. For PC2, the 45 to 50% gradient bin has the highest positive loading, while there are stronger negative loadings for the 0 to 5% as well as 95 to 100% gradient bins. This separates the models of the black cluster at highest positive PC2 scores and mainly the blue cluster at high negative PC2 scores. Therefore, models of the black cluster are characterized by the presence of many low to moderately inclined surfaces in a geometry (depending on the variance in a data distribution) and an overall more rounded appearance (see e.g., the highlighted black example model "pillow(rounded)_-batholithV4" in Fig. 2.11a). Meanwhile, the blue models and other models at high negative PC2 scores are characterized by the abundance of steep-dipping to vertical surfaces. Thus, PC2 is an indicator for the overall steepness of the lateral parts of a structure or, on the other hand, its sphericity.

The PC3 vs. PC4 cluster plot is shown in Fig. 2.11b. For PC3, large positive contributions are spread among the 0 to 5% and 95 to 100% horizontal bins as well as the 95 to 100% vertical bin and the 0 to 5% and 45 to 50% gradient bins, while the only considerable negative loading is exhibited by the 10 to 15% gradient bin. Datasets at very positive PC3 scores belong to the vermilion and blue clusters. The largest negative PC3 scores are seen for the reddish-purple cluster. Very positive PC3 scores indicate anisotropy, rather flat top surfaces and steep-dipping to vertical lateral walls (see e.g., the highlighted vermilion "dyke"). In contrast, however, datasets at largest negative PC3 scores, cannot be linked to very high data percentages in that 10 to 15% gradient bin; its loading (-0.27) not being the main cause of the observed negative PC3 scores. PC4 shows considerable positive loadings for the 50 to 55% bin of the vertical data and the 0 to 5% and 95 to 100% gradient bins. Meanwhile, large negative loadings are seen for the 0 to 5% and 95 to 100% horizontal bins, the 95 to 100% vertical bin and the 80 to 85% gradient bin. These contributions mainly drive the differentiation of the reddish-purple and vermilion clusters (negative PC4 scores) from the other clusters apart from some sky-blue models. Since the horizontal and vertical bins contributing very negatively are the same horizontal and vertical bins contributing particularly positively to PC3, it can be deduced that the overall position of the vermilion models in the PC3 vs. PC4 diagram is more driven by these horizontal and vertical bins. Meanwhile, the datasets from the reddish-purple and sky-blue models are comparatively influenced more by the 80 to 85% gradient bin also showing a considerable negative loading. Still, most datasets from these clusters at negative PC4 scores can be considered as rather anisotropic geometries with mainly steeper (but not vertical) lateral walls, while models at higher positive PC4 scores exhibit uniform vertical extents and steep-dipping to vertical lateral walls. This explains the position of the isolated blue model at highest positive PC4 scores ("volcanic.pipe"; highlighted in Fig. 2.11b; see also Fig. 2.8h for the gradient distribution), completing the separation of the blue cluster from the rest of the data.

The cluster plot of PC5 vs. PC6 can be seen in Fig. 2.11c. PC5 shows strong positive contributions for the 0 to 5% vertical bin and the 50 to 55% and 95 to 100% gradient bins, while stronger negative loadings are given by the 50 to 55% vertical bin and the 0 to 5% gradient bin. This separates the majority of the sky-blue cluster (highest positive PC5 scores) from the rest of the datasets. As this corresponds to the first appearance of the 0 to 5% vertical bin among considerable contributing bins, most of the associated models are characterized by widespread low vertical extents and few much larger ones, as seen in overhang configurations (for example, see the model "laccolith" in Fig. 2.2). PC6 is mainly influenced by the gradient data, where the 10 to 15% bin contributes the most negatively and the 80 to 85% bin contributes positively. Once again (as for PC3), the 10 to 15% gradient bin, however, does not seem to be the main reason for

the separation of the reddish-purple cluster at very negative PC6 scores. Similarly, the sky-blue models at higher positive PC6 scores do not exhibit particularly large high percentages in the respective bin.

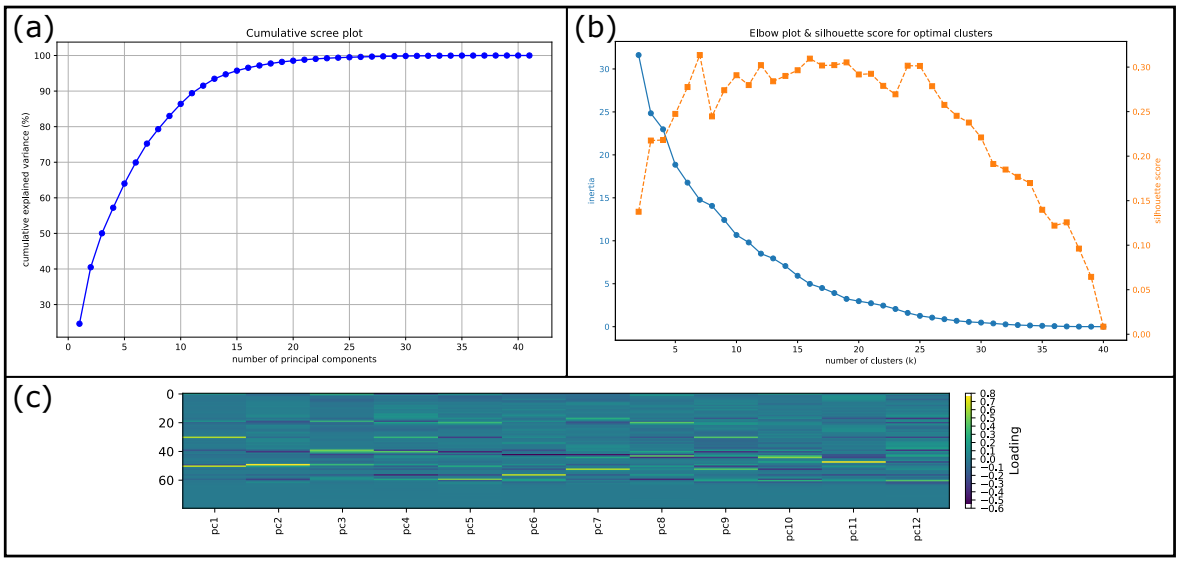


Figure 2.10: Calculated supplementary information for the setup and interpretation of the cluster analysis after principal component analysis. a) Cumulative scree plot, showing the explained variance with increasing number of principal components. b) Elbow plot and silhouette score to determine number of clusters. c) Contribution matrix showing the contribution of the input data (percentiles of the probability density functions of measured parameters) to the principal components

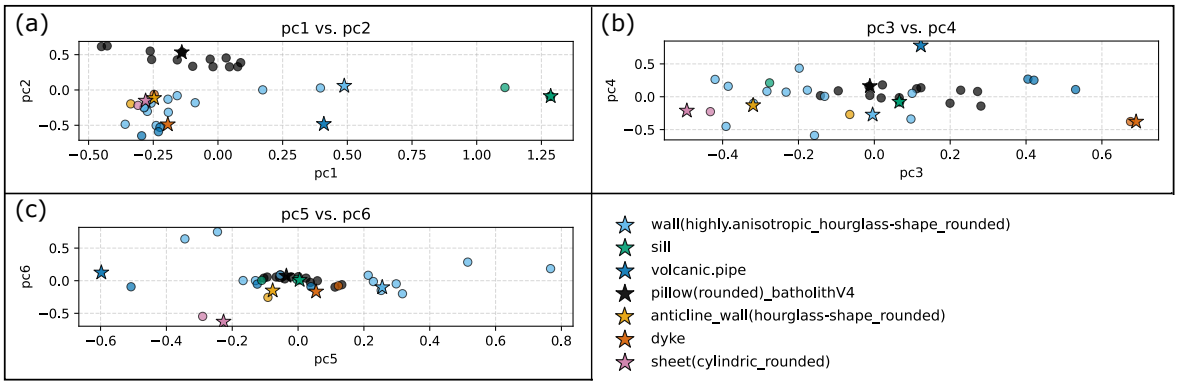


Figure 2.11: Matrix plot of principal components (PC's) explaining 70% of the variance in the data (see also Fig. 2.10a). Larger stars mark example models for clusters (see legend)

The overall cluster results validate that the flat and/or cuboidal geometries (vertical extent $\leq$ horizontal extent and/or exclusively straight lateral surfaces) mostly differ considerably from the other structures designed to represent intrusive subsurface bodies: the flat/cuboidal geometries are mainly distributed among the bluish-green, blue and vermilion clusters (see Fig. 2.11). As recognized above, these three clusters can be differentiated from the other models within the first four PC's. Only the "laterally.eroded.layer_pinchout" is located outside, in the sky-blue cluster, although representing a flat geometry. The K-means cluster analysis furthermore indicates that

some standard geometries are similar across all parameters. Therefore, it was assessed whether certain standard geometries are redundant to simplify the benchmark selection process. The pairs of flattened and rounded versions show high similarities, leading to the exclusion of the flattened models while retaining the "uneroded" structures. The models "batholithV3" and "pillow(rounded)_batholithV4" cluster closely, differing only in vertical elongation; thus, "batholithV3" is excluded. Although similarities exist between models with varying lateral characteristics, both "cylindric" and "hourglass" shape variations are retained. This also applies to various "sheets" and the "anticline_-wall(hourglass-shape_rounded)", which exhibit similar PC scores in some, but not all cluster plots. Lastly, some of the flat and cuboidal bodies in the bluish-green cluster ("flat.layer", "sill" and "cube") are nearly identical in position. The "cube" is excluded from the benchmark collection, while the other two geometries are merged, keeping the shape of the "sill".

Given these exclusions based on structural similarity, the collection is condensed from 36 to 25 standard geometries (see Fig. 2.12). Decreasing the database by validating the bodies' geometrical dissimilarity facilitates the decision making on the best suitable benchmark for a case study. Despite our reduction efforts, this list is not expected to be exhaustive: we would like to encourage users to suggest additional geometries based on their expertise and/or literature, to ensure that suitable benchmark models are available for as many geomodeling applications as possible.

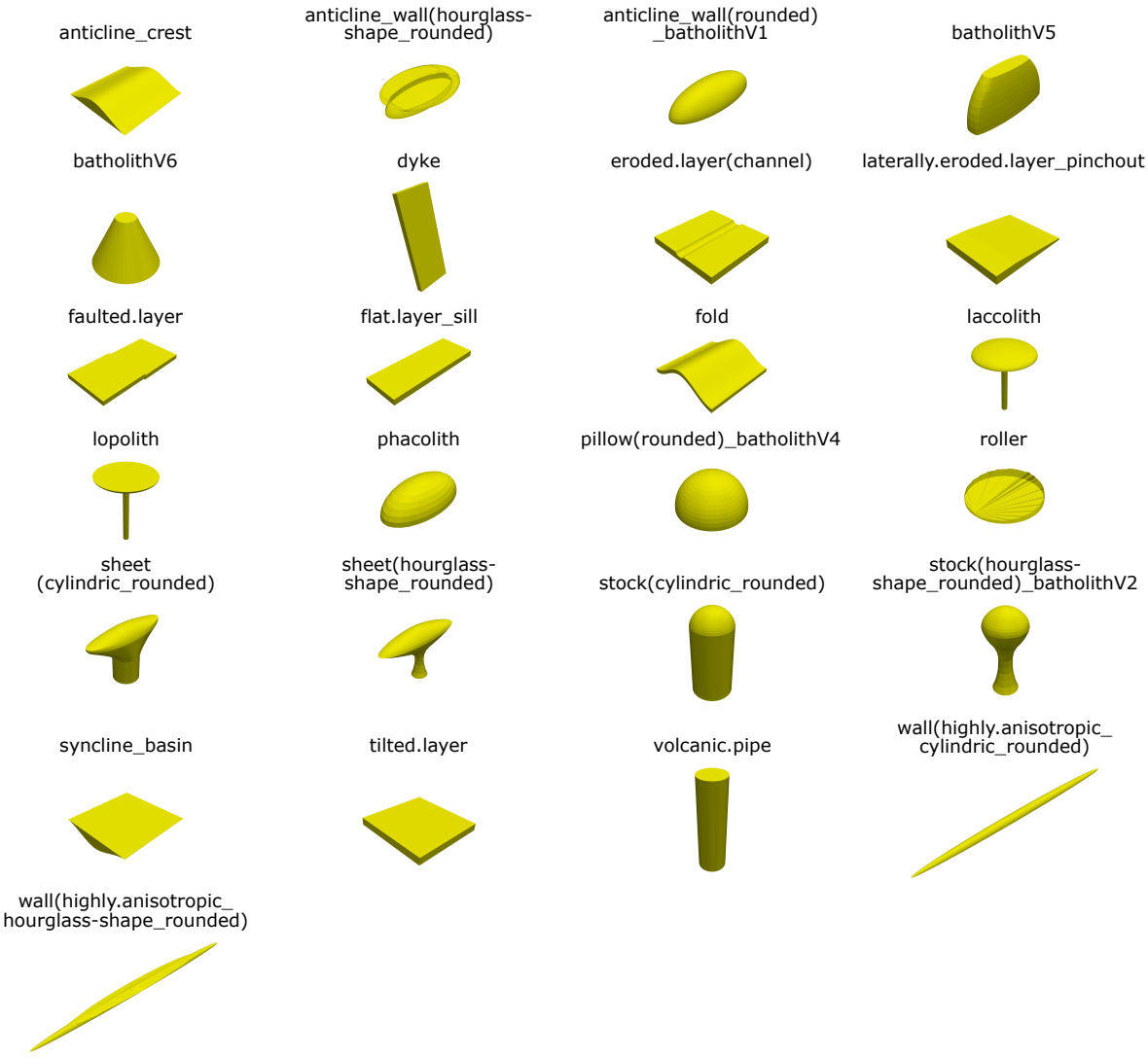


Figure 2.12: Condensed collection of standard geometries after application of the quantification method.

2.4 Discussion

By applying a set of defined geometrical descriptors to systematically generated 3D benchmark models, this study establishes a framework for the quantitative comparison of shape properties. The analysis highlights how key attributes such as anisotropy, surface morphology, and sphericity vary across models, offering a structured perspective on their geometric dis-/similarities. These outcomes prompt a deeper discussion of how well the proposed descriptors capture meaningful shape differences and how this quantitative framework advances the analysis of unmodeled data and 3D geological structures.

2.4.1 Comparison of existing methods for 3D shape characterization with the proposed workflow

The workflow of this study differs considerably – both in the scale of the test subjects as well as the purpose of the methods – from the quantitative comparative approaches used in material sciences (Subsect. 2.1.1). The material-scientific studies mainly operate on millimeter- to centimeter-scales and have a higher emphasis on parameters exploring the sphericity/angularity (or similar metrics) of objects, as these characteristics are fundamental in this field, where properties and applicability of composite building materials heavily depend on mechanical interactions between individual particles (Kakani and Kakani 2004). Meanwhile, the proposed approach aims at characterizing 3D structures and 2D sections at the meter- to kilometer-scale (although the applicability is scale-independent in theory), through direction-dependent measurements of geometrical parameters, thereby providing datasets suited for quantitative comparison.

Studies presenting approaches that show similarities to ours are Celenk (1995), Schweizer et al. (2017) and Lindsay et al. (2013). Celenk (1995) determines the horizontal main axes of equally-spaced cross sections as well, but does so to align sections of two different objects. Comparison is then achieved by computing the averaged shape difference of sections between the objects in four directions along the main axes. Key differences of our approach therefore involve the segmented assemblage of cross sections in the orthogonal direction (following the respective segmented horizontal main axis) and the exact measurement of the dimensional extents on the sections. Hence, our method opts for the determination of larger datasets of absolute measurements on a single object, that are compared to other bodies in subsequent steps. Meanwhile, Celenk (1995) computes the relative measure that is the averaged shape difference, representing a faster, but more approximate approach of object comparison, as the author does not segment the horizontal main axis along the larger extent. Schweizer et al. (2017) do not try to compare the dimensions of individual 3D structures, but use the Jaccard distance and the normalized city-block distance as measures for model dissimilarity instead. The two parameters are being applied as measures for the similarity in position of certain geological units between two model realizations of the same study site. In a similar fashion, the Hausdorff distance has been used before (see e.g., Suzuki et al. 2008). These dissimilarity distances were not applied in our study, as they could only act as size indicators rather than shape descriptors and would not give any indication on where two structures differ spatially. Meanwhile, our approach provides insight into both shape and size differences of objects, which is crucial for geological modeling. Lindsay et al. (2013) explore geometric uncertainty across multiple realizations of a study site, evaluating parameters like depth, volume and curvature, which

parallel those in our study. However, their parameters are often tied to stratigraphic units and may not apply directly to individual 3D structures. Both studies utilize PCA to analyze geometric variability and model differences, although executed differently.

Despite these existing methodologies, we opted for a straightforward approach, allowing us to efficiently replicate the main geometric characteristics of input datasets. Our algorithm is computationally efficient, easily interpretable with basic geological knowledge, and accessible to a non-specialist audience.

2.4.2 Assumptions and compromises of the algorithm ensuring its universal applicability

Despite the strengths of our methodology, certain limitations must be acknowledged. The reliance on discrete differential geometries (Bobenko et al. 2008) means that the input dataset must represent a single, compact, and topologically connected structure (Thiele et al. 2016a). For objects separating from one to the next cross section into multiple strands, split algorithms are available. However, this comes at the cost of interpretability of the statistics of geometric properties. Moreover, the method functions optimally for convex hulls (Rockafellar 1970), although a follow-up study will show, that the full geometric diversity of intrusive salt structures and crystalline bodies from the German subsurface can be quantitatively compared without major limitations. These assumptions should be considered when interpreting results in other domains.

The focus of this study was to establish a generalized algorithm to quantitatively describe the shape of objects and to infer dis-/similarity between geometries. Given the wide range of potential and available models, the algorithm requires some trade-offs to be universally applicable. Discussion of the data distributions for the geometrical parameters (see Fig. 2.6) focuses on the results from measuring the sphere, representing a comprehensible case with distinct expected data distributions: The nature of a sphere is a similar shape of any section through the center, eventually resulting in a normal distribution of the levelled distance measurements in both horizontal and vertical directions. This expected distribution is not produced in our case due to the generation approach of the orthogonal cross sections: The assembled sections follow the contour of the structure (see Fig. 2.5g & h), which results in larger measurements for the orthogonal horizontal data and a slightly tailed distribution of the combined horizontal data, similar to an ellipsoid with a low contrast in the main axes. As this situation is rarely seen in geological modeling, the impact is small since anisotropic geometries are measured accurately with our segmentation algorithm. The gradient and curvature data reflect the effects of our approach as well: While the gradient diagram of the sphere shows a symmetric distribution as expected, the relative elongation of

the orthogonal sections increases the frequency of lower gradient measurements. Due to this accumulating effect, the presence of low-dipping surfaces of a structure is overestimated by the data. Furthermore, the exclusion of marginal cross sections leads to vertical clipping that introduces infinite gradient measurements (representing two consecutive vertices being exactly vertical) that would not exist when measuring the sections in a rounded, unclipped state. The curvature data is influenced by this clipping as well, that results in few large values where the three consecutive vertices form a large angle. These measurements increase the variance of curvature data considerably, with the majority of data for most datasets being located within the 0 to 5% and 5 to 10% bins.

However, the discriminability of the standard geometries and basic 3D objects in the cluster analysis is ensured despite these compromises made in the methodology: structures of varying anisotropy plot in different parts of cluster diagrams showing contribution of the combined horizontal data, as the highest contribution of horizontal data comes from the first and last distribution bins (see Fig. 2.10c). Similarly, as vertical and gradient data distributions of flattened geometries show the discussed characteristic properties, they differ in their PC scores from their rounded counterparts. Furthermore, the discussed increased frequency of gradient measurements around 0 does not change cluster patterns as it applies to all datasets. The same is true for the artifact-influenced curvature data and its impact on the general clustering of similar structures. Still, its squeezed nature shows an effect on the overall clustering results, as the curvature data does not show any considerable contribution in PC dimensions.

2.4.3 Intended direct application and potential further usage of the quantification method and the standard geometries

The methodology will be a part of a larger framework to model and compare geological structures based on sparse data in the context of the German site selection. For most regions of interest for nuclear waste disposal, seismic 2D data are available frequently with a few boreholes. This is similar to the cross sections established through the benchmark models here, allowing for a fast model selection based on the geometrical properties and potentially further constraining hyper parameter selection for interpolation. However, for the integration of unmodeled sparse input data in the initial conceptualization of geological models, some adoptions of the workflow are needed. Obviously, the creation of segmented sections is omitted as the starting point are cross sections, which can be analyzed as described. The number of geometrical data is restricted by the number of available cross sections, thus a comparison will be conducted on a less complete statistical basis. Consequently, a user likely has to solely rely on

the Kullback-Leibler divergence and cluster analysis to assess the reasonableness of various shapes. In case these analyses do not limit the range of standard geometries sufficiently, additional experience-based benchmarks could be created and clustered among the available models to test whether a closer fit applies. Here, more complex structural configurations could easily be approached by superposition of basic benchmarks. Thus, the choice of the conceptual model is based on the quantification and does not rely on the expert knowledge only. After interpolation resulted in a series of stochastic prior realizations, the method will be used for falsification by data (e.g., boreholes). Furthermore, the application of the framework to purely quantify the shape of a modeled 3D body can be very useful in the context of the site selection. Here, the comparative parts of our proposed analysis (i.e., Kullback-Leibler divergence and cluster analysis) might be of little value and thus be omitted. Additionally, applying our methodology also supports testing for the minimum amount of data necessary for geological modeling, as different data densities and configurations can be inserted into the algorithm. The open-access collection of benchmarks for geomodeling is also a convenient tool to visualize the range of three-dimensional geometries of the different rock types to a broader audience, which aids in the communication of uncertainties and decisions for geoscientists and stakeholders in various settings (see Zehner 2021).

2.5 Conclusion

In our publication, we presented a methodology to quantitatively describe, compare and systematize 2D and 3D datasets, and proposed a set of regular standard geometries as benchmark models in geomodeling approaches. Demonstrating the quantification method on the 3D standard geometries, their geometrical dis-/similarity is assessed. The combined evaluation of data distributions and a cluster analysis reproduces the main geometrical characteristics of input meshes and visualizes differences between various datasets. While distributions of combined horizontal extensional measurements provide insight into the anisotropy of datasets and the potential existence of overhangs, distributions of the vertical extent indicate the character of the top surface of structures and support or falsify the presence of overhangs. Distributions of gradient and curvature data (1) indicate the prevailing character of the slope of the lateral surfaces of structures, (2) further emphasize potentially present flat top surfaces and (3) give a general indicator on the sphericity of a structure. Cluster analysis of normalized, dimensionally reduced data groups and systematizes input structures based on the combined measured statistical parameters. In our application to synthetic datasets, clustering also serves to identify and exclude or merge benchmark models showing large geometrical similarity. Apart from cluster analysis and assessment of data distributions, comparison of parameter distributions is furthermore achieved using the

Kullback-Leibler divergence. The proposed method and standard geometries are intended to be used at several stages within a workflow for structural geomodeling, both for initial conceptualization, potential adjustment of the interpolation method and examination of structural reasonableness of resulting models. Furthermore, general shape quantification for exploration/storage estimates can be realized.

As indicated earlier, the first follow-up study aims at applying the method to a large database of structural geological models. Afterwards, the method will be applied to datasets of sparse, unmodeled input data and coupled with a spatial interpolation algorithm in a study focusing on geomodeling based on progressively reduced datasets.

Code and data availability

Method development was carried out in Python. The method mostly relies on the capabilities of the libraries Shapely (https://shapely.readthedocs.io/en/stable/, last access: 26.2.25), PyVista (https://pyvista.org/, last access: 26.2.25) and Plotly (https://plotly.com/, last access: 26.2.25). The python code, the condensed database of standard geometries (as .vtk-files) and the datasets of raw extensional, gradient and curvature data are stored at https://doi.org/10.5281/zenodo.15795851, (Carl 2025).

Author contribution

FC: writing–original draft; writing–review and editing; method development; data acquisition and analysis; conceptualization; visualization. JY: writing–review and editing. MCC: writing–review and editing. FW: writing–review and editing; supervision; funding acquisition. PA-Z: writing–review and editing; conceptualization; supervision; funding acquisition.

Competing interests

The authors declare the following financial interests/personal relationships which may be considered as potential competing interests: Friedrich Carl, Jian Yang and Marlise Colling Cassel are funded by the German Federal Company for Radioactive Waste Disposal (BGE). Other authors declare that they have no conflict of interest.

Acknowledgements

This study was conducted as part of the GeoBlocks project. GeoBlocks is a collaboration of RWTH Aachen University, University of Aberdeen and the German Federal Institute for Geosciences and Natural Resources (BGR) within the research cluster URS (Uncertainty and Robustness with regard to the Safety of a repository for high-level radioactive waste), funded by the German Federal Company for Radioactive Waste Disposal (BGE), with the main objective being the creation of an open-source workflow for geological modeling that includes the quantification and visualization of uncertainties and aims at the optimization of sampling procedures. We thank for the financial support by BGE. The authors would also like to thank BGR for the data provided to the study. Mark Lindsay and Mark Jessell are thanked for their constructive and thorough reviews, which helped to improve the paper significantly.

References

Al Rousan, T., Masad, E., Tutumluer, E., and Pan, T. (2007). "Evaluation of image analysis techniques for quantifying aggregate shape characteristics". In: *Construction and Building Materials* 21.5, pp. 978–990. ISSN: 0950-0618. DOI: 10.1016/j.conbuildmat.2006.03.005. URL: https://www.sciencedirect.com/science/article/pii/S0950061806000377 (visited on 10/22/2025).

Altuhafi, F., O'Sullivan, C., and Cavarretta, I. (2013). "Analysis of an Image-Based Method to Quantify the Size and Shape of Sand Particles". EN. In: *Journal of Geotechnical and Geoenvironmental Engineering* 139.8, pp. 1290–1307. ISSN: 1943-5606. DOI: 10.1061/(ASCE)GT.1943-5606.0000855. URL: https://ascelibrary.org/doi/10.1061/%28ASCE%29GT.1943-5606.0000855 (visited on 10/22/2025).

BGE (2020). *Zwischenbericht Teilgebiete gemäß § 13 StandAG*. Tech. rep. URL: https://www.bge.de/fileadmin/user_upload/Standortsuche/Wesentliche_Unterlagen/Zwischenbericht_Teilgebiete/Zwischenbericht_Teilgebiete_barrierefrei.pdf (visited on 04/04/2026).

— (2023). *Vorgehen zur Ermittlung von Standortregionen aus den Teilgebieten*. Tech. rep. URL: https://www.bge.de/fileadmin/user_%20upload/Standortsuche/Wesentliche_Unterlagen/Methodik/%20Phase_I_Schritt_2/20231004_Vorgehen_zur_Ermittlung_von_%20Standortregionen_aus_den_Teilgebieten_barrierefrei.pdf (visited on 01/22/2026).

BGR, LAGB, LBEG, LBGR, LLUR, and LUNG (2022). *3D-Modell des geologischen Untergrundes des Norddeutschen Beckens (Projekt TUNB) Erstveröffentlichung 2021, Version 2022*. DOI: https://gst.bgr.de. URL: https://gst.bgr.de,%20Abgerufen%20am%201.12.xn--2024%20allgemeine%20geschftsbedingungen,%20siehe%20https:-qde//www.bgr.bund.de/AGB%20General%20terms%20and%20conditions,%20see%20https://www.bgr.bund.de/AGB_en.%E2%80%9C (visited on 12/01/2024).

Bobenko, A. I., Schröder, P., Sullivan, J. M., and Ziegler, G. M. (2008). *Discrete Differential Geometry*. en-US. Accepted: 2016-09-23T15:42:10Z. Birkhäuser Basel. ISBN: 978-3-7643-8620-7. URL: http://publications.mfo.de/handle/mfo/521 (visited on 12/01/2024).

Bond, C. E., Johnson, G., and Ellis, J. F. (2015). "Structural model creation: the impact of data type and creative space on geological reasoning and interpretation". English. In: *Special Publication - Geological Society of London* 421, pp. 83–97. ISSN: 0375-6440. DOI: 10.1144/SP421.4. URL: https://abdn.elsevierpure.com/en/publications/structural-model-creation-the-impact-of-data-type-and-creative-sp (visited on 08/06/2025).

Bond, C. E., Gibbs, A. D., Shipton, Z. K., and Jones, S. (2007). "What do you think this is?: "Conceptual uncertainty" In geoscience interpretation". English. In: *GSA Today* 17.11, pp. 4–10. ISSN: 1052-5173.

DOI: 10.1130/GSAT01711A.1. URL: https://abdn.elsevierpure.com/en/publications/what-do-you-think-this-is-conceptual-uncertainty-in-geoscience-in (visited on 08/06/2025).

Cardone, A., Gupta, S. K., and Karnik, M. (2003). "A Survey of Shape Similarity Assessment Algorithms for Product Design and Manufacturing Applications". In: *Journal of Computing and Information Science in Engineering* 3.2, pp. 109–118. ISSN: 1530-9827. DOI: 10.1115/1.1577356. URL: https://doi.org/10.1115/1.1577356 (visited on 11/21/2025).

Carl, F. (2025). *Code and datasets of the quantification algorithm and benchmark model collection*. DOI: https://doi.org/10.5281/zenodo.15795851.

Carl, F., Angeles Gonzalez de Lucio, G. de los, Yang, J., Achtziger-Zupančič, P., Kukla, P. A., Bense, F., and Wellmann, J. F. (2023). "Host rock analysis for the German nuclear waste disposal site-selection: review of subsurface geometries and input data for geological modelling". In: *RING*. URL: https://www.ring-team.org/research-publications/ring-meeting-papers?view=pub&id=223007 (visited on 12/02/2024).

Celenk, M. (1995). "Three-dimensional object recognition using cross-sections". In: *Proceedings of the Twenty-Seventh Southeastern Symposium on System Theory*. Starkville, MS, USA: IEEE Comput. Soc. Press, pp. 92–96. ISBN: 978-0-8186-6985-9. DOI: 10.1109/SSST.1995.390611. URL: http://ieeexplore.ieee.org/document/390611/ (visited on 02/12/2025).

Cox, M. R. and Budhu, M. (2008). "A practical approach to grain shape quantification". In: *Engineering Geology* 96.1, pp. 1–16. ISSN: 0013-7952. DOI: 10.1016/j.enggeo.2007.05.005. URL: https://www.sciencedirect.com/science/article/pii/S0013795207001123 (visited on 10/22/2025).

Gardoll, S. J., Groves, D. I., Knox-Robinson, C. M., Yun, G. Y., and Elliott, N. (2000). "Developing the tools for geological shape analysis, with regional- to local-scale examples from the Kalgoorlie Terrane of Western Australia". In: *Australian Journal of Earth Sciences* 47.5, pp. 943–953. ISSN: 0812-0099. DOI: 10.1046/j.1440-0952.2000.00822.x. URL: https://doi.org/10.1046/j.1440-0952.2000.00822.x (visited on 10/22/2025).

Hudec, M. R., Jackson, M. P. A., Cottington, N., Vendeville, B. C., Schultz-Ela, D. D., and Dooley, T. P. (2011). *The salt mine: a digital atlas of salt tectonics*. Bureau of Economic Geology Udden book series no. 5. Austin, Tex. : Tulsa, Okla: Bureau of Economic Geology, Jackson School of Geosciences, University of Texas at Austin ; American Association of Petroleum Geologists. ISBN: 978-0-615-51836-7.

Hudec, M. R. and Jackson, M. P. A. (2006). "Growth of allochthonous salt sheets in passive margins and orogens." en. In: *AAPG Bulletin* 90, pp. 1535–1564. DOI: doi:10.1306/05080605143.. URL: https://www.researchgate.net/publication/273336919_Growth_of_allochthonous_salt_sheets_in_passive_margins_and_orogens (visited on 11/30/2024).

— (2007). "Terra infirma: Understanding salt tectonics". In: *Earth-Science Reviews* 82.1, pp. 1–28. ISSN: 0012-8252. DOI: 10.1016/j.earscirev.2007.01.001. URL: https://www.sciencedirect.com/science/article/pii/S0012825207000025 (visited on 11/30/2024).

Jackson, M. P. A. and Talbot, C. J. (1991). "A Glossary of Salt Tectonics". en. In: *Geological Circular* 91-4. DOI: doi.org/10.23867/gc9104D. URL: https://www.beg.utexas.edu/publications/glossary-salt-tectonics (visited on 04/04/2025).

Jolliffe, I. T. (2002). *Principal Component Analysis*. en. Springer Series in Statistics. New York: Springer-Verlag. ISBN: 978-0-387-95442-4. DOI: 10.1007/b98835. URL: http://link.springer.com/10.1007/b98835 (visited on 04/23/2025).

Kakani, S. L. and Kakani, A. (2004). *Material Science*. New Age International. ISBN: 978-81-224-1528-5. URL: https://gateformme.wordpress.com/wp-content/uploads/2017/04/material-science-kakani.pdf (visited on 04/04/2026).

Kullback, S. and Leibler, R. A. (1951). "On Information and Sufficiency". en. In: *The Annals of Mathematical Statistics* 22.1, pp. 79–86. ISSN: 0003-4851. DOI: 10.1214/aoms/1177729694. URL: http://projecteuclid.org/euclid.aoms/1177729694 (visited on 12/01/2024).

Laga, H., Guo, Y., Tabia, H., Fisher, R. B., and Bennamoun, M. (2019). *3D Shape Analysis: Fundamentals, Theory, and Applications*. John Wiley & Sons, p. 368. ISBN: 978-1-119-40510-8. URL: https://content.e-bookshelf.de/media/reading/L-12043375-484a419330.pdf (visited on 04/04/2026).

Lindsay, M. D., Jessell, M. W., Ailleres, L., Perrouty, S., Kemp, E. de, and Betts, P. G. (2013). "Geodiversity: Exploration of 3D geological model space". In: *Tectonophysics* 594, pp. 27–37. ISSN: 0040-1951. DOI: 10.1016/j.tecto.2013.03.013.

URL: https://www.sciencedirect.com/science/article/pii/S004019511300187X (visited on 04/04/2025).

Markl, G. (2015). *Minerale und Gesteine: Mineralogie – Petrologie – Geochemie*. de. Berlin, Heidelberg: Springer. ISBN: 978-3-662-44627-0. DOI: 10.1007/978-3-662-44628-7. URL: https://link.springer.com/10.1007/978-3-662-44628-7 (visited on 04/04/2025).

Maystrenko, Y., Bayer, U., Brink, H.-J., and Littke, R. (2008). "The Central European Basin System – an Overview". In: *Dynamics of Complex Intracontinental Basins. The Central European Basin System*. Ed. by R. Littke, U. Bayer, D. Gajewski, and S. Nelskamp. Springer Berlin, pp. 15–34. ISBN: 978-3-540-85084-7.

Meyer-Baese, A. and Schmid, V. J. (2014). *Pattern Recognition and Signal Analysis in Medical Imaging*. Elsevier, 467 p. ISBN: 978-0-12-416615-8.

Nichols, G. (2009). *Sedimentology and Stratigraphy*. 2nd Edition. ISBN: 978-1-118-68777-2. URL: https://www.kufunda.net/publicdocs/Sedimentology%20and%20Stratigraphy%20-%20Copy.pdf (visited on 04/04/2026).

Nie, Z., Qi, Q., Wang, X., Liang, Z., and An, A. (2023). "Shape quantification of volcanic cinders and the influence of particle shape indexes on accumulation characteristics". In: *International Journal of Pavement Engineering* 24.1, p. 2001816. ISSN: 1029-8436. DOI: 10.1080/10298436.2021.2001816. (Visited on 10/22/2025).

Parquer, M. N., Kemp, E. A. de, Brodaric, B., and Hillier, M. J. (2025). "Checking the consistency of 3D geological models". English. In: *Geoscientific Model Development* 18.1, pp. 71–100. ISSN: 1991-959X. DOI: 10.5194/gmd-18-71-2025. URL: https://gmd.copernicus.org/articles/18/71/2025/ (visited on 10/24/2025).

Philpotts, A. and Ague, J. (2009). *Principles of Igneous and Metamorphic Petrology*. 2nd ed. Cambridge: Cambridge University Press. DOI: 10.1017/CBO9780511813429. (Visited on 06/04/2025).

Rockafellar, R. T. (1970). "Convex analysis". In: *Princeton mathematical series* 28, p. 451. URL: https://books.google.de/books?id=1TiOka9bx3sC&printsec=frontcover&redir_esc=y#v=onepage&q&f=false (visited on 04/04/2026).

Scheck-Wenderoth, M., Maystrenko, Y., Hübscher, C., Hansen, M., and Mazur, S. (2008). "Dynamics of salt basins". In: *Dynamics of complex intracontinental basins : The Central European Basin System*. Ed. by R. Littke, U. Bayer, D. Gajewski, and S. Nelskamp. Springer-Verlag Berlin, pp. 307–322. ISBN: 978-3-540-85084-7. URL: https://gfzpublic.gfz-potsdam.de/pubman/faces/ViewItemOverviewPage.jsp?itemId=item_237971_1 (visited on 11/30/2024).

Schweizer, D., Blum, P., and Butscher, C. (2017). "Uncertainty assessment in 3-D geological models of increasing complexity". English. In: *Solid Earth* 8.2, pp. 515–530. ISSN: 1869-9510. DOI: 10.5194/se-8-515-2017. URL: https://se.copernicus.org/articles/8/515/2017/ (visited on 04/04/2025).

Selley, R. (2000). *Applied Sedimentology*. Academic Press, 523 p. ISBN: 9780080527475. URL: https://www.kufunda.net/publicdocs/Applied%20Sedimentology%20-%20By%20Richard%20C.%20Selley.pdf (visited on 04/04/2026).

Shamir, A. (2008). "A survey on Mesh Segmentation Techniques". de. In: *Computer Graphics Forum* 6, pp. 1539–1556. ISSN: 1467-8659. DOI: DOI:10.1111/j.1467-8659.2007.01103.x. URL: https://doi.org/10.1111/j.1467-8659.2007.01103.x (visited on 05/27/2025).

Stephenson, P. (2018). "The Shoelace Formula & Pick's Theorem". In: *Mathematics in School* 47.4, pp. 35–38. ISSN: 0305-7259. URL: https://www.jstor.org/stable/26534777 (visited on 12/01/2024).

Stollhofen, H., Bachmann, G. H., Barnasch, J., Bayer, U., Beutler, G., Franz, M., Kästner, M., Legler, B., Mutterlose, J., and Radies, D. (2008). "Upper Rotliegend to Early Cretaceous basin development". In: *Dynamics of Complex Intracontinental Basins : the Example of the Central European Basin System*. Ed. by R. Littke, U. Bayer, D. Gajewski, and S. Nelskamp. Springer Verlag Berlin, pp. 181–210. ISBN: 978-3-540-85084-7. URL: https://gfzpublic.gfz-potsdam.de/pubman/faces/ViewItemFullPage.jsp?itemId=item_238813_1 (visited on 11/30/2024).

Suzuki, S., Caumon, G., and Caers, J. (2008). "Dynamic data integration for structural modeling: model screening approach using a distance-based model parameterization". en. In: *Computational Geosciences* 12.1, pp. 105–119. ISSN: 1573-1499. DOI: 10.1007/s10596-007-9063-9. URL: https://doi.org/10.1007/s10596-007-9063-9 (visited on 06/10/2025).

Thiele, S. T., Jessell, M. W., Lindsay, M., Ogarko, V., Wellmann, J. F., and Pakyuz-Charrier, E. (2016a). "The topology of geology 1: Topological analysis". In: *Journal of Structural Geology* 91, pp. 27–38. ISSN: 0191-8141. DOI: 10.1016/j.jsg.2016.08.009.

URL: https://www.sciencedirect.com/science/article/pii/S0191814116301110 (visited on 12/01/2024).

Thiele, S. T., Jessell, M. W., Lindsay, M. D., Wellmann, J. F., and Pakyuz-Charrier, E. (2016b). "The topology of geology 2: Topological uncertainty". In: *Journal of Structural Geology* 91, pp. 74–87. ISSN: 0191-8141. DOI: 10.1016/j.jsg.2016.08.010. URL: https://www.sciencedirect.com/science/article/pii/S0191814116301122 (visited on 07/24/2025).

Wellmann, J. F. and Caumon, G. (2018). "3-D Structural Geological Models: Concepts, Methods, and Uncertainties". English. In: *Advances in Geophysics*. 59. Elsevier, pp. 1–121. DOI: https://doi.org/10.1016/bs.agph.2018.09.001. (Visited on 04/04/2026).

Winter, J. (2013). "Principles of Igneous and Metamorphic Petrology". en. In: URL: https://elibrary.pearson.de/book/99.150005/9781292034768 (visited on 04/04/2025).

Zehner, B. (2021). "On the visualization of 3D geological models and their uncertainty". en. In: *Zeitschrift der Deutschen Gesellschaft für Geowissenschaften*, pp. 83–98. ISSN: , DOI: 10.1127/zdgg/2020/0251. URL: https://www.schweizerbart.de/papers/zdgg/detail/172/96734/On_the_visualization_of_3D_geological_models_and_t?af=crossref (visited on 06/05/2025).

Zhao, B. and Wang, J. (2016). "3D quantitative shape analysis on form, roundness, and compactness with μCT". In: *Powder Technology* 291, pp. 262–275. ISSN: 0032-5910. DOI: 10.1016/j.powtec.2015.12.029. URL: https://www.sciencedirect.com/science/article/pii/S0032591015302345 (visited on 10/22/2025).

CHAPTER

THREE

QUANTITATIVE COMPARISON OF SUBSURFACE STRUCTURES: AN APPLICATION TO SALT DOMES AND CRYSTALLINE BODIES

This chapter was published as a peer-reviewed article:

Carl, F., Yang, J., Colling Cassel, M., Wellmann, F., Achtziger-Zupančič, P., 2026b. Quantitative comparison of subsurface structures: an application to salt domes and crystalline bodies, Journal of Structural Geology, 205, https://doi.org/10.1016/j.jsg.2026.105633.

Abstract

Structural geological models are valuable instruments to visualize the subsurface for various scientific and economic interests. However, as geomodels only represent potential realizations of subsurface conditions, quantitative comparison of multiple probable models or model scenarios is important. This study applies an algorithm for the geometric shape quantification. The method quantitatively assesses the geometry of geological structures based on cross sections oriented perpendicular to the structures' horizontal main axes. The resulting data are analyzed and clustered statistically: Histogram analysis of dimensional data provides insight into the anisotropy of structures, the presence of overhangs and the character of the top surface of the structures. Gradient and curvature data offer insight into the slopes of the lateral walls of the structures and their sphericity as well as top surface. Cluster analysis reveals geometric affilia-

tions, as the methodology is applied to 239 datasets of intrusive salt geometries from the North German Basin and 67 datasets of crystalline basement structures from Saxony (Germany). The resulting clusters are assigned to a catalogue of benchmark models exhibiting high geometric similarity. The cluster results are contextualized in the regional geology of the North German Basin and the basement of Saxony in Germany. The relation of geometric statistics and regional geology demonstrates the application of the catalogue of benchmark models to model geological bodies.

3.1 Introduction

Geological modeling is an essential tool for the characterization of the subsurface and to guide decision making in economic as well as scientific projects (Turner and Gable 2007). Geomodeling in general does equally rely on the available input data and on the knowledge of the user regarding the geological setting and the subsurface structures to be modelled (Wellmann and Caumon 2018). Since the knowledge can be as variable as the quantity and quality of the input data, possible model realizations can differ strongly for a specific case study. And although the "true" geological subsurface cannot be evaluated directly, the comparison of multiple realizations of composite models or individual subsurface structures is valuable nonetheless to assess the possible range of geological features or the geological rationality of modeling results (Wellmann and Caumon 2018). Here, quantitative comparative approaches are preferred over qualitative ones, enabling the geologist to look at the models beyond pure visual examination. This study presents the application of the methodology to quantitatively analyze the external, three-dimensional geometry of subsurface structures using dimensional measurements as well as gradients and curvatures, determined on 2D cross-sections, that has been established by Carl et al. (2026). 239 datasets of intrusive salt structures from the North German Basin and 67 models of crystalline structures from Saxony (Germany) are analyzed with the methodology ("crystalline" as defined by the German federal company for radioactive waste disposal (Bundesgesellschaft für Endlagerung, BGE; see Subsect. 3.1.2.1). Besides quantifying the geometric dis-/similarity of the subsurface models, they are also compared to a set of regular benchmarks models established in Carl et al. (2026). Furthermore, the results of the methodology are put into the context of the regional geology.

3.1.1 Previous studies

The intrusive salt structures from the North German Basin and their development have been studied extensively since decades (e.g., Jaritz 1974; Sannemann 1968; Trusheim 1971). While some publications examine the development of the basin as a whole (e.g.,

Scheck-Wenderoth and Lamarche 2005; Stollhofen et al. 2008), many studies concentrate on salt structure evolution in specific sub-basins or grabens. For the Northeast German Basin, Kossow et al. (2000) study the evolution of salt pillows in the northern part of the area, while Scheck et al. (2003) follow up with a general examination of salt movements in response to the post-Permian tectonic evolution. In Scheck-Wenderoth et al. (2008), where the authors analyze the dynamic salt mobilization following tectonic triggers since the Permian for the whole Central European Basin System, one focused case study is from the Northeast German Basin as well. The Glückstadt Graben situated in Schleswig-Holstein and the northernmost parts of Lower Saxony is another major structural element appearing as a case study in Scheck-Wenderoth et al. (2008). Furthermore, Maystrenko et al. (2005a) and Maystrenko et al. (2005b) focus on the Glückstadt Graben, assessing its evolution and salt tectonics since the Mesozoic using seismic data. South of that lies the Lower Saxony Basin, whose evolution has been studied for instance by Betz et al. (1987) and Brink et al. (1992). Further to the west, East Frisia is studied by Kukla et al. (2008) who use data from the region to assess the connection of salt geometries and kinematics, thus providing an overview of the regional tectonic evolution as well. Lastly, offshore to the North, the geological history of the southern Horn Graben is analyzed by Best et al. (1983) based on seismic and well data. Despite the decades-long research on the North German Basin, up to this day, there are studies conducted on the structural evolution of sub-basins. For instance, Ahlrichs et al. (2020) evaluate the structural evolution at the Northeast North German Basin Margin based on recent seismic data. While studies on the salt structures in the NGB are numerous, yet inherently connected by looking at a single specific rock type, the situation is different for the Saxonian regions of interest. The geological, structural and mineralogical heterogeneity of the Ore Mountains and adjacent areas results only in few overview publications (e.g., Pälchen and Walter 2011; Rötzler 2025; Sebastian 2013). Instead, publications tend to focus on specific rock types in various geoscientific fields of study. Here, geometric questions are rarely the main focus. Kuschka (2002) describes the geology and tectonics of hydrothermal systems across Saxony, while Hiller (1995) goes into detail on the structural framework of the Haemmerlein und Tellerhaeuser hydrothermal sites. Andreani et al. (2014) present a geomorphological approach applied to the Ore Mountains, using digital elevation models to assess interactions between tectonics and landscapes. For geometric analysis, this might only help in the evaluation of top surfaces of subsurface structures. Geomechanical studies like Achtziger-Zupančič et al. (2017) are more concerned with fault networks within rock bodies rather than the external geometry of a given structure, or focus on much smaller scales (e.g., Schulmann et al. 1996). Focusing on the external geometry of structures, to our knowledge a quantitative examination of the dis-/similarity of intrusive subsurface bodies has not been conducted on this structural scale and a database of

such size before. For salt structures, most comparative studies have been executed on a basin scale (e.g., Liro 1992; Neff 1960; Stokes 1982; Tari et al. 2003), not quantifying differences between individual structures, but only assessing variations in structural evolution and the range of structural types. Jackson and Talbot (1986) compile some data on the approximate size of salt structures in different basins from numerous studies, but do not conduct detailed analyses either. For crystalline intrusive structures, the situation is similar: the geometry of structures within regions has been assessed in several studies, partially classified but not quantified (e.g., Eide et al. 2017; Köpping et al. 2022; Mark et al. 2020).

Given that our study is based on the work done in Carl et al. (2026), it is reviewed briefly, with the approach being revisited and enhanced in Sect. 3.2 of our contribution. The methodology for the quantitative comparison of the geometry of 3D objects was established after reviewing approaches from material sciences (e.g., Altuhafi et al. 2013; Cox and Budhu 2008; Zhao and Wang 2016) and geosciences (e.g., Lindsay et al. 2013; Schweizer et al. 2017). Furthermore, a set of regular benchmark models for geomodeling ("standard geometries") was derived, applicable also to salt and crystalline rocks, and five additional simple test geometries were defined. Subsequently, a description of the methodology including a pseudocode for reference followed. Results of the algorithm were then analyzed exemplarily for a sphere and a model of a real intrusive salt structure, "Altenbruch-Beverstedt", that is also included in our database. Next, the usage of a cluster analysis for the quantitative comparison of datasets was illustrated, analyzing dis-/similarities between the standard geometries. Then, the preceding results were analyzed, leading to an exclusion of certain standard geometries from the open access collection of benchmarks due to high geometric similarity. The discussion focused on 1) the distinction of the method from previous approaches for 3D structural comparison, 2) its compromises to ensure universal applicability and 3) the question of how this quantitative framework advances the analysis of 3D geological structures.

3.1.2 Brief introduction to the case study

3.1.2.1 Database: subsurface datasets and benchmark models

The methodology presented by Carl et al. (2026) was developed aiming to aid in the German national search for a disposal site for high-level radioactive waste, which is performed by the BGE. In the German site selection, four potential host rock types have been defined: claystone/shale, "stratiform" salt, "steep" salt and crystalline rocks. The geometric complexity among the host rocks is largest for "steep" salt rock and crystalline rocks, therefore, the methodology was applied to these rock types (see Fig. 3.1). Example structures for both rock types are visible in Fig. 3.2. The database

was compiled from two different online sources: The salt bodies were taken from the TUNB model of the German Federal Institute for Geosciences and Natural Resources (BGR et al. 2022), being open meshes in the .vtk-file format. The .vtk-input models of crystalline rocks originate from the composite models "Altenberg-Teplice" (LfULG and CGS 2012), "Aue" (LfULG 2010), "Elbezone" (LfULG 2012), "Erzgebirge-Fichtelgebirge-Komplex" (LfULG n.d.), "Neiße-Grenzregion" (LfULG 2014), "Schienenneubaustrecke Dresden-Prag 2015" (TUBAF and LfULG 2015) and "Schienenneubaustrecke Dresden-Prag 2020" (LfULG and CGS 2020), being compiled at the online viewer of 3D geomodels provided by the Saxon State Office for Environment, Agriculture and Geology (LfULG). Please note, that for some crystalline composite models, naming conventions for model elements are ambiguous. Thus, despite intensive research, it was not possible to check in every case, if a modelled body is a crystalline structure. However, this is negligible for our study, as for the respective composite models, all model elements are geometrically similar.

When applying the approach to real cases of intrusive salt and crystalline bodies, one has to consider benchmark models with known geometric properties based on geometric systematizations in order to assign the real bodies to geometric types of subsurface structures. The set of 25 benchmark models ("standard geometries") seen in Fig. 3.3 is taken from Carl et al. (2026). It is based on a geometric systematization of the potential host rocks in the German site selection and has been established initially by Carl et al. (2023). For the rock types of our case study, the systematization shall be reviewed shortly.

Salt rock (i.e., halite) can develop a variety of structures in the subsurface due to the uniqueness of salt tectonics (Hudec and Jackson 2007). The most common classification subdivides the geometries into concordant and intrusive structures with respect to the overburden (Hudec and Jackson 2007; see Fig. 3.1), with only the latter being relevant for our study: stocks, sheets and walls. In addition to this systematization, a subdivision according to the length-to-width ratio of salt bodies is discussed as well (e.g., Hudec et al. 2011), supplementary to the main classification. Here, structures are called anticlines or walls, respectively, when they exhibit a length-to-width ratio higher than 2 in map view, therefore being considerably anisotropic. Consequently, the rather isotropic geometries (length-to-width ratio smaller than 2) are pillows, stocks and, at least in their early developmental stages, sheets. An additional aspect in the classification of salt structures is, whether the salt of the structure is autochthonous or allochthonous. Here, sheets represent the only structure belonging to the latter category: If the bulb of a stock or wall is sub-horizontally oriented or moderately dipping above the autochthonous salt source layer, these structures would be classified as salt sheets (Hudec and Jackson 2006).

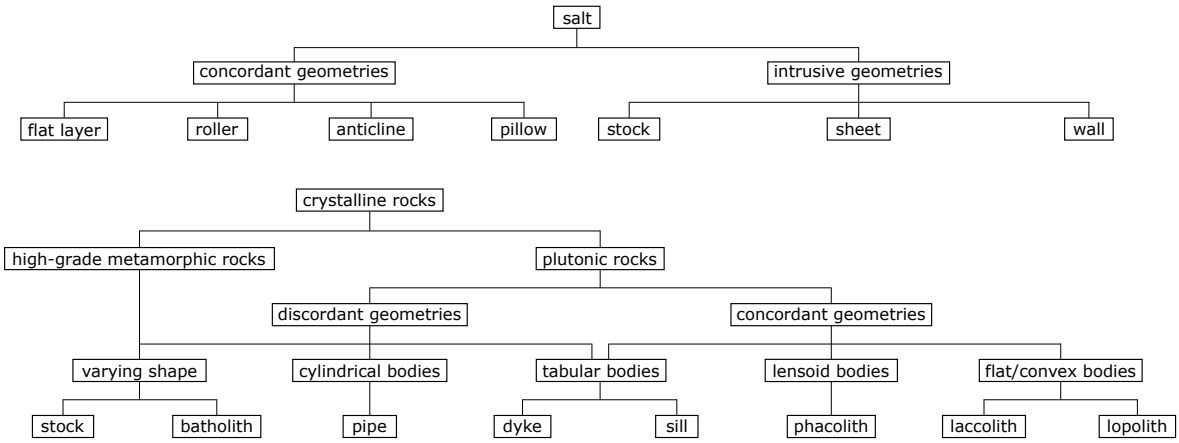


Figure 3.1: Geometrical systematization of the rock types encompassed by our database. Adapted from Carl et al. (2023)

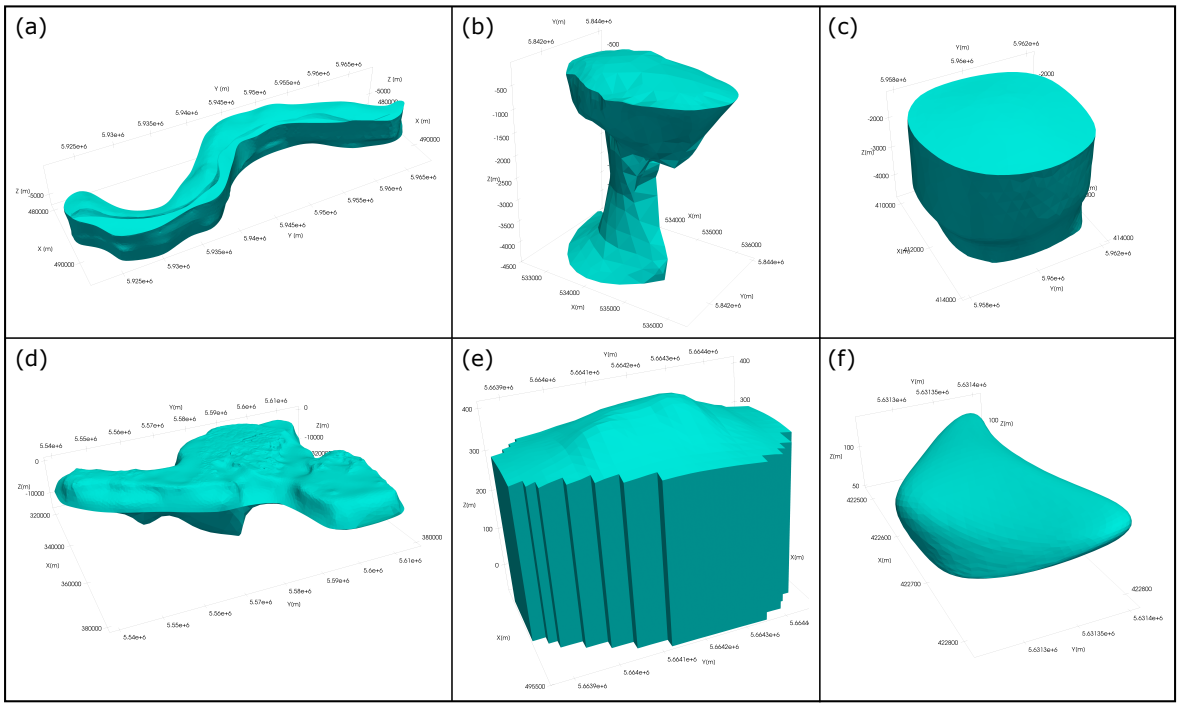


Figure 3.2: Example models from the database of the present study. a) the intrusive salt structure "Altenbruch-Beverstedt". b) the intrusive salt structure "Eilte". c) the intrusive salt structure "Spiekeroog". d) the "Eibenstock" granite. e) the intrusive igneous body of unknown composition "hgk455_HYE93001_2". f) a "biotite-muscovite-potash feldspar orthogneiss" body

Crystalline rocks as systematized by Carl et al. (2023) encompass both metamorphic rocks as well as plutonic rocks. The combination of both groups complicates the establishment of a coherent geometric systematization as metamorphic rocks are formed from various protoliths, resulting in a variety of geometries. Orthogneisses and part of the migmatites, for example, originate from plutonic protoliths and resemble the geometries of these rocks. In contrast, paragneisses and the remaining migmatites result from various sedimentary sources. Their geometry depends not only on the structure of the original geological body but also on their deformation history during the

metamorphosis. Therefore, the geometric end members defined by Carl et al. (2023) were partially represented by several regular standard geometries in Carl et al. (2026), to represent the range of varying geometries (see Fig. 3.3). For plutonic rocks, the systematization established by Carl et al. (2023) is based on the combination of the shape of the geological bodies and their relationship to the overlying strata (concordance or discordance; Philpotts and Ague 2009): batholiths (larger than 100 km^2) and stocks (smaller than 100 km^2) are defined as discordant structures of varying shape and are represented by the same benchmark models as the metamorphic rocks. Moreover, cylindrical, discordant bodies are present in the subsurface mainly representing feeder pipes for magma ascendancy. Furthermore, two types of tabular geometries can be distinguished: sills (mostly concordant) and dikes (discordant). Additionally, three other concordant geometries were defined: laccoliths exhibit a roughly flat base and a convex top, while lopoliths show a roughly flat top and a shallow convex base, whereas phacoliths lack flat sides as they are lensoid. These classifications were the basis for the set of standard geometries (Fig. 3.3). In the literature review preceding their setup in Carl et al. (2026), it became apparent that some of these benchmark models are non-unique for rock types but can be used in different environments, e.g., stocks/batholiths for salt and crystalline basement. This is indicated in the model titles. Thus, the rock types considered in the present study overlap in their geometric range and can partially be approximated by the same benchmark models. Given our focus on the external geometry of subsurface bodies, we decided to analyze all the intrusive rock types together, thereby also demonstrating their geometric similarities as important insights for geological modeling.

3.1.2.2 Geological overview and location of case study regions

The North German Basin (NGB) featuring the salt structures (see Fig. 3.4a) is part of the Central European Basin System (CEBS) in northern central Europe, originating during the Late Carboniferous-Early Permian as a result of extended rifting and igneous pulses (e.g., Abramovitz and Thybo 1999; Bayer et al. 1999; Dadlez et al. 1995; Gast 1988; Plein 1990; Scheck et al. 2002; Ziegler 1990). Both CEBS and NGB strike NW-SE. Salt deposits involved in halo-tectonics in the NGB are mainly of Late Permian age, with minor rock volumes also being deposited during the Early Permian (Schröder et al. 1995), Middle Triassic (Röhling 2000), Late Triassic (Bachmann et al. 2008) and Late Jurassic (Fischer et al. 2018). During the Triassic, extensional tectonics resulted in widespread salt movements and the development of deep rim synclines within the NGB, creating complex internal structures and accommodation space in the sub-basins (Kukla et al. 2008). The Triassic salt movements led to the development of salt anticlines, pillows and intrusive structures within the NGB and locally to rafting of cap rock at several points in time. By the Late Triassic, most of the salt walls

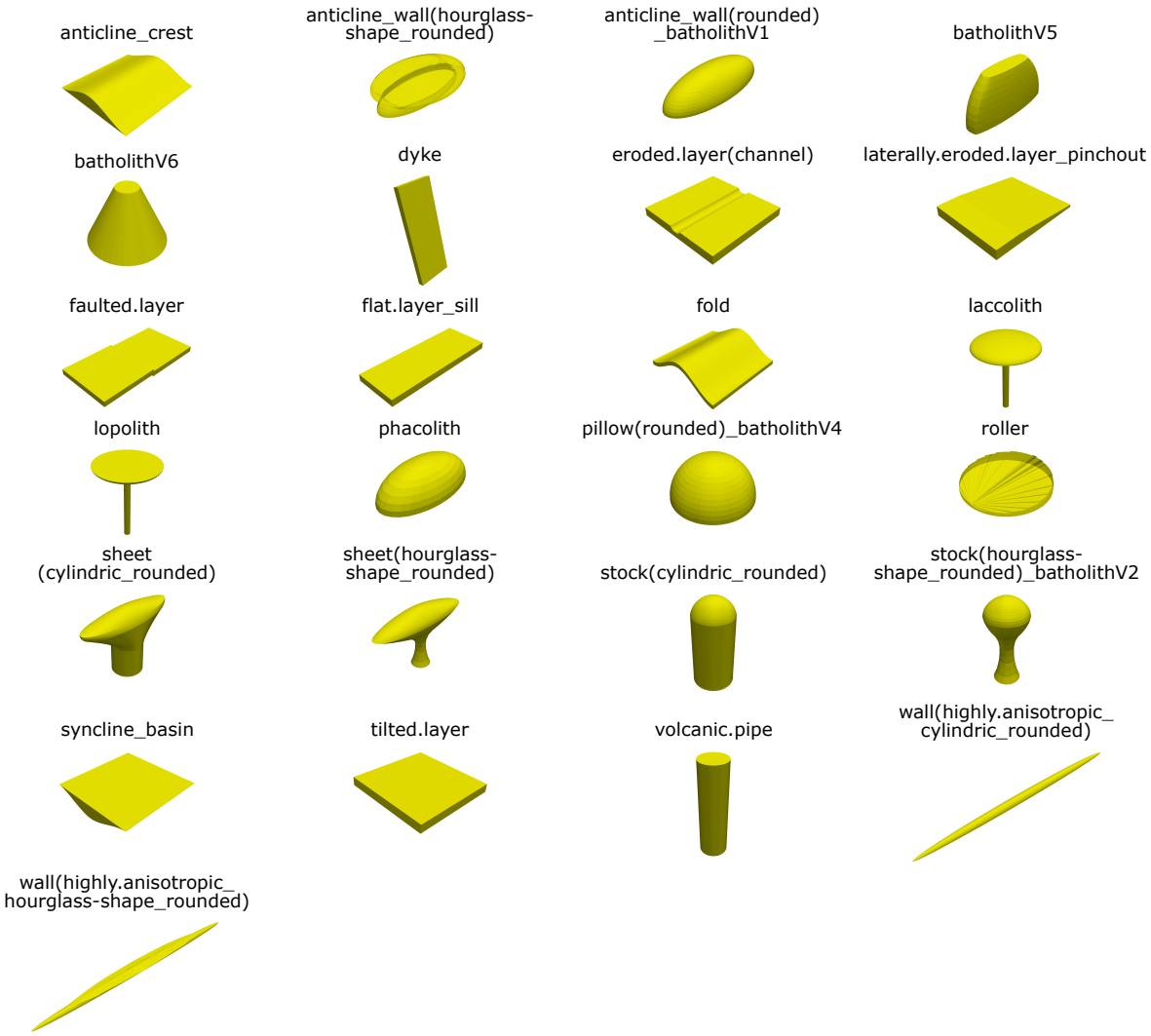


Figure 3.3: Set of benchmark models ("standard geometries") employed in this study. Taken from Carl et al. (2026)

with N-S-strike direction were already initiated in the respective grabens and troughs, parallel to their axes. Some of these salt structures reflect strong deformation intensity as they were formed to be up to 200 km long and several kilometers high and wide, reaching the paleo-surface, which caused leaching of the salt bodies and erosion of the overburden (Scheck-Wenderoth et al. 2008). Between the Jurassic and the Cenozoic, a succession of accelerated halo-tectonics during rifting phases, especially intensive along N-S trending structures, and less activity during compression took place (e.g., Scheck-Wenderoth et al. 2008; Stollhofen et al. 2008).

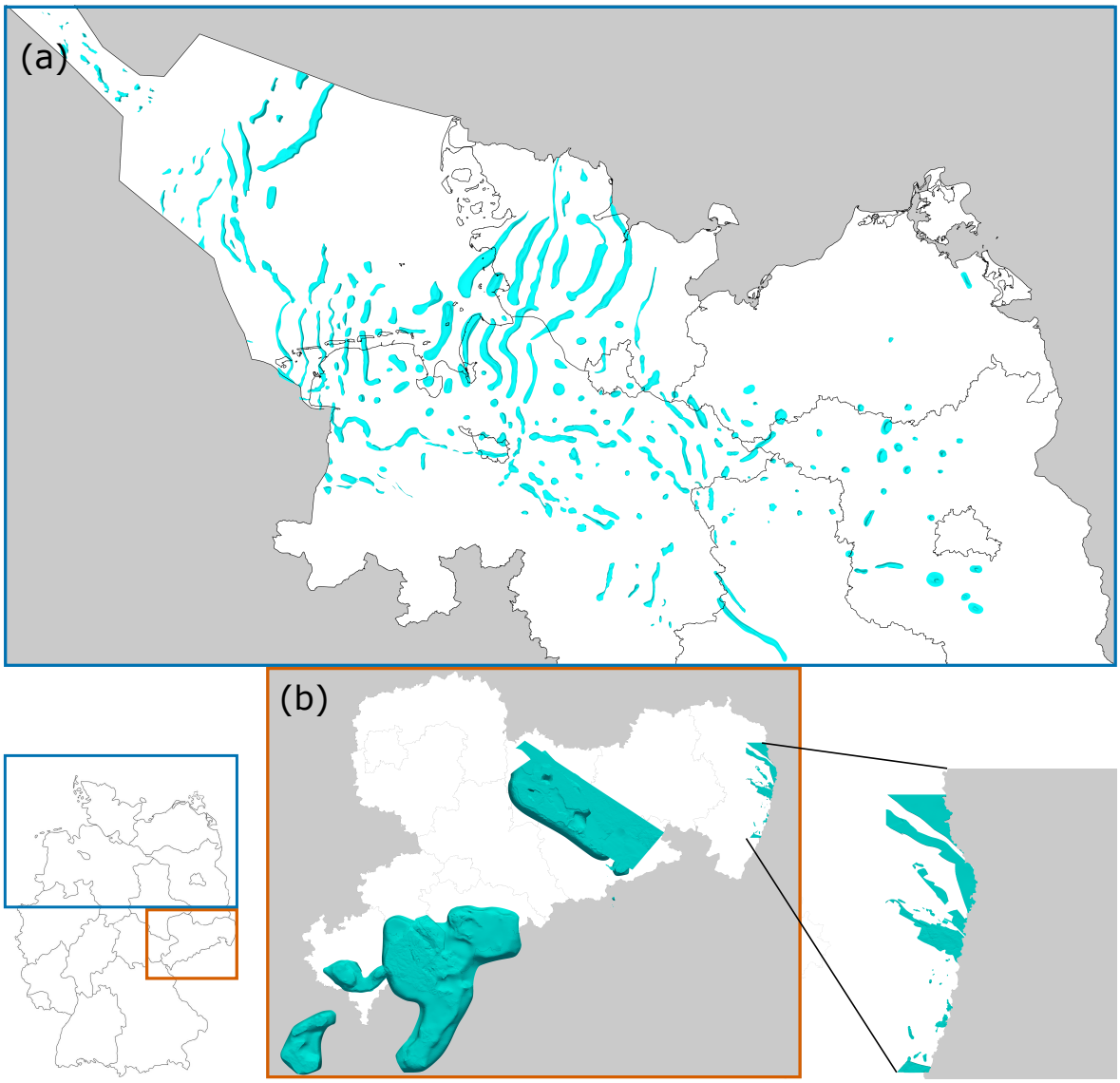


Figure 3.4: Location of the subsurface structures assessed with our method. a) intrusive salt structures from the North German Basin, taken from BGR et al. (2022). b) crystalline structures from Saxony, assembled from the online viewer of 3D geomodels provided by LfULG. The maps were created in ParaView

In today's spatial distribution of NW-SE and N-S-oriented anisotropic salt structures and of the isotropic structures (Fig. 3.4a), the formation history of the region can be recognized. In general, abundance of intrusive salt structures decreases from west to east, reflecting the underlying trend in deformation intensity (Scheck-Wenderoth et al. 2008). In the northwestern part of the study area (Schleswig-Holstein and the NW-part of Lower Saxony), which is the central part of the CEBS, approximately N-S-striking salt walls with a regular spacing prevail. In contrast, more marginal further to the south and southeast, NW-SE- to W-E-striking salt walls are present. Going further to the east, into the Northeastern German Basin, most salt structures are isotropic, as this region reacted as a stable block where fault zones developed only marginally. Overall, the maturity of the structures is lower in this sub-basin.

The crystalline structures from our database are located in the Saxonian Ore Mountains as well as in the adjacent Vogtland area to the southwest and the Elbezone and Neiße areas to the northeast (Fig. 3.4b). The basement of the region is Cadomic, with the majority of protoliths being granodiorites and greywackes (Sebastian 2013). The rocks of the Ore Mountains were metamorphized during the Variscan orogeny around 340 Ma. The presence of rocks from greenschist to eclogite facies reflects the influence of increasing P-T conditions on a prograde path (e.g., Sebastian 2013). Exhumation of the Ore Mountains happened in the Cenozoic (mainly Eocene to Miocene) as a result of the Alpine orogenesis, while the Eger Graben to the South was formed, accompanied by basaltic volcanism (Kuschka 2002).

The majority of metamorphic rocks are gneiss domes surrounded by schists, with various compositions owing to the diversity of educts (e.g., Sebastian 2013). In the later stages of the Variscan orogeny around 325 Ma, granitic plutons intruded into the Ore Mountains as well as the Vogtland and Meißen area (e.g., Sebastian 2013; Wenzel 1999). In the eastern part of the Ore Mountains, explosive rhyolithic vulcanism formed the calderas of Altenberg-Teplice and Tharandt, leaving feeder pipes behind. These magmatic rocks did not experience any metamorphic overprint.

3.1.3 Content and motivation of this study

The method for the quantitative comparison of subsurface structures established by Carl et al. (2026) on regular synthetic geometries is applied to the database of 306 structural models of real intrusive subsurface bodies, demonstrating its applicability to the full range of external geometric complexity shown by the intrusive structures in the German subsurface. The basic algorithm is adjusted to allow for the analysis of open meshes. The method and benchmark models introduced by Carl et al. (2026) facilitate common workflows for structural geomodeling at several stages. They are applicable in the setup or selection of a basic conceptual model, aid in the selection of hyper parameters for interpolation, and in the evaluation and selection of resulting model realizations. However, the present study will show that the method and benchmarks can also be utilized to assess 1) the geometric affiliations between irregular structures in a large geometrically diverse database and 2) the geometric dis-/similarities of these irregular structures to a set of benchmarks. Given the results, the potential context between the data and the regional geology is then analyzed, assessing, how the geometric properties relate to geological processes shaping the geo-bodies. The overall approach is meant to enable the efficient geometric systematization of compilations of large geological models without the necessity of visual interpretation by an experienced geoscientist and without the need to run a full-scale implicit comparison of these models. The method is an approximate approach to quantitative shape comparison: the

main geometric characteristics of input datasets are reproduced fast and visualized, but the determined parameters are not assessed at every possible location of a model (see also Carl et al. 2026), and the cluster analysis could be subdivided into individual parameters to allow for a more detailed interpretation of dis-/similarities between smaller subsets of the database. Furthermore, the approach does not allow for the analysis of implicit input models directly from a scalar field. The paper is structured as follows: Sect. 3.2 presents the methodology set up by Carl et al. (2026) briefly and explains the additions necessary to allow for the analysis of open meshes. Sect. 3.3 shows the results of applying the approach to the irregular structural models and the attempt to put the cluster results into the context of the regional geology. Meanwhile, Sect. 3.4 discusses the performance of the method for irregular bodies, the implications from the contextualization of the results with regional geology and the contribution of this study to the initial method by Carl et al. (2026). Finally, Sect. 3.5 concludes with potential future research.

3.2 Methods

3.2.1 Measurement of geometric parameters

The method for the quantification of 3D structures based on a set of geometric parameters as established in Carl et al. (2026) is expanded in our contribution. In general, while the method currently runs with .vtk-files (Schroeder et al. 2006) as input, other open source file formats should be implementable as well. The only precondition would be, that the input data needs to either be a mesh with extractable vertices or a data frame of vertex coordinates themselves.

The first part of the method is a geometric segmentation algorithm where the horizontal and vertical extents of 3D bodies are determined on equidistant cross sections that are oriented perpendicular to the two horizontal main axes of the structures (see Fig. 3.6). Thus, two sets of cross sections need to be created separately. First, the mesh is discretized into 22 sections with the normal direction parallel to the longer horizontal axis of the mesh's bounding box (Fig. 3.6a). The cross sections normal to the longitudinal main axis of the structure (first direction) are sequentially rotated to reach their optimal orientation based on the minimization of their cross-sectional area (Stephenson 2018; Fig. 3.5, Part 1). Meanwhile, the cross sections normal to the first set are assembled by rastering the established sections vertically, then firstly connecting raster lines of consecutive sections and secondly the resulting trapezoidal segments (Fig. 3.5, Part 3; Fig. 3.6c). Following a multistep approach for the correction of artifacts in the sections of both sets (Fig. 3.5, Part 2; Fig. 3.6b), the methodology of Carl et al. (2026) is enhanced to enable the processing of open input meshes that require the definition

of a base level for vertical dimensional measurements. To establish an individual base level for every input mesh, the cross sections of both directions are cropped and leveled at a fixed depth interval (see Fig. 3.5, Part 4). Determination of the base level bases on the interquartile range method (Upton and Cook 1996) on the Z-coordinate of the last vertex. Outliers which are not cropped are defined as being above the upper bound ($= \textit{third quartile} + 1.5 \cdot \textit{interquartile range}$) in terms of Z-values. In most cases, a few 100 m have been removed from the vertical extent in order to create a base level, depending on the input mesh's homogeneity of the vertical extent prior to base level creation. Given the sections of both sets (Fig. 3.6d), horizontal and vertical measurements are then carried out on each cross section at 5 equidistant transects, between the intersections of measurement lines and the polygon (Fig. 3.5, Part 5; Fig. 3.6e). As the first and last sections of both sets are excluded from the measurements as they could (undesirably) slice irregular shapes several times, 20 sections per direction are considered for every input structure. Thus, 100 values are obtained respectively for the two horizontal parameters and 200 measurements for the vertical extent. Gradients and curvatures are additionally calculated between consecutive vertices of a section (Fig. 3.5, Part 5). The curvature in 2D is determined as the reciprocal of the circumradius of a triangle, and thus calculated between three consecutive vertices in either the xz- or yz-plane. First, the side lengths of the triangle of the points are determined, then the semiperimeter of the triangle and the area through Heron's formula. Then, the curvature is obtained. For both parameters, the different numbers of vertices in the input meshes used in this study resulted in varying amounts of data between 573 and 17,037 measurements per model.

3.2.2 Data analysis

The data obtained from the geometric measurements were compiled into a database, analyzed using the first three statistical moments, the standard deviation and the median and displayed through histograms and cumulative distribution functions (CDF's). Comparative analyses of histograms and data distributions and clustering analyses after principal component analysis (PCA) was conducted on the measurements: Semi-quantitative comparison of histograms was carried out for the dimensional data as well as gradient and curvature data. Overflow bins for gradient and curvature data were employed to aid interpretability (see Carl et al. 2026). Cluster analysis was carried out on the irregular input meshes and standard geometries after data normalization to a range of -1 to 1 and principal component analysis (e.g., Jolliffe 2002). The purpose of PCA is the reduction of the number of variables in the data while preserving the highest amount of original variance possible. 20 percentiles of the PDF's of the different parameters were used as features in the PCA. The number of clusters of the

```
Part 1:
Input: initial cross sections
Output: cross sections rotated perpendicular to longer horizontal main axis by minimization of cross section area
for each initial section do
    for each of 38 rotation steps (0° to 180° in 5° increments) do
        Compute rotation angle (theta)
        Apply rotation matrix to original normal ([1,0,0] or [0,1,0]) to get rotated normal
    end for
    for each rotated normal do
        Slice mesh using rotated normal and center point of section
        Retrieve vertices from rotated slice
        Project cross section into YZ plane to calculate area
        Compute centroid of this projected section
        Sort points by angle relative to centroid
        Compute area of polygon using sorted points and shoelace formula
    end for
end for

Part 2:
Input: rotated cross sections
Output: rotated cross sections after artifact correction
Step 1:
for each rotated cross section do
    set vertex with lowest z-value as vertex index=0
    perform normalized nearest neighbour algorithm
end for

Step 2:
for each section after normalized nearest neighbour algorithm do
    apply correction criterion
    if correction criterion = True then
        initialize manual vertex order correction in plotly.dash
        for each section with artifacts do
            correct vertex order by clicking on previous (correct) vertex then incorrect vertex
        end for
    end if
end for

Part 3:
Input: corrected cross sections of 1st direction
Output: corrected cross sections of orthogonal direction
for each section of 1st direction do
    raster section vertically into 22 vertical lines
    for each vertical line do
        retrieve X, Y and Zmin+Zmax - coordinates
    end for
end for

for 2 consecutive sections of 1st direction do
    for all vertical lines in both sections do
        extract X, Y and Zmin+Zmax (=2 points per section)
        combine 4 points into trapezoidal segment
    end for
end for

for every index of vertical lines do
    combine trapezoidal segments to assemble uncorrected orthogonal section
end for

for uncorrected cross sections of orthogonal direction
    repeat Part 2

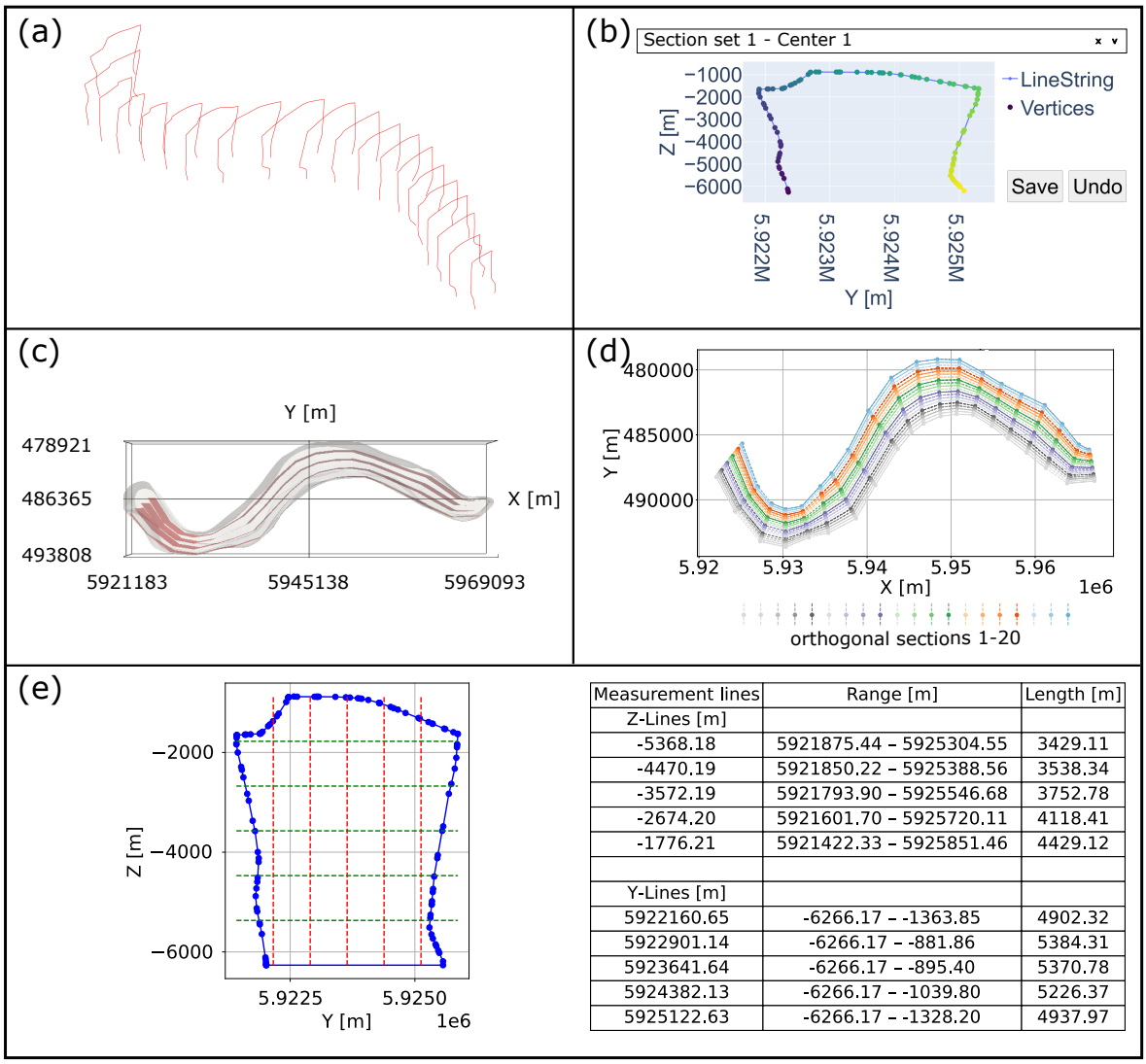
Part 4:
Input: corrected cross sections of both directions
Output: cross sections cropped at fixed baselevel + uncropped outliers
for each cross section do
    retrieve Z-value of last vertex
end for
Apply IQR on all last Z-values to detect sections not to be cropped
for all sections to be cropped do
    crop linestring at median of Z-values of last vertex (eliminate vertices below)
    add vertex at each end of linestring at median of Z-values of last vertex (base level)
end for

Part 5:
Input: all cross sections
Output: horizontal and vertical dimensional measurements
for each cross section of 1st direction except index 0 & 21 do
    rotate & project section onto YZ plane
    create 5 horizontal and vertical measurement transects
    measure horizontal and vertical dimensions between intersections of transect and polygon
end for

for each cross section of orthogonal direction except index 0 & 21 do
    rescale sections (corresponds to rotation & projection onto YZ plane)
    create 5 horizontal and vertical measurement transects
    measure horizontal and vertical dimensions between intersections of transect and polygon
end for

for all cross sections do
    compute gradients
    compute curvatures
end for
```

Figure 3.5: Pseudocode of the algorithm that creates the cross sections of both directions and measures the dimensional extents, gradients and curvatures on these sections. For further information, see Subsect. 3.2.1. Adapted from Carl et al. (2026)



Measurement lines	Range [m]	Length [m]
Z-Lines [m]		
-5368.18	5921875.44 – 5925304.55	3429.11
-4470.19	5921850.22 – 5925388.56	3538.34
-3572.19	5921793.90 – 5925546.68	3752.78
-2674.20	5921601.70 – 5925720.11	4118.41
-1776.21	5921422.33 – 5925851.46	4429.12
Y-Lines [m]		
5922160.65	-6266.17 – -1363.85	4902.32
5922901.14	-6266.17 – -881.86	5384.31
5923641.64	-6266.17 – -895.40	5370.78
5924382.13	-6266.17 – -1039.80	5226.37
5925122.63	-6266.17 – -1328.20	4937.97

Figure 3.6: Visual representation of the segmentation and measurement algorithm for the intrusive salt structure Altenbruch-Beverstedt. a) initial segmentation of the input mesh. b) Plotly.dash app for vertex-order correction. c) Subset of orthogonal cross sections. d) Coverage of input structure with cross sections (top view). e) Example of dimensional measurement results. Adapted from Carl et al. (2026)

K-means algorithm was determined based on silhouette score and elbow plot. Geometric interpretation of clusters was approached relying on the features showing the highest contributions to respective principal components.

3.3 Results

The 306 datasets are comprised of complete, individual 3D structural representations of subsurface geometries. Each dataset is presented as one possible realization of the respective geological body, with all associated data uncertainties, methodological uncertainties, and subjective bias being incorporated (see Wellmann and Caumon 2018). Since the geometric properties of these models are examined – irrespective of which

geomodeling method was employed in their creation – they are utilized as appropriate input data for the workflow. An important limitation must be noted for the following analyses: certain datasets should be interpreted as representing minimum extents only. This constraint arises because the corresponding geological structures are situated in border regions of Germany, where the modeling meshes were truncated at the national border by the modelers. The respective cases are: "Bettina-Sued", "Bettina-West", "Boertange", "Delia", "Greta", "Hannelore-Hilda-Erika", "Lia", "Liane-Emshoern", "Neusustrum", "Paapsand", "Tellingstedt_Osterbruch-Basdahl", "Warnau" and "Wybelsum".

3.3.1 Analysis of histograms and data distributions of the geometric data

Given that real 3D geological bodies exhibit anisotropy to varying degrees and based on the axis definition (Subsect. 3.2.1), the horizontal distance properties derived from cross sections perpendicular to the longitudinal main axis are observed to be smaller on average than those measured parallel to it (see Table 3.1). Since structural anisotropy can only be assessed when data from both measurement directions are considered, the two horizontal properties have been merged into a single parameter termed the "combined horizontal extent". This parameter exhibits the largest values for both variance and standard deviation, as anticipated. Moreover, it represents the only parameter for which a positive average skewness is observed.

Figure 3.7 presents the range of the four dimensional parameters, by showing how many datasets extend beyond any given length measurement. The cumulative distribution functions (CDF's) for all parameters are visualized in integrated diagrams as well (Fig. 3.8). For horizontal data normal to the longitudinal axis (Fig. 3.7a), less than 50 input meshes exhibit measurements larger than 5,000 m. Horizontal data along the longitudinal axis (Fig. 3.7b) and the combined horizontal data (Fig. 3.7c) show a much higher range and a larger portion of datasets extending well over 10,000 m. Vertical data (Fig. 3.7d) exhibit a portion of approximately 50 datasets with maximum ranges less than 300 m. Beyond that, the pattern is similar to that seen in Fig. 3.7a, although the scale is different: the vast majority of meshes does not extend past 4,000 m vertically. CDF diagrams display P10, P50, and P90 quantiles in color with individual datasets in grey for clarity (Fig. 3.8). The shape of the P10 and P90 quantiles of the horizontal data normal to the longitudinal main axis (Fig. 3.8a) reflects the presence of a large amount of positively skewed data distributions (see P90), while there are less negatively skewed distributions (see P10). This pattern is reversed for the horizontal data along the longitudinal main axis as many more datasets exhibit a negative skew (Fig. 3.8b): there are more significantly curved CDF's with higher

probabilities at larger normalized values. The combined horizontal data (Fig. 3.8c) shows the prevalence of bimodal distributions, as indicated by the kink seen in both the quantiles and many individual distributions. Vertical data (Fig. 3.8d) exhibit the greatest CDF shape variability, ranging from quasi-linear to exponential forms. Many distributions seem to be negatively skewed, as reflected in the P10.

Table 3.1: Averaged statistical moments, median and standard deviation for the four dimensional parameters measured for all input meshes of the database.

(a)	Mean	Median	Variance	Standard deviation	Skewness
Horizontal extent normal to longitudinal main axis	1,936 m	1,951 m	1,942,165 m^2	832 m	-0.1
Horizontal extent along longitudinal main axis	10,053 m	10,815 m	24,892,330 m^2	2,781 m	-1.1
Combined horizontal extent	6,277 m	3,550 m	77,294,350 m^2	5,035 m	0.2
Vertical extent	1,619 m	1,713 m	6,824,23 m^2	580 m	-0.8

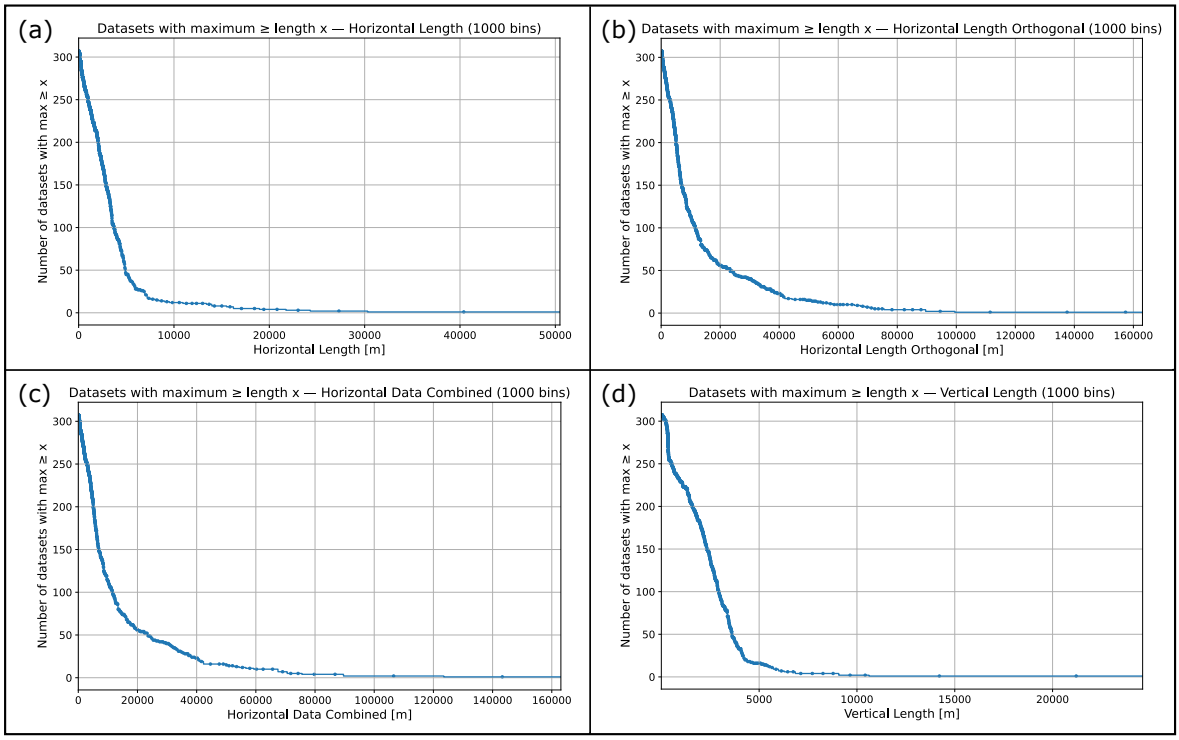


Figure 3.7: Range of parameter measurements for all irregular input meshes of the database. Visualized is the number of datasets whose maximum measurement is larger than a given length x. a) Horizontal data normal to the longitudinal main axis. b) Horizontal data along the longitudinal main axis. c) Combined horizontal data. d) Vertical data

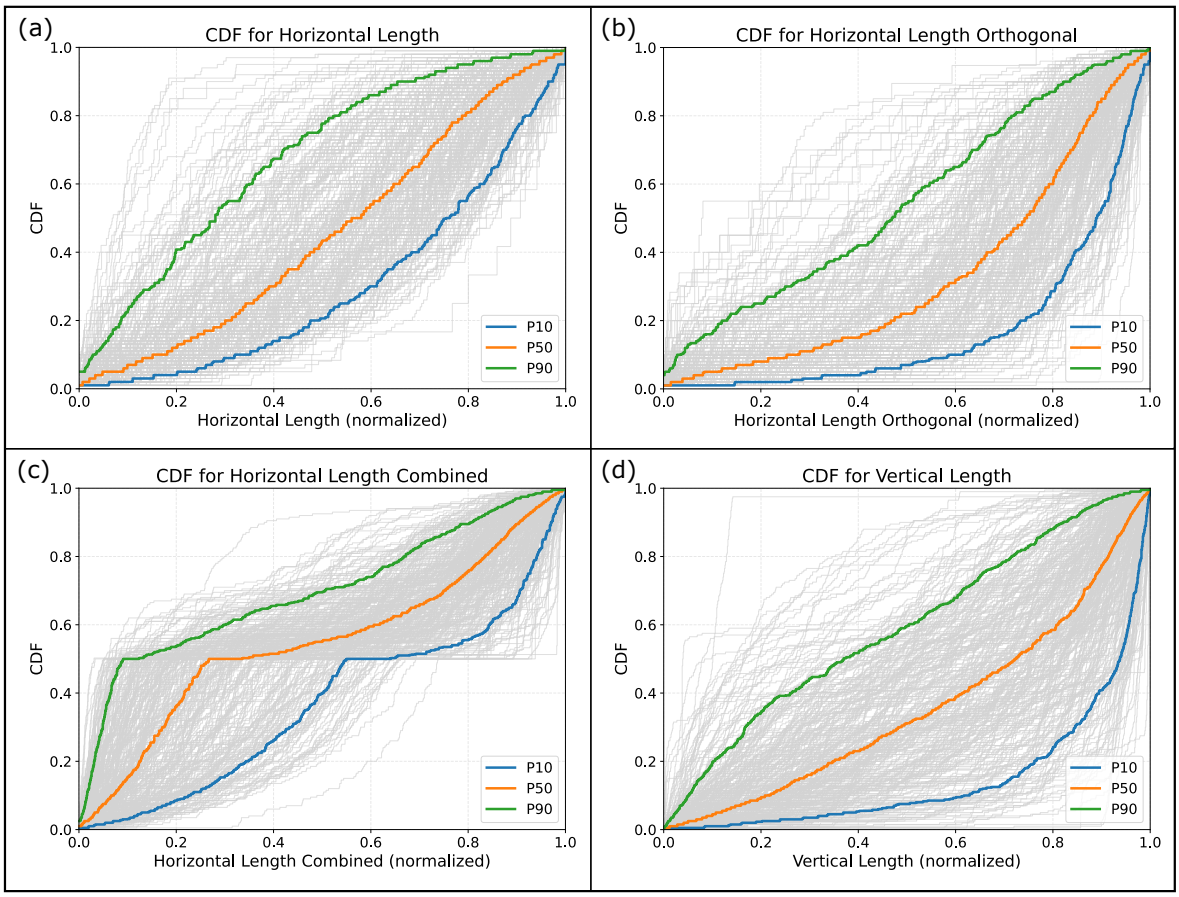


Figure 3.8: Combined cumulative distribution functions of all irregular input meshes of the database. a) CDF's of the horizontal data normal to the longitudinal main axis. b) CDF's of the horizontal data along the longitudinal main axis. c) CDF's of the combined horizontal data. d) CDF's of the vertical data

Figure 3.9 illustrates the variability of data distributions (blue) plotted against corresponding CDF's (red). Across all four dimensional parameters, distributions exhibiting distinct negative skew (Fig. 3.9a), positive skew (Fig. 3.9b), bimodal patterns (Fig. 3.9c), approximately normal distributions (Fig. 3.9d), and approximately uniform distributions (Fig. 3.9e) are observed, with the latter two appearing less frequently. Row (f) of Fig. 3.9 exhibits shapes of distributions standing out for the given parameter. For horizontal data normal to the longitudinal main axis (Fig. 3.9, column 1, "1st direction"), distributions with pronounced positive skew are most prevalent (34%), though not overwhelmingly so, as negatively skewed distributions comprise approximately 26%. This shows that a lot of structures exhibit narrow shapes across most of their extent normal to the longitudinal main axis, corresponding to the limited size of most test bodies either overall (having a small isotropic shape) or in one dimension (showing an anisotropic form). Meanwhile, larger measurements either represent overhangs at the top of geometries or other lateral enlargements across the vertical extents.

In contrast, the horizontal data along the longitudinal axis (Fig. 3.9, column 2, "orthogonal direction") exhibits less variation, with 67% showing pronounced negative skew. This mainly results from the approach of constructing those cross sections: the assemblage from trapezoidal segments with vertical lateral edges potentially results in the same horizontal extent for several measurements of a single section. Furthermore, centrally located cross sections of a structure tend to be of similar length for many geometries. Thus, many histograms end up showing negative skewness as many measurements of a dataset are rather similar, falling in a limited number of neighboring large histogram bins.

When the two horizontal measures are combined (Fig. 3.9, column 3), bimodal distributions become predominant (48%). These appear in two characteristic forms: 28% of datasets display closely positioned, potentially overlapping subordinate distributions (Fig. 3.9c, column 3), while a second group (ca. 20%, Fig. 3.9f, column 3) exhibits widely separated subordinate distributions. The combined horizontal extent reflects (an-)isotropy. In general, data analysis reveals that rather isotropic structures are characterized by a monomodal distribution as their horizontal extent is similar along both horizontal main axes. The skew of combined distributions for isotropic structures is usually negative. This is often the case due to the assembled sections of the second (orthogonal) set following the contour of a structure, which results in larger measurements for the horizontal data along the longitudinal axis (see also Carl et al. 2026). In contrast, the prevalent bimodal distributions are characteristic for anisotropic structures, where the observed increasing distance between the two subordinate distributions indicates increasing anisotropy. As recognized by Carl et al. (2026), multimodal distributions can also indicate the presence of overhang configurations (variations in lateral extents over the vertical range), when a similar distribution shape is present for the vertical data as well (example in Fig. 3.10; distributions visible as well in Fig. 3.9).

For the vertical data (Fig. 3.9, column 4), the CDF diagram (Fig. 3.8d) reveals that many data distributions are negatively skewed. Furthermore, a distinct property of the distributions indicates a characteristic of many underlying geometries, particularly of intrusive salt structures in the German subsurface: flat top surfaces. The majority of histograms are characterized by monomodal distributions with maxima at the highest measurement bins, while frequencies in lower bins decline rapidly. This pattern is quantified by determining the percentages of data in the last two bins of vertical distributions and assessing their ratio. In case the data in the last bin is at least twice as frequent as data in the second-to-last bin, structures are assumed to possess relatively flat top surfaces. This estimate applies to 70% of salt models, although this can only represent an approximation, as there is no literature published on this matter and our applied method being rather simple. Still, flat top surfaces can be regarded

as a common characteristic among German intrusive salt structures. The structures either pierced their cap rock at some point (which most notably happened in the Late Triassic and Cretaceous; Scheck-Wenderoth et al. 2008), or the cap rock was eroded temporarily as it happened regionally in the NGB during the Cretaceous due to uplift (Scheck-Wenderoth et al. 2008), both of which resulting in the dissolution of halite. For crystalline structures, vertical distributions are more varied, although flat top surfaces seem to be present regularly as well (calculated value at 34%), for instance representing modern-day topography.

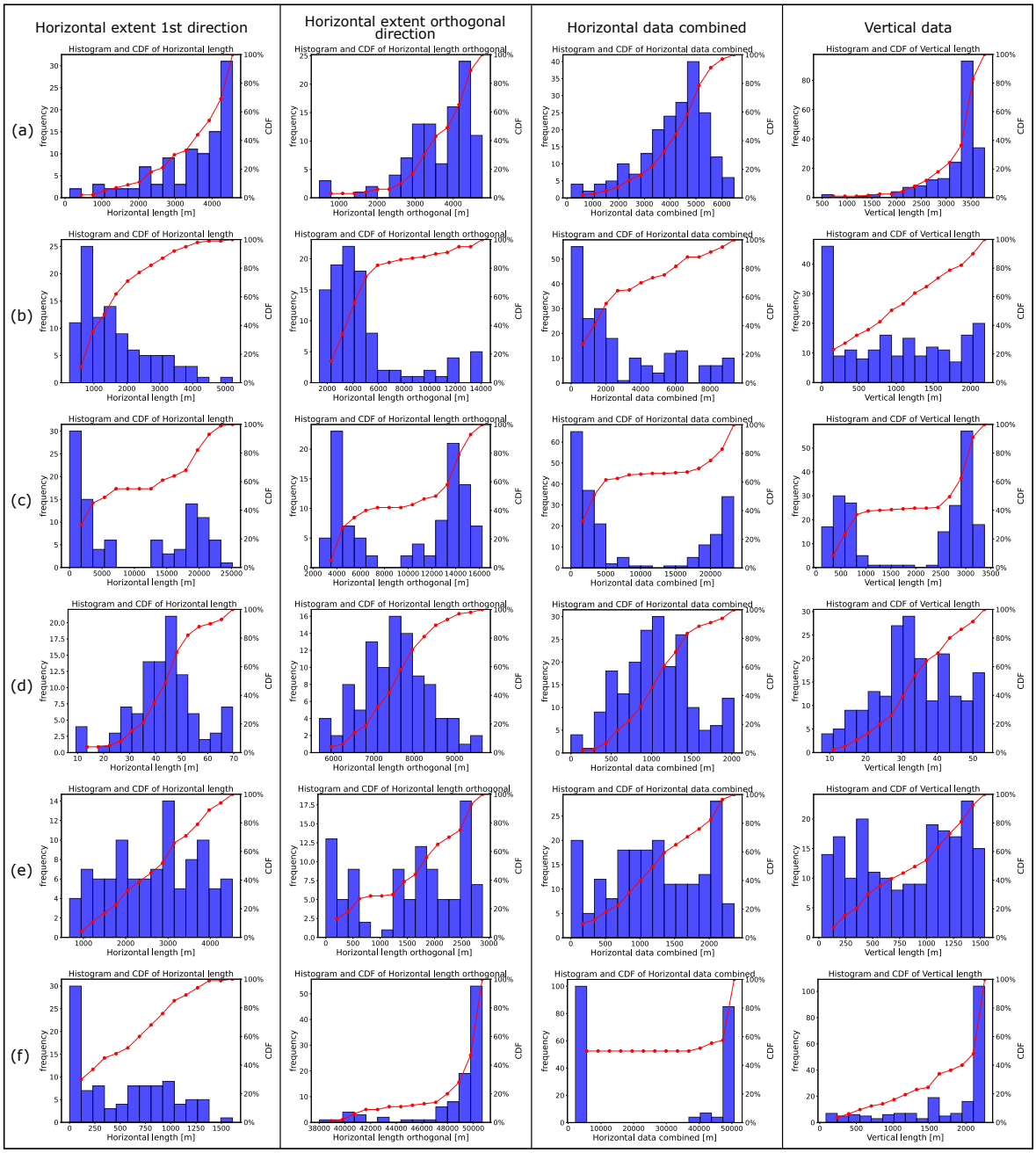


Figure 3.9: Example cases for the variability of data distributions (blue) along the corresponding CDF's (red) among dimensional parameters. Row (f) shows distributional shapes standing out for the given parameter

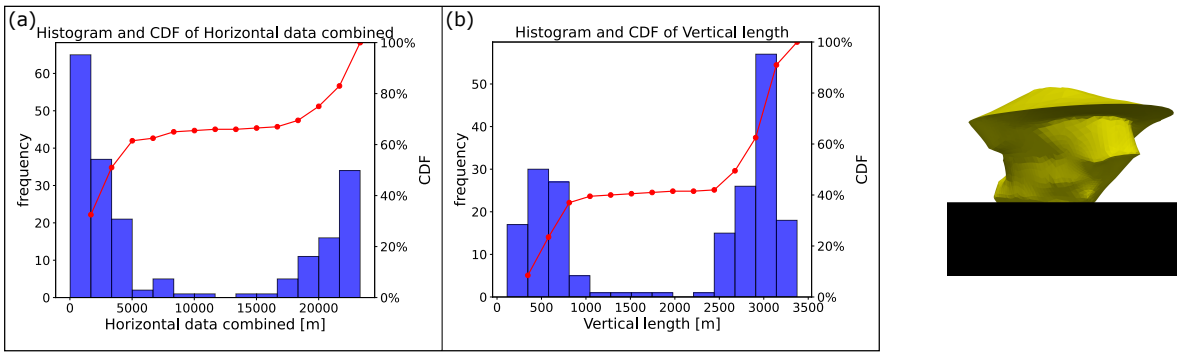


Figure 3.10: Example of a subsurface structure showing overhang configurations ("Neuenhuntorf"), as identifiable from the wide bimodal data distributions of both the combined horizontal as well as vertical data. Model taken from BGR et al. (2022)

Gradient and curvature distributions (Fig. 3.11) display a narrower range of shapes. Gradient data predominantly exhibit unimodal distributions with peak frequencies around zero, though variance differs considerably among datasets (Fig. 3.11a & c). Small subordinate maxima are observed in overflow bins representing extreme gradient values. Curvature histograms (Fig. 3.11b & d) consistently show monomodal distributions with positive skew, as data are constrained to positive values, with the majority concentrated in the smallest value bins. Gradient and curvature data deliver information on the shape of a body through various ways. The amount of infinite gradient values corresponds to the number of vertical line segments within the input mesh. These data combined with very high (positive and negative) gradient values give a good indication of the portion of steep-dipping areas of the subsurface structure (Fig. 3.11a). In contrast, a dominance of gradient values at 0 usually suggests a rather flat top surface, which supports potential corresponding findings from the vertical histogram data, if present. Meanwhile, the prevalence of many small to intermediate gradient data indicates a rather rounded appearance (Fig. 3.11c) and potentially hints at (rounded) overhang configurations. However, curvature data excels at indicating how spherical a given geometry is (see Fig. 3.11d). Although the distributions from both parameters can visually indicate sphericity, the curvature graph does highlight the higher sphericity of a given geometry in comparison to other models (for instance Fig. 3.11b) more clearly.

3.3.2 Cluster analysis after normalization and dimensional reduction

3.3.2.1 Mean-centering for all parameters

Cluster analysis after dimensional reduction was carried out on the data of the irregular input meshes and standard geometries, with 20 percentiles of 5% of the PDF's of the combined horizontal data, vertical data, gradients and curvatures as features, respec-

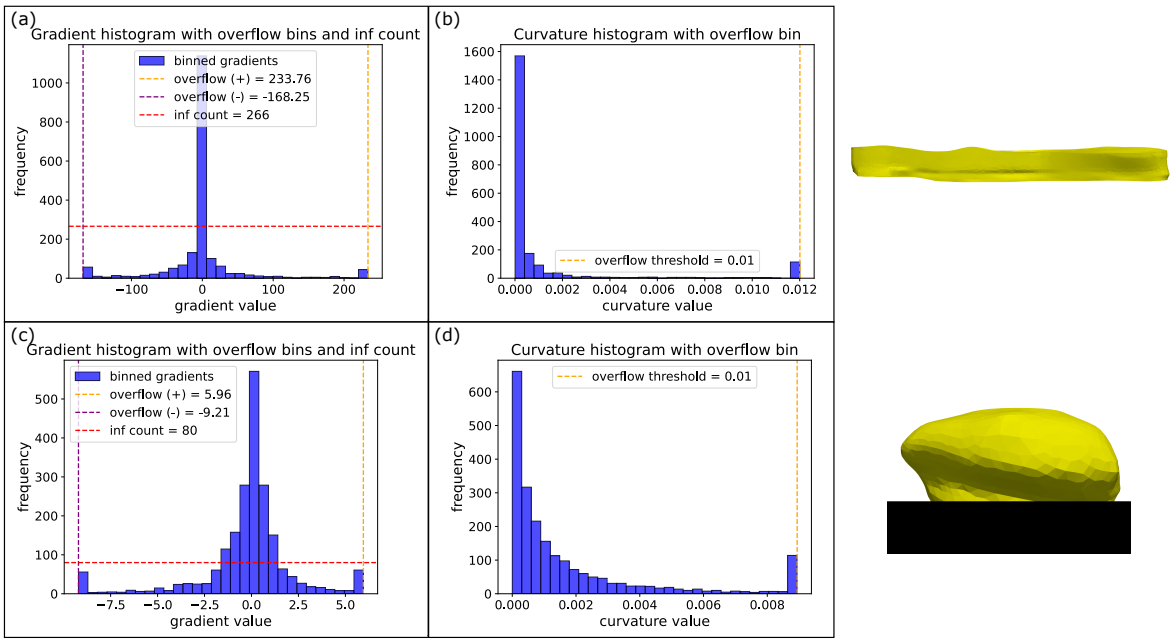


Figure 3.11: Example cases of gradient and curvature data. a) & b) structure "Bevern-Oldendorf"; c) & d) structure "Sievershuetten". Models taken from BGR et al. (2022). The comparatively high sphericity of "Sievershuetten" is captured best in the curvature data

tively. With the combined analysis of the elbow plot and silhouette score (Fig. 3.12b), a cluster number of 18 was determined. The first 14 principal components have to be considered to cover 80% of the variance, as the sum of the first two principle components only explains 25% of the variance (see Fig. 3.12a). The contribution ("loadings") of the different percentiles of the PDF's of the four parameters to the principal components (PC's) is given by the feature contribution matrix (Fig. 3.12c), where bright yellowish colors represent strong positive contributions and dark blue colors considerable negative loadings. In the contribution matrix, the percentiles 0 to 19 correspond to the PDF of the combined horizontal data, followed by the vertical data (20 to 39), gradients (40 to 59) and curvatures (60 to 79). The principal component matrix plot for the PC's 1 to 8 is visible in Fig. 3.13. PC's 9 to 14 were disregarded due to the nature of the cluster results outlined below.

Analyzing the contribution matrix reveals a dominance of gradient percentiles among the function bins showing high (positive or negative) loadings: From PC1 to PC4, higher loadings are exclusively present between the 35 to 40% and 60 to 65% as well as the 95 to 100% gradient bins. PC5 is the first PC exhibiting notable contribution from the vertical data (positively from the 95 to 100% bin) and a more varied distribution from the gradient data. Meanwhile, PC6 marks the first considerable appearance of the horizontal data (higher negative loading from the 0 to 5% bin). The 0 to 5% and 95 to 100% bins of the horizontal data and the 95 to 100% vertical bin are the only bins of these parameters reappearing as considerably contributing bins in later PC's. The curvature data never contributes to a higher degree in our algorithm, as already

noted by Carl et al. (2026). Due to the repeated strong contribution from a small number of gradient bins, informational value of this cluster analysis is limited. The reason for this lies in the per-feature variance being much higher for most gradient bins compared to the bins of the other parameters (Fig. 3.14a). This reflects the nature of the input data: Even though almost all gradient data distributions from the irregular structures have their distinct maximum at small gradients around 0, the variance of positive and negative gradients differs. Thus, when normalizing the data distributions to a range of -1 to 1, the maximum around 0 ends up in different positions in the normalized diagrams between datasets, explaining the large variance seen across most gradient bins. Only PC scores which are influenced strongly by the high loading of the 95 to 100% gradient bin (present in PC1 to PC3; see Fig. 3.12c and Fig. 3.13a & b) reveal additionally, that the corresponding structures show predominantly steep-dipping to vertical surfaces, often located in lateral walls. This mainly applies to the black circle as well as bluish-green square cluster and, probably not universally, to the orange circle, bluish-green diamond and sky-blue circle clusters (color definition after Wong 2011; see also legend of Fig. 3.13). The exceptionally large variance of the 95 to 100% gradient bin (see Fig. 3.14) is caused by the incorporation of infinite gradient values: to enable PCA computation, these values had to be replaced with the highest finite gradient value present in a dataset.

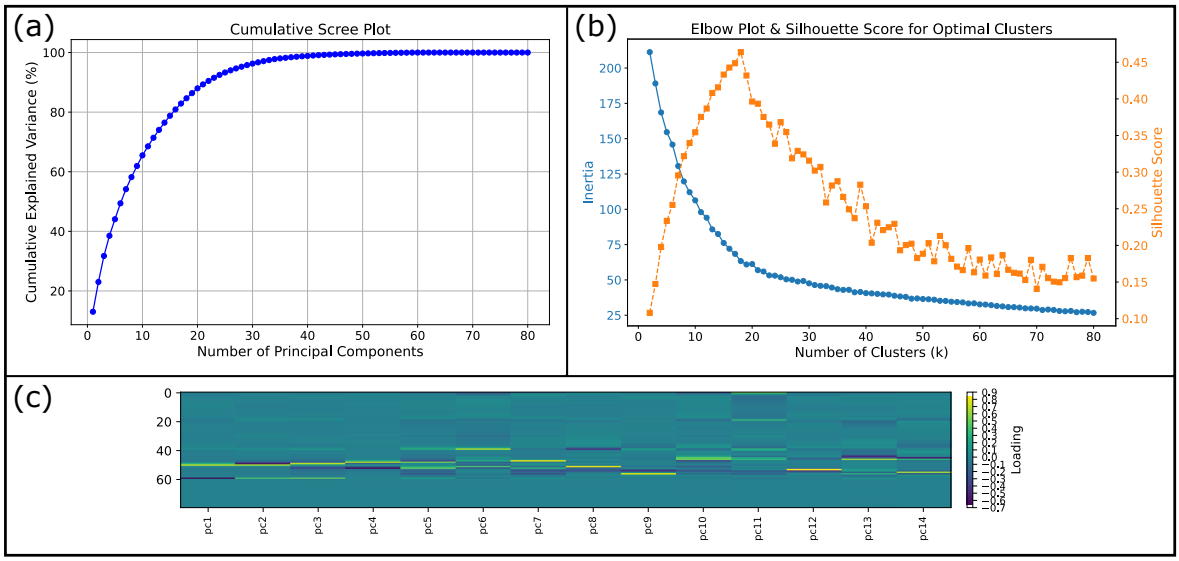


Figure 3.12: Calculated supplementary graphs for the setup and interpretation of the first cluster analysis. a) Cumulative scree plot, visualizing the explained variance with increasing number of principal components. b) Elbow plot and silhouette score for the determination of the cluster number. c) Contribution matrix showing the contribution of the input data (percentiles of the probability density functions of measured parameters) to the principal components

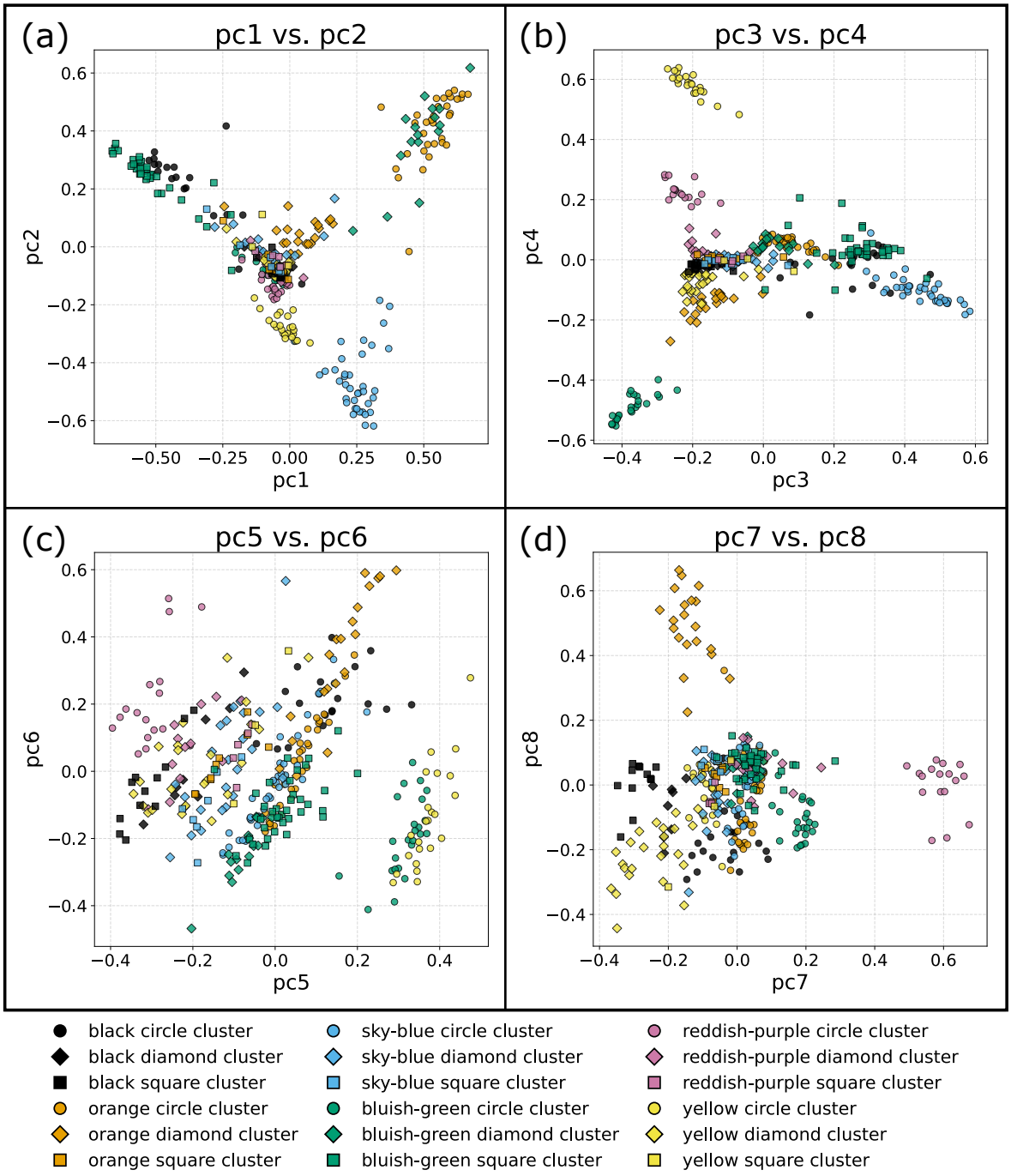


Figure 3.13: Matrix plot of principal components (PC's) for the first cluster analysis, containing 18 clusters. Informational value of this cluster analysis is limited due to a dominating strong contribution from a small number of gradient bins

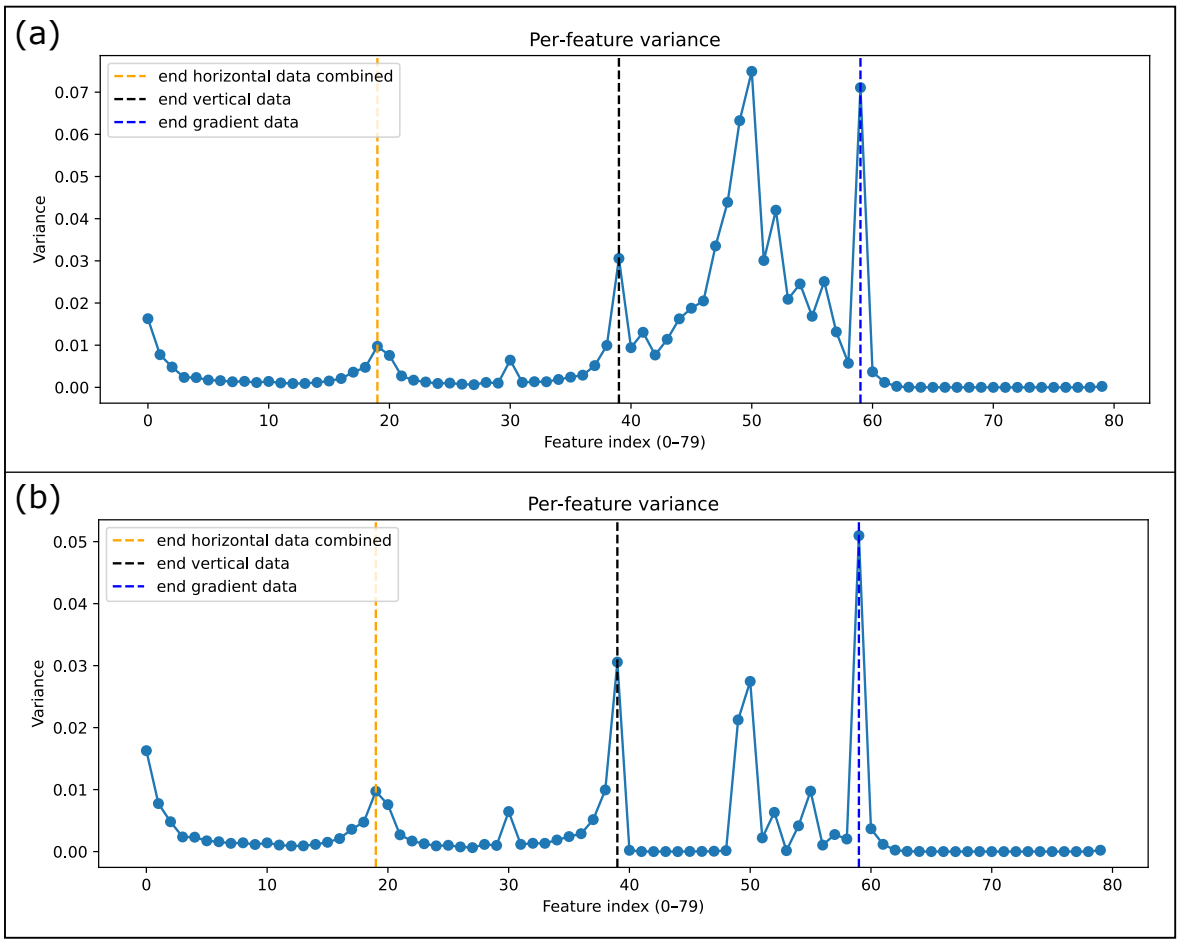


Figure 3.14: Variance per feature (percentiles of the PDF's of the input parameters) in the cluster analyses. a) Using mean centering, the variance is highest for most gradient bins. b) In the second cluster approach, gradients = 0 are aligned with normalized 0, thus correcting the artifact seen from gradient data

3.3.2.2 Gradient data aligned with normalized 0

Given that the first cluster analysis virtually only provides information about gradient data variations between datasets, a second clustering was performed. Here, the varying position of the gradient maximum in the distributions is accounted for by aligning the position of gradients = 0 with the value of 0 in the normalized distributions. Meanwhile, centering of the other parameters was kept unchanged. With this correction, the relative per-feature variance of the respective bins of these parameters gets much higher (see Fig. 3.14b). It could be argued that using two different approaches for centering artificially distorts the input data situation. However, this artifact correction ensures that the peak of very small gradients is co-located for every dataset, thus improving the representation of the unnormalized input data. The cluster number of five in the second cluster analysis was determined based on Fig. 3.15b. The first 14 principal components are considered to cover 85% of the variance (Fig. 3.15a). The feature

contribution matrix is visible in Fig. 3.15c, with the percentiles 0 to 19 corresponding to the PDF of the combined horizontal data, followed by the vertical data (20 to 39), gradients (40 to 59) and curvatures (60 to 79).

The contribution matrix reveals that structures at high positive PC1 scores are mainly influenced by a large data frequency in the 95 to 100% gradient bin, while considerable negative loadings are visible for the 45 to 50% and 50 to 55% gradient bins. For PC2, high positive loadings are seen especially for the 95 to 100% vertical bin and to a minor degree for the 90 to 95% vertical bin. Meanwhile, large negative contributions are present from the 0 to 5% horizontal bin. Additionally, slightly elevated negative loadings are visible for the 5 to 10% and 95 to 100% horizontal bins, the 50 to 55% vertical bin and the 50 to 55% gradient bin. The separation of positive PC1 and PC2 scores is characteristic for the black cluster (see Fig. 3.16a). Given the PC1 scores, black models thus exhibit steep to vertical lateral walls, while PC2 indicates the presence of flat top surfaces. The bluish-green cluster shows positive PC1 and mainly negative PC2 scores, hint-ing at steep-dipping to vertical lateral walls as well, and potential anisotropy. The sky-blue cluster exhibits a range of negative to positive PC1 scores, but it characterized by predominantly negative PC2 values, indicating anisotropy. The orange cluster is predominantly showing negative PC1 scores but varies in PC2. This hints at the presence of more rounded structures and/or the existence of overhang configurations. The reddish-purple cluster combines structures at positive and negative PC1 scores but is exclusively positive regarding PC2. Thus, flat top surfaces for these structures are indicated.

High positive PC3 values are mostly influenced by loadings of the 0 to 5% and 95 to 100% horizontal bins, of the 95 to 100% vertical bin, as well as the 50 to 55% gradient bin. Meanwhile, the only considerably elevated negative contribution is seen from the 45 to 50% gradient bin. For PC4, considerable positive contributions are seen from the 50 to 55% and 95 to 100% gradient bins, and to a minor degree from the 0 to 5% and 50 to 55% vertical bins. On the other hand, elevated negative loadings are primarily given by the two horizontal bins between 0 and 10% and the 45 to 50% as well as 75 to 80% gradient bins. The PC3 and PC4 scores do not add clear information for the interpretation of the black, orange and reddish-purple clusters, as their models range in positive and negative scores for both PC's (see Fig. 3.16b). The bluish-green cluster exhibits predominantly negative PC3 scores, indicating that the top surfaces of the corresponding structures are rather rounded and/or, that overhang configurations are present. Similarly, the mostly negative PC4 scores of the sky-blue cluster indicate, that the models are rather rounded as well and/or exhibit overhangs, in addition to being anisotropic. Particularly high positive contributions to PC5 are given by the 90 to 100% horizontal bins and the 80 to 95% vertical bins. Meanwhile,

considerable negative loadings are seen from the 0 to 10% vertical bin. For PC6, the 0 to 5% horizontal bin, the 95 to 100% vertical bin as well as the 45 to 50% and 95 to 100% gradient bins contribute stronger positively. Elevated negative loadings are given by the 75 to 80% gradient bin. PC5 and PC6 are not useful when interpreting the sky-blue and reddish-purple cluster. Black models are characterized by positive PC6 scores, that underline their interpretation as showing steep-dipping lateral walls and flat top surfaces (see Fig. 3.16c). The additional data from the horizontal bins hints at anisotropy in some cases. Similarly, the positive PC6 scores of most bluish-green models support the hypothesis that these models are steep-dipping and anisotropic. Lastly, for orange models at predominantly negative PC6 scores, the interpretation of a more rounded appearance gets supported. For the PC's 7 to 14, clusters do not show delimitable ranges of positive or negative scores anymore, thus not revealing additional information on the potential model appearances.

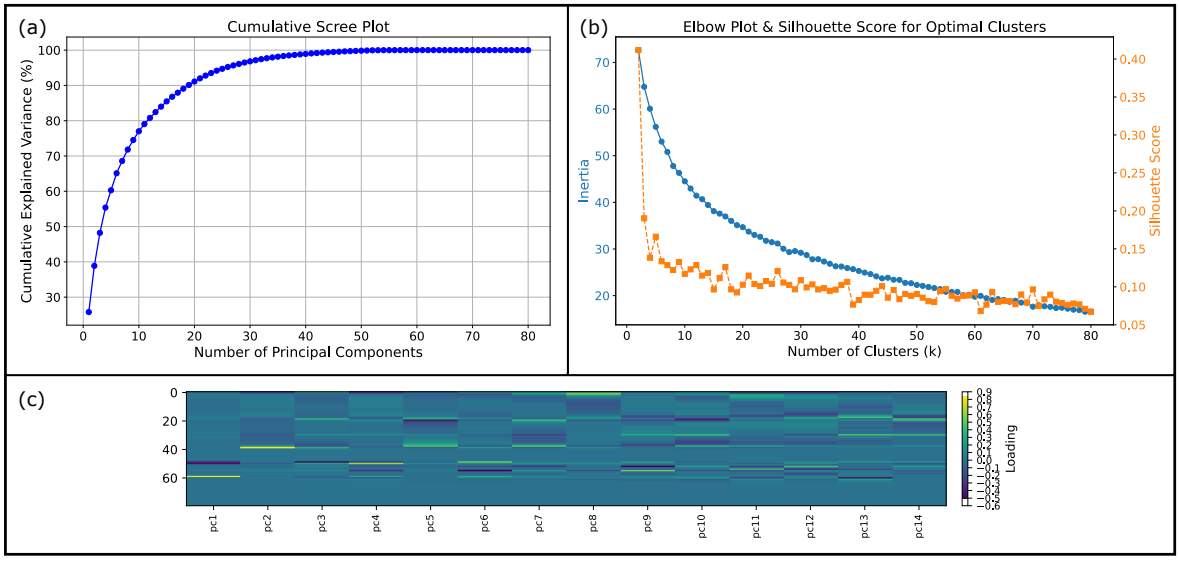


Figure 3.15: Calculated supplementary graphs for the setup and interpretation of the second cluster analysis. a) Cumulative scree plot. b) Elbow plot and silhouette score. c) Contribution matrix showing the contribution of the input data to the principal components. For additional information on the graphs, see text and the caption of Fig. 3.12

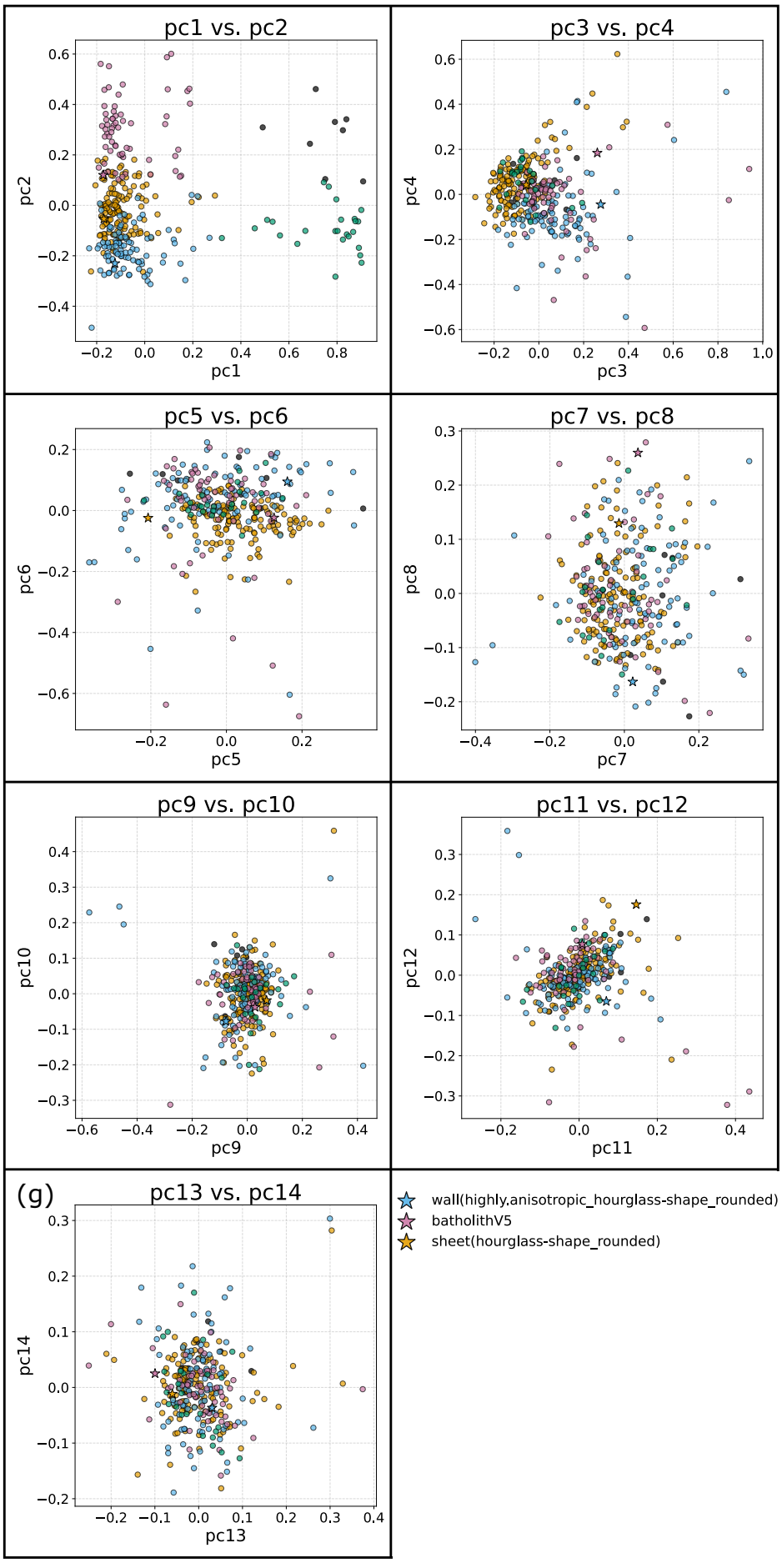


Figure 3.16: Matrix plot of principal components (PC's) for the second cluster analysis aligning gradients = 0 with normalized 0. Larger stars mark a representative benchmark model (standard geometry) per cluster (see legend and Fig. 3.3; note: the other standard geometries are part of the plots as well)

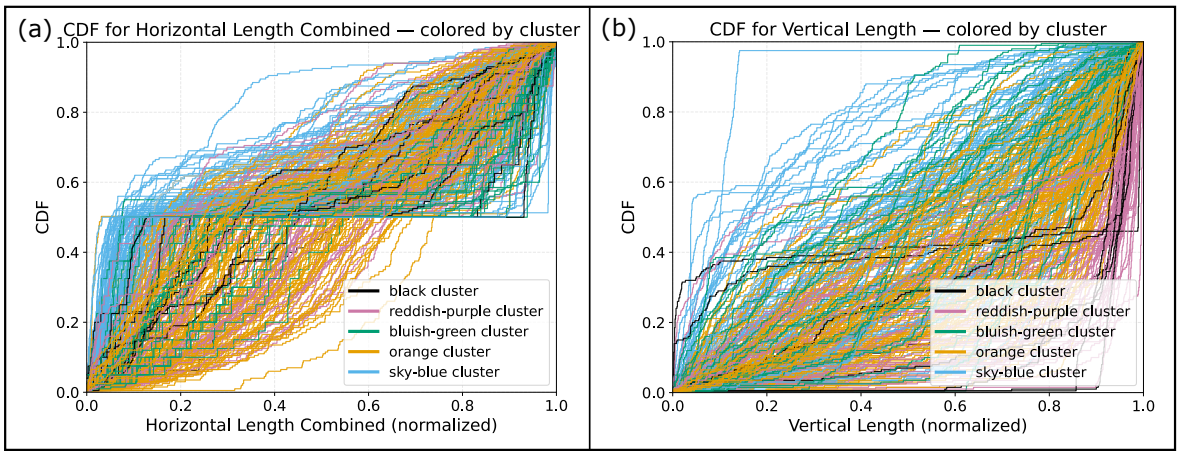


Figure 3.17: Combined cumulative distribution functions of all irregular input meshes of the database colorized according to the results of the second cluster approach. a) CDF's of the combined horizontal data. b) CDF's of the vertical data. For separated plots per cluster, see appendix Fig. A3.1

Figure 3.17 illustrates the cluster results of the second approach on the CDF's of the irregular input models: the CDF of every structure is colorized according to its cluster affiliation (for separated plots per cluster, see appendix A3.1). The kink in many of the respective functions in Fig. 3.17a supports the interpretation that the sky-blue and bluish-green models are predominantly considerably anisotropic, while the structures in the other clusters are rather isotropic to slightly anisotropic in most cases. The flat appearance of top surfaces for most reddish-purple and black models is indicated in Fig. 3.17b, by the exponential shapes of the CDF's. The interpreted overhang configurations partially present in the orange, bluish-green and sky-blue clusters are difficult to identify, as this would require the simultaneous assessment of both combined horizontal and vertical distributions of individual datasets (see also Subsect. 3.3.1).

Figure 3.18 shows the distances of datasets from the respective cluster centroid across dimensions. The mean distance and standard deviations are indicated in the histograms. The coefficient of variation ($CV = \textit{standard deviation} / \textit{mean}$) is indicated just like the amount of outliers defined by mean + 3 standard deviations. The respective distance of the chosen representative standard geometry (see below) is marked as a vertical bluish-green line. Note, that there are no standard geometries located in the bluish-green and black clusters. The lowest CV's are visible for the black and bluish-green clusters (Fig. 3.18a & c), while the highest values can be reported for the reddish-purple and sky-blue clusters (Fig. 3.18b & e). The standard deviations reveal similar trends to the CV's: The narrowest distributions are seen for the black and bluish-green clusters, while the spread of the other three clusters is much larger. However, in general, Figs. 3.16 and 3.18 clearly show, that clusters are not very compact and overlap. The low compactness of clusters reproduces the nature of the underlying input data: As subsurface structures vary in distinct ranges regarding the assessed geometric parameters, clear cluster separation is not to be expected. The stretch of

clusters across positive and negative PC scores for most PC diagrams and clusters indicates that a higher number of clusters potentially could have facilitated the cluster interpretability regarding the geometric appearance of input models. In all histograms of Fig. 3.18, the outlier models seen in Fig. 3.16 are clearly recognizable. These mainly correspond to specific standard geometries (see below).

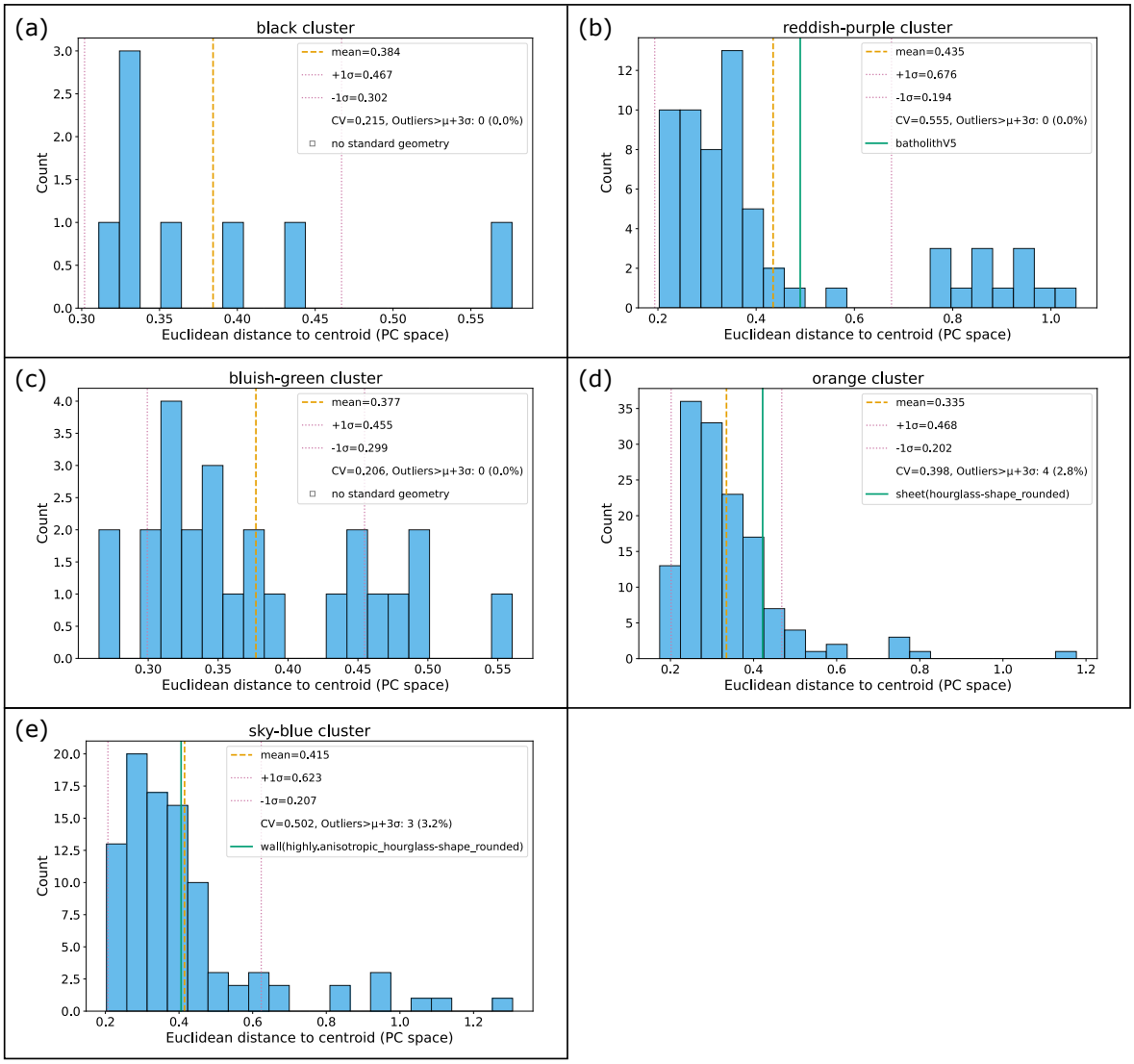


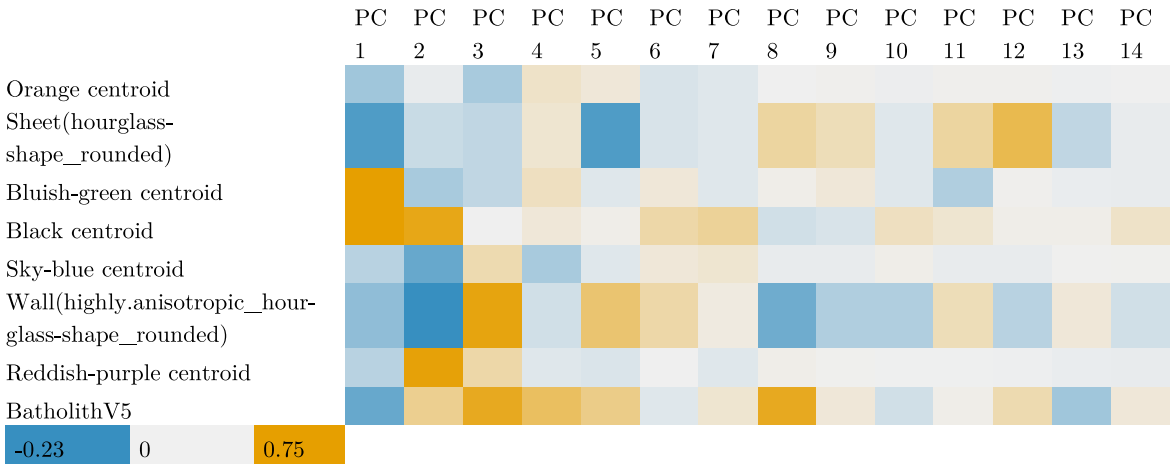
Figure 3.18: Distance histograms of datasets to the respective cluster centroid. Mean model distance and standard deviations are marked in orange and reddish-purple, respectively. The corresponding standard geometry to that cluster is marked in bluish-green

Relying on the results of the second cluster approach, the subsurface datasets can be categorized and assigned to representative standard geometries. As establishing 25 groups of datasets (corresponding to 25 standard geometries) would be too compartmentalized, we attempted to link the clusters of the second cluster approach to a representative standard geometry reproducing the cluster's geometric characteristics (see highlighted models in Fig. 3.16). For the black and bluish-green clusters, no standard geometries cluster among the real subsurface datasets. Assignment of standard

geometries to clusters does not always correspond to a "perfect" representation, as standard geometries are distributed heterogeneously. This is shown in Table 3.2, indicating the differences in PC scores between the cluster centroids and the respective standard geometry chosen to represent a cluster (numeric PC scores and the data of the other standard geometries are provided in the appendix). For the reddish-purple cluster, the standard geometry "batholithV5" exhibits the main property identified to be typical, being characterized by a flat top surface (see Fig. 3.3). For the orange cluster, the marked benchmark is the "sheet(hourglass-shape_rounded)", showing a typical rounded vertical profile and an overhang configuration. Other standard geometries clustering well within the range of real models are the benchmarks "phacolith" and "sheet(cylindric_-rounded)". The two models "wall(highly.anisotropic_hourglass-shape_rounded)" and "wall(highly.anisotropic_cylindric_rounded)" (the former is marked) are representative for the sky-blue cluster, as they exhibit considerable anisotropy and a rounded vertical profile.

While many standard geometries seem to be representative of the geometric range of subsurface datasets in the second cluster approach, some benchmark models plot outside these limits (see Table A3.1 in appendix). The only standard geometry being located outside in all cluster diagrams is the "volcanic.pipe". The "laterally.eroded.layer_-pinchout" plots outside across PC1 to PC4. Meanwhile, the "dyke", "eroded.layer (channel)", "faulted.layer", "flat.layer_sill" and "tilted.layer" cluster outside only in the PC3 vs PC4 diagram, at high PC3 scores. This reflects that although these standard geometries were designed to represent "stratiform" geometries, they still fit to our database of intrusive structures. This is mainly the case, because many crystalline geometries were modelled as "blocky" bodies, horizontally restricted by vertical faults or fault traces and vertically by a rather flat topography. In general, the proximity of the highlighted standard geometries to the subsurface models of similar geometric appearance underlines the applicability of the standard geometries as benchmark models in geomodeling approaches, as discussed by Carl et al. (2026).

Table 3.2: Color-coded PC scores of cluster centroids and assigned standard geometries of the second cluster approach. The representative synthetic standard geometries do not necessarily correspond to the "average" structure (i.e., the centroid) of a cluster. Note that the numeric PC scores can be found in the appendix Table A3.1, alongside the PC scores of the remaining standard geometries



3.3.3 Cluster results in the context of the regional geology

To circle back from the abstraction of the cluster analysis to the geological nature of the input data, the cluster results of the second approach have also been visualized on the maps showing the modelled input meshes in the German subsurface (Fig. 3.19). The maps of Fig. 3.19 were assembled in ParaView. The input meshes are colored corresponding to the five determined clusters. Note that there are no salt structures belonging to the bluish-green and black clusters. The maps allow to assess 1) whether geometrically similar models have been clustered together and 2) how the cluster results correspond to geological features at a higher scale.

In the North German Basin (Fig. 3.19a), anisotropic salt walls are predominantly associated with graben and trough structures of similar orientation (e.g., Maystrenko et al. 2008; Scheck-Wenderoth et al. 2008). Two main groups can be identified: 1) roughly N-S striking structures in the Glückstadt Graben and adjacent Westholstein, Eastholstein and Hamburg Troughs as well as the Horn Graben. These are all situated in the northern parts of the covered area. 2) Walls in WNW-ESE oriented grabens and sub-basins following the main direction of the Central European Basin System, the largest one being the Lower Saxony Basin. Both groups of walls are mainly covered by the sky-blue cluster, that also includes most considerably anisotropic walls not being associated with large structural elements. However, some walls have also been clustered among the other two clusters. This is especially true for the orange cluster, but a very prominent structure in the Westholstein Trough has been assigned to the reddish-purple cluster as well. This is due to additional geometric characteristics discussed below. Away from the large structural elements facilitating wall develop-

ment, most intrusive salt bodies are isotropic to slightly anisotropic. This is captured largely by the orange and reddish-purple clusters. Given the visualized cluster results in Fig. 3.19a, the cluster approach does a reasonable job at differentiating geometries of varying anisotropy, thus also separating salt domes originating in different structural settings. However, as our approach is purely geometric and independent of a body's orientation, it cannot indicate the strike of a salt wall, which can add valuable information to geological interpretation. Another geometric characteristic assessable from the cluster analysis is the shape of the top surfaces. Among the intrusive salt structures, flat top surfaces and more rounded shapes can be observed. This reflects the major variations of the tectonic regime throughout geological times, that repeatedly led to uplift and erosion in some sub-basins, grabens and troughs, while other areas experienced concurrent subsidence (e.g., Maystrenko et al. 2008; Scheck-Wenderoth et al. 2008; Stollhofen et al. 2008): Areas of predominant sedimentation were shifting from N-S striking structural elements in the Triassic to more marginal, formerly eroding areas in the Jurassic-Early Cretaceous, before inversion especially of the southern parts of the CEBS starting in the Late Cretaceous reversed the overall trend once again. Given this evolution, the character of the top surface of individual salt domes is dependent on the rates of subsidence and uplift in their surrounding region in the past, as well as sedimentation rates of younger strata throughout the Mesozoic. In the cluster analysis, this aspect is reflected through a differentiation between the reddish-purple cluster (interpreted as showing flat top surfaces) and the orange and sky-blue clusters (more rounded appearances or rather flat tops while exhibiting overhangs). This pattern is only partially visible in Fig. 3.19a, as some sky-blue and orange structures without overhangs are rather flat as well. However, as erosion and thus flat top surfaces is recognizable in all parts of the NGB given the geological history, it is difficult to assess for which salt bodies the interpretation of the cluster results might not match. However, the assignment of the already-mentioned wall in the Westholstein Trough to the reddish-purple cluster is based on the flat top surface that this body clearly exhibits. The third major characteristic being assessable from the data of our method is the lateral character of the top of a structure. Overhang configurations or hourglass shapes in salt rocks are geometries mostly developed by passive diapirism, as a result of the relative rate of diapir rise being larger than the rate of adjacent sediment accumulation (Hudec and Jackson 2007). In contrast, equal rates lead to cylindric diapir shapes with steep-dipping lateral walls, while higher sediment aggradation rates result in upward tapering. In accordance with the cluster analysis, considerable overhang configurations are present in the sky-blue and orange clusters.

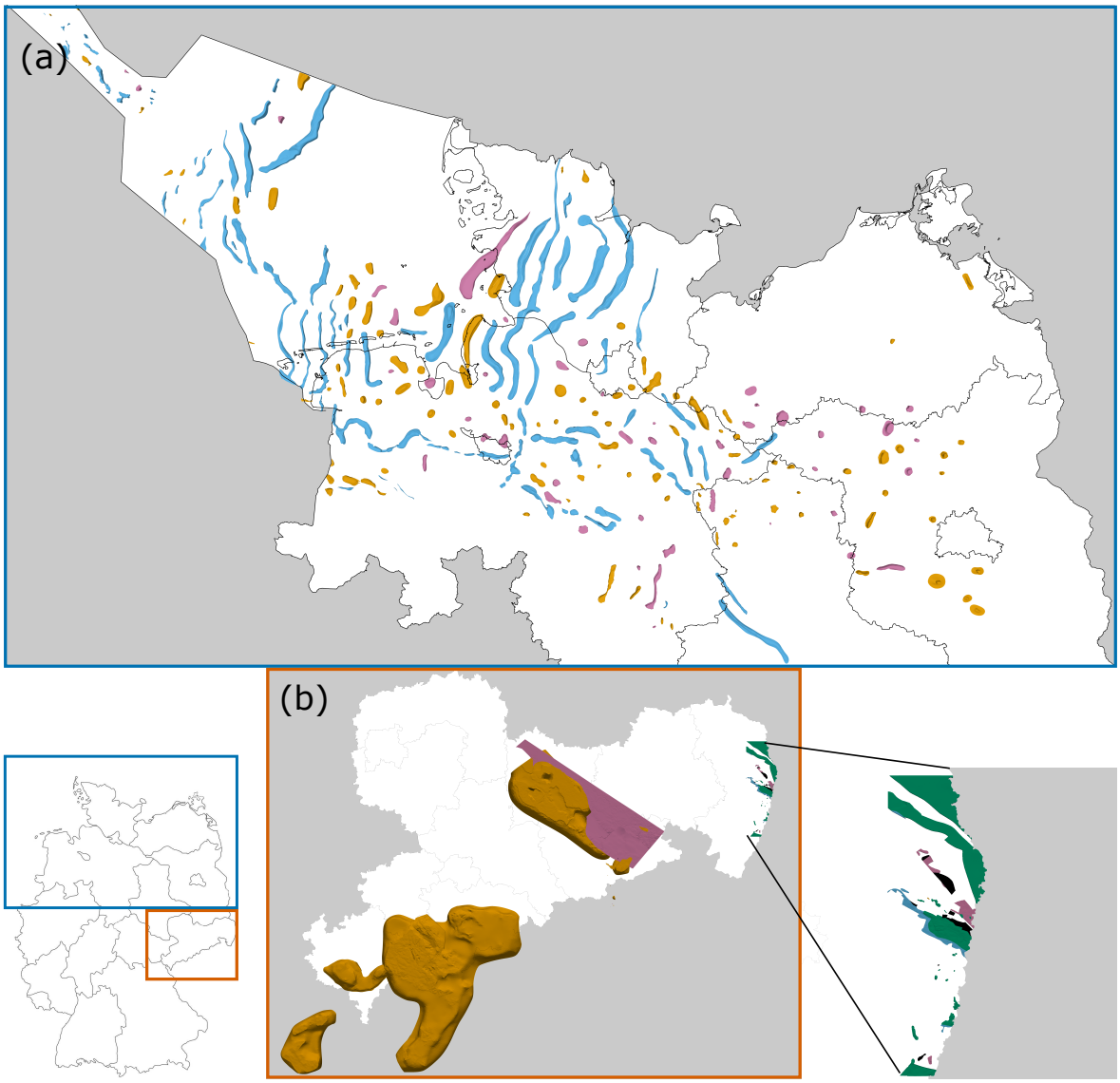


Figure 3.19: Cluster results from the second approach (see also Fig. 3.16) translated onto the 3D models from BGR et al. (2022) and LfULG, to assess the link between geology and clustering results (see text). a) intrusive salt structures from the North German Basin. b) crystalline intrusives from Saxony

In Saxony, the structures covered in the database vary considerably in scale (Fig. 3.19b). Some of the geometric differences observed between models result from differences in input data and model construction, as discussed in Subsect. 3.4.2. These differences are reproduced by the cluster analysis. In addition, some geological features can be put into context with the geometric properties of the clustering as well. The mostly large intrusive structures in the central and southwestern part of the study area are mainly Variscan granitoids with various geochemical and mineralogical characteristics (Eibenstock, Gottesberg, Markersbach, Stolpen and Meissen granites; Sebastian 2013). Their assignment to the orange cluster reflects their heterogenous vertical profiles. Furthermore, the clustering reveals their only slightly anisotropic nature, as similarly recognized for salt structures. The remaining large structure of this region

was assigned to the reddish-purple cluster. This is a part of the Lausitzer Granodioritic massif consisting of cadomic granodiorites and granites (Berger et al. 2011). 31 types of intrusions have been distinguished in the past (Schust and Wasternack 2002), from which many were modelled together by LfULG (2012). The cluster assignment mainly results from the modelled rather flat top surface (largely the modern-day topography), similar to the mentioned case of a large salt wall in Fig. 3.19a.

The smaller area of Saxon models within our database corresponds to the Neiße region. The included structures partially belong to the Lausitzer Granodioritic massif as well, with the remaining being of volcanic origin (Krentz et al. 2015). In the cluster analysis, most models in the Neiße region have been assigned to the bluish-green and black clusters. The models of both clusters are characterized by steep-dipping to vertical lateral walls, indicating that these bodies were modelled laterally based on faults and fault traces. What differentiates the clusters is mostly the existence of bluish-green structures showing overhangs and/or rather rounded top surfaces, while the tops of black models are predominantly flat. Overhang configurations in magmatic rocks result from doming during the ascendancy of melts (Markl 2015): depending on the geomechanical and petrophysical properties of the overburden and the temperature as well as viscosity of the melt, magma advancement is more vertical or lateral. Thus, it can be inferred that the bluish-green bodies have been more viscous and cooler (potentially being granitoid), while the magma of black bodies have been more basaltic/alkaline or encountered overburden more favorable for ascendancy. Meanwhile, the larger, mostly more anisotropic structures that have been assigned to both clusters as well as the other three clusters represent larger complexes/massifs encompassing several individual geo-bodies.

3.4 Discussion

By applying the quantification method to a set of 306 subsurface structures alongside 25 standard geometries, this study validates the functionality of the workflow for irregular 3D objects. The analysis shows what types of subsurface structures are present in the database, by interpreting the varying data distributions to assess key geometric properties such as anisotropy, sphericity and surface morphology. Clustering quantifies geometric dis-/similarities between individual structures and within model groups. The context between the cluster results and regional geology is assessed. These results motivate a discussion on the required adaptations of the quantification method to enable the coverage of irregular open input models, the influence of variations in the

model construction process on the study results, whether such a statistical approach can replace visual analysis of input data for geometric interpretation of datasets and how the present study contributes to the initial method by Carl et al. (2026).

3.4.1 Implications from the method application to irregular meshes

While the overall method as developed and tested on the regular standard geometries required some assumptions and compromises already (see Carl et al. 2026), additional aspects have to be considered applying the method to the variety of irregular structures.

Carl et al. (2026) noted that the orientation of cross sections normal to the horizontal main axes avoids the creation of several disconnected polygons that could have resulted from measuring the horizontal extents along a regular measurement grid. Still, a structure can be cut multiple times in the horizontal and/or vertical direction if a section slices the input mesh where it shows large variations in its horizontal or vertical extent, due to lateral thickness variations or overhangs, respectively. Thus, the method can produce some inaccurate values when covering highly irregular structures. However, this was found to only have a minor impact on the assignment of models to structural types/regular benchmark geometries.

As described by Carl et al. (2026), the setup of the orthogonal cross sections following the contour of a structure generally results in enlarged measurements for the orthogonal horizontal data and a slightly tailed distribution of the combined horizontal data. Furthermore, as the nature of the segmented approach in irregular structures can lead to a somewhat erratic appearance of an orthogonal section in top view, consecutive segments of it can exhibit considerable differences in their vertical range, depending on the 3D-shape of the input mesh. This might be visible in the cross sections in planar view and is potentially captured in the measurements of the vertical extents.

Our interquartile range (IQR)-based approach to determine the individual base level for vertical dimensional measurements is prone to two types of contrasting exceptional cases: 1) sections might get extended to depth although representing an enclosed polygon, therefore not requiring an artificial reference base level. 2) sections might get detected as an outlier, resulting in them not being extended to depth, although they do not represent closed polygons. Both problems were found to concern at most 20 out of 200 measurements that did not seem to affect the resulting statistics and characteristics of the histograms considerably.

As hypothesized by Carl et al. (2026), covering all input structures scale-independent with two sets of 20 cross sections and a fixed amount of measurements ensures the direct comparability between the datasets of different geo-bodies, but cannot represent

the geometric complexity of larger bodies as well as that of smaller ones. However, as the aim of the methodology is to establish a direct comparability between datasets, having equally sized datasets outweighs the drawback of potentially missing lateral irregularities of large structures. This holds especially true, since 1) most large structures are highly anisotropic salt walls with little lateral irregularity and 2) our overall approach already characterizes the input meshes based on a limited amount of 2D sections. Thus, creating a variable number of sections based on the extents of a structure would not eliminate the general uncertainty arising from this type of discretization.

3.4.2 Influence of input model construction on study results

The input models of our database are structural models created in different projects at different times, using varying software and modeling algorithms. Furthermore, raw input data for modeling varied. For instance, seismic data is available more frequently for northern German salt structures than for crystalline basement geo-bodies from Saxony (LBEG n. d.). Consequently, compromises made during modeling are apparent in the structural models, like the (near) verticality of the lateral walls of many crystalline structures, as they have been modeled based on steep-dipping faults or only on fault traces. Another aspect to consider is the resolution of the structural models, varying according to their intended purpose and input data. However, irrespective of potential weaknesses of these models and input data being used, our method is applicable: (near) vertical lateral walls are recognized as such in the gradient and curvature measurements, while the resolution of a model is bypassed using equidistant transects for dimensional measurements. This makes the quantification approach particular interesting for any measurement that is capable of producing cross sections (thus almost all geophysical measurements and all field geologist interpretations).

3.4.3 Cluster results in the context of the regional geology – implications

Given our assessments, the cluster results can be partially put into the context of the regional geology even though our approach at its core is purely geometric. Divergences result from the nature of the quantitative method (overestimating the anisotropy of more isotropic structures) and the limited depth of the interpretation of the clustering results: as all bins contribute to the PC scores of a dataset, analyzing the highest loadings can only give a general idea of a bodies' characteristics. This is especially true since we attribute few geometric properties to clusters containing dozens of models with partially large PC value ranges. To improve the "accuracy" of interpreting the cluster analysis to assess certain geometric properties like (an-)isotropy, one could consider splitting up parameters into several cluster analyses (for instance using only horizontal

and vertical data at first). Thus, the influence of the variance of certain distribution bins on PC scores of individual datasets would be increased. Given its performance, our approach allows for the quantitative geometric systematization of large subsurface databases without the need to interpret the shape of bodies visually.

3.4.4 Contribution of this study to the initial quantification method

Our work considerably enhances the method established by Carl et al. (2026). After developing the core method based on closed meshes of synthetic, regular geometries in the previous paper and discussing its intended applications, the present study expands the algorithm to open meshes and demonstrates its applicability to the full geometric range of intrusive geo-bodies in the German subsurface. Since intrusive structures tend to exhibit more complex external shapes compared to concordant strata, the applicability of the method to such geo-bodies is anticipated as well. This is especially true, since some intrusive structures of the database of the present study were modelled as rather "blocky" shapes with vertical lateral walls and flat top surfaces, which is a typical appearance of concordant strata in many structural geomodels, where only orientation axes are switched. From a perspective of computational efficiency, the method application to 306 meshes demonstrates that the algorithm is a very efficient tool for the geometric analysis of large databases of large geomodels: the cluster analysis presents all properties at once without requiring a full-scale comparative analysis of implicit model representations with millions of degrees of freedom. While establishing and demonstrating the universal applicability of the method, the present study also proofs that geo-bodies of different rock types relevant as host rocks for nuclear waste disposal show geometric similarities, thus reinforcing the corresponding finding of Carl et al. (2026) based on literature and model reviews. This has implications for the usability of the set of standard geometries for model conceptualization in structural geomodeling as described in Carl et al. (2026): it validates that a large geometric range of synthetic models should be potentially considered in the setup of an early conceptual model instead of a small, manual selection. Furthermore, the present study contextualizes the statistics of the geometric properties with the shaping geological processes of the regional geology. It thus supports the analysis of geometric patterns in regional geology, which aids the assessment of selection criteria for storage capabilities of subsurface geo-bodies. However, in their core, the method results do not require visualization on the 3D models. By approaching the data analysis as shown in Subsect. 3.3.1 and 3.3.2, the introduction of subjective bias in decision making is avoided, for instance regarding the selection of a subset of structures for extensive exploration in an economic project.

3.5 Conclusion

In this publication, we demonstrated the applicability of the shape quantification method established by Carl et al. (2026) to the full geometric range of irregular subsurface structures from the North German Basin and Saxony. The shape quantification algorithm has been extended to allow its application to open input meshes. Analysis of data distributions and CDF's enables the geometric characterization of individual geo-bodies and the determination of the frequency of key structural properties (e.g., considerable anisotropy) in our database. The cluster analysis required an enhancement of the workflow proposed by Carl et al. (2026), as gradient data dominated the data variance in the measured database of the case study. The second cluster approach aligning gradients = 0 to normalized 0 uncovered geometric affiliations between the 306 input structures and the geometric dis-/similarities to the applied set of standard geometries. Furthermore, the clustering revealed that the geometric properties of clusters can be partially put into the context of the regional geology. This is the case despite the discussed challenges that the geometrically diverse database presents to the methodology. With the present study, the capabilities of the method and benchmark models established by Carl et al. (2026) are enhanced and their universal applicability is demonstrated, visualizing an application to a large geometrically diverse database of structural models of different rock types. In the next step, the quantification method will be coupled with a spatial interpolation algorithm. It will then be applied to datasets of sparse, unmodeled input data in a framework studying the impact of progressively reduced datasets on geomodeling results.

Code and data availability

Method development was carried out in Python. The methodology mostly relies on the capabilities of the libraries Shapely (https://shapely.readthedocs.io/en/stable/), PyVista (https://pyvista.org/) and Plotly (https://plotly.com/). The python code, the meshes of standard geometries and subsurface models (as .vtk-files) and the datasets of raw dimensional, gradient and curvature data are stored at
https://doi.org/10.5281/zenodo.17611418, Carl (2025).

Author contribution

F. Carl: writing - original draft, writing - review and editing, methodology, software, investigation, formal analysis, conceptualization, visualization. J. Yang: writing - review and editing, conceptualization. M. Colling Cassel: writing - review and editing,

conceptualization. F. Wellmann: writing - review and editing, supervision, funding acquisition. P. Achtziger-Zupančič: writing - review and editing, conceptualization, supervision, funding acquisition.

Declaration of competing interest

The authors declare the following financial interests/personal relationships which may be considered as potential competing interests: Friedrich Carl, Jian Yang and Marlise Colling Cassel are funded by the German Federal Company for Radioactive Waste Disposal (BGE). Other authors declare that they have no conflict of interest.

Declaration of generative AI and AI-assisted technologies in the manuscript preparation process

During the preparation of this work the authors used ChatGPT in order to accelerate code generation, for debugging and to improve documentation. After using this tool/service, the authors reviewed and edited the content as needed and take full responsibility for the content of the published article.

Acknowledgements

This study was conducted as part of the GeoBlocks project. GeoBlocks is a collaboration of RWTH Aachen University, University of Aberdeen and the German Federal Institute for Geosciences and Natural Resources (BGR) within the research cluster URS (Uncertainty and Robustness with regard to the Safety of a repository for high-level radioactive waste), funded by the German Federal Company for Radioactive Waste Disposal (BGE), with the main objective being the creation of an open-source workflow for geological modeling that includes the quantification and visualization of uncertainties and aims at the optimization of sampling procedures. We thank for the financial support by BGE. The authors would also like to thank BGR and LfULG for the data provided to the study. Two anonymous reviewers are thanked for their constructive and thorough reviews, which helped to improve the paper significantly.

References

Abramovitz, T. and Thybo, H. (1999). "Pre-Zechstein structures around the MONA LISA deep seismic lines in the southern Horn Graben area". en. In: *Bulletin of the Geological Society of Denmark* 45, pp. 99–116. DOI: 10.37570/bgsd-1998-45-10. URL: https://www.researchgate.net/publication/238620830_Pre-Zechstein_structures_around_the_MONA_LISA_deep_seismic_lines_in_the_southern_Horn_Graben_area (visited on 11/30/2024).

Achtziger-Zupančič, P., Loew, S., and Hiller, A. (2017). "Factors controlling the permeability distribution in fault vein zones surrounding granitic intrusions (Ore Mountains/Germany)". en. In: *Journal of Geophysical Research: Solid Earth* 122.3, pp. 1876–1899. ISSN: 2169-9356. DOI: 10.1002/2016JB013619. URL: https://onlinelibrary.wiley.com/doi/abs/10.1002/2016JB013619 (visited on 06/29/2025).

Ahlrichs, N., Hübscher, C., Noack, V., Schnabel, M., Damm, V., and Krawczyk, C. M. (2020). "Structural Evolution at the Northeast North German Basin Margin: From Initial Triassic Salt Movement to Late Cretaceous-Cenozoic Remobilization". en. In: *Tectonics* 39.7. ISSN: 1944-9194. DOI: 10.1029/2019TC005927. URL: https://onlinelibrary.wiley.com/doi/abs/10.1029/2019TC005927 (visited on 06/29/2025).

Altuhafi, F., O'Sullivan, C., and Cavarretta, I. (2013). "Analysis of an Image-Based Method to Quantify the Size and Shape of Sand Particles". EN. In: *Journal of Geotechnical and Geoenvironmental Engineering* 139.8, pp. 1290–1307. ISSN: 1943-5606. DOI: 10.1061/(ASCE)GT.1943-5606.0000855. URL: https://ascelibrary.org/doi/10.1061/%28ASCE%29GT.1943-5606.0000855 (visited on 10/22/2025).

Andreani, L., Stanek, K. P., Gloaguen, R., Krentz, O., and Domínguez-González, L. (2014). "DEM-Based Analysis of Interactions between Tectonics and Landscapes in the Ore Mountains and Eger Rift (East Germany and NW Czech Republic)". en. In: *Remote Sensing* 6.9, pp. 7971–8001. ISSN: 2072-4292. DOI: 10.3390/rs6097971. URL: https://www.mdpi.com/2072-4292/6/9/7971 (visited on 01/12/2026).

Bachmann, G., Voigt, T., Bayer, U., Eynatten, H. von, Legler, B., and Littke, R. (2008). "Depositional history and sedimentary cycles in the Central European Basin System". In: *Dynamics of Complex Intracontinental Basins : the Example of the Central European Basin System*. Ed. by R. Littke, U. Bayer, D. Gajewski, and S. Nelskamp. Springer Berlin, pp. 156–172. ISBN: ISBN: 978-3-540-85084-7. URL: https://gfzpublic.gfz-potsdam.de/pubman/faces/ViewItemFullPage.jsp?itemId=item_238809_1 (visited on 11/30/2024).

Bayer, U., Scheck-Wenderoth, M., Rabbel, W., Krawczyk, C. M., Götze, H.-J., Stiller, M., Beilecke, T., Marotta, A. M., Barrio-Alvers, L., and Kuder, J. (1999). "An integrated study of the NE German Basin". In: *Tectonophysics* 314.1-3, pp. 285–307. DOI: 10.1016/S0040-1951(99)00249-8. URL: https://gfzpublic.gfz-potsdam.de/pubman/faces/ViewItemFullPage.jsp?itemId=item_227768_3 (visited on 11/30/2024).

Berger, H., Felix, M., Görne, S., Koch, E., Krentz, O., Förster, H., Konietzky, H., Lunow, C., Walter, K., Schütz, H., Stanek, L., and Wagner, S. (2011). "Tiefengeothermie Sachsen". In: *Schriftenreihe des LfULG* 09/2011. URL: https://www.researchgate.net/publication/310440017_Tiefengeothermie_Sachsen (visited on 04/04/2026).

Best, G., Kockel, F., and Schöneich, H. (1983). "Geological History of the Southern Horn Graben". en. In: *Petroleum Geology of the Southeastern North Sea and the Adjacent Onshore Areas: (The Hague, 1982)*. Ed. by J. P. H. Kaasschieter and T. J. A. Reijers. Dordrecht: Springer Netherlands, pp. 25–33. ISBN: 978-94-009-5532-5. DOI: 10.1007/978-94-009-5532-5_2. URL: https://doi.org/10.1007/978-94-009-5532-5_2 (visited on 06/29/2025).

Betz, D., Führer, F., Greiner, G., and Plein, E. (1987). "Evolution of the Lower Saxony Basin". In: *Tectonophysics*. Compressional Intra-Plate Deformations in the Alpine Foreland 137.1, pp. 127–170. ISSN: 0040-1951. DOI: 10.1016/0040-1951(87)90319-2. URL: https://www.sciencedirect.com/science/article/pii/0040195187903192 (visited on 11/30/2024).

BGR, LAGB, LBEG, LBGR, LLUR, and LUNG (2022). *3D-Modell des geologischen Untergrundes des Norddeutschen Beckens (Projekt TUNB) Erstveröffentlichung 2021, Version 2022*. DOI: https://gst.bgr.de. URL: https://gst.bgr.de,%20Abgerufen%20am%201.12.xn--2024%20allgemeine%20geschftsbedingungen,%20siehe%20https:-qde//www.bgr.bund.de/AGB%20General%20terms%20and%20conditions,%20see%20https://www.bgr.bund.de/AGB_en.%E2%80%9C (visited on 12/01/2024).

Brink, H. J., Dürschner, H., and Trappe, H. (1992). "Some aspects of the late and post-Variscan development of the Northwestern German Basin". In: *Tectonophysics*. The European Geotraverse, Part 8 207.1, pp. 65–95. ISSN: 0040-1951. DOI: 10.1016/0040-1951(92)90472-I. URL: https://www.sciencedirect.com/science/article/pii/004019519290472I (visited on 01/12/2026).

Carl, F. (2025). *FriedrichCarl97/Carlet- al.-b-in-review: Carl. et al.(b) assets V. 1.0, Zenodo [code and data set]*. DOI: 10.5281/zenodo.17611419.

Carl, F., Angeles Gonzalez de Lucio, G. de los, Yang, J., Achtziger-Zupančič, P., Kukla, P. A., Bense, F., and Wellmann, J. F. (2023). "Host rock analysis for the German nuclear waste disposal site-selection: review of subsurface geometries and input data for geological modelling". In: *RING*. URL: https://www.ring-team.org/research-publications/ring-meeting-papers?view=pub&id=223007 (visited on 12/02/2024).

Carl, F., Yang, J., Colling Cassel, M., Wellmann, F., and Achtziger-Zupančič, P. (2026). "Quantitative comparison of three-dimensional bodies using geometrical properties to validate the dissimilarity of a standard collection of 3D geomodels". English. In: *Solid Earth* 17.1, pp. 155–178. ISSN: 1869-9510. DOI: 10.5194/se-17-155-2026. URL: https://se.copernicus.org/articles/17/155/2026/ (visited on 02/04/2026).

Cox, M. R. and Budhu, M. (2008). "A practical approach to grain shape quantification". In: *Engineering Geology* 96.1, pp. 1–16. ISSN: 0013-7952. DOI: 10.1016/j.enggeo.2007.05.005. URL: https://www.sciencedirect.com/science/article/pii/S0013795207001123 (visited on 10/22/2025).

Dadlez, R., Narkiewicz, M., Stephenson, R. A., Visser, M. T. M., and Wees, J.-D. van (1995). "Tectonic evolution of the Mid-Polish Trough: modelling implications and significance for central European geology". In: *Tectonophysics* 252.1, pp. 179–195. ISSN: 0040-1951. DOI: 10.1016/0040-1951(95)00104-2. URL: https://www.sciencedirect.com/science/article/pii/0040195195001042 (visited on 11/30/2024).

Eide, C. H., Schofield, N., Jerram, D. A., and Howell, J. A. (2017). "Basin-scale architecture of deeply emplaced sill complexes: Jameson Land, East Greenland". In: *Journal of the Geological Society* 174.1, pp. 23–40. DOI: 10.1144/jgs2016-018. URL: https://www.lyellcollection.org/doi/full/10.1144/jgs2016-018 (visited on 09/03/2025).

Fischer, K., Herrendorf, G., Luppold, F. W., Meinsen, J., Poßin, W., Schwarz, C., and Thomas, M. (2018). *GeoBerichte 31 - Neue Erkenntnisse zu Quartär, Jura und Unterkreide in Niedersachsen*. Tech. rep. 31. Landesamt für Bergbau, Energie und Geologie. DOI: 10.48476/geober_31_2018. URL: https://nibis.lbeg.de/doi/DOI.aspx?doi=10.48476/geober_31_2018 (visited on 11/30/2024).

Gast, R. E. (1988). "Rifting im Rotliegenden Niedersachsens". en. In: *Geowissenschaften* 6.4, pp. 115–122. URL: https://www.researchgate.net/publication/302950657_Rifting_im_Rotliegenden_Niedersachsens (visited on 11/30/2024).

Hiller, A. (1995). "Geologischer Bau der Lagerstaetten Haemmerlein und Tellerhaeuser im Westerzgebirge". In: *Z. Geol. Wiss* 23, pp. 599–608.

Hudec, M. R., Jackson, M. P. A., Cottington, N., Vendeville, B. C., Schultz-Ela, D. D., and Dooley, T. P. (2011). *The salt mine: a digital atlas of salt tectonics*. Bureau of Economic Geology Udden book series no. 5. Austin, Tex. : Tulsa, Okla: Bureau of Economic Geology, Jackson School of Geosciences, University of Texas at Austin ; American Association of Petroleum Geologists. ISBN: 978-0-615-51836-7.

Hudec, M. R. and Jackson, M. P. A. (2006). "Growth of allochthonous salt sheets in passive margins and orogens." en. In: *AAPG Bulletin* 90, pp. 1535–1564. DOI: doi:10.1306/05080605143.. URL: https://www.researchgate.net/publication/273336919_Growth_of_allochthonous_salt_sheets_in_passive_margins_and_orogens (visited on 11/30/2024).

— (2007). "Terra infirma: Understanding salt tectonics". In: *Earth-Science Reviews* 82.1, pp. 1–28. ISSN: 0012-8252. DOI: 10.1016/j.earscirev.2007.01.001. URL: https://www.sciencedirect.com/science/article/pii/S0012825207000025 (visited on 11/30/2024).

Jackson, M. and Talbot, C. J. (1986). "External shapes, strain rates, and dynamics of salt structures". In: *GSA Bulletin* 97.3, pp. 305–323. ISSN: 0016-7606. DOI: 10.1130/0016-7606(1986)97<305:ESSRAD>2.0.CO;2. URL: https://doi.org/10.1130/0016-7606(1986)97%3C305:ESSRAD%3E2.0.CO;2 (visited on 09/03/2025).

Jaritz, W. (1974). "Zur Entstehung der Salzstrukturen Nordwestdeutschlands". de. In: *(Geologisches Jahrbuch Reihe A* A 10. ISBN: 9783510964833. URL: https://www.schweizerbart.de/publications/detail/artno/186001030/Zur-Entstehung-der-Salzstrukturen-Nordwestdeutschlands (visited on 11/30/2024).

Jolliffe, I. T. (2002). *Principal Component Analysis*. en. Springer Series in Statistics. New York: Springer-Verlag. ISBN: 978-0-

387-95442-4. DOI: 10.1007/b98835. URL: http://link.springer.com/10.1007/b98835 (visited on 04/23/2025).

Köpping, J., Magee, C., Cruden, A. R., Jackson, C. A.-L., and Norcliffe, J. R. (2022). "The building blocks of igneous sheet intrusions: Insights from 3-D seismic reflection data". In: *Geosphere* 18.1, pp. 156–182. ISSN: 1553-040X. DOI: 10.1130/GES02390.1. URL: https://doi.org/10.1130/GES02390.1 (visited on 09/03/2025).

Kossow, D., Krawczyk, C., McCann, T., Strecker, M., and Negendank, J. F. (2000). "Style and evolution of salt pillows and related structures in the northern part of the Northeast German Basin". en. In: *International Journal of Earth Sciences* 89.3, pp. 652–664. ISSN: 1437-3262. DOI: 10.1007/s005310000116. URL: https://doi.org/10.1007/s005310000116 (visited on 06/29/2025).

Krentz, O., Riedel, P., Reinhardt, S., Bretschneider, M., and Hofmann, K. (2015). "TransGeoTherm – Erdwärmepotenzial in der Neiße-Region". In: *Schriftenreihe des LfULG* 10. URL: https://publikationen.sachsen.de/bdb/artikel/24461 (visited on 04/04/2026).

Kukla, P., Urai, J., and Mohr, M. (2008). "Dynamics of salt structures". In: *Dynamics of Complex Intracontinental Basins: the Example of the Central European Basin System*. Ed. by R. Littke, U. Bayer, D. Gajewski, and S. Nelskamp. Springer Berlin, pp. 291–306. ISBN: 978-3-540-85084-7.

Kuschka, E. (2002). *Zur Tektonik, Verbreitung und Mineralogie sächischer hydrothermaler Mineralgänge*. Freiberg: Sächsisches Landesamt für Umwelt und Geologie. URL: https://swb.bsz-bw.de/DB=2.304/PPNSET?PPN=117296095X (visited on 03/04/2025).

LBEG (n. d.). *Hydrocarbon Information System (KW-FIS)*. URL: https://www.lbeg.niedersachsen.de/energie_rohstoffe/erdoel_und_erdgas/fachinformationssystem/kohlenwasserstoff-fachinformationssystem-kw-fis-670.html (visited on 04/04/2026).

LfULG (2010). *Geologisches 3D Modell Aue*. URL: https://www.umwelt.sachsen.de/umwelt/infosysteme/gst3/?view=7063a8c0-4868-11ed-83fd-8b057a3766b1 (visited on 04/04/2026).

— (2012). *Geologisches 3D Modell der Elbtalzone*. URL: https://www.umwelt.sachsen.de/umwelt/infosysteme/gst3/?view=7063a8c0-4868-11ed-83fd-8b057a3766b1 (visited on 04/04/2026).

— (2014). *Geologisches 3D Modell TransGeoTherm*. URL: https://www.umwelt.sachsen.de/umwelt/infosysteme/gst3/?view=7063a8c0-4868-11ed-83fd-8b057a3766b1 (visited on 04/04/2026).

— (n.d.). *Geologisches 3D Modell Erzgebirge-Fichtelgebirge-Komplex*. URL: https://www.umwelt.sachsen.de/umwelt/infosysteme/gst3/?view=7063a8c0-4868-11ed-83fd-8b057a3766b1 (visited on 04/04/2026).

LfULG and CGS (2012). *Geologisches 3D Modell der Altenberg-Teplice-Caldera (ATC)*. URL: https://www.umwelt.sachsen.de/umwelt/infosysteme/gst3/?view=7063a8c0-4868-11ed-83fd-8b057a3766b1 (visited on 04/04/2026).

— (2020). *Geologisches 3D Modell Neubaustrecke Dresden-Prag 2020*. URL: https://www.umwelt.sachsen.de/umwelt/infosysteme/gst3/?view=7063a8c0-4868-11ed-83fd-8b057a3766b1 (visited on 04/04/2026).

Lindsay, M. D., Jessell, M. W., Ailleres, L., Perrouty, S., Kemp, E. de, and Betts, P. G. (2013). "Geodiversity: Exploration of 3D geological model space". In: *Tectonophysics* 594, pp. 27–37. ISSN: 0040-1951. DOI: 10.1016/j.tecto.2013.03.013. URL: https://www.sciencedirect.com/science/article/pii/S004019511300187X (visited on 04/04/2025).

Liro, L. M. (1992). "Distribution of shallow salt structures, lower slope of the northern Gulf of Mexico, USA". In: *Marine and Petroleum Geology* 9.4, pp. 433–451. ISSN: 0264-8172. DOI: 10.1016/0264-8172(92)90053-H. URL: https://www.sciencedirect.com/science/article/pii/026481729290053H (visited on 09/03/2025).

Mark, N. J., Holford, S. P., Schofield, N., Eide, C. H., Pugliese, S., Watson, D. A., and Muirhead, D. (2020). "Structural and lithological controls on the architecture of igneous intrusions: examples from the NW Australian Shelf". en. In: *Petroleum Geoscience* 26.1, pp. 50–69. ISSN: 1354-0793. DOI: 10.1144/petgeo2018-067. URL: https://www.earthdoc.org/content/journals/10.1144/petgeo2018-067 (visited on 09/03/2025).

Markl, G. (2015). *Minerale und Gesteine: Mineralogie – Petrologie – Geochemie*. de. Berlin, Heidelberg: Springer. ISBN: 978-3-662-44627-0. DOI: 10.1007/978-3-662-44628-7. URL: https://link.springer.com/10.1007/978-3-662-44628-7 (visited on 04/04/2025).

Maystrenko, Y., Bayer, U., and Scheck-Wenderoth, M. (2005a). "Structure and evolution of the Glueckstadt Graben due to salt movements". In: *International Journal of Earth Sciences* 94.5-6, pp. 799–814. DOI: 10.1007/s00531-005-0003-4. URL: https://gfzpublic.gfz-potsdam.de/pubman/faces/ViewItemFullPage.jsp?itemId=item_233973_1 (visited on 11/30/2024).

— (2005b). "The Glueckstadt Graben, a sedimentary record between the North and Baltic Sea in north Central Europe". en. In: *Tectonophysics* 397.1-2, pp. 113–126. ISSN: 00401951. DOI: 10.1016/j.tecto.2004.10.004. URL: https://linkinghub.elsevier.com/retrieve/pii/S0040195104004482 (visited on 11/30/2024).

Maystrenko, Y., Bayer, U., Brink, H.-J., and Littke, R. (2008). "The Central European Basin System – an Overview". In: *Dynamics of Complex Intracontinental Basins. The Central European Basin System*. Ed. by R. Littke, U. Bayer, D. Gajewski, and S. Nelskamp. Springer Berlin, pp. 15–34. ISBN: 978-3-540-85084-7.

Neff, A. W. (1960). "Comparisons Between the Salt Anticlines of South Persia and Those of the Paradox Basin". en-US. In: pp. 56–68. URL: https://archives.datapages.com/data/fcgs/data/005/005001/56_four-corners050056.htm (visited on 09/03/2025).

Pälchen, W. and Walter, H. (2011). *Geologie von Sachsen I: Geologischer Bau und Entwicklungsgeschichte*. Stuttgart: E. Schweizerbart'sche Verlagsbuchhandlung (Nägele u. Obermiller). ISBN: 978-3-510-65239-6.

Philpotts, A. and Ague, J. (2009). *Principles of Igneous and Metamorphic Petrology*. 2nd ed. Cambridge: Cambridge University Press. DOI: 10.1017/CBO9780511813429. (Visited on 06/04/2025).

Plein, E. (1990). "The Southern Permian Basin and its Paleogeography". en. In: *Sediments and Environmental Geochemistry: Selected Aspects and Case Histories*. Ed. by D. Heling, P. Rothe, U. Förstner, and P. Stoffers. Berlin, Heidelberg: Springer, pp. 124–133. ISBN: 978-3-642-75097-7. DOI: 10.1007/978-3-642-75097-7_7. URL: https://doi.org/10.1007/978-3-642-75097-7_7 (visited on 11/30/2024).

Röhling, S. (2000). "Der Mittlere Muschelkalk in Bohrungen Norddeutschlands: Fazies, Geochemie, Zyklo- und Sequenzstratigraphie". PhD thesis. Martin-Luther-Universität Halle-Wittenberg. DOI: https://doi.org/10.23689/fidgeo-397. URL: https://e-docs.geo-leo.de/entities/publication/eb8dd734-1b27-46f6-bc41-9018e44508ed (visited on 04/04/2026).

Rötzler, K. (2025). "Die geologische Entwicklung und Metamorphose im Erzgebirge, Ein Exkursionsführer durch das Erzgebirge". en. In: *Geologica Saxonica – Journal of Central European Geology* 71, pp. 31–59. ISSN: 2750-8242, 1617-8467. DOI: 10.3897/gs.71.e147496. URL: https://geologica-saxonica.arphahub.com/article/147496/ (visited on 06/29/2025).

Sannemann, D. (1968). "Salt-stock families in northwestern Germany". In: *AAPG Mem* 8, pp. 261–270.

Scheck, M., Bayer, U., and Lewerenz, B. (2003). "Salt movements in the Northeast German Basin and its relation to major post-Permian tectonic phases; results from 3D structural modelling, backstripping and reflection seismic data". In: *Tectonophysics* 361.3-4, pp. 277–299. DOI: doi:10.1016/S0040-1951(02)00650-9. URL: https://gfzpublic.gfz-potsdam.de/pubman/faces/ViewItemOverviewPage.jsp?itemId=item_229407 (visited on 11/30/2024).

Scheck, M., Thybo, H., Lassen, A., Abramovitz, T., and Laigle, M. (2002). "Basement structure in the southern North Sea, offshore Denmark, based on seismic interpretation". In: *Geological Society, London, Special Publications* 201.1, pp. 311–326. DOI: 10.1144/GSL.SP.2002.201.01.15. URL: https://www.lyellcollection.org/doi/abs/10.1144/GSL.SP.2002.201.01.15 (visited on 11/30/2024).

Scheck-Wenderoth, M. and Lamarche, J. (2005). "Crustal memory and basin evolution in the Central European Basin System—new insights from a 3D structural model". In: *Tectonophysics*. Integration of Geophysical and Geological Data and Numerical Models in Basins 397.1, pp. 143–165. ISSN: 0040-1951. DOI: 10.1016/j.tecto.2004.10.007. URL: https://www.sciencedirect.com/science/article/pii/S0040195104004500 (visited on 01/12/2026).

Scheck-Wenderoth, M., Maystrenko, Y., Hübscher, C., Hansen, M., and Mazur, S. (2008). "Dynamics of salt basins". In: *Dynamics of complex intracontinental basins : The Central European Basin System*. Ed. by R. Littke, U. Bayer, D. Gajewski, and S. Nelskamp. Springer-Verlag Berlin, pp. 307–322. ISBN: 978-3-540-85084-7. URL: https://gfzpublic.gfz-potsdam.de/pubman/faces/ViewItemOverviewPage.jsp?itemId=item_237971_1 (visited on 11/30/2024).

Schröder, L., Plein, E., and Bachmann, G. H. (1995). "Stratigraphische Neugliederung des Rotliegend im - Norddeutschen Becken". de. In: *Geologisches Jahrbuch* A.148. (Visited on 11/30/2024).

Schroeder, W., Martin, K. M., and Lorensen, W. (2006). *The Visualization Toolkit, An Object-Oriented Approach To 3D Graphics*. Kitware. ISBN: 978-1-930934-19-1. (Visited on 11/10/2025).

Schulmann, K., Mlčoch, B., and Melka, R. (1996). "High-temperature microstructures and rheology of deformed granite, Erzgebirge, Bohemian Massif". In: *Journal of Structural Geology* 18.6, pp. 719–733. ISSN: 0191-8141. DOI: 10.1016/S0191-8141(96)80007-1. URL: https://www.sciencedirect.com/science/article/pii/S0191814196800071 (visited on 06/29/2025).

Schust, F. and Wasternack, J. (2002). "Granitoid-Typen in postkinematischen Granitoidplutonen: Abbildungilder von autonomen Intrusionsschüben - Beispiele vom Nordrand des Böhmischen Massivs (Erzgebirge-Harz-Flechtinger Scholle-Lausitz)." In: *Z. geol. Wiss* 30, pp. 77–117. URL: http://www.zgw-online.de/en/media/077-021.pdf (visited on 04/04/2026).

Schweizer, D., Blum, P., and Butscher, C. (2017). "Uncertainty assessment in 3-D geological models of increasing complexity". English. In: *Solid Earth* 8.2, pp. 515–530. ISSN: 1869-9510. DOI: 10.5194/se-8-515-2017. URL: https://se.copernicus.org/articles/8/515/2017/ (visited on 04/04/2025).

Sebastian, U. (2013). *Die Geologie des Erzgebirges*. de. Berlin, Heidelberg: Springer. ISBN: 978-3-8274-2976-6 978-3-8274-2977-3. DOI: 10.1007/978-3-8274-2977-3. URL: http://link.springer.com/10.1007/978-3-8274-2977-3 (visited on 03/04/2025).

Stephenson, P. (2018). "The Shoelace Formula & Pick's Theorem". In: *Mathematics in School* 47.4, pp. 35–38. ISSN: 0305-7259. URL: https://www.jstor.org/stable/26534777 (visited on 12/01/2024).

Stokes, W. L. (1982). "Geologic Comparisons and Contrasts, Paradox and Arapien Basins". en-US. In: pp. 1–12. URL: https://archives.datapages.com/data/uga/data/051/051001/1_ugs510001.htm (visited on 09/03/2025).

Stollhofen, H., Bachmann, G. H., Barnasch, J., Bayer, U., Beutler, G., Franz, M., Kästner, M., Legler, B., Mutterlose, J., and Radies, D. (2008). "Upper Rotliegend to Early Cretaceous basin development". In: *Dynamics of Complex Intracontinental Basins : the Example of the Central European Basin System*. Ed. by R. Littke, U. Bayer, D. Gajewski, and S. Nelskamp. Springer Verlag Berlin, pp. 181–210. ISBN: 978-3-540-85084-7. URL: https://gfzpublic.gfz-potsdam.de/pubman/faces/ViewItemFullPage.jsp?itemId=item_238813_1 (visited on 11/30/2024).

Tari, G., Molnar, J., and Ashton, P. (2003). "Examples of salt tectonics from West Africa: a comparative approach". In: *Petroleum Geology of Africa: New Themes and Developing Technologies*. Ed. by T. Arthur, D. S. MacGregor, and N. R. Cameron. Vol. 207. Geological Society of London, pp. 85–104. ISBN: 978-1-86239-128-4. DOI: 10.1144/GSL.SP.2003.207.5. URL: https://doi.org/10.1144/GSL.SP.2003.207.5 (visited on 09/03/2025).

Trusheim, F. (1971). "Zur Bildung der Salzlager im Rotliegenden - und Mesozoikum Mitteleuropas." de. In: *Beihefte zum Geologischen Jahrbuch* 112. URL: https://www.schweizerbart.de/publications/detail/isbn/9783510967391/Beih_112_z_Geol_Jahrb (visited on 06/29/2025).

TUBAF and LfULG (2015). *Geologisches 3D Modell Neubaustrecke Dresden-Prag 2015*. URL: https://www.umwelt.sachsen.de/umwelt/infosysteme/gst3/?view=7063a8c0-4868-11ed-83fd-8b057a3766b1 (visited on 04/04/2026).

Turner, A. K. and Gable, C. W. (2007). "A REVIEW OF GEOLOGICAL MODELING". In: URL: https://api.semanticscholar.org/CorpusID:32656351 (visited on 04/04/2026).

Upton, G. and Cook, I. (1996). *Understanding Statistics*. en. OUP Oxford. ISBN: 978-0-19-914391-7. URL: https://books.google.de/books?id=vXzWG09_SzAC&printsec=frontcover&hl=de&source=gbs_ge_summary_r&cad=0#v=onepage&q&f=false (visited on 04/04/2026).

Wellmann, J. F. and Caumon, G. (2018). "3-D Structural Geological Models: Concepts, Methods, and Uncertainties". English. In: *Advances in Geophysics*. 59. Elsevier, pp. 1–121. DOI: https://doi.org/10.1016/bs.agph.2018.09.001. (Visited on 04/04/2026).

Wenzel, T. (1999). "Mantel- und Krustenkomponenten in den Granitoiden des Meißener Massivs (Elbezone)". In: *Z. geol. Wiss.* 27, pp. 417–426. (Visited on 04/04/2026).

Wong, B. (2011). "Points of view: Color blindness". en. In: *Nature Methods* 8.6, pp. 441–441. ISSN: 1548-7105. DOI: 10.

1038/nmeth.1618. URL: https://www.nature.com/articles/nmeth.1618 (visited on 09/05/2025).

Zhao, B. and Wang, J. (2016). "3D quantitative shape analysis on form, roundness, and compactness with μCT". In: *Powder Technology* 291, pp. 262–275. ISSN: 0032-5910. DOI: 10.1016/j.powtec.2015.12.029. URL: https://www.sciencedirect.com/science/article/pii/S0032591015302345 (visited on 10/22/2025).

Ziegler, P. A. (1990). *Geological Atlas of Western and Central Europe*. Shell Internationale Petroleum Maatschappij B.V. ISBN: 978-90-6644-125-5. (Visited on 04/04/2026).

CHAPTER

FOUR

MINIMUM DATA QUANTITY REQUIREMENTS FOR STRUCTURAL GEOLOGICAL MODELING

This chapter is the draft of a manuscript (April 2026):

Carl, F., Yang, J., Back, S., Wellmann, F., Achtziger-Zupančič, P., in prep. Minimum data quantity requirements for structural geological modeling.

Abstract

The appearance and reliability of structural geological models depend strongly on the quality, quantity and spatial distribution of input data. As input data acquisition is expensive and time-consuming, the spatial distribution is commonly sparse and heterogeneous. Thus, it is of great importance to evaluate how much data is required to create realistic geological geometries from typically available subsurface information such as 2D seismic interpretations and boreholes. This study establishes and applies two metrics to assess minimum requirements for data quantities: The mean averaged Kullback-Leibler divergence and the mean Euclidean distance in principal component space, measured between condensed model realizations and a reference. Two 3D models of intrusive salt structures from the German subsurface have been selected statistically as test cases alongside a sphere to cover very diverse geometries. Synthetic datasets in 15 data configurations are randomly extracted from the meshes and interpolated implicitly in 3D to provide an entity of 1500 models per structure as the basis for the analyses. Model realizations are condensed into five different percentile threshold mod-

els per data configuration. These threshold models and the references are geometrically characterized using a previously established shape quantification algorithm. Horizontal, vertical and gradient data is obtained, providing information on the (an-)isotropy, sphericity and surface morphology of models. The geometric data represents the input for the established metrics. The mean averaged Kullback-Leibler divergence assesses model similarity to the reference based on the similarity of parameter distributions. The mean Euclidean distance in principal component space is based on dimensionally reduced parameter data. For both metrics, intermediate values are obtained for every single combination of data configuration and threshold model. Intermediate datasets are analyzed, before the values of the five threshold models per data configuration are averaged to obtain the final metrics. The 15 values per metric are ordered by increasing model similarity to the respective reference, to identify increases of data quantities coinciding with considerable improvements of model similarity. Minimum data quantity requirements are indicated for all three test cases, with the requirements being larger, the higher the structural complexity.

4.1 Introduction

Three-dimensional (3D) geological modeling is an important tool for the visualization and understanding of the subsurface, producing possible realizations of subsurface conditions. At the present day, various input data types can be used in geomodeling, such as surface data, 2D maps and cross sections, borehole data and various geophysical data like e.g., seismics (Wellmann and Caumon 2018). While all obtainable data is considered when building a model, the available subsurface data in an area of interest is usually sparse. This is mostly due to the high acquisition costs of many subsurface data (Bjørlykke 2015). Therefore, sparse, heterogeneously distributed data is the standard in most cases where geoscientists are instructed to create geomodels. It is thus of great interest, to explore how much data is required to create realistic realizations of subsurface geometries with a reasonable uncertainty.

4.1.1 Previous studies

Given the commonly sparse data, various studies have been conducted to assess the impact of the incorporation of additional subsurface data on structural geomodels. In most cases, the influence is evaluated by studying the resulting reduction of model uncertainties. For instance, Wellmann and Regenauer-Lieb (2012) describe the concepts of information entropy (Shannon 1948), fuzzy set entropy (Luca and Termini 1993) and total model entropy/mean entropy in the geomodeling context, as cell/voxel-based measures for the quantitative description and comparison of uncertainties. In essence,

the information entropy quantifies the amount of information that is missing with regard to the position of a geological unit. In their study, the effects of the addition of data as well as different conceptual geological hypotheses have been explored. While data integration mostly reduces the model information entropy, varying hypotheses like the presence of a fault can also increase the entropy in some areas. Wellmann (2013) complements the study of Wellmann and Regenauer-Lieb (2012), by adapting the concepts of joint entropy, mutual information and conditional entropy in the geomodeling context. Joint entropy quantifies the combined uncertainty at two positions in space, while mutual information represents a measure for shared information between two locations. Conditional entropy reveals how new information at a single point can reduce spatial uncertainties, and multivariate conditional entropy extends this concept to information at multiple locations. The introduced measures from information theory are explored in two simple geological scenarios where the reduction of uncertainty regarding the depth of a geological layer by the drilling of a borehole is studied. Schweizer et al. (2017) focus on the effect of data integration on model uncertainty as well, as they apply the concepts of information entropy, total model entropy and fuzzy set entropy as described by Wellmann and Regenauer-Lieb (2012) to a case study from southern Germany. Four geomodels are created with progressively larger and more varied datasets, concurrently increasing model complexity as more structural elements are identified. The growing geometric complexity is recognized in the quantitative assessment of model uncertainty, as it increases uncertainties in some model parts while data integration has been found to reduce uncertainties in other model cells. A similar research objective to Schweizer et al. (2017) is pursued by Wang et al. (2022), who assess the influence of progressively added data on the uncertainties in a geological model used as a basis for simulations of groundwater flow and land subsidence. Lindsay et al. (2012) approach uncertainty quantification through the concept of "stratigraphic variability" to assess model reliability. After perturbing strike and dip data to set up model realizations, their concept is introduced, determining 1) how many stratigraphic units exist among the realizations in individual voxets (the "stratigraphic possibility"), 2) which unit is present most often, and 3) how frequent the other units are ("stratigraphic variability frequency"). After the establishment of the method, it is applied in a case study from southeastern Australia, to quantify the value of additional seismic input data in constraining the geometry of geo-bodies and in reducing uncertainties. Meanwhile, Jessell et al. (2010) study how input data constrain the resulting geomodels by defining a set of misfit functions applicable to assess how well a model realization honors input data and other available information. Spatial information such as outcrop locations, contact coordinates of horizons in boreholes, and orientation data are considered as well as temporal relationships. A reference model based on synthetic input data is created, before 20 randomly perturbed input

datasets and subsequent model realizations are created respectively in four different perturbation configurations. The misfit functions are calculated and partially visualized between the 80 models and the reference, providing quantitative views on how the appearances of geomodels can be constrained given variations in input data. Putz et al. (2006) test the effects of progressively reduced data densities on modeling results for the 2D outcrop map of their 3D model of the Plattengneis Shear Zone in the Eastern Alps. The input dataset is progressively reduced nine times in 10% steps, by randomly removing data of geological contacts and orientations. Based on visual comparison, the authors state that the similarity to the initial model remains rather high until a reduction to 30% of the original input data. While they notice that model quality decreases steadily as expected from the beginning, only the last model of lowest data quantities is seen as being unrecognizable compared to the reference. Carmichael and Ailleres (2016) evaluate the influence of surface orientation data density on geomodels as well, as they assess the performance of six automatic upscaling methods in reproducing the main geological trends in an input dataset. The computation of an initial best-case model considering all data is followed by the application of the upscaling methods with different thresholds for data density to create new datasets. Implicit model realizations are created based on the datasets, and geodiversity metrics after Lindsay et al. (2013) are applied to assess the dis-/similarity in the results between the combinations of upscaling methods and data density thresholds, as a comparison to the initial model. Self-organizing maps are used for the quantified clustering of the models based on these dis-/similarities. The influence of data density on model appearances is also assessed visually, using the stratigraphic variability of Lindsay et al. (2012). Weighted upscaling methods are observed to outperform stochastic removal techniques at preserving dominant geological trends in the initial input data, given similar data quantities. Models of low data densities are identified as statistical outliers of low similarity.

Other more practice-oriented approaches on the data sparsity problem focus on optimized data acquisition, to determine where additional data would cause the highest information gain/reduction in uncertainty. Many studies aim at optimizing drillhole placement, for instance through simulation-based approaches (e.g., Afonseca and Miguel-Silva 2022) or using geostatistical methods (e.g., Hossein-Morshedy et al. 2023). Scheidt et al. (2026) propose a framework combining these different strategies, integrating both statistical learning and geostatistical simulation to assess optimal drillhole placement when data is present in areas adjacent to a target showing sparse data. The statistical relationships between surface geochemistry, geophysical inversions, and models of intrusion and ore grade in the well-explored areas are captured and inform a set of prior realizations of intrusion and ore grade distribution for the target area. Subsequently, these models are used to quantitatively assess the expected uncertainty reduction for each potential drillhole.

Geomodeling with sparse data is prone to produce model realizations showing inconsistencies by ignoring data or geological knowledge. Thus, consistency checking and falsification of realizations are important steps. Parquer et al. (2025) establish a framework for checking the consistency of 3D geomodels automatically based on digitally encoded spatial, temporal and polarity relations as well as geological principles. The framework incorporates all consistent and inconsistent geological situations potentially present between nine types of geological objects in a model, considering a combination of all above-mentioned relations and knowledge. The framework is demonstrated using a proof-of-concept tool, testing parts of it in four case studies. The established tool evaluates the relations within a given geomodel in comparison to the set of all possible relations defined in the framework. Therefore, Parquer et al. (2025) advance the automatic and quantified verification of geological rationality of structural geomodels.

4.1.2 Database

The initial data for the comparative analyses to assess minimum data requirements for representative structural geomodeling have been obtained from pre-modeled meshes. Two structural 3D models of intrusive salt bodies were selected statistically from the TUNB model of the northern German subsurface (BGR et al. 2022), and a sphere model has been chosen additionally to facilitate demonstrating the methodology (see Fig. 4.1). TUNB model selection was based on the cluster analysis in Carl et al. (2026b), as the two models were clustered closest to the respective cluster centroid. This approach ensures that the example structures are geometrically very dissimilar and thus, a wide variety of geometries is covered, when considering the sphere as well. While the structure "Gielow" consists of a stock with a considerable overhang (variations in lateral extents over the vertical range), the structure "Juliusburg_Koestorf-Rosenthal" is a considerably anisotropic salt wall with overhangs (for the salt classification terms, see Hudec and Jackson 2007). Synthetic datasets have been extracted from the meshes, as described in Subsect. 4.2.1.

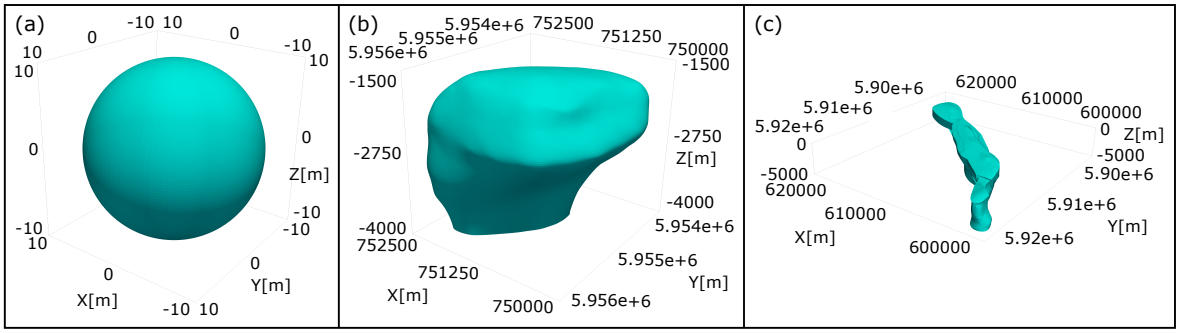


Figure 4.1: 3D models of the three tested structures. a) Sphere. b) Gielow. c) Juliusburg_Koestorf-Rosenthal. Salt bodies in b) and c) are taken from the TUNB model (BGR et al. 2022)

4.1.3 Content and aims of this study

As shown, geoscientific research mostly incorporates the assessment of uncertainty reduction through data integration. To our knowledge only Putz et al. (2006) and Carmichael and Ailleres (2016) have specifically explored how much data is necessary to produce realistic structural geomodels. However, the experiments of Putz et al. (2006) on the effects of reduced data densities on a geomodel have been based only on visual examination, and although the results of Carmichael and Ailleres (2016) are quantitative, they restricted their research to surface orientation data instead of subsurface data types, without identifying the minimum data required in their structural geomodeling case. Therefore, we deem that quantitative metrics are necessary to explore such requirements, that are a key parameter in cost-benefit analyses in exploration. For instance, in the German site selection for a nuclear waste disposal site, regional comparison currently has to be done based on existing, often sparse datasets, before additional data will be acquired in the next stage of the process (BGE 2023). Thus, current geomodeling attempts based on sparse data have a considerable influence on the site selection decision. Consequently, it has to be ensured that these geomodels realistically represent subsurface conditions, despite the variations in input data quantity, spatial distribution and types of available data.

Given the apparent lack of published studies on this topic, we aim at assessing the performance of two quantitative metrics to evaluate minimum required data quantities for geomodeling: the (mean) averaged Kullback-Leibler divergence and the (mean) Euclidean distance in principal component space, measured between condensed model realizations and a reference. To allow for the application of these metrics, the three selected reference models have to be reproduced with different input data densities, and all models have to be geometrically quantified using the algorithm established and applied by Carl et al. (2026a) and Carl et al. (2026b). 15 data configurations of varying amounts of 1D and 2D data, representing e.g., 1D boreholes and 2D geophysical data, have been synthetically extracted from the references and interpolated to create 100 model realizations respectively. The model realizations have been reduced to five threshold models per data configuration, that are compared to the reference models.

Given the resulting data from the quantification algorithm, the mean averaged Kullback-Leibler divergence and the mean distance in principal component space are computed. Thus, it is assessed whether configurations are present, for which increases in data quantities coincide with considerable improvements of model similarity compared to the respective reference. Therefore, potential minimum requirements for input data quantities are identified. Subsequently, the performance of both metrics is discussed. With this contribution, we aim to define metrics that shed light on the question of how much data is required for reasonably uncertain structural geomodeling for deci-

sions. As data situations for modeling are sparse in most real cases, the application of this method is wide within geosciences and economy. Our paper is subdivided as follows: Sect. 4.2 describes the generation of synthetic datasets, their interpolation and the generation of threshold models, reviews the shape quantification algorithm of Carl et al. (2026a) and outlines the data analysis. Sect. 4.3 presents the two metrics alongside intermediate results. Sect. 4.4 discusses the method design and the comparative performance of both metrics, reflects on what external factors influence the requirements of minimum data quantities and compares the workflow to previously proposed approaches for quantified uncertainty assessment. Sect. 4.5 concludes the study summarizing its main outcomes.

4.2 Methods

4.2.1 Generation of synthetic datasets, model realizations and threshold models

Datasets have been randomly extracted from the triangulated meshes of the sphere and the two intrusive salt structures. This required closed meshes. Thus, the meshes of the TUNB models have been closed with the capabilities of the vtk-python package (Schroeder et al. 2006). From the 3D models, 100 datasets consisting of a fixed amount of randomly oriented vertical 2D cross sections and 1D vertical lines have been created for 15 different data configurations, respectively (see Table 4.1). In the 3D interpolation using the implicit kriging-based method implemented in the open-source Python package GemPy (de la Varga et al. 2019), the sections are discretized into points. For the interpolation, orientation data is required. To mimic the prevalent lack of orientation data in most 2D geophysical dataset types, a single orientation with normal direction [0, 0, 1] (in-plane) has been created at the highest point in terms of z-coordinates of each 2D section (see Fig. 4.2). One accurate orientation has been generated at every point where a borehole intersects the input mesh, without adding measurement uncertainty.

Table 4.1: Overview of the 15 data configurations tested in this study, ranging from very sparse to extensive data situations.

0 sections 10 boreholes	2 sections 2 boreholes	4 sections 4 boreholes
1 section 1 borehole	2 sections 3 boreholes	5 sections 5 boreholes
1 section 2 boreholes	3 sections 1 borehole	8 sections 8 boreholes
1 section 3 boreholes	3 sections 2 boreholes	10 sections 0 boreholes
2 sections 1 borehole	3 sections 3 boreholes	10 sections 10 boreholes

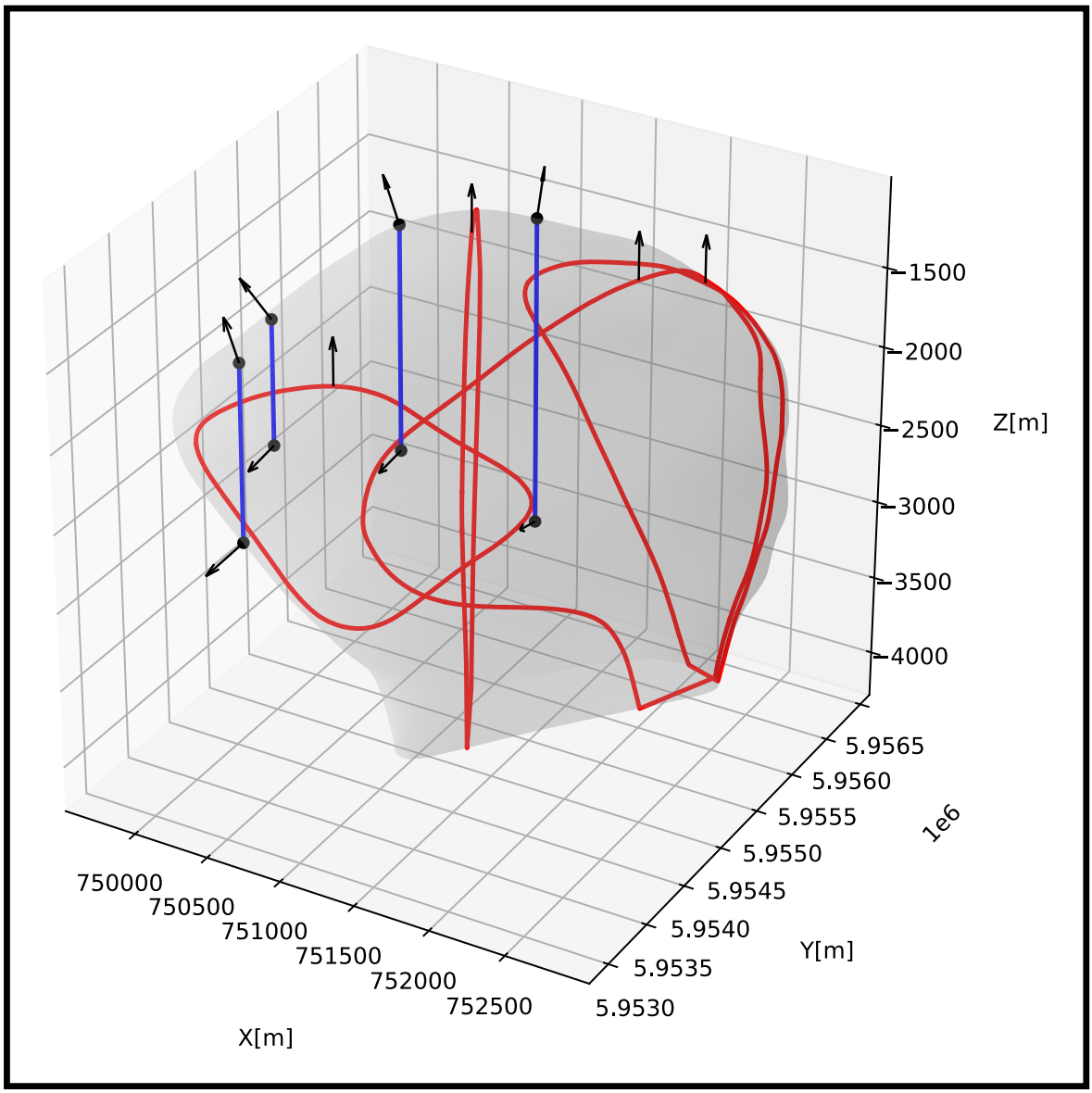


Figure 4.2: Exemplary visualization of the synthetic datasets extracted from the input meshes of the test structures. One orientation in 3D is extracted at every point where a borehole intersects the input mesh. In contrast, only one orientation per cross section is created at its highest point, pointing vertically upwards

After their computation, the 100 model realizations per data configuration have been condensed into 1%-, 25%-, 50%-, 75%- and 99%-explicit percentile block models, including all cells where at least the respective number of model realizations exist for a data configuration. Internal cell faces of block models have been removed, and the exterior surfaces have been smoothened using the capabilities of the vtk-python package, to enable the processing of the block models with the algorithm established by Carl et al. (2026a), as outlined in Subsect. 4.2.2. Using percentile threshold models allows for the comparative analysis of the geometric range of the 100 model realizations in between data configurations with reduced computational effort compared to the analysis of all 1500 realizations per structure. Differences between low and high data quantity

configurations are recognized best in the marginal thresholds. The 1% models often consist of many cells of the model space, as the probability of at least 1/100 realizations being present in a cell is very high. However, the higher the similarity between the realizations of a configuration, the less cells are present in the 1% percentile model, and the higher is also the similarity of this threshold model to the respective reference. The 99% models on the other hand often only consist of few cells, as only cells remain that are present in virtually all model realizations. In fact, for some data configurations of the input structures, the 99% threshold has not been computable, as realizations have been too dissimilar (see e.g., Subsect. 4.3.2.3). Thus, the sizes of the databases are 74 for the sphere and Gielow instead of 75, and 69 for Juliusburg_Koestorf-Rosenthal. Consequently, for the 99% threshold, higher similarity between realizations leads to more remaining cells in the corresponding percentile model, potentially resulting in a higher similarity of the percentile model to the given reference. In contrast to the marginal thresholds, the intermediate percentiles like the 50% models are more similar in between data configurations and compared to the respective reference. On one hand, geometric outliers present in the small percentiles like the 1% thresholds are filtered out, while on the other hand, the shape is not as constrained as in the higher percentiles that show increasingly lower co-occurrences of realizations in the cells. In case all 100 realizations of a data configuration are very similar, all five threshold models are virtually equal as well. The five block models of the data configuration "4 sections 4 boreholes" of all three tested structures are visualized in Fig. 4.3 exemplarily, representing a configuration of intermediate to high data quantities among the chosen sets.

4.2.2 Measurement of geometric data

The threshold models and references have been segmented, and geometric parameters have been measured on the resulting cross sections following the method for the quantitative characterization and comparison of 3D structures established in Carl et al. (2026a). Please refer to the mentioned reference for a detailed explanation of the following algorithm. With this quantification method, the geometric characterization of objects is independent of their orientation in the subsurface, as measurements are conducted along the horizontal main axes of the bodies. The models have been discretized into two sets of cross sections. First, 32 equidistant cross sections whose normal direction is parallel to the longer horizontal axis of the mesh's cuboidal bounding box have been created. These cross sections have been sequentially rotated to reach their targeted orientation normal to the longitudinal main axis of the structure, determined based on the minimized values of the cross-sectional area (Stephenson 2018). Then, cross sections orthogonal to the first set have been assembled from trapezoidal seg-

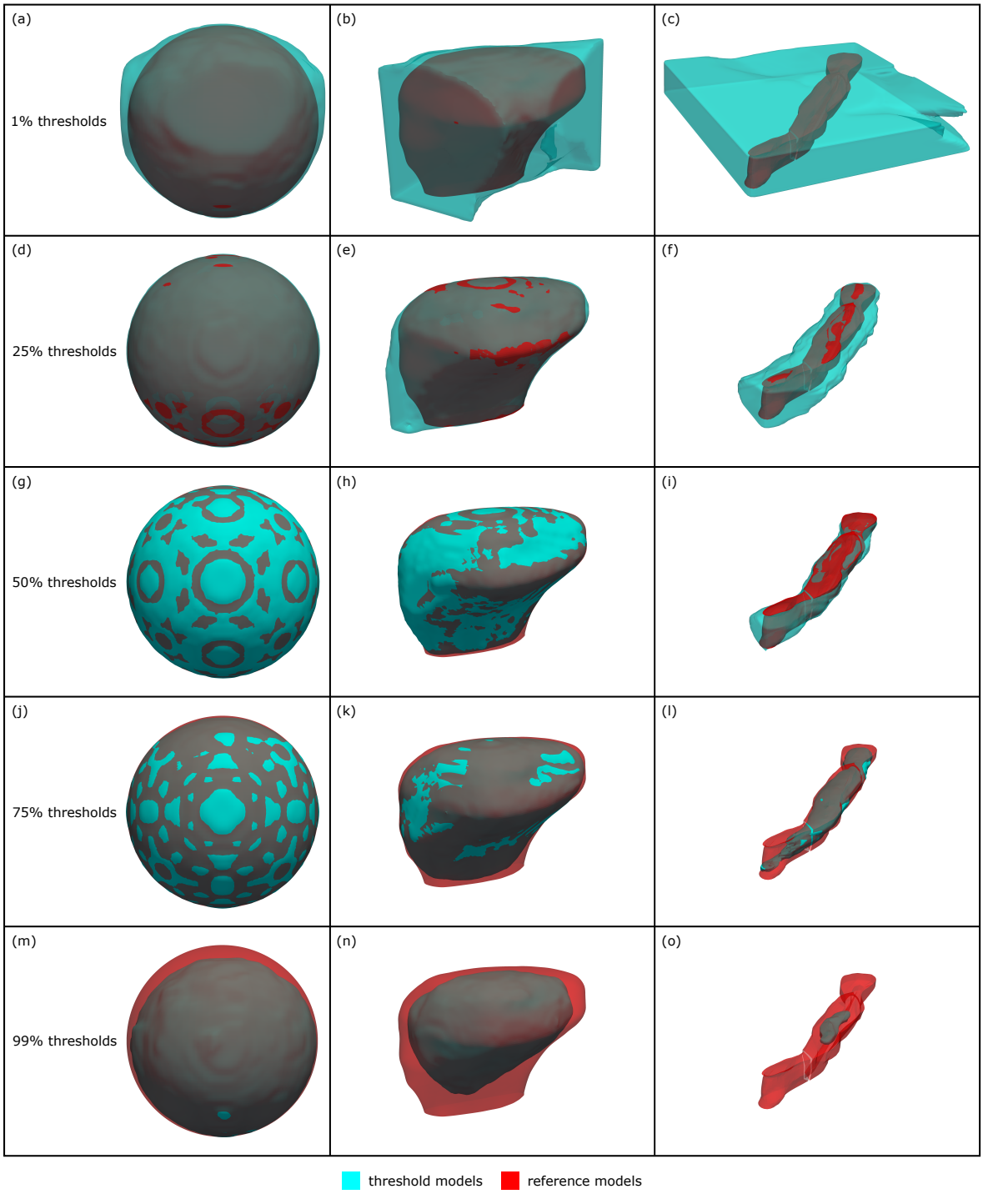


Figure 4.3: Exemplary visualization of the threshold models measured and compared in the present study, alongside the respective reference mesh. Shown are the threshold models of the configuration "4 sections 4 boreholes", a setup of intermediate to high data quantities among the tested range. Coordinate axes are omitted for visual clarity (for the size of the objects, see Fig. 4.1)

ments in between the sections of the first set. Subsequently, artifacts in the vertex order within sections have been corrected. After the establishment of both sets of cross sections, horizontal and vertical measurements have been carried out on all cross sections except for the first and last section of each set, at 10 equidistant transects. Thus, 300 measurements have been obtained for the two horizontal parameters and 600 values for the vertical extent. This represents a considerable increase from the amount of data obtained in the original methodology proposed by Carl et al. (2026a) (5 equidistant measurements on 20 sections per section set). Although the increase of the amount of computed cross sections coincided with a noticeable comparative enlargement of computation times, the extension of the database has been deemed necessary to ensure that the following data analysis could capture the partially small geometric differences between the different threshold models of a structure. Gradient data is extracted from the cross sections as well, between consecutive polygon points.

4.2.3 Data analysis

The data analysis focuses on the comparison of the individual percentile threshold models to the respective reference model, to identify input data quantities required to produce interpolated shapes that resemble the geometry of the reference structure. The geometric data has been compiled into a database, and the horizontal measurements of both cross-sectional sets have been combined into an additional parameter, as established in Carl et al. (2026a) and Carl et al. (2026b). Parameter distributions have been compared between the threshold models and references using the Kullback-Leibler divergence (KLD; Kullback and Leibler 1951), and after principal component analysis (PCA; e.g., Jolliffe 2002) has been conducted on the measurements.

The three KLDs of individual geometric parameters (combined horizontal data, vertical and gradient data) between a threshold model and the reference have been averaged to obtain a singular averaged KLD per assessed threshold model for a data configuration. These averaged KLDs between data configurations and the initial 3D model have been compared separately for the five percentile thresholds. Then, the five values of a data configuration have been averaged to obtain a mean averaged KLD ("mean avKLD") that is plotted among data configurations, ordered by increasing model similarity to the respective reference. When interpreting the averaged Kullback-Leibler divergences, it has to be considered that they do not indicate which individual parameters are more dis-/similar between two models (see Carl et al. 2026a). Furthermore, it has to be noted that gradient distributions have been altered in the computation, as infinite values had to be replaced by the highest finite gradient value of a given dataset to allow for the calculation of the KL divergence. Thus, the highest bin is inflated in the gradient distributions. Additionally, gradients = 0 have been aligned with normalized 0, to

avoid artificial mismatches of the main gradient maxima (see also Carl et al. 2026b). Both adjustments to the gradient data had to be performed prior to the principal component analyses as well. All five groups of threshold models alongside the reference have been analyzed separately. 20 percentiles of the PDFs of the combined horizontal data, vertical data and gradients have been used as features in the PCA. The distance in principal component space between threshold models and the respective reference has been determined and plotted. Then the values of the five threshold models per data configuration have been averaged to obtain the metric of mean distance in PC space, sorted as well by increasing model similarity to the respective reference.

4.3 Results

4.3.1 Geometric characteristics of the reference models

The three reference models for the data analysis show different geometric characteristics as revealed by the quantification algorithm of Carl et al. (2026a). To provide a visual reference for the geometric properties to facilitate the understanding of the results of the metrics, these characteristics shall be described shortly. The description is based on the histogram data of the measured geometric parameters (see Fig. 4.4), as established by Carl et al. (2026a). The combined horizontal data of both cross-sectional sets of the sphere (Fig. 4.4a) reflect the isotropy of the structure. The slight bimodality of the histogram is the consequence of the setup of the orthogonal cross sections following the contour of the structure, which results in enlarged measurements for the orthogonal horizontal data and a slightly tailed distribution of the shown combined horizontal data (see Carl et al. 2026a). The vertical data (Fig. 4.4b) is influenced by the differences in both sets of cross sections as well, resulting in the nonmonotonic increase of the underlying probability density function. In contrast, the gradient distribution (Fig. 4.4c) is symmetric, as all sections are circular (except for the vertical edges of the orthogonal sections), irrespective of the contour-alignment of the second set. The combined horizontal data of Gielow (Fig. 4.4d) reflect the isotropy of the structure through the narrow distribution shape. The presence of the two maxima at higher values indicates the existing overhang configurations, which are also recognizable in the multimodality of the vertical data (Fig. 4.4e). The gradient diagram (Fig. 4.4f) clearly reflects the rounded nature of the structure, by the presence of many intermediate gradients (see also Fig. 4.4c & i). For Juliusburg_Koestorf-Rosenthal, the strong bimodality of the combined horizontal data reflects the considerable anisotropy of the structure (Fig. 4.4g). The bimodality of the vertical data reveals the presence of lateral overhang configurations (Fig. 4.4h). The gradient histogram (Fig. 4.4i) is strongly influenced by the rather coarse input mesh of the TUNB model, that results

in both the prevalence of small gradients as well as the presence of large values, as seen by the large threshold values of the 5th- and 95th-percentile overflow bins. Rather spherical parts of the structure are represented by less data and thus less curved. If the input mesh had been finer, the gradient data would have shown more intermediate values. However, re-meshing of the reference models had not been considered prior to the measurements.

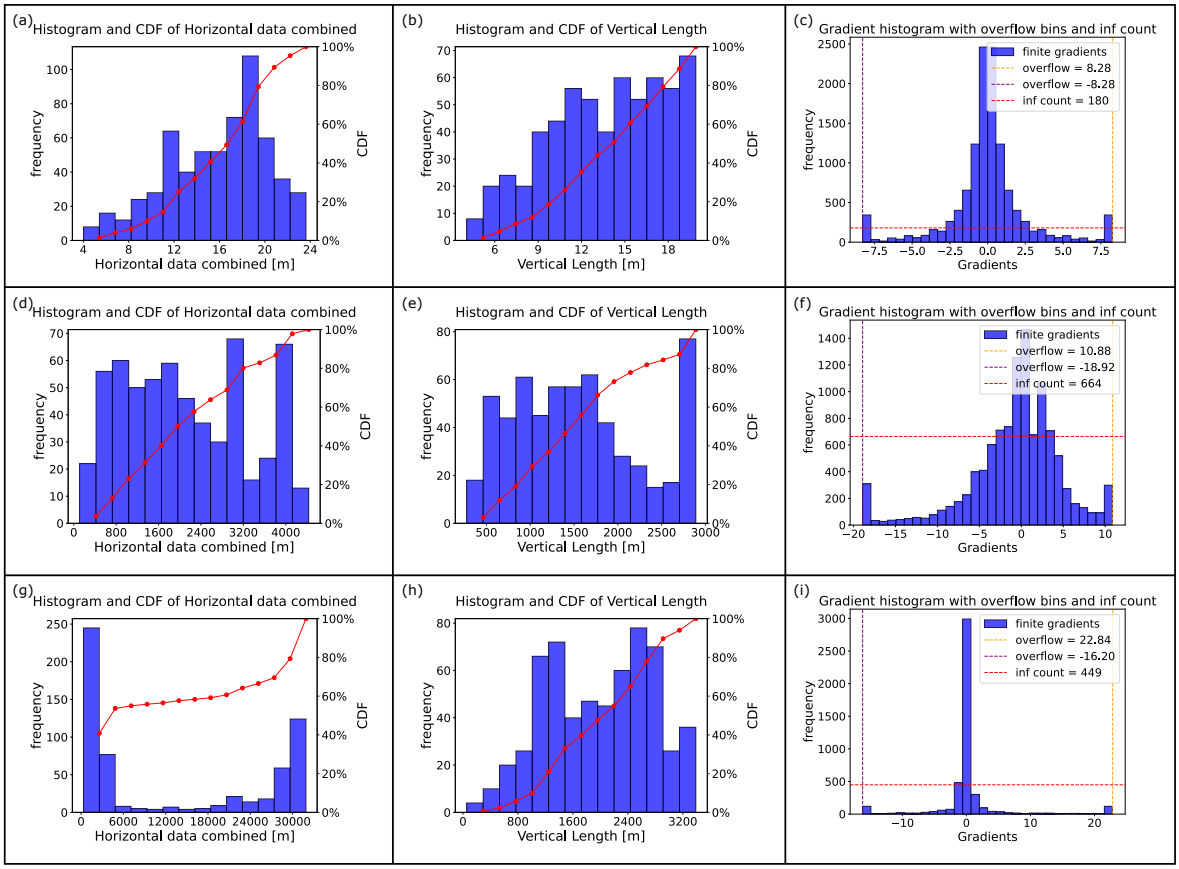


Figure 4.4: Data distributions of the geometric parameters for the three tested reference structures. First column: combined horizontal data of both sets of cross sections alongside the respective cumulative distribution function (CDF) in red. Second column: vertical data. Third column: gradient data, with the amount of infinite measurements as a horizontal red line, and 5th and 95th percentile overflow bins. a) – c): sphere. d) – f): Gielow. g) – i) Juliusburg_Koestorf-Rosenthal

4.3.2 (Mean) averaged Kullback-Leibler divergences

For the three example structures, the Kullback-Leibler divergence has been calculated to quantitatively assess the similarity between the threshold models and the initial reference. The distributions of the three parameters (the combined horizontal data, the vertical data and the gradients) have been compared between the models, and the average of these three values has been used as a comparative metric for the overall dis-/similarity between meshes. The similarity of two distributions – and two structures – is larger, the smaller the KL divergence is, with a value of 0 indicating equality of the distributions/structures. Figures 4.5 - 4.7 visualize the averaged KL divergences

("avKLDs") between the threshold models and the initial 3D model, subdivided into the groups of five percentile thresholds. Furthermore, the five averaged KL divergences of every data configuration have been averaged again, to obtain the single value of "mean avKLD", respectively. This enables the evaluation of dis-/similarity between data configurations and the respective reference structure in a single diagram (see Figs. 4.5f - 4.7f). Thus, it is indicated whether the addition of specific quantities of sections/boreholes has a considerable impact on the similarity of model results.

4.3.2.1 Sphere

The 1% threshold group of the sphere (Fig. 4.5a) reveals large differences in the appearances of the percentile models. The models "1 section 1 borehole", "2 sections 1 borehole" and "1 section 2 boreholes" are (partially) cuboidal, filling (nearly) the entire model space, as the underlying model realization sets are very dissimilar, respectively. Beyond that, increases of data quantities coincide well with increases of model similarity. The percentile model of the "0 sections 10 boreholes"-configuration already shows a very spherical appearance. For the 25% group (Fig. 4.5b), the correspondence of improving similarity and increasing amounts of data is visible as well. However, most threshold models are already very close to the reference, indicating that all 100 realizations per setup are similar as well, respectively. Only the models "1 section 1 borehole" and "2 sections 1 borehole" exhibit comparatively larger avKLD values. The 50% group (Fig. 4.5c) shows universally spherical appearances, as all the avKLD values are below 0.1. The overall same pattern is visible for the 75% threshold models (Fig. 4.5d), with the avKLD values of low quantity data configurations being slightly larger in comparison. The 99% threshold models (Fig. 4.5e) exhibit lower similarities for most setups, as less cells are co-occuring in 99/100 realizations, thus not producing completely spherical shapes anymore.

The mean avKLD diagram (Fig. 4.5f) shows a mostly smooth trend of improving model similarity that coincides well with increasing data quantities. Given the plots in Fig. 4.5a – e, the diagram pattern is mainly influenced by the data of the 1% group, where differences between the data configurations are largest. This reflects that for virtually all data configurations, a varying number of realizations is deviating from spherical shapes. With increasing amounts of input data in the setups, the number of these geometric outliers decreases, thus increasing the sphericity of the resulting combined threshold model and the similarity to the reference. The highest overall similarity to the reference is seen for the "0 sections 10 boreholes"-model, indicating that the complete absence of sections lacking accurate orientation data is beneficial at very high data quantities in the case of the sphere.

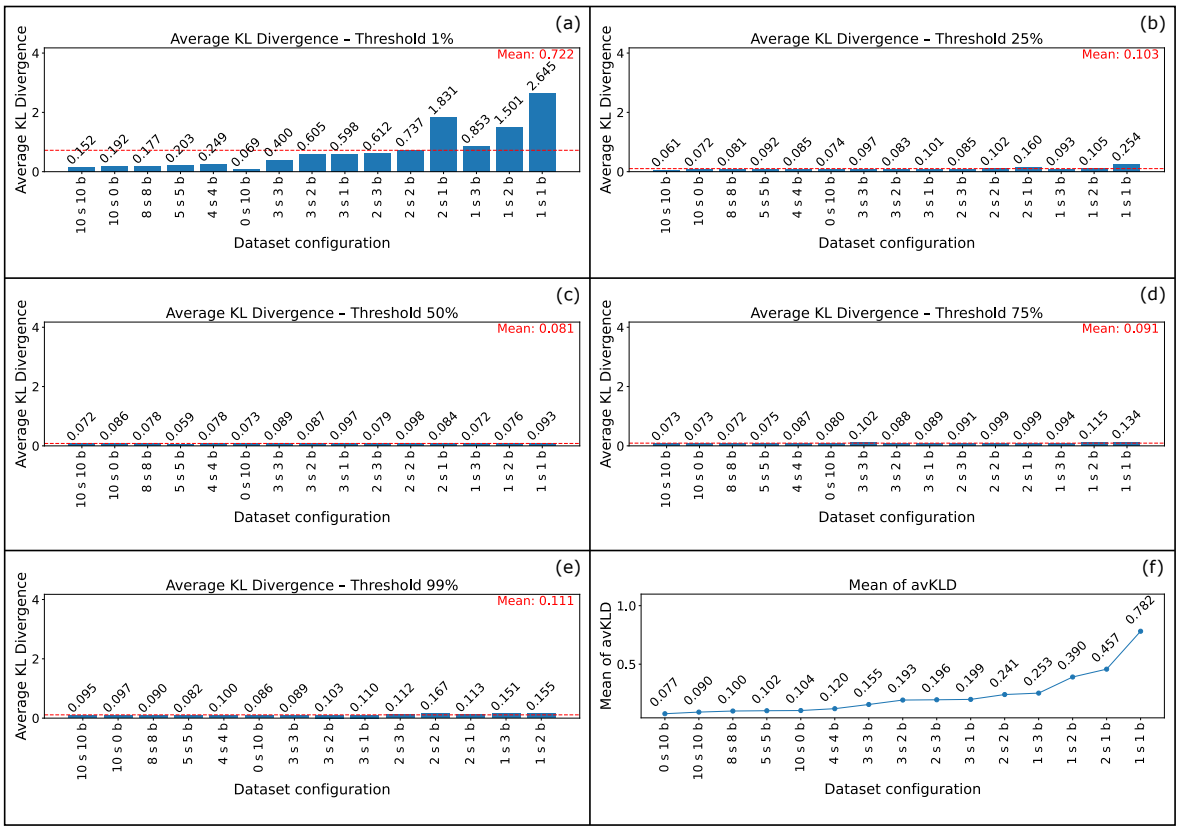


Figure 4.5: a) – e) Averaged Kullback-Leibler divergence (avKLD) values between threshold models and the reference model for the sphere, separated into threshold groups (see diagram titles). Data configurations in numerical order from right to left, except for the setup "0 sections 10 boreholes". f) Mean averaged Kullback-Leibler divergence (mean avKLD) in ascending order, obtained by averaging the respective values of a data configuration from a) to e)

4.3.2.2 Gielow

For Gielow, the 1% group (Fig. 4.6a) is characterized by similarly high avKLDs for many percentile models of low data quantity, representing cuboidal model appearances. Lower values are present for data configurations combining more than 6 sections and/or boreholes, and for the setup "3 sections 1 borehole". The latter is likely caused by the variability in the 100 input datasets per data configuration and would most likely be smoothened if more realizations had been computed. The 25% group (Fig. 4.6b) shows uniformly lower avKLDs with one outlier in the pattern. The configuration "3 sections 1 borehole" exhibits a high avKLD value compared to adjacent setups. In contrast, slight outliers of low values from the general trend of decreasing avKLDs with increasing amounts of data are seen at configurations with three boreholes. For the 50% group (Fig. 4.6c), the "10 sections 0 boreholes"-model is an outlier of large values, with an avKLD approximately two times higher than the value of adjacent models. An outlier of a comparatively low value is present for the setup "3 sections 3 boreholes". Overall, all data configurations show a generally higher similarity to the initial TUNB model, with low avKLD values between 0.065 and 0.160. The 75% group (Fig. 4.6d) shows a

stronger differentiation of most high-quantity setups at lower avKLDs again. This is especially true for the configurations "4 sections 4 boreholes", "8 sections 8 boreholes" and "10 sections 10 boreholes". Another outlier of low avKLD is visible for the "3 sections 2 boreholes"-model, likely again due to the randomness in input data creation. For the 99% block model set (Fig. 4.6e), the values of most setups are higher, as it is to be expected (see Subsect. 4.2.1). An outlier of high avKLD is present for the configuration "3 sections 1 borehole", while outliers of comparatively low values given adjacent setups are "4 sections 4 boreholes", "2 sections 3 boreholes" and "1 section 2 boreholes".

In the mean avKLD diagram of Gielow (Fig. 4.6f), model improvements correspond well with increasing data quantities. At lowest similarities, a sharp decrease from the "1 section 1 borehole"-configuration to the next lower one is observable. This is mainly due to the lack of a 99% percentile of this setup. Afterwards, the decrease of mean avKLD is rather moderate between adjacent configurations, until larger differences are visible between the setups "1 section 3 boreholes" and "3 sections 1 borehole", as well as between "3 sections 1 borehole" and "3 sections 3 boreholes". However, only beyond the latter, improvement of model results with increasing data quantities are largest in the diagram. Thus, it is indicated that at least four sections and boreholes are required respectively to model Gielow realistically. However, even between the data configurations of largest similarity to the reference, value differences are still large, indicating that data integration still has a considerable impact.

4.3.2.3 Juliusburg_Koestorf-Rosenthal

For Juliusburg_Koestorf-Rosenthal, the 1% set (Fig. 4.7a) almost exclusively consists of cuboidal geometries. This includes the configuration "10 sections 0 boreholes", whose avKLD value is even higher. This is mainly due to a mismatch of the gradient data distribution compared to the reference (see Subsect. 4.4.2). The 25% group shows lower avKLDs for high quantity configurations as expected, but compared to the sphere and Gielow, values are almost universally higher (Fig. 4.7b). While the "10 sections 0 boreholes"-configuration is recognizable again as an outlier of high values due to the same reason as before, the inclusion of three boreholes does seem to have a positive influence on avKLD values, as partially observed for Gielow. In the 50% group (Fig. 4.7c), four setups show comparatively high avKLD values: "10 sections 0 boreholes", "3 sections 1 borehole", "2 sections 1 borehole" and "1 section 1 borehole". Thus, a lack of 3D orientations from boreholes is indicated to be associated with poor modeling performance. While the values for the other data configurations are notably lower, there is no clear trend of improving modeling results with increasing data quantities. In fact, the lowest avKLD value is visible for the setup "1 section 3 boreholes" at the

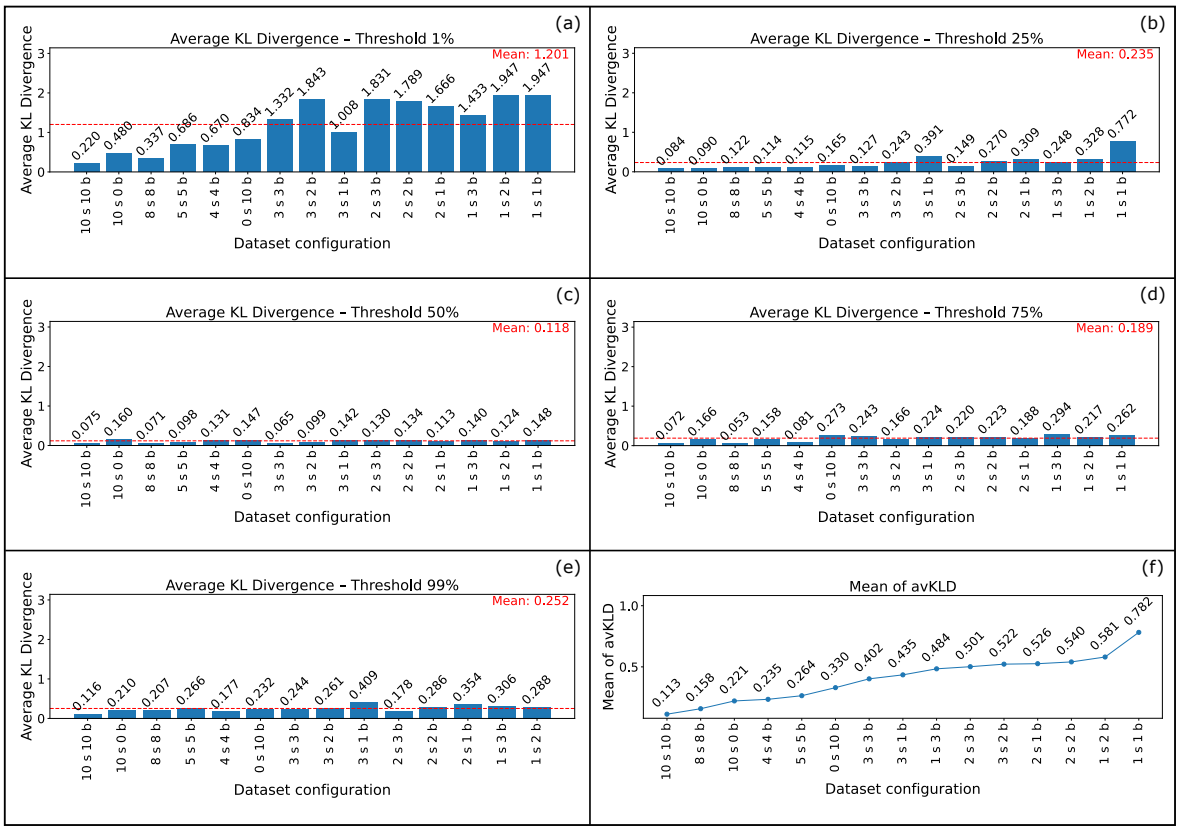


Figure 4.6: a) – e) Averaged Kullback-Leibler divergence (avKLD) values between threshold models and the TUNB reference model for Gielow, separated into threshold groups (see diagram titles). Data configurations in numerical order from right to left, except for the setup "0 sections 10 boreholes". f) Mean averaged Kullback-Leibler divergence (mean avKLD) in ascending order, obtained by averaging the respective values of a data configuration from a) to e)

lower quantity-end. Thus, for Juliusburg_Koestorf-Rosenthal, lower values in the 50% threshold are mostly resulting randomly from the variability of the underlying 100 datasets and model realizations. For the 75% models (Fig. 4.7d), values are much more uniform across the database in comparison to the previous thresholds. This is explainable by the nature of the quantification algorithm: as it compares shapes scale-independently, higher similarities can be detected if model geometries consisting of fewer cells (hence showing smaller dimensions) exhibit a more similar shape to the reference. This is especially the case if a large number of model realizations of a configuration miss entire marginal parts of the heterogeneous salt wall, instead of poorly constraining these parts. The 99% group (Fig. 4.7e) shows larger values across all remaining data configurations, indicating lower geometric similarity. For six data configurations of low quantities, the 99% percentile could not be computed as the 100 model realizations are too dissimilar, respectively.

The mean avKLD plot (Fig. 4.7f) shows a rather smooth trend where the values are generally much higher compared to the data from the sphere and Gielow. Given the mean avKLD values of the best-performing data configurations, higher data quantities

than tested seem to be required to model such a complex both anisotropic and overhanging shape realistically. Improving modeling results correspond only very roughly with increasing data quantities according to the mean avKLD graph, especially among the low- to medium-quantity configurations. The lowest similarity to the reference is indicated for the high quantity configuration "10 sections 0 boreholes" though. As already indicated, this aspect is due to mismatching data (see Subsect. 4.4.2). The seemingly (partially) arbitrary order of data configurations showing decreasing mean avKLD values in Fig. 4.7f raises the question whether the mean avKLD is a suitable metric to evaluate required minimum data quantities for Juliusburg_Koestorf-Rosenthal. In addition to the influences of mismatching data and the geometric complexity, the unordered and high mean avKLD values are also partially resulting from the scale-independent quantification algorithm (see above). While on one hand, not covering marginal parts can still result in an anisotropic shape somewhat resembling the larger reference structure, on the other hand, values of high similarity get increasingly unlikely the more anisotropic a structure is. This is due to the increasingly lower probability of constraining the full length of the structure reasonably by input data of random location and orientation.

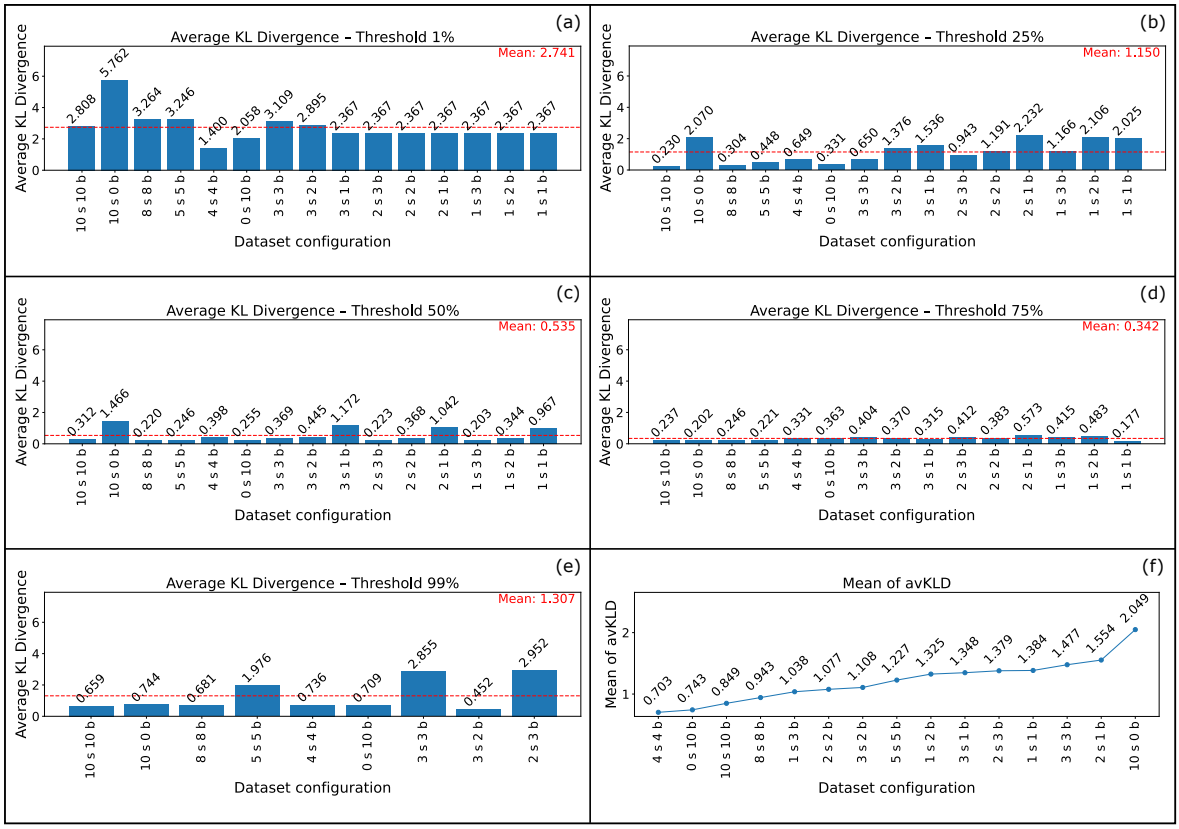


Figure 4.7: a) – e) Averaged Kullback-Leibler divergence (avKLD) values between threshold models and the TUNB reference model for Juliusburg_Koestorf-Rosenthal, separated into threshold groups (see diagram titles). Data configurations in numerical order from right to left, except for the setup "0 sections 10 boreholes". f) Mean averaged Kullback-Leibler divergence (mean avKLD) in ascending order, obtained by averaging the respective values of a data configuration from a) to e)

4.3.3 (Mean) Euclidean distances in principal component space

Similar to the analysis of the averaged Kullback-Leibler divergences between threshold models and the respective reference, one can analyze the Euclidean distances in PC space between threshold models and the reference after principal component analyses. Furthermore, averaging the values of the five threshold models respectively for the data configurations provides an alternative quantitative measure to the mean avKLD, and thus another opportunity to explore, what the minimum data configuration for realistic and reliable structural geomodeling might be. To facilitate the comparison of the PC space distance with the avKLD figures, the order of data configurations in the diagrams is the same. As for the (mean) avKLD, lower values of (mean) PC space distance reflect higher model similarity to the reference.

4.3.3.1 Sphere

In comparison to the avKLD diagram (Fig. 4.5a), the 1% threshold plot of the PC space distances (Fig. 4.8a) shows a very similar pattern. The same is true for the 25% threshold diagram (Fig. 4.8b in comparison with Fig. 4.5b) and the 50% diagram (Fig. 4.8c; compared to Fig. 4.5c). Subtle differences in the diagram pattern are recognizable for the 75% threshold models (Fig. 4.8d), as the PC space distance values among low quantity configurations are more uniform compared to the corresponding avKLD values in Fig. 4.5d. Otherwise, the pattern between the two diagrams is very similar again. In the 99% diagram (Fig. 4.8e), the pattern is more uniform than in the avKLD counterpart as well.

When averaging the PC space distance values per data configuration (Fig. 4.8f), a similar pattern to the corresponding diagram of mean avKLD (Fig. 4.5f) is visible. High similarities to the reference are indicated by data configurations of at least four to five combined sections and boreholes. Small differences in Fig. 4.8f include for instance, that three plateaus of values are recognizable in the lower half of the data quantity spectrum, with every plateau consisting of setups with similar data quantities. Furthermore, all data configurations of high quantities, starting with "10 sections 0 boreholes" show similar values. This indicates that beyond a number of four respective sections and boreholes, additional data does not improve the modeling results notably anymore. This also explains the position of the "5 sections 5 boreholes"-setup, being more similar to the reference than "10 sections 10 boreholes" and "8 sections 8 boreholes": differences in this group of data configurations mostly result from the variability in the 100 input datasets per data configuration.

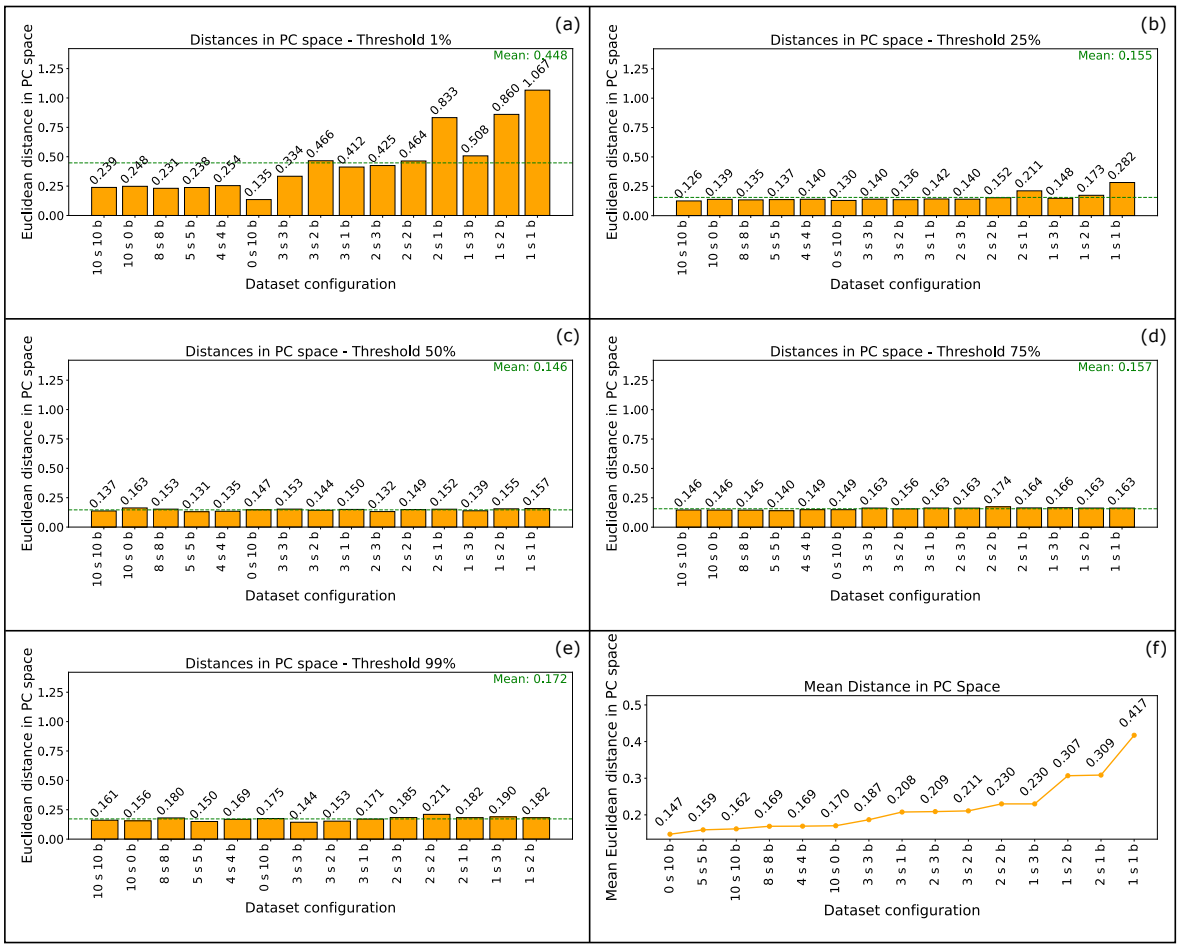


Figure 4.8: a) – e) Euclidean distance values in principal component (PC) space between threshold models and the reference model for the sphere, separated into threshold groups (see diagram titles). Data configurations in numerical order from right to left, except for the setup "0 sections 10 boreholes". f) Mean Euclidean distance in PC space in ascending order, obtained by averaging the respective values of a data configuration from a) to e)

4.3.3.2 Gielow

Comparing the 1% threshold diagram in Fig. 4.9a to the respective diagram of the avKLD (Fig. 4.6a), it is noticeable that the model of the configuration "2 sections 3 boreholes" has an equally low value as "3 sections 1 borehole", that is an outlier in Fig. 4.6a. Furthermore, in Fig. 4.9a, the values of the other low-quantity setups are more uniform. Otherwise, the patterns of both diagrams are similar, as there is an improvement in similarity with increasing data quantities starting with the setup "3 sections 3 boreholes". In the comparison of the 25% threshold diagrams (Figs. 4.6b & 4.9b), overall patterns are similar. In Fig. 4.9b, the setup "3 sections 1 borehole" is no outlier of large values though. In the 50% threshold diagram (Fig. 4.9c), the outlier of large values that is the "10 sections 0 boreholes"-model distance is smaller, while the relative value of the "3 sections 3 boreholes"-setup is higher compared to Fig. 4.6c, but still exhibits the overall lowest value. Similarly, the values of the configurations "10 sections 10 boreholes" and "8 sections 8 boreholes" are comparatively higher. Among

the 75% percentile models (Fig. 4.9d), the three outliers of "10 sections 10 boreholes", "8 sections 8 boreholes" and "4 sections 4 boreholes" show comparatively higher values as well. The same is true for the setup "3 sections 2 boreholes". The 99% distance diagram (Fig. 4.9e) exhibits a very similar pattern to its avKLD counterpart. Most notably, the "3 sections 1 borehole"-setup represents less of an outlier of large values.

Averaging the respective values per data configuration (Fig. 4.9f) reveals a similar pattern in comparison to the mean avKLD diagram (Fig. 4.6f), with minor differences in the order of data configurations being visible for low-quantity setups. However, the strongest improvements of model similarity with increasing data quantities are visible earlier, between the trio of "3 sections 1 borehole", "2 sections 3 boreholes" and "3 sections 3 boreholes". Beyond that, the data still indicates though, that the improvement of modeling results with data integration is considerable. Thus, even though the benefit of data integration is higher already at overall lower data quantities according to the mean PC space distance metric, the performance of high data quantities is still notably better.

4.3.3.3 Juliusburg_Koestorf-Rosenthal

When comparing the 1% threshold diagram of the PC space distances (Fig. 4.10a) with its avKLD counterpart (Fig. 4.7a), the pattern appears to be very different at first, which mostly comes down to the data configuration "10 sections 0 boreholes" not being an outlier of large values compared to adjacent setups in Fig. 4.10a. Instead, starting with the setup "0 sections 10 boreholes" (but excluding "5 sections 5 boreholes"), there is a clear trend of improving modeling results with increasing data quantities. Meanwhile, for the data configurations with 3 or less respective sections and boreholes, the diagram patterns are similar. In the 25% threshold diagram (Fig. 4.10b), the data configuration "10 sections 0 boreholes" is less of an outlier of large values compared to Fig. 4.7b. Besides, the overall diagram pattern is different as well. While the data configurations of highest similarities are the same ("10 sections 10 boreholes", "8 sections 8 boreholes" and "0 sections 10 boreholes"), the PC space distance diagram shows rather uniform values for most of the other setups, while the avKLD diagram is more varied. A setup of high values in Fig. 4.10b is "1 section 1 borehole". This configuration does not appear with a notably large value in the avKLD diagram. The 50% threshold model (Fig. 4.10c) shows a different pattern compared to the corresponding avKLD diagram (Fig. 4.7c) as well. As previously, the data configuration "10 sections 0 boreholes" is less of an outlier of large values. The same is true for the setups "3 sections 1 borehole", "2 sections 1 borehole" and "1 section 1 borehole". Overall, the relative value range in Fig. 4.10c is thus smaller again compared to the corresponding avKLD diagram. Still, neither exhibit a distinct trend of improving model similarity with increasing

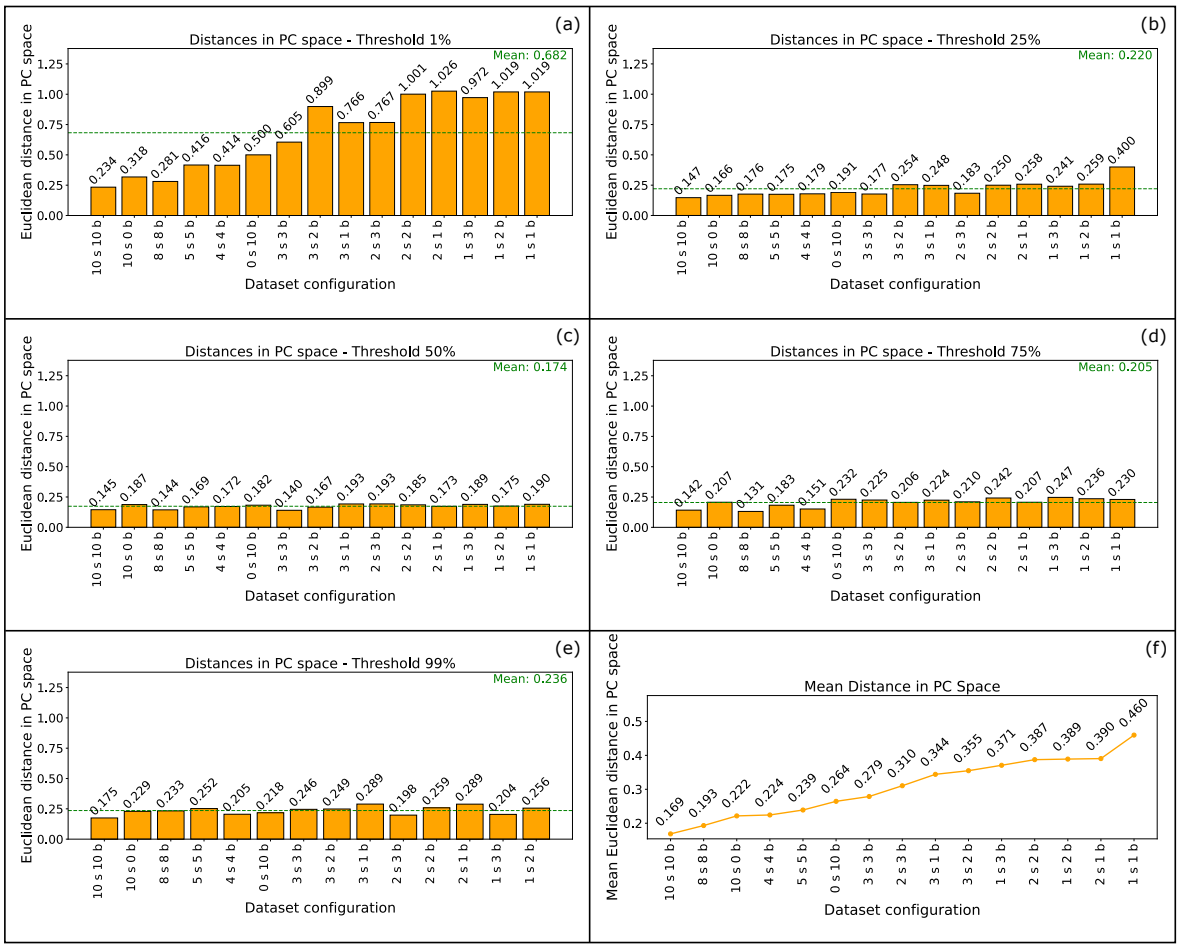


Figure 4.9: a) – e) Euclidean distance values in principal component (PC) space between threshold models and the reference model for Gielow, separated into threshold groups (see diagram titles). Data configurations in numerical order from right to left, except for the setup "0 sections 10 boreholes". f) Mean Euclidean distance in PC space in ascending order, obtained by averaging the respective values of a data configuration from a) to e)

data quantities. Regarding the 75% percentiles, the patterns between the PC space distance diagram (Fig. 4.10d) and the avKLD diagram (Fig. 4.7d) are rather similar. In both cases, the relative value ranges are rather small. However, in Fig. 4.10d, highest similarities to the reference are visible for the configurations "10 sections 10 boreholes" and "8 sections 8 boreholes", while in the avKLD plot, the lowest value of the metric is given by the data setup "1 section 1 borehole" (see Fig. 4.7d). In the 99% diagram (Fig. 4.10e), there are no outliers of large values. This differentiates the plot from the corresponding avKLD diagram (Fig. 4.7e), where the setups "5 sections 5 boreholes", "3 sections 3 boreholes" and "2 sections 3 boreholes" are noticeable in that regard. In contrast, the models "3 sections 2 boreholes" and "8 sections 8 boreholes" show comparatively low values in Fig. 4.10e.

The large differences identified between the values and patterns of both metrics for Juliusburg_Koestorf-Rosenthal are recognizable in the diagram of the mean PC space distances (Fig. 4.10f). It shows a much better correlation of improving modeling

results with increasing data quantities. This includes for instance the positions of the setups "10 sections 0 boreholes", "4 sections 4 boreholes" and "5 sections 5 boreholes" (compare Fig. 4.7f). The overall trends between both plots are quite similar though, as both exhibit mainly rather small value changes between adjacent data configurations. The exception in Fig. 4.10f is the large step between "0 sections 10 boreholes" and "8 sections 8 boreholes", that implies a large improvement of the modeling results. In contrast to the result from the mean avKLD plot, this indicates that Juliusburg_-Koestorf-Rosenthal can be modeled realistically with the tested data configurations.

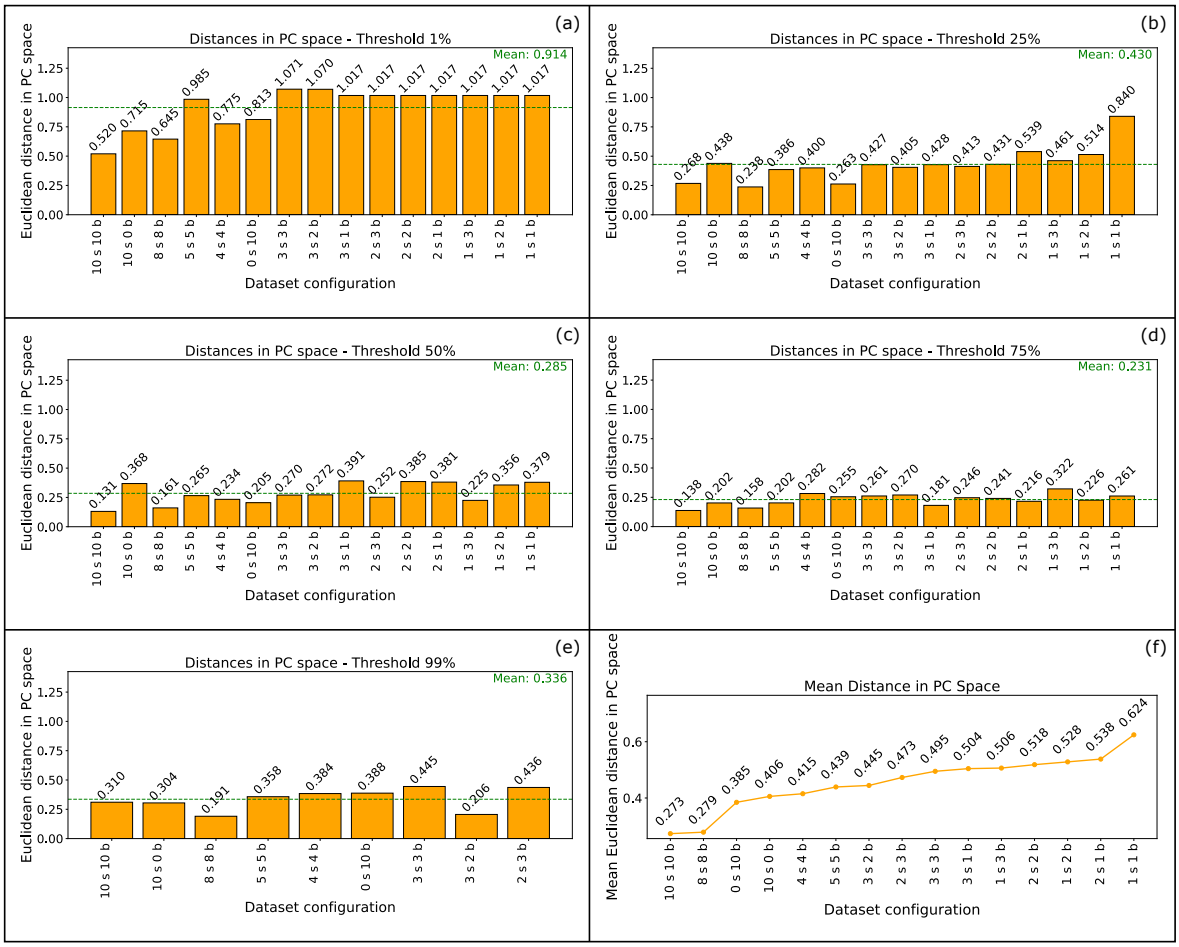


Figure 4.10: a) – e) Euclidean distance values in principal component (PC) space between threshold models and the reference model for Juliusburg_Koestorf-Rosenthal, separated into threshold groups (see diagram titles). Data configurations in numerical order from right to left, except for the setup "0 sections 10 boreholes". f) Mean Euclidean distance in PC space in ascending order, obtained by averaging the respective values of a data configuration from a) to e)

4.3.4 Comparison of the results of both metrics between the structures

Assessing the mean avKLD graph of the sphere in Fig. 4.5f reveals strong effects of data integration on modeling results already at low data quantities, followed by comparatively minor improvements of the similarity between adjacent data configurations for most of the setups. For Gielow and Juliusburg_Koestorf-Rosenthal (Figs. 4.6f & 4.7f), the trend is reversed, with less of an effect among low quantity setups, and a stronger benefit when increasing the data quantities. According to the data, for the sphere, some of the setups of four combined sections and boreholes already produce modeling results closer to the respective reference as it is the case for all data configurations of the other structures except for the two best-performing setups of Gielow. This is not unexpected given the spheres' regular shape.

The mean PC space distance diagrams (Figs. 4.8f - 4.10f) reveal differences both compared to the respective avKLD plots as well as between each other. Comparing the data of Gielow to the sphere, similarly low mean PC space distance values require more input data, but the difference according to this metric is smaller as indicated by the mean avKLD: the setup "4 sections 4 boreholes" performs similarly for Gielow as the configurations of four to five combined sections and boreholes perform for the sphere. Furthermore, for Gielow, the addition of data between adjacent data configurations has a larger impact on average on the modeling results. The mean PC space distance values are generally highest for Juliusburg_Koestorf-Rosenthal. Between the setups "0 sections 10 boreholes" and "8 sections 8 boreholes", the largest similarity increase between two adjacent data configurations across all three structures is recognizable, when disregarding the lowest quantity setup "1 section 1 borehole" always being influenced by the absence of 99% threshold models. Apart from this step at high quantities, the average increase of model similarities with increasing data quantities between adjacent setups is larger than for the sphere, but smaller than for Gielow.

4.3.5 Assessment of minimum data requirements

The effect of data integration on model similarity is visualized best on the sphere (Fig. 4.11). Given the overall comparability of the results of both metrics for the sphere, for simplicity, we only refer to the respective PC space distance values from Fig. 4.8f. Compared are the data configuration "1 section 2 boreholes" at a mean PC space distance value of 0.307 to the setup "2 sections 3 boreholes" at higher threshold model similarities (mean value = 0.209), and the setup "4 sections 4 boreholes" (mean value = 0.169) in the group at the high end of the similarity spectrum. Based on Fig. 4.8f, the configuration "2 sections 3 boreholes" has been identified as reproducing the sphere

sufficiently well. The 1% model of "1 section 2 boreholes" is rather blocky (Fig. 4.11a), indicating that in most cells, at least one realization is present. In contrast, for the "2 sections 3 boreholes"-model, the sphericity of the underlying reference is way more apparent (Fig. 4.11b), with extrapolations well beyond the bounds of the reference mostly being present laterally. The "4 sections 4 boreholes"-model is already very spherical with only rather minor lateral extrapolations (Fig. 4.11c). This reflects that very few of the 100 model realizations of that configuration deviate from the spherical reference. In the case of the 25% models (Fig. 4.11d – f), deviations from the reference are minor for all three models, underlining the low overall number of extreme outliers for all data configurations. Still, the benefit of additional data integration is recognizable laterally. The 50% model of "1 section 2 boreholes" exhibits a slight mismatch compared to the reference at the top of the structure (Fig. 4.11g). This mismatch gets reduced with additional data (Fig. 4.11h) and is absent in the "4 sections 4 boreholes"-model (Fig. 4.11i). Otherwise, all three models are very similar to each other as well as to the reference (see also Fig. 4.8c). For the 75% percentile threshold, the model of "1 section 2 boreholes" is already notably smaller than the reference (Fig. 4.11j), especially in the upper hemisphere. A similar yet less pronounced trend is observable for the intermediate model of "2 sections 3 boreholes" (Fig. 4.11k), while the model of the setup "4 sections 4 boreholes" is still very close to the reference (Fig 4.11l). The marginal 99% threshold models visualize the influence of different data densities very clearly again (Fig. 4.11m – o). The model of "1 section 2 boreholes" is rather resembling an upward-facing ellipsoid than a sphere. The result of the setup "2 sections 3 boreholes" still reproduces a roughly spherical shape, although notably smaller than the reference. The percentile model of "4 sections 4 boreholes" validates that the ensemble of the 100 underlying realizations is very similar, resulting in a good representation of the sphere apart from some deviations mainly in the upper hemisphere. Overall, for the sphere it is validated that differences between the modeling results of different data configurations are mainly recognizable in the marginal threshold models, underlining their importance for the methodology to assess 1) the modeling performance of data configurations and 2) the minimum data requirements for structural geomodeling.

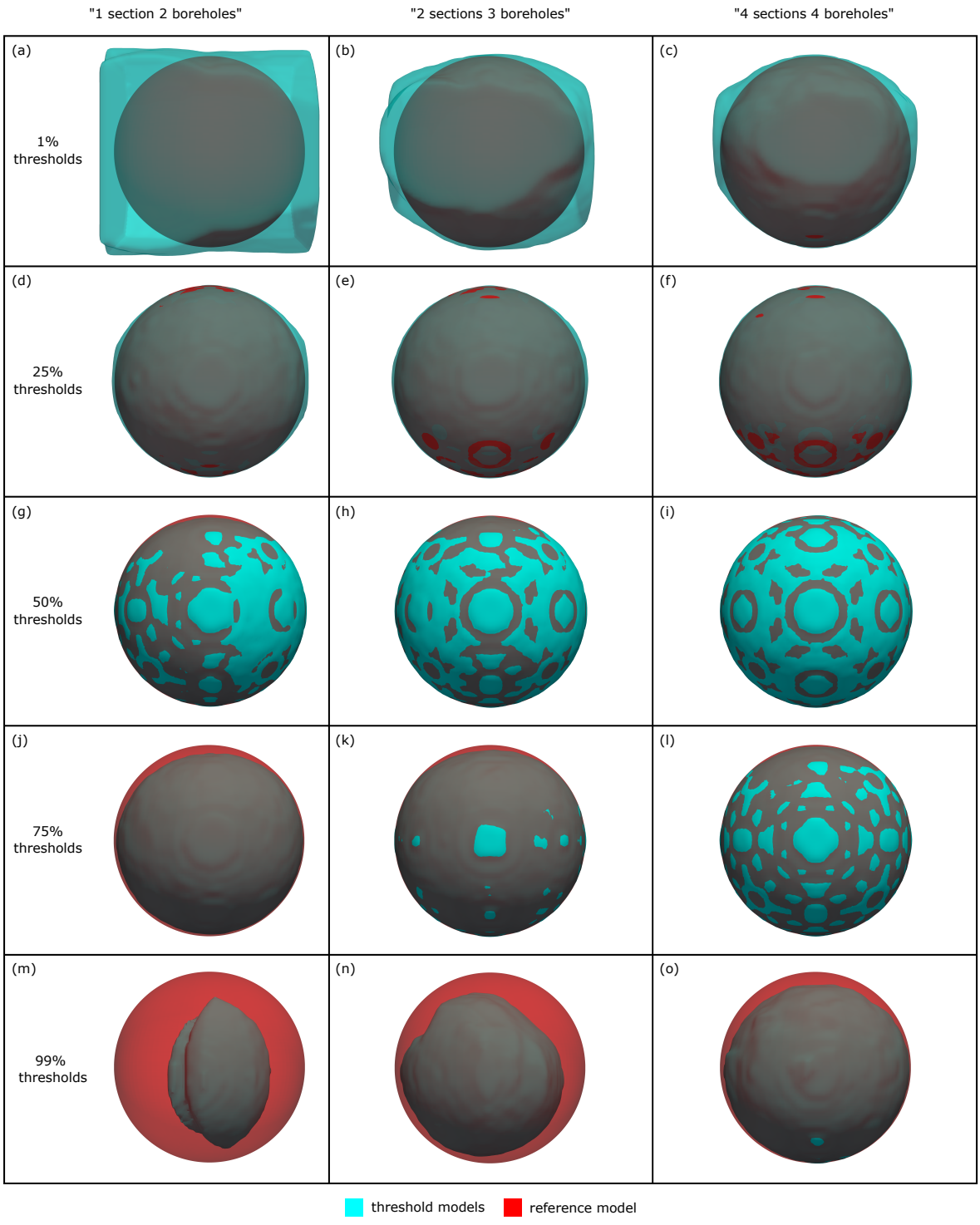


Figure 4.11: Exemplary visualization of the effect of data integration on threshold models for the sphere (compare also Fig. 4.8f). Compared are the low quantity configuration "1 section 2 boreholes" (first column) to the medium quantity setup "2 sections 3 boreholes" (second column) that has been identified as the minimum data requirement, and the medium to high quantity configuration "4 sections 4 boreholes" (third column). Coordinate axes are omitted for visual clarity (for the size of the sphere, see Fig. 4.1)

For the two TUNB structures, the minimum data requirements are larger. In the case of Gielow, the mean PC space distance values are mostly affected by the outliers recognizable in the 1% threshold models. Considering this aspect, we would argue that the setup "3 sections 3 boreholes" performs reasonably at reproducing the reference (see Fig. 4.12). The improvements of model similarity with further data integration (see Figs. 4.3 & 4.9f) reduce the number of large outliers, thus improving the similarity especially of the 1% threshold. Furthermore, in the 75% threshold, the coverage of the lower parts of the structure is generally notably improved. In the 99% model, positive effects of data integration vary, due to the scale-independency of the quantification algorithm. As observed in Subsect. 4.3.3.3, the mean PC space distance plot for Juliusburg_Koestorf-Rosenthal indicates that the tested data configurations are marginally sufficient to model the highly anisotropic, partially overhanging structure. This is mainly the case as most data setups fail to reproduce the overhang configurations (see e.g., Fig. 4.3, right column). Furthermore, while the general anisotropy is reproduced for many data configurations and threshold models, the constraint of the shape in the "short" horizontal direction is mostly poor. Even the large jump in similarity between the setups "0 sections 10 boreholes" and "8 sections 8 boreholes" fails to result in a mean PC space distance value indicating particularly high similarity to the reference model (Fig. 4.13). Still, when recognizing the strong geometric outliers in the 1% threshold model, the "8 sections 8 boreholes"-setup reproduces the reference reasonably well (with the exact same mean PC space distance value as the setup "3 sections 3 boreholes" for Gielow). However, in contrast to Gielow, the determined "sufficient" data configuration for Juliusburg_Koestorf-Rosenthal is rather unrealistic in its availability, when disregarding the possible presence of a 3D seismic survey. Overall, given the results for all three structures, a clear correlation between increasing minimum data quantity requirements and increasing structural complexity is identified.

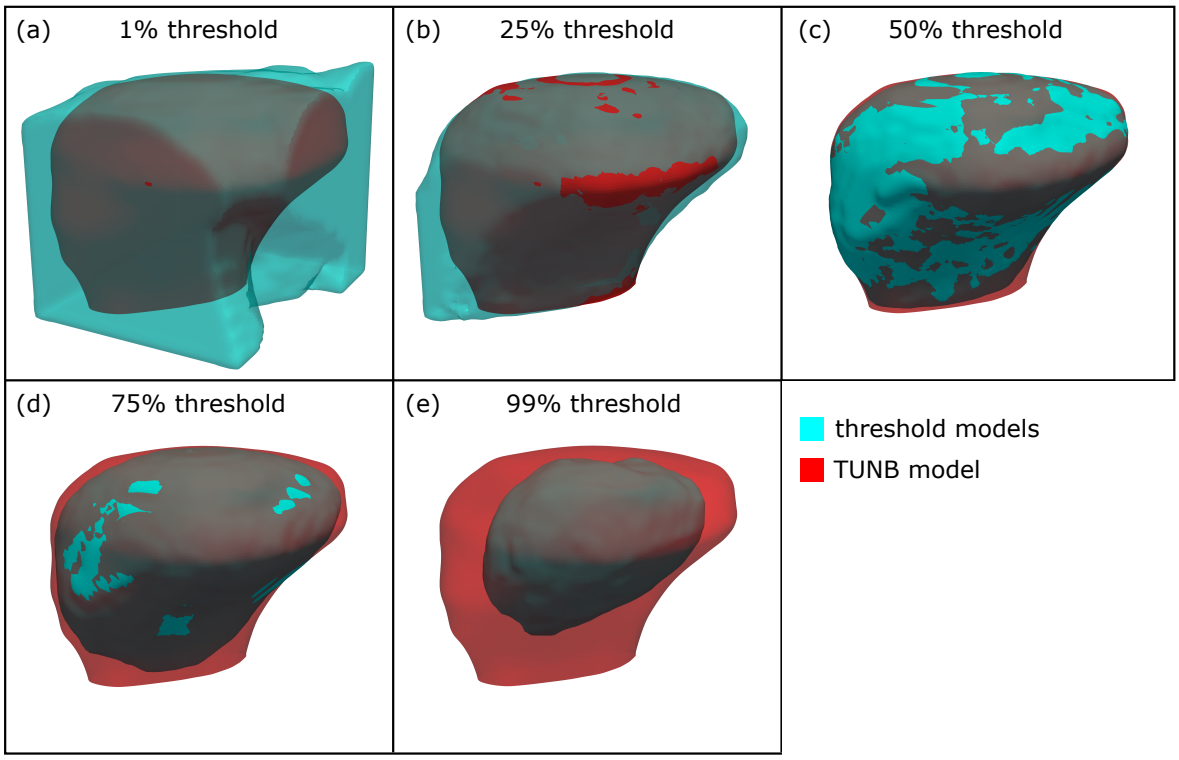


Figure 4.12: Visualization of the threshold models of the configuration "3 sections 3 boreholes" for Gielow, that has been identified as the minimum data requirement (compare also Figs. 4.3 & 4.9f). Coordinate axes are omitted for visual clarity (for the dimensions of Gielow, see Fig. 4.1)

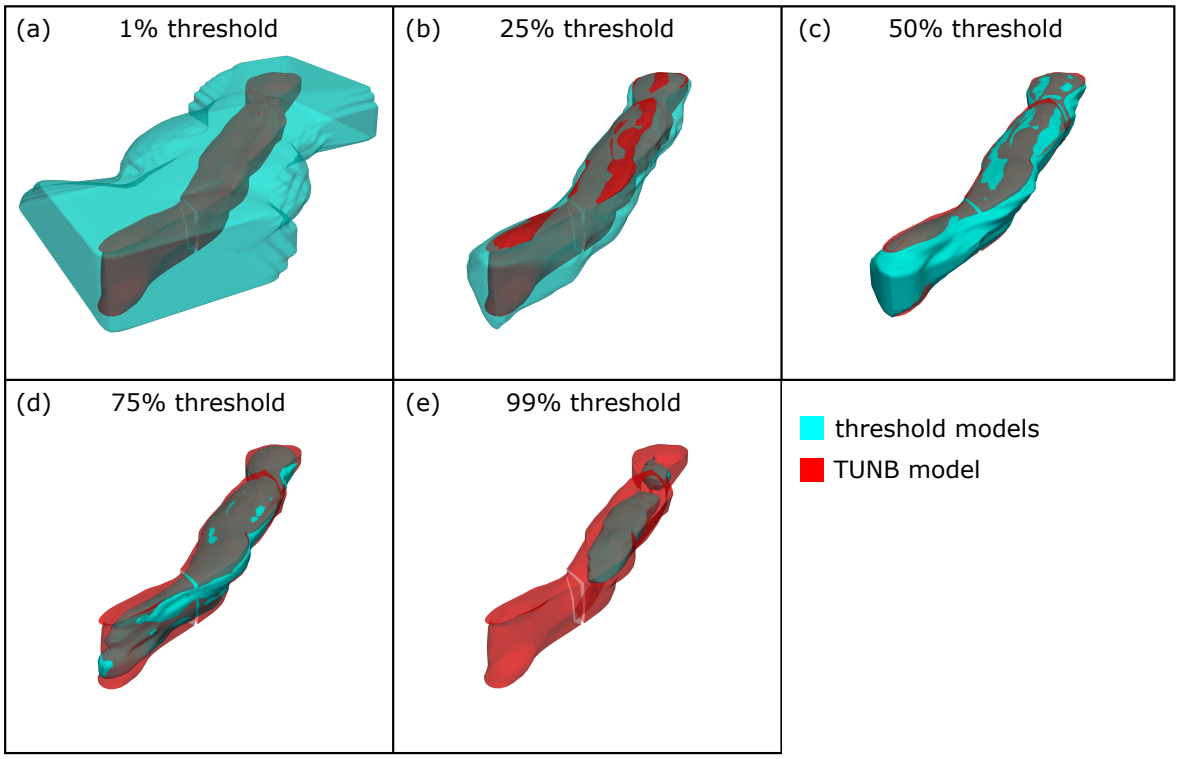


Figure 4.13: Visualization of the threshold models of the configuration "8 sections 8 boreholes" for Juliusburg_Koestorf-Rosenthal, that has been identified as the minimum data requirement (compare also Figs. 4.3 & 4.10f). Coordinate axes are omitted for visual clarity (for the dimensions of Juliusburg_Koestorf-Rosenthal, see Fig. 4.1)

4.4 Discussion

4.4.1 Methodology – data and model generation and setup of metrics

The objective of establishing metrics to assess minimum data requirements is challenging in many aspects. The choice of employing synthetic datasets to represent real geological and geophysical input data types requires decision-making on the design of the data types; the relative amounts (configurations) in which they should be obtained; and input/reference models from which these datasets should be extracted. The design of the data types is also dependent on the interpolation algorithm to be used. After computing the model realizations, further decision-making is required regarding the setup of the metrics. In the case of this study, this was mainly concerned with the representation of the model realizations by threshold models and the choice of the statistical methods providing the foundation for the metrics.

In the initial data generation, the choice of configurations has been based on the data situation in the German subsurface. The regional distribution of seismic data has been evaluated using the German Hydrocarbon Information System (LBEG n. d.), and the density of boreholes has been assessed with the Borehole Map of Germany (Staatliche geologische Dienste 2016). Based on these databases, the 15 data configurations were designed to cover both realistic/typical data situations as well as unrealistic extensive "best case scenarios". This explains both the prevalence of data setups with three or less respective sections and boreholes, as well as the chosen high quantity configurations. Furthermore, it has to be noted, that extremely sparse data situations ("1 section 0 boreholes" and "0 sections 1 borehole") have not been covered as they could not be interpolated in 3D without additional information that was not incorporated intentionally to avoid subjective bias. Overall, data configurations have thus been chosen based on evaluations of regional patterns rather than specific case studies. Given the data configurations, the placement of orientations required for the chosen interpolation method is supposed to mimic real data situations. Regarding borehole data, one can assume that a single respective orientation measurement at the inlet and outlet of a borehole in a geo-body is obtainable in most cases. While additional measurements inside the structure might be possible, we did not intend to cover internal structures of geo-bodies, and thus did not obtain data inside the geometries. In the case of real geophysical 2D sections, it is less likely that acquisition of orientation data is conducted simultaneously. However, as the interpolation method utilized in our study requires orientations, we chose a single in-plane orientation with normal direction [0, 0, 1] at the shallowest z-coordinate of each section, to have the lowest possible impact on mod-

eling results. With the influence of the vertical orientations from the sections being intentionally small, the 3D orientations from the boreholes are vital for the modeling results. For the 3D interpolation, the cross sections are automatically discretized into points. Thus, the input datasets effectively consist of points and orientations. The number of 100 datasets and interpolated realizations has been chosen to represent the geometric uncertainty that is to be expected based on the approach. The amount is assumed to be of minor importance, i.e., it might influence the order of similarity whenever differences between two data configurations are small but will have no effect on large differences.

When interpolating the input datasets, the model space has been kept constant. This was done to limit the cost of computing the model realizations. The downside of this approach is that extreme geometric outliers get truncated at the boundary of the model space, as frequently seen in 1% threshold models of low quantity configurations (see e.g., Figs. 4.12a, 4.13a). While these 1% models therefore not completely cover the geometric range of dissimilar model realizations, the essence of the threshold models and the corresponding values of both metrics remains: the specific models are very dissimilar compared to the given reference. Furthermore, the choice of a restricted model domain has the advantage that cuboidal threshold models indicating dissimilar model realizations are identifiable immediately in the bar charts of both metrics due to their constant values. Thus, more similar threshold models compared to the reference are obvious without deeper analysis. The same is true for differences in the structural complexity of various geometries: a prevalence of cuboidal shapes in the 1% threshold (see e.g., Fig. 4.10a compared to Figs. 4.8a & 4.9a) indicates a larger structural complexity of the underlying geo-body.

As described in Subsect. 4.2.1, the computation of the threshold models instead of the individual evaluation of the 1500 model realizations per structure represents a computationally efficient way to assess structural dis-/similarity between the realizations of different data configurations and a reference. The small 1% and 25% thresholds reproduce the quantity of geometric outliers for a data configuration, while the 75% and 99% percentiles reflect the similarity between the majority of the underlying 100 model realizations. While the alternative individual comparison of model realizations to the reference would have defined the number of outliers more precisely, combining the realizations into threshold models still reproduces well the differences between the modeling results of the various data configurations. Thus, the threshold models are sufficient and efficient approximations of the respective total realization ensemble, given that the research question has been the assessment of minimum data requirements rather than the exact geometric characterization of a realization set. The setup of the metrics required averaging of values at several points, possibly smoothing outliers and

thus potentially hiding relevant information. However, the averaging of the three KLD values per threshold model to obtain the avKLD between that threshold model and the reference is the best way to process the data. As the geometry of a structure is defined by the combination of all three individual geometric parameters (see Carl et al. 2026a; Carl et al. 2026b), establishing three KLD-related metrics for minimum data requirements based on the individual properties would be unreasonable. This holds true for the PC space distance metric as well. Regarding the averaging of the five respective values from the threshold models of a data configuration to obtain the final metrics, no information get lost for the interpreter. The presence of geometric outliers resulting in values of lower similarity for threshold models is still detectable in the intermediate bar charts.

4.4.2 Comparison between both metrics

Based on the results, both metrics often produce somewhat comparable patterns of similarity for the sphere and Gielow, but very dissimilar plots for Juliusburg_Koestorf-Rosenthal. In general, differences are to be expected and attributed to two factors (see for example Jolliffe 2002; Kullback and Leibler 1951): 1) While the KLD is computed per parameter, the distance in PC space is calculated from a concatenated feature vector. 2) While the KLD treats every percentile of the PDFs equally, PCA emphasizes directions of largest variance and thus inherently weighs original features. Overall, as a result of these factors, the outliers of PC space distance values in the bar charts of the threshold groups are less extreme than the outliers seen in the avKLD plots. The very distinct differences between the results of both metrics for Juliusburg_Koestorf-Rosenthal are resulting mainly from mismatches in the gradient data distributions compared to the reference, as most prominently present for the data configuration "10 sections 0 boreholes" (see Fig. 4.14). Such often slight mismatches in the distributions can cause large differences in the resulting Kullback-Leibler divergences, especially if the distributions consist of few main maxima of data with little data in between, as it is the case for many normalized gradient datasets (see also Subsect. 4.2.3). In contrast, PCA is not prone to such mismatches and better detects and translates variations in the input data to the respective metric when inherently weighing the input. We would thus argue that the mean PC space distance is the better performing metric.

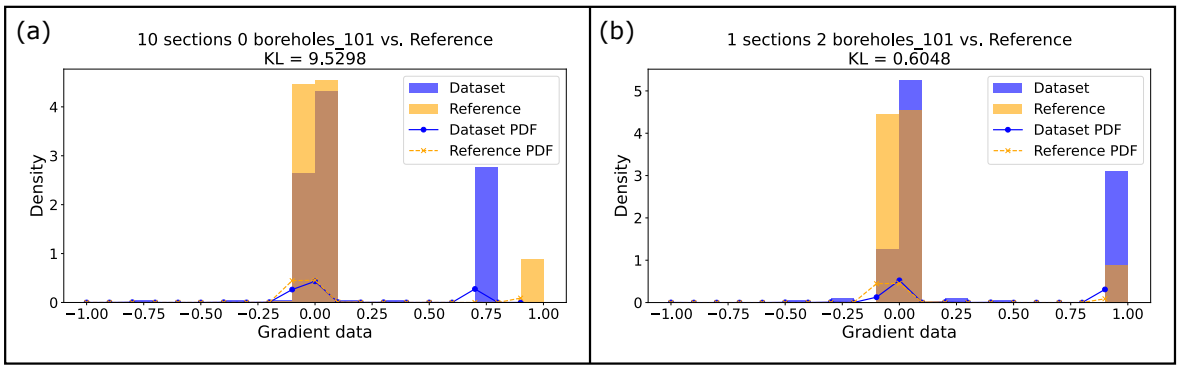


Figure 4.14: Visualization of the Kullback-Leibler divergence calculation and mismatches of data maxima. Note that the bars in the graph are for visualization only, the KLDs are computed on the PDFs. a) Large KLD following a mismatch of the large positive gradients while the other maxima correspond well. b) Much smaller KLD given the overlap of all three maxima, although the maxima around 0 correspond not as good as it is the case for the threshold model in a)

4.4.3 Further considerations on minimum data requirements

Besides the impact of structural complexity on the required amounts of input data, another aspect is the applied modeling method. For an explicit geomodel, more input data might be required, scaling with the number of geo-objects to be modeled, as every object has to be explicitly defined by a mesh whose vertices are either exactly or approximately tied to the input data (Wellmann and Caumon 2018). In contrast, in implicit interpolation algorithms, the geological boundaries of an object are represented as an isosurface within a volumetric scalar field. This is helpful when conformable packages of strata are modeled, as less input is required. However, in general, the aspect of the modeling method is less important when a single geo-body is to be modeled, as all input data belong to that structure anyway. In addition to the potential impact of different modeling methods, it has to be considered as well that in reality, the relative value of borehole data compared to any type of 2D geophysical data is dissimilar. Cores most often offer rather precise information on the depth and orientation of rock interfaces in the subsurface that may lack representativity for the larger volume though. Meanwhile, geophysical data come with comparatively more uncertainties introduced in data acquisition, processing and interpretation, but mostly have a larger spatial coverage (Wellmann and Caumon 2018). Furthermore, every type of data is able to resolve the subsurface differently, with the resolution of many geophysical data being comparatively coarser.

4.4.4 Comparison of the workflow to previously proposed approaches

The reduction of uncertainties in geological models with data integration has been explored by various authors (e.g., Lindsay et al. 2012; Schweizer et al. 2017; Wang et al. 2022; Wellmann and Regenauer-Lieb 2012; Wellmann 2013), but among these studies, none has assessed the inverse problem of minimum data quantity requirements. Putz et al. (2006) approach such a problem by progressively reducing input data for geomodeling, but do not apply any quantitative measures in their analysis. Carmichael and Ailleres (2016) quantitatively assess the influence of data density on modeling results through their performance evaluation of upscaling methods, but do not attempt to derive minimum data quantity requirements. Their approach might be adaptable for that purpose given their basis of quantitative model comparison, but would require an exploration of similarity sufficiency to the initial reference.

The adaptability of the other approaches outlined in the introduction for similar purposes compared to our metrics varies. The model entropy described by Wellmann and Regenauer-Lieb (2012) is very useful for the visualization of uncertainty quantification and reduction and for hypothesis testing, and the mean entropy and fuzziness entropy work well for model comparison. The latter two metrics describe uncertainty with a single number, which is similar to our proposed approach, in that higher values for our metrics (corresponding to lower similarity compared to the reference) also represent higher uncertainty regarding the shape of a geometry. Entropy considerations for our cases of single, isolated structures would be binary systems. In cells where all 100 realizations are present (a 100% percentile model) or on the other hand no realizations exist, the entropy would be zero. Meanwhile, in all cells where the existence of realizations is equally as probable as their absence, entropy would be maximal. Visualizing the entropy cell-wise would thus give a good indication for the dis-/similarity of all 100 realizations and roughly for the shape of the 50% percentile. Furthermore, computing the mean entropy of the realization set of a data configuration would reflect with a single value, how similar all model realizations are to each other. Given a low mean entropy, the overlap of all realizations would be high, and they would be well constrained to the same shape. In contrast, if the mean entropy was high, this would indicate that the realizations are dissimilar and do not constrain a structure reasonably. Therefore, the single value of mean entropy could also be used to compare the modeling results of different data configurations. However, the comparison to a reference would not be possible. Thus, although it is unlikely, it could be theoretically possible that the 100 realizations of a configuration produce a shape similar to each other but not to the reference one might like to reproduce. This would not be visible through the mean entropy. Furthermore, it remains unexplored, what value of mean entropy would

indicate a "sufficiently reasonable" modeling result. The concept of stratigraphic variability introduced by Lindsay et al. (2012) represents a viable quantitative measure for cell-based uncertainty characterization and reduction assessment given additional data as well. For our evaluation of minimum data quantities, its value is however limited. While for our database, the stratigraphic possibility would only indicate, whether at least one realization is present respectively in the cells (thus corresponding to a 1% threshold model of the present study), the stratigraphic variability frequency would reflect how high the probability of a realization being present in a cell is. The latter could thus be used alternatively to create percentile threshold models, when summing up all cells for which a value is higher than a threshold percentage. However, these threshold models would need to be analyzed similarly to our approach. Jessell et al. (2010) compute their misfit functions (structural, lithological, gravity and magnetic misfits) between model realizations and references and are thus closer to our approach in that regard, especially as one value per misfit function is obtained. Thus, similarly to the approach proposed herein, plotting the variations in the misfit function values among model realizations may determine whether specific realizations are closer to the reference. Consequently, the misfit functions of Jessell et al. (2010) could work similarly to our metrics, provided that the assessed realization sets differ in the amount of underlying input data.

The methods investigating the optimal location of data acquisition (e.g., Afonseca and Miguel-Silva 2022; Hossein-Morshedy et al. 2023; Scheidt et al. 2026; Wellmann 2013) cannot be translated directly to our objective, as we solely looked into required data quantities so far, while randomly varying the placement of the input. However, a combination of both types of approaches would be interesting: where would data need to be acquired to cover the object of interest in a way, that the resulting geomodels are both sufficiently realistic and produced with as little data as possible? This is essentially an objective of optimal experimental design (see e.g., Nowak and Guthke 2016; Seidler et al. 2016; White and Royer 2003), that requires at least basic conceptual knowledge. The approach of assessing the realism of geo-objects through consistency checking as recently shown by Parquer et al. (2025) is currently not applicable to isolated 3D geo-objects we are concerned with, but would be a viable method to check the minimum data quantity requirements for typical "composite" geomodels consisting of several stratigraphic units. If too many realizations failed the consistency check, it would be indicated that more data is needed to model a subsurface object configuration reliably. Here, thresholds could easily be defined.

4.4.5 Implications of the study results

Given the results of this study and the aspects discussed, several general outcomes are identified. The established framework allows for an assessment of minimum data quantity requirements for structural geomodeling. Between the two established metrics, the mean PC space distance performs better at reproducing the differences of the modeling results of various data configurations. The results validate that the minimum data requirements to model a structure realistically scale with the geometric complexity. While this relationship is not yet well defined based on the three tested structures, expanding such tests to a larger diversity of geo-bodies may result in a database that allows to infer minimum requirements for an "untested" case as long as there is a conceptual understanding of the structure to be modeled. Furthermore, provided there is a well-established relationship, one might consider "extrapolating" the minimum requirements for a complex situation based on the data of more "simple" models.

The possibility is thus anticipated to use the framework to evaluate whether an unmodeled dataset is sufficient for geomodeling with reasonable uncertainty given a basic conceptual understanding of the specific subsurface situation. This understanding is quantitatively improvable when employing the set of benchmark geometries presented by Carl et al. (2026a): based on the input dataset, a subset of benchmarks may be selected, before the framework presented herein is applied. By applying the different benchmark models as possible reference geometries and comparing the similarity results of the input dataset, it can be tested which benchmark approximates the subsurface situation best, thus improving the conceptual understanding. On the other hand, if the input dataset fails to realistically reproduce any of the tested benchmarks, it is indicated that the data situation or the range of selected benchmarks is insufficient.

4.5 Conclusion

In this publication, we have established and applied two metrics to evaluate, how much geological and/or geophysical input data is required to create realistic structural geomodels of isolated subsurface structures. A sphere and two pre-modeled meshes of geometrically diverse intrusive salt structures from the German subsurface have been used as starting points and references for the analyses. 100 synthetic datasets of 2D vertical cross sections and 1D vertical boreholes have been randomly extracted for 15 different data configurations. Datasets have been interpolated in 3D using the implicit modeling method implemented in GemPy, and the resulting model realizations have been condensed into five threshold models per data configuration. Threshold models and references have been segmented and measured using the quantitative shape characterization and comparison method established by Carl et al. (2026a) and Carl et

al. (2026b). This method provides datasets of horizontal and vertical extensional data as well as gradients, therefore characterizing the (an-)isotropy, sphericity and surface morphology of tested geo-objects. This data has been utilized as the input for both tested metrics for minimum data quantity requirements:

1. The mean averaged Kullback-Leibler divergence (mean avKLD) is an averaged measure for model similarity based on data distributions. With the basic KLD, the distributions of the three geometric parameters are quantitatively compared between the individual threshold models of the 15 data configurations and the reference model. The three Kullback-Leibler divergence values for a threshold model of a data configuration are averaged to obtain the averaged Kullback-Leibler divergence of that model. The avKLDs are visualized and analyzed in bar charts. Subsequently, the five values of the threshold models of a data configuration are averaged again to produce the single mean averaged Kullback-Leibler divergence of that configuration.
2. The mean Euclidean distance in principal component (PC) space is an averaged measure for model similarity based on dimensionally reduced data. The 15 models of a threshold group are dimensionally reduced together with the reference model through principal component analysis. The Euclidean distances in PC space between the models of a threshold and the reference are thus determined. The five distance values of the threshold models of a data configuration are averaged to obtain the single mean distance in PC space of that data configuration.

After respectively analyzing the bar charts of the intermediate averaged Kullback-Leibler divergences and Euclidean distances in PC space for the five individual thresholds, a line plot has been created for each of the two final metrics. Values have been sorted in ascending order to reflect increasing similarity of data configurations to the respective reference. The two diagrams have been analyzed to recognize increases of data quantities that coincide with considerable improvements of model similarity. The mean PC space distance has been identified as the superior metric, as PCA weighs the geometric input data and thus determines where input structures vary the most. For the geometrically simple sphere, minimum data requirements to acquire reasonable geomodeling results are lowest. For Gielow, a moderate data quantity requirement is identified when considering the presence of few geometric outliers. The structurally most complex salt wall Juliusburg_Koestorf-Rosenthal can only be modeled reliably with the data configurations of largest quantities, whose availability in reality is rather unlikely for most subsurface situations. The experimental results validate that the established framework is utilizable to assess the minimum data requirements for struc-

tural geomodeling. Furthermore, it is anticipated that the approach is applicable to evaluate the sufficiency of an unmodeled dataset for realistic modeling, as long as there is a basic conceptual understanding of the subsurface situation.

Given the results of the present study, a follow-up step could be to apply the mean PC space distance to additional meshes of subsurface structures, to better establish the relationship of increasing minimum data quantity requirements with increasing structural complexity. Furthermore, the application of the concept to unmodeled datasets could be demonstrated: instead of randomly extracting datasets from meshes, one could progressively reduce the geological and geophysical data available for a given subsurface structure. This would likely result in fewer data configurations as tested herein, but the respective impact of individual boreholes or geophysical sections on constraining the shape of the structure could be assessed. In case the conceptual understanding of the subsurface situation was poor, benchmark models could be employed as described in Subsect. 4.4.5.

Code and data availability

Code creation was carried out in Python. The approach mostly relies on the capabilities of the packages Shapely (https://shapely.readthedocs.io/en/stable/), PyVista (https://pyvista.org/), vtk (https://docs.vtk.org/en/latest/api/python.html), Plotly (https://plotly.com/) and GemPy (https://github.com/gempy-project/gempy). The python code, the threshold models and references (both as .vtk-files), and the datasets of raw horizontal, vertical and gradient data are stored at
https://doi.org/10.5281/zenodo.19406122, Carl (2026).

Author contribution

FC: writing–original draft; writing–review and editing; method development; data acquisition and analysis; conceptualization; visualization. JY: writing–review and editing; conceptualization. SB: writing–review and editing; data acquisition. FW: writing–review and editing; supervision; funding acquisition. PA-Z: writing–review and editing; conceptualization; supervision; funding acquisition.

Declarations

The authors declare the following financial interests/personal relationships which may be considered as potential competing interests: Friedrich Carl and Jian Yang are funded by the German Federal Company for Radioactive Waste Disposal (BGE). Other authors declare that they have no conflict of interest.

Acknowledgements

This study was conducted as part of the GeoBlocks project. GeoBlocks is a collaboration of RWTH Aachen University, University of Aberdeen and the German Federal Institute for Geosciences and Natural Resources (BGR) within the research cluster URS (Uncertainty and Robustness with regard to the Safety of a repository for high-level radioactive waste), funded by the German Federal Company for Radioactive Waste Disposal (BGE), with the main objective being the creation of an open-source workflow for geological modeling that includes the quantification and visualization of uncertainties and aims at the optimization of sampling procedures. We thank for the financial support by BGE. The authors would also like to thank BGR for the data provided to the study.

References

Afonseca, B. C. and Miguel-Silva, V. (2022). "Defining optimal drill-hole spacing: A novel integrated analysis from exploration to ore control". en. In: *Journal of the Southern African Institute of Mining and Metallurgy* 122.6, pp. 305–315. ISSN: 2225-6253. DOI: 10.17159/2411-9717/2024/2022. URL: http://www.scielo.org.za/scielo.php?script=sci_abstract&pid=S2225-62532022000600009&lng=en&nrm=iso&tlng=en (visited on 03/03/2026).

BGE (2023). *Vorgehen zur Ermittlung von Standortregionen aus den Teilgebieten*. Tech. rep. URL: https://www.bge.de/fileadmin/user_%20upload/Standortsuche/Wesentliche_Unterlagen/Methodik/%20Phase_I_Schritt_2/20231004_Vorgehen_zur_Ermittlung_von_%20Standortregionen_aus_den_Teilgebieten_barrierefrei.pdf (visited on 01/22/2026).

BGR, LAGB, LBEG, LBGR, LLUR, and LUNG (2022). *3D-Modell des geologischen Untergrundes des Norddeutschen Beckens (Projekt TUNB) Erstveröffentlichung 2021, Version 2022*. DOI: https://gst.bgr.de. URL: https://gst.bgr.de,%20Abgerufen%20am%201.12.xn--2024%20allgemeine%20geschftsbedingungen,%20siehe%20https:-qde//www.bgr.bund.de/AGB%20General%20terms%20and%20conditions,%20see%20https://www.bgr.bund.de/AGB_en.%E2%80%9C (visited on 12/01/2024).

Bjørlykke, K., ed. (2015). *Petroleum Geoscience: From Sedimentary Environments to Rock Physics*. en. Berlin, Heidelberg: Springer. ISBN: 978-3-642-34131-1 978-3-642-34132-8. DOI: 10.1007/978-3-642-34132-8. URL: https://link.springer.com/10.1007/978-3-642-34132-8 (visited on 10/13/2025).

Carl, F. (2026). *FriedrichCarl97/Carl-et-al.-c-in-prep: Carl. et al.(c) assets V. 1.0*. DOI: https://doi.org/10.5281/zenodo.19406121.

Carl, F., Yang, J., Colling Cassel, M., Wellmann, F., and Achtziger-Zupančič, P. (2026a). "Quantitative comparison of three-dimensional bodies using geometrical properties to validate the dissimilarity of a standard collection of 3D geomodels". English. In: *Solid Earth* 17.1, pp. 155–178. ISSN: 1869-9510. DOI: 10.5194/se-

17-155-2026. URL: https://se.copernicus.org/articles/17/155/2026/ (visited on 02/04/2026).

— (2026b). "Quantitative comparison of subsurface structures: an application to salt domes and crystalline bodies". In: *Journal of Structural Geology* 205, p. 105633. ISSN: 0191-8141. DOI: 10.1016/j.jsg.2026.105633. URL: https://www.sciencedirect.com/science/article/pii/S0191814126000192 (visited on 02/12/2026).

Carmichael, T. and Ailleres, L. (2016). "Method and analysis for the upscaling of structural data". In: *Journal of Structural Geology* 83, pp. 121–133. ISSN: 0191-8141. DOI: 10.1016/j.jsg.2015.09.002. URL: https://www.sciencedirect.com/science/article/pii/S0191814115300353 (visited on 03/11/2026).

de la Varga, M., Schaaf, A., and Wellmann, F. (2019). "GemPy 1.0: open-source stochastic geological modeling and inversion". English. In: *Geoscientific Model Development* 12.1, pp. 1–32. ISSN: 1991-959X. DOI: 10.5194/gmd-12-1-2019. URL: https://gmd.copernicus.org/articles/12/1/2019/ (visited on 02/21/2026).

Hossein-Morshedy, A., Khorram, F., and Emery, X. (2023). "A Multi-Objective Approach for Optimizing the Layout of Additional Boreholes in Mineral Exploration". en. In: *Minerals* 13.10, p. 1252. ISSN: 2075-163X. DOI: 10.3390/min13101252. URL: https://www.mdpi.com/2075-163X/13/10/1252 (visited on 03/03/2026).

Hudec, M. R. and Jackson, M. P. A. (2007). "Terra infirma: Understanding salt tectonics". In: *Earth-Science Reviews* 82.1, pp. 1–28. ISSN: 0012-8252. DOI: 10.1016/j.earscirev.2007.01.001. URL: https://www.sciencedirect.com/science/article/pii/S0012825207000025 (visited on 11/30/2024).

Jessell, M. W., Ailleres, L., and Kemp, E. A. de (2010). "Towards an integrated inversion of geoscientific data: What price of geology?" In: *Tectonophysics* 490.3, pp. 294–306. ISSN: 0040-1951. DOI: 10.1016/j.tecto.2010.05.020. URL: https://www.sciencedirect.com/science/article/pii/S0040195110002246 (visited on 02/18/2026).

Jolliffe, I. T. (2002). *Principal Component Analysis*. en. Springer Series in Statistics. New York: Springer-Verlag. ISBN: 978-0-387-95442-4. DOI: 10.1007/b98835. URL: http://link.springer.com/10.1007/b98835 (visited on 04/23/2025).

Kullback, S. and Leibler, R. A. (1951). "On Information and Sufficiency". en. In: *The Annals of Mathematical Statistics* 22.1, pp. 79–86. ISSN: 0003-4851. DOI: 10.1214/aoms/1177729694. URL: http://projecteuclid.org/euclid.aoms/1177729694 (visited on 12/01/2024).

LBEG (n. d.). *Hydrocarbon Information System (KW-FIS)*. URL: https://www.lbeg.niedersachsen.de/energie_rohstoffe/erdoel_und_erdgas/fachinformationssystem/kohlenwasserstoff-fachinformationssystem-kw-fis-670.html (visited on 04/04/2026).

Lindsay, M. D., Jessell, M. W., Ailleres, L., Perrouty, S., Kemp, E. de, and Betts, P. G. (2013). "Geodiversity: Exploration of 3D geological model space". In: *Tectonophysics* 594, pp. 27–37. ISSN: 0040-1951. DOI: 10.1016/j.tecto.2013.03.013. URL: https://www.sciencedirect.com/science/article/pii/S004019511300187X (visited on 04/04/2025).

Lindsay, M. D., Aillères, L., Jessell, M. W., Kemp, E. A. de, and Betts, P. G. (2012). "Locating and quantifying geological uncertainty in three-dimensional models: Analysis of the Gippsland Basin, southeastern Australia". In: *Tectonophysics* 546-547, pp. 10–27. ISSN: 0040-1951. DOI: 10.1016/j.tecto.2012.04.007. URL: https://www.sciencedirect.com/science/article/pii/S0040195112002004 (visited on 07/31/2025).

Luca, A. de and Termini, S. (1993). "A Definition of a Nonprobabilistic Entropy in the Setting of Fuzzy Sets Theory". en-US. In: *Readings in Fuzzy Sets for Intelligent Systems*. Morgan Kaufmann, pp. 197–202. DOI: 10.1016/B978-1-4832-1450-4.50020-1. URL: https://www.sciencedirect.com/science/chapter/edited-volume/abs/pii/B9781483214504500201 (visited on 02/23/2026).

Nowak, W. and Guthke, A. (2016). "Entropy-Based Experimental Design for Optimal Model Discrimination in the Geosciences". en. In: *Entropy* 18.11, p. 409. ISSN: 1099-4300. DOI: 10.3390/e18110409. URL: https://www.mdpi.com/1099-4300/18/11/409 (visited on 03/06/2026).

Parquer, M. N., Kemp, E. A. de, Brodaric, B., and Hillier, M. J. (2025). "Checking the consistency of 3D geological models". English. In: *Geoscientific Model Development* 18.1, pp. 71–100. ISSN: 1991-959X. DOI: 10.5194/gmd-18-71-2025. URL: https://gmd.copernicus.org/articles/18/71/2025/ (visited on 10/24/2025).

Putz, M., Stüwe, K., Jessell, M., and Calcagno, P. (2006). "Three-dimensional model and late stage warping of the Plattengneis Shear Zone in the Eastern Alps". In: *Tectonophysics* 412.1, pp. 87–103. ISSN: 0040-1951. DOI: 10.1016/j.tecto.2005.10.003. URL: https://www.sciencedirect.com/science/article/pii/S0040195105004531 (visited on 02/18/2026).

Scheidt, C., Neto, F. T., Yin, D. Z., and Caers, J. K. (2026). "Optimizing Drilling in Brownfield Ni-Cu Depositional Systems Based on the Integration of Geochemical, Geophysical and Drill-Hole Data". en. In: *Minerals* 16.1, p. 82. ISSN: 2075-163X. DOI: 10.3390/min16010082. URL: https://www.mdpi.com/2075-163X/16/1/82 (visited on 03/03/2026).

Schroeder, W., Martin, K. M., and Lorensen, W. (2006). *The Visualization Toolkit, An Object-Oriented Approach To 3D Graphics*. Kitware. ISBN: 978-1-930934-19-1. (Visited on 11/10/2025).

Schweizer, D., Blum, P., and Butscher, C. (2017). "Uncertainty assessment in 3-D geological models of increasing complexity". English. In: *Solid Earth* 8.2, pp. 515–530. ISSN: 1869-9510. DOI: 10.5194/se-8-515-2017. URL: https://se.copernicus.org/articles/8/515/2017/ (visited on 04/04/2025).

Seidler, R., Padalkina, K., Bücker, H. M., Ebigbo, A., Herty, M., Marquart, G., and Niederau, J. (2016). "Optimal experimental design for reservoir property estimates in geothermal exploration". en. In: *Computational Geosciences* 20.2, pp. 375–383. ISSN: 1573-1499. DOI: 10.1007/s10596-016-9565-4. URL: https://doi.org/10.1007/s10596-016-9565-4 (visited on 03/06/2026).

Shannon, C. E. (1948). "A mathematical theory of communication". In: *The Bell System Technical Journal* 27.3, pp. 379–423. ISSN: 0005-8580. DOI: 10.1002/j.1538-7305.1948.tb01338.x. URL: https://ieeexplore.ieee.org/document/6773024 (visited on 06/11/2025).

Staatliche geologische Dienste (2016). *Deutscher Bohrungsnachweis*. URL: https://numis.niedersachsen.de/trefferanzeige;jsessionid=7B84630628B1FBF2573ED801916273B6?docuuid=e255206f-49c2-46f8-9995-a023c5520bbb (visited on 04/04/2026).

Stephenson, P. (2018). "The Shoelace Formula & Pick's Theorem". In: *Mathematics in School* 47.4, pp. 35–38. ISSN: 0305-7259. URL: https://www.jstor.org/stable/26534777 (visited on 12/01/2024).

Wang, S.-J., Nguyen, Q. C., Lu, Y.-C., Doyoro, Y. G., and Tran, D.-H. (2022). "Evaluation of geological model uncertainty caused by data sufficiency using groundwater flow and land subsidence modeling as example". en. In: *Bulletin of Engineering Geology and the Environment* 81.8, p. 331. ISSN: 1435-9537. DOI: 10.1007/s10064-022-02832-7. URL: https://doi.org/10.1007/s10064-022-02832-7 (visited on 02/19/2026).

Wellmann, F. and Regenauer-Lieb, K. (2012). "Uncertainties have a meaning: Information entropy as a quality measure for 3-D geological models". In: *Tectonophysics*. Modelling in Geosciences 526-529, pp. 207–216. ISSN: 0040-1951. DOI: 10.1016/j.tecto.2011.05.001. URL: https://www.sciencedirect.com/science/article/pii/S0040195111001788 (visited on 07/24/2025).

Wellmann, J. F. (2013). "Information Theory for Correlation Analysis and Estimation of Uncertainty Reduction in Maps and Models". en. In: *Entropy* 15.4, pp. 1464–1485. ISSN: 1099-4300. DOI: 10.3390/e15041464. URL: https://www.mdpi.com/1099-4300/15/4/1464 (visited on 08/08/2025).

Wellmann, J. F. and Caumon, G. (2018). "3-D Structural Geological Models: Concepts, Methods, and Uncertainties". English. In: *Advances in Geophysics*. 59. Elsevier, pp. 1–121. DOI: https://doi.org/10.1016/bs.agph.2018.09.001. (Visited on 04/04/2026).

White, C. D. and Royer, S. A. (2003). "Experimental Design as a Framework for Reservoir Studies". en. In: OnePetro. DOI: 10.2118/79676-MS. URL: https://dx.doi.org/10.2118/79676-MS (visited on 03/06/2026).

CHAPTER

FIVE

CONCLUDING REMARKS

5.1 Synopsis and conclusions

The research presented in this thesis focused on a method for the quantitative geometric characterization and comparison of subsurface structures, and on two developed metrics for the assessment of minimum data quantity requirements for realistic structural geomodeling. The main results of the thesis are the following:

- A framework for the geometric quantification of datasets has been established. Extensional data, gradients and curvatures are measured on 2D cross sections of 3D structures, perpendicular to the two horizontal main axes of the objects. The analyzed data provides insight into the anisotropy, sphericity and surface morphology of the investigated structures. The Kullback-Leibler divergence and the dimensionally reduced cluster analysis serve for the quantitative comparison and geometric systematization of the tested datasets. The methodology is established and demonstrated on a set of regular benchmark models for structural geomodeling. Through the method application, the dissimilarity of the final model set is quantified. The framework of the quantification algorithm and the benchmarks aims at aiding in several phases of geomodeling workflows. It is utilizable in the initial conceptualization of a modeling case, in the parametrization of the interpolation method, for the evaluation of geometric reasonableness of probabilistic model realizations after interpolation, and for the geometric characterization of final models. In comparison to previous advances for the quantitative description and/or comparison of geological structures and models, the established algorithm fills a niche. Unlike the dissimilarity distance functions as applied for instance by Schweizer et al. (2017) and Suzuki et al. (2008), the methodology is capable of

providing insight into both shape and size differences of objects. A similar conclusion can be drawn considering the mean entropy as described by Wellmann and Regenauer-Lieb (2012), and the misfit functions of Jessell et al. (2010): both measures provide singular values for model comparison that cannot indicate where two structures differ spatially. The geodiversity metrics of Lindsay et al. (2013) and their assessment exhibit many similarities to the established approach of this thesis, but the metrics are mainly tied to the coexistence of several stratigraphic units and are thus not directly applicable to individual geo-objects. Gardoll et al. (2000) determine geometric parameters like aspect ratios and the sphericity of geological bodies, but their method is only applicable to shallow horizontal data. Overall, the measurement of geometric parameters for shape difference quantification as described in this thesis is more common in material science (e.g., Altuhafi et al. 2013; Zhao and Wang 2016) and computer sciences (e.g., Celenk 1995). While the methodology of this thesis is more approximating than other algorithms given its setup of cross section-based data acquisition, it is efficient in reproducing the main geometric characteristics of input datasets. The results are interpretable with basic geological knowledge and thus accessible to a broader audience.

- The established benchmark models fill a gap in another aspect: thus far, only Pellerin et al. (2015) have proposed benchmark models in the context of structural geomodeling. However, these have been designed for "composite" structural models consisting of several stratigraphic units. The created set of "standard geometries" of this thesis usable for isolated geo-bodies therefore represents a step towards a more complete and varied database of benchmarks, that is utilizable for many geomodeling applications. In the context of the German site selection, the standard geometries could also serve visualization purposes, showing the geometric range of the potential host rocks for nuclear waste disposal to a non-specialist audience.
- The application of the quantification method to the full range of geometric complexity of the geological structures in the German subsurface validates the universal applicability of the framework. After adapting the method to open meshes, 239 datasets of intrusive salt structures and 67 models of crystalline intrusives have been covered, from which some exhibit appearances similar to those typical for concordant rock bodies. The minor compromises of the method to ensure its universal applicability have been found to not have a significant impact on the results. Similarly, differences in the construction of the assessed input models and in the used input data do not influence the applicability of the method either, as the framework is purely geometric at its core. Its geometric foundation also

has the advantage that the method results do not require visualization of the 3D models for their interpretation. This can avoid the introduction of subjective bias when applying the framework for decision-making, for instance when selecting a subset of structures for extensive exploration in an economic project. The cluster results have furthermore been found to be contextualizable with the respective regional geology in many parts, although it is indicated that a subdivision of the input data into multiple cluster analyses would uncover the relationships even better. The contextualization facilitates the evaluation of geometric patterns in the regional geology, which supports the assessment of selection criteria for storage capabilities of subsurface geo-bodies. Overall, the second study underlines the computational efficiency of the framework for the geometric analysis of large databases of geomodels, as the cluster analysis is capable of presenting all properties at once without requiring a full-scale comparative analysis of implicit model representations with millions of degrees of freedom.

- The results of the second study furthermore demonstrate the application of the catalogue of benchmark models to the full geometric range of subsurface geo-bodies. This also proves the hypothesis based on literature and model reviews, that the different rock types relevant as potential host rocks for nuclear waste disposal show geometric similarities and can partially be approximated with the same benchmark models. This validates, that when applying the benchmarks for the purpose of conceptualization of a structural geomodel, a large geometric range of standard geometries should be considered in the creation of an early conceptual model instead of a small, manual selection.
- Little research has been published so far on quantified minimum data requirements. To address this objective, two metrics have been established: the mean averaged Kullback-Leibler divergence and the mean Euclidean distance in principal component space, evaluated between condensed model realizations and a reference. Two models from the German subsurface have been selected as input and references based on the cluster results of the second study. In combination with a sphere model, a range of geometric diversity is thus assessed. Synthetic datasets have been extracted from the meshes in 15 data configurations and interpolated implicitly. Model realizations have been condensed into five percentile threshold models per data configuration, and these models as well as the references are analyzed with the shape quantification method of the thesis. The resulting geometric data is the input for the two metrics and their intermediate measures that are analyzed as well. The two final metrics reflect how similar the geometric modeling results based on different data configurations are compared to the initial reference models. Increases of data quantities coinciding with consider-

able improvements of model similarity are thus identifiable, just as minimum data quantity requirements for the different structures. The results differ between the metrics due to their varying statistical setup, and the mean Euclidean distance in principal component space has been identified as being superior. Minimum data quantities are recognizable for all three tested structures, and are larger, the higher the geometric complexity. It is anticipated that the framework is applicable to assess whether an unmodeled data situation is sufficient for reasonable geomodeling, as long as a basic conceptual understanding of the subsurface is present. The established metrics and the experimental findings advance the research on required data densities, that has not been approached quantitatively with the same research objective before. In previous studies (e.g., Lindsay et al. 2012; Schweizer et al. 2017; Wang et al. 2022; Wellmann and Regenauer-Lieb 2012), the focus often has been on the effect of data integration on geomodels rather than assessing how much data is required to produce realistic modeling results in the first place.

In the context of the GeoBlocks project, this thesis has substantially contributed to the research on the quantified assessment and comparison of different uncertainties that arise in the process of geological modeling. While the project is affiliated with the German search for a nuclear waste disposal site, the methodologies and further results of this thesis are usable in different scientific and economic contexts. Within the framework of the GeoBlocks project, this doctorate was initially meant to be concerned with three aspects:

1. the quantitative description of the geometric variability of the potential host rocks
2. the development of methods for the comparison of regions showing different data sparsity situations from different acquisition sources
3. the assessment of the influence of data quality on modeling results

The first point has been addressed with the quantitative method for the geometric characterization and comparison, and with the set of benchmark models. The framework has been applied to the full range of geometric complexity of the German subsurface and can be integrated into geomodeling workflows and structural analyses. The second research focus has been approached with the metrics to assess the minimum requirements for data quantities and with the corresponding experimental results. While several directions for future research remain (see Subsect. 5.2), the work done in this thesis represents a foundation for further exploration. The third topic has been covered by co-researchers.

5.2 Recommendations for future research

For future research, two main directions are identified: the advancement and further application of the geometric shape quantification method and the further investigation of minimum data requirements for structural geomodeling. One of the primary aspects to aim for in the improvement of the quantification method is its potential automatization, given that currently, some geometric artifacts in the cross-sectional polygons need to be corrected manually. A successful automatization of the quantification method would optimize it for different proposed usages, like the falsification of large realization sets by data. Furthermore, the efficiency of the approach compared to implicit comparison methods could be directly assessed. As postulated in chapter 2, the applicability of the method and benchmarks to unmodeled input data in early model conceptualizations still needs proof. The results of the cluster analysis in chapter 3 have been found to be contextualizable with the regional geology. However, it has been hypothesized that a more compartmentalized set of cluster analyses instead of a single large one, and a more detailed cluster interpretation would provide superior results, which is assessable in another case study. Overall, the direct integration of the quantification method and the benchmarks into a complete workflow for structural geomodeling with quantified uncertainty is the final goal. There is the opportunity to combine the framework with open-source methods for 3D interpolation (e.g., de la Varga et al. 2019; Yang et al. 2025) and automatic consistency checking (Parquer et al. 2025) to efficiently address uncertainties in all stages of geomodeling.

However, the quantification algorithm is applicable beyond the field of structural geomodeling. Somewhat congeneric application fields would be material science – where the direction-dependent (micro-)structure of building materials is assessed – and remote sensing, where landscape elements like river channels, lava flows or coastlines may be evaluated along their main axes. Additional applications are envisioned where the direction-dependent characterization of objects is followed by an assessment of deviation compared to a clearly defined set of references. These preconditions are found in medicine, where the geometry of organs or blood vessels of patients may deviate from known ranges and standard values. Similarly, in civil engineering, the geometry of infrastructure like underground cables, pipes or curved bridges may be measured direction-dependent, to detect for instance deformation or corrosion when compared to the initial construction plans. In both cases, deviations from the norm could be quickly identified with the established method.

As the study in chapter 4 represents a first step towards the definition of minimum data quantity requirements for structural geomodeling, several possibilities for future research and experiments are recognized. The first follow-up step is the application of

the superior metric of the mean Euclidean distance in principal component space to a larger geometric variety of subsurface structures. While the minimum requirements have been found to correlate with structural complexity, a better investigation into that relationship is needed for scientific and economic considerations. Secondly, an application of the metric to unmodeled input data is of interest: for instance, borehole data and seismic sections prior to modeling could be used instead of randomly created synthetic data. While the number of data configurations would likely be smaller, the influence of individual datasets (boreholes and sections) on constraining the bodies' shape could be assessed. This evaluation is integrable with other research conducted within GeoBlocks, to assess whether multiple interpretations of uncertain seismic lines influence the amount of data required. What is needed as well is the investigation of minimum data quantity requirements for "composite" geomodels consisting of several stratigraphic units. For that purpose, for instance methods for consistency checking like the one introduced by Parquer et al. (2025) might be adapted. From a technical perspective, the approach proposed in this thesis could be improved by the already-mentioned potential automatization of the shape quantification algorithm. Furthermore, automatic re-meshing of input models prior to the approach is a task of future development, as well as an investigation on how scale differences in threshold models and model realizations may be accounted for.

A last research question where all methods and results of this thesis may contribute is a quantified definition of complexity among geomodels and underlying subsurface configurations. While measures for geological complexity quantification in the context of the site selection are explored (see BGE 2022), the framework of this thesis may help: what could be defined on a scale to represent single components of a composite complexity measure are 1) the data density and its sufficiency for reasonably uncertain geomodeling, 2) the anticipated anisotropy of a structure, and 3) the lateral character of a body (i.e., the potential presence and spatial extent of overhangs).

References

Altuhafi, F., O'Sullivan, C., and Cavarretta, I. (2013). "Analysis of an Image-Based Method to Quantify the Size and Shape of Sand Particles". EN. In: *Journal of Geotechnical and Geoenvironmental Engineering* 139.8, pp. 1290–1307. ISSN: 1943-5606. DOI: 10.1061/(ASCE)GT.1943-5606.0000855. URL: https://ascelibrary.org/doi/10.1061/%28ASCE%29GT.1943-5606.0000855 (visited on 10/22/2025).

BGE (2022). *Konzept zur Durchführung der repräsentativen vorläufigen Sicherheitsuntersuchungen gemäß Endlagersicherheitsuntersuchungsverordnung.* Tech. rep. URL: https://www.bge.de/fileadmin/user_upload/Standortsuche/Wesentliche_Unterlagen/Methodik/Phase_I_Schritt_2/rvSU-Methodik/20220328_Konzept_zur_Durchfuehrung_der_rvSU_barrierefrei.pdf (visited on 04/04/2026).

Celenk, M. (1995). "Three-dimensional object recognition using cross-sections". In: *Proceedings of the Twenty-Seventh Southeastern Symposium on System Theory.* Starkville, MS, USA: IEEE Comput. Soc. Press, pp. 92–96. ISBN: 978-0-8186-6985-9. DOI: 10.1109/SSST.1995.390611. URL: http://ieeexplore.ieee.org/document/390611/ (visited on 02/12/2025).

de la Varga, M., Schaaf, A., and Wellmann, F. (2019). "GemPy 1.0: open-source stochastic geological modeling and inversion". English. In: *Geoscientific Model Development* 12.1, pp. 1–32. ISSN: 1991-959X. DOI: 10.5194/gmd-12-1-2019. URL: https://gmd.copernicus.org/articles/12/1/2019/ (visited on 02/21/2026).

Gardoll, S. J., Groves, D. I., Knox-Robinson, C. M., Yun, G. Y., and Elliott, N. (2000). "Developing the tools for geological shape analysis, with regional- to local-scale examples from the Kalgoorlie Terrane of Western Australia". In: *Australian Journal of Earth Sciences* 47.5, pp. 943–953. ISSN: 0812-0099. DOI: 10.1046/j.1440-0952.2000.00822.x. URL: https://doi.org/10.1046/j.1440-0952.2000.00822.x (visited on 10/22/2025).

Jessell, M. W., Ailleres, L., and Kemp, E. A. de (2010). "Towards an integrated inversion of geoscientific data: What price of geology?" In: *Tectonophysics* 490.3, pp. 294–306. ISSN: 0040-1951. DOI: 10.1016/j.tecto.2010.05.020. URL: https://www.sciencedirect.com/science/article/pii/S0040195110002246 (visited on 02/18/2026).

Lindsay, M. D., Jessell, M. W., Ailleres, L., Perrouty, S., Kemp, E. de, and Betts, P. G. (2013). "Geodiversity: Exploration of 3D geological model space". In: *Tectonophysics* 594, pp. 27–37. ISSN: 0040-1951. DOI: 10.1016/j.tecto.2013.03.013. URL: https://www.sciencedirect.com/science/article/pii/S004019511300187X (visited on 04/04/2025).

Lindsay, M. D., Aillères, L., Jessell, M. W., Kemp, E. A. de, and Betts, P. G. (2012). "Locating and quantifying geological uncertainty in three-dimensional models: Analysis of the Gippsland Basin, southeastern Australia". In: *Tectonophysics* 546-547, pp. 10–27. ISSN: 0040-1951. DOI: 10.1016/j.tecto.2012.04.007. URL: https://www.sciencedirect.com/science/article/pii/S0040195112002004 (visited on 07/31/2025).

Parquer, M. N., Kemp, E. A. de, Brodaric, B., and Hillier, M. J. (2025). "Checking the consistency of 3D geological models". English. In: *Geoscientific Model Development* 18.1, pp. 71–100. ISSN: 1991-959X. DOI: 10.5194/gmd-18-71-2025. URL: https://gmd.copernicus.org/articles/18/71/2025/ (visited on 10/24/2025).

Pellerin, J., Caumon, G., Julio, C., Mejia-Herrera, P., and Botella, A. (2015). "Elements for measuring the complexity of 3D structural models: Connectivity and geometry". In: *Computers & Geosciences* 76, pp. 130–140. ISSN: 0098-3004. DOI: 10.1016/j.cageo.2015.01.002. URL: https://www.sciencedirect.com/science/article/pii/S0098300415000035 (visited on 08/12/2025).

Schweizer, D., Blum, P., and Butscher, C. (2017). "Uncertainty assessment in 3-D geological models of increasing complexity". English. In: *Solid Earth* 8.2, pp. 515–530. ISSN: 1869-9510. DOI: 10.5194/se-8-515-2017. URL: https://se.copernicus.org/articles/8/515/2017/ (visited on 04/04/2025).

Suzuki, S., Caumon, G., and Caers, J. (2008). "Dynamic data integration for structural modeling: model screening approach using a distance-based model parameterization". en. In: *Computational Geosciences* 12.1, pp. 105–119. ISSN: 1573-1499. DOI: 10.1007/s10596-007-9063-9. URL: https://doi.org/10.1007/s10596-007-9063-9 (visited on 06/10/2025).

Wang, S.-J., Nguyen, Q. C., Lu, Y.-C., Doyoro, Y. G., and Tran, D.-H. (2022). "Evaluation of geological model uncertainty caused by data sufficiency using groundwater flow and land subsidence modeling as example". en. In: *Bulletin of Engineering Geology and the Environment* 81.8, p. 331. ISSN: 1435-9537. DOI: 10.1007/s10064-022-02832-7. URL: https://doi.org/10.1007/s10064-022-02832-7 (visited on 02/19/2026).

Wellmann, F. and Regenauer-Lieb, K. (2012). "Uncertainties have a meaning: Information entropy as a quality measure for 3-D geological models". In: *Tectonophysics*. Modelling in Geosciences 526-529, pp. 207–216. ISSN: 0040-1951. DOI: 10.1016/j.tecto.2011.05.001. URL: https://www.sciencedirect.com/science/article/pii/S0040195111001788 (visited on 07/24/2025).

Yang, J., Carl, F., Achtziger-Zupančič, P., and Wellmann, F. (2025). "Flexible Geological Modeling with Radial Basis Functions Integrating External Drift". en. In: *Mathematical Geosciences*. ISSN: 1874-8953. DOI: 10.1007/s11004-025-10250-0. URL: https://doi.org/10.1007/s11004-025-10250-0 (visited on 02/04/2026).

Zhao, B. and Wang, J. (2016). "3D quantitative shape analysis on form, roundness, and compactness with μCT". In: *Powder Technology* 291, pp. 262–275. ISSN: 0032-5910. DOI: 10.1016/j.powtec.2015.12.029. URL: https://www.sciencedirect.com/science/article/pii/S0032591015302345 (visited on 10/22/2025).

APPENDIX

Chap. 2 - Supplementary material (Carl et al., 2026a)

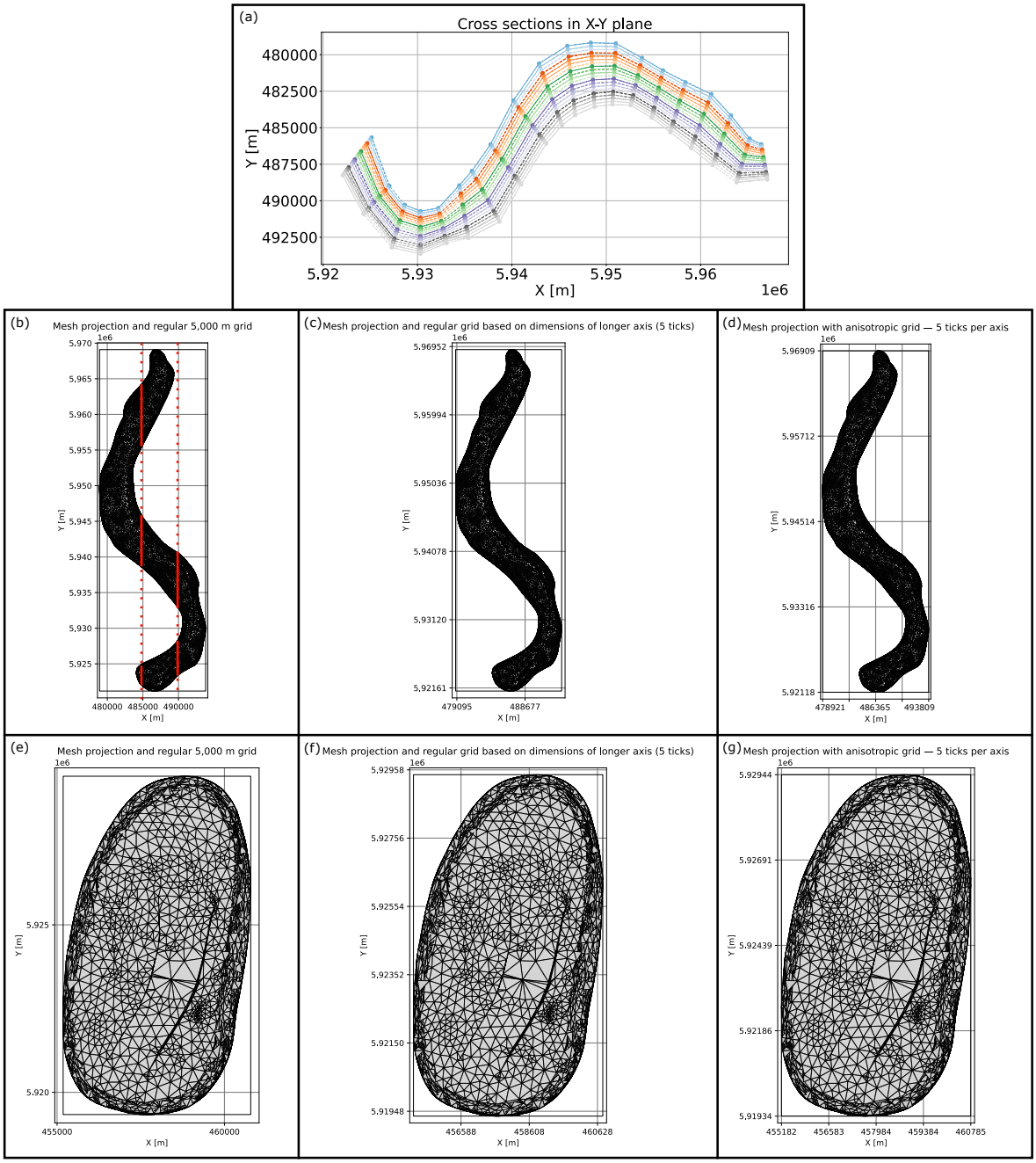


Figure A2.1: Visualization of the advantages of measuring the extents of input meshes on sections normal to their horizontal main axes. Lower row: model "Seefeld" from BGR et al. (2022) for comparative purposes. a): Sections using the proposed method on "Altenbruch-Beverstedt" (top view). b) & e): hypothetical measurement of the horizontal extent along a regular grid (grey lines) of constant size for all datasets (example: 5000 m grid size for both). c) & f): measurement along a mesh-specific regular grid based on the extent of the longer axis of the mesh's bounding box. d) & g): measurement along an anisotropic grid to have an equal amount of sections per direction. Multiple cuts along a horizontal measuring line for an irregular structure are visualized in (b)

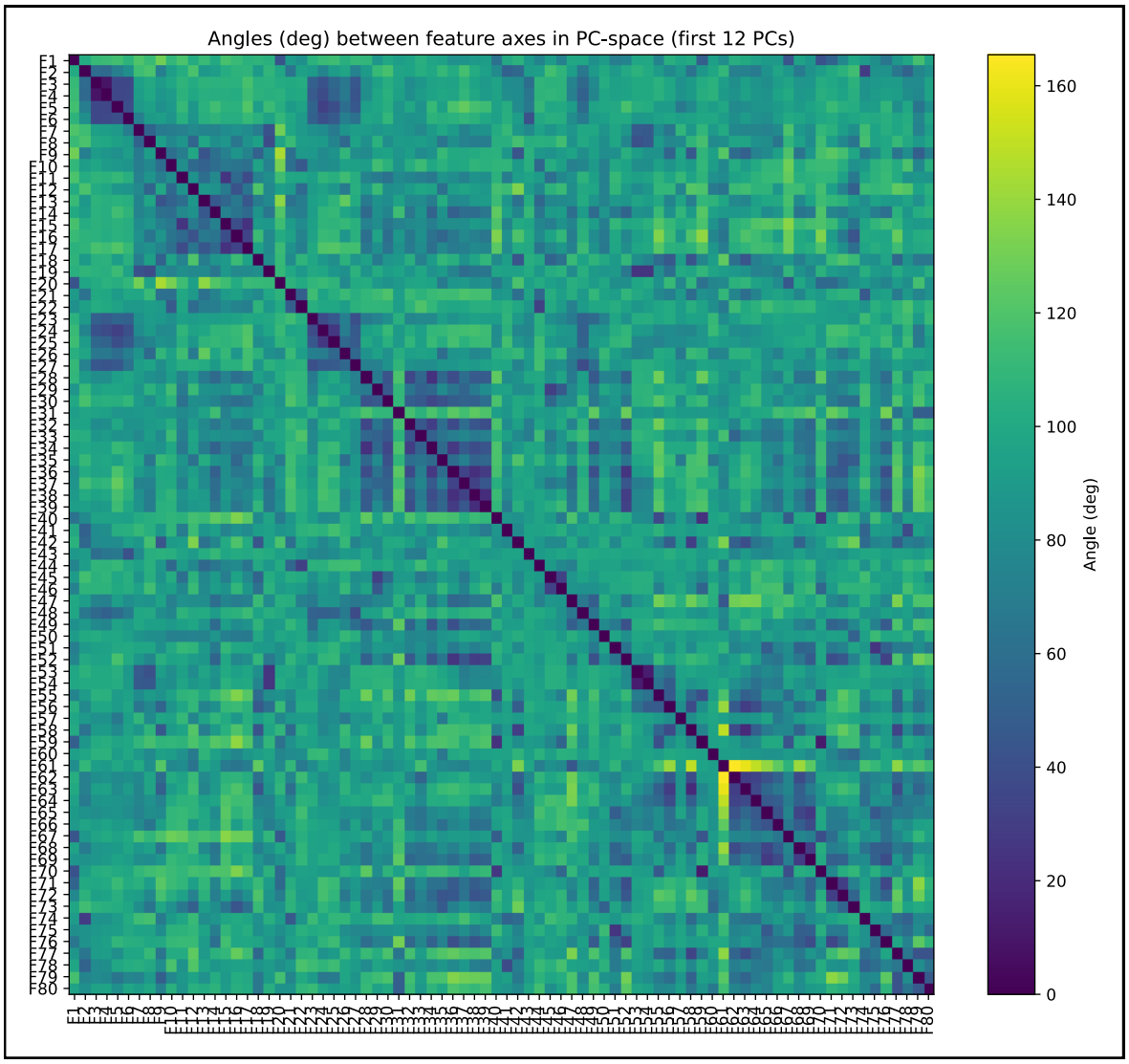


Figure A2.2: Matrix plot for the angles between feature axes in PC space. The plot is used to assess the dependencies among the features (percentiles of the parameter PDF's) in the cluster analysis. Small angles (dark blue) and large angles (bright yellowish) indicate strong dependency between individual features. This can be seen for instance between F3-F6; F32-F39 and F61-F69, with the exception of F67 (F61 is inversely dependant from F62-F64). The strong inter-feature dependencies result in a weak cluster separation beyond PC6. Thus, PC7 to 12 are not shown in Fig. 2.11

Chap. 3 - Supplementary material (Carl et al., 2026b)

Table A3.1: PC scores of cluster centroids and standard geometries in the second cluster analysis.

Geometry/centroid	PC1	PC2	PC3	PC4	PC5	PC6	PC7	PC8	PC9	PC10	PC11	PC12	PC13	PC14
orange centroid	-0.1	-0.01	-0.09	0.05	0.03	-0.03	-0.02	0.001	0.005	-0.005	0.004	0.004	-0.003	-0.001
sheet(hourglass-shape_-rounded)	-0.2	-0.05	-0.06	0.04	-0.2	-0.03	-0.02	0.1	0.07	-0.02	0.1	0.2	-0.06	-0.01
bluish-green centroid	0.3	-0.09	-0.06	0.06	-0.02	0.03	-0.02	0.01	0.03	-0.02	-0.08	0.004	-0.008	-0.01
black centroid	0.3	0.27	0	0.03	0.01	0.09	0.11	-0.04	-0.03	0.06	0.04	0.01	0.01	0.05
sky-blue centroid	-0.07	-0.17	0.08	-0.09	-0.02	0.03	0.04	-0.01	-0.01	0.01	-0.01	-0.01	0.002	0.003
wall(highly.anisotropic_-hourglass-shape_rounded)	-0.12	-0.23	0.28	-0.04	0.16	0.09	0.02	-0.16	-0.08	-0.08	0.07	-0.07	0.03	-0.04
reddish-purple centroid	-0.07	0.29	0.09	-0.02	-0.027	0.001	-0.02	0.01	0.003	-0.002	-0.002	-0.003	-0.008	-0.01
batholithV5	-0.17	0.12	0.26	0.18	0.13	-0.02	0.04	0.26	0.03	-0.04	0.01	0.08	-0.1	0.03
anticline_wall_-batholithV1(rounded)	-0.12	-0.12	0.08	0.19	0.08	-0.14	-0.11	0.01	-0.01	-0.15	0.18	0.02	0.02	0.02
anticline_crest	-0.18	-0.12	0.38	0.30	0.18	-0.03	-0.07	0.06	0.06	-0.18	0.06	0.19	-0.04	-0.06
anticline_wall(hourglass-shape_rounded)	-0.16	-0.05	-0.10	0.11	0.13	-0.07	0.04	-0.04	-0.09	-0.07	0.01	0.06	-0.08	-0.02
batholithV6	0.00	-0.06	0.04	0.14	-0.08	-0.27	-0.10	-0.07	-0.04	0.09	0.02	-0.01	-0.01	0.01
dyke	-0.13	0.37	0.94	0.11	0.12	0.19	-0.05	0.05	-0.05	-0.13	0.02	0.07	-0.03	0.04
eroded.layer_channel	0.19	0.40	0.85	-0.03	0.04	0.20	-0.09	-0.01	-0.08	-0.13	0.09	0.03	-0.05	0.01
laterally.eroded.layer_pinchout	0.29	0.04	0.21	0.39	0.07	-0.11	-0.05	0.04	-0.07	-0.07	-0.13	-0.03	-0.04	0.04
faulted.layer	0.20	0.04	0.60	0.24	-0.22	0.03	0.34	0.24	-0.09	-0.19	-0.18	-0.06	0.15	0.04
flat.layer_sill	-0.22	-0.49	0.84	0.45	0.34	-0.05	-0.18	-0.02	0.30	0.32	0.10	-0.08	-0.02	-0.11
fold	0.15	0.11	0.31	0.21	-0.29	-0.30	0.03	-0.12	-0.28	-0.31	0.00	-0.13	0.03	0.05
laccolith	-0.20	-0.17	0.17	0.41	-0.35	-0.17	0.31	-0.14	-0.15	-0.18	-0.07	0.01	-0.06	0.02
lopolith	-0.23	-0.17	0.17	0.41	-0.36	-0.17	0.32	-0.15	-0.16	-0.21	-0.07	0.00	-0.05	0.05
phacolith	-0.11	-0.07	-0.07	0.11	0.01	-0.13	-0.13	-0.07	-0.02	-0.13	0.16	-0.04	-0.02	0.02
pillow(rounded)_batholithV4	-0.18	-0.08	0.05	0.32	0.06	-0.16	-0.05	-0.05	0.00	0.02	-0.03	-0.05	-0.01	0.01
roller	-0.17	-0.13	-0.01	0.24	0.00	-0.10	-0.10	-0.03	0.00	0.00	-0.10	-0.02	-0.04	-0.04
sheet(cylindric_rounded)	-0.16	-0.03	0.01	0.14	-0.15	-0.08	-0.02	0.07	0.02	-0.09	0.25	0.09	0.06	0.01
stock(hourglass-shape_-rounded)_batholithV2	-0.19	0.15	0.08	0.15	-0.12	0.03	0.03	-0.06	0.00	0.05	0.01	0.07	-0.07	-0.04
stock(cylindric_rounded)	-0.08	-0.08	0.07	0.25	0.09	-0.15	-0.05	-0.07	-0.01	0.04	-0.03	-0.09	0.02	0.01
syncline_basin	-0.19	-0.12	0.39	0.32	0.19	-0.03	-0.06	0.06	0.06	-0.20	0.08	0.17	-0.04	-0.06
tilted.layer	0.14	0.22	0.57	0.31	0.21	0.05	0.11	0.02	-0.04	-0.10	0.02	0.13	-0.07	0.00
volcanic.pipe	-0.01	-0.26	0.35	0.62	0.17	-0.23	-0.23	-0.01	0.31	0.46	-0.07	-0.23	0.00	-0.12
wall(highly.anisotropic_-cylidric_rounded)	-0.13	-0.26	0.35	0.01	0.12	0.05	-0.02	-0.19	-0.08	-0.07	0.18	-0.06	0.00	0.04

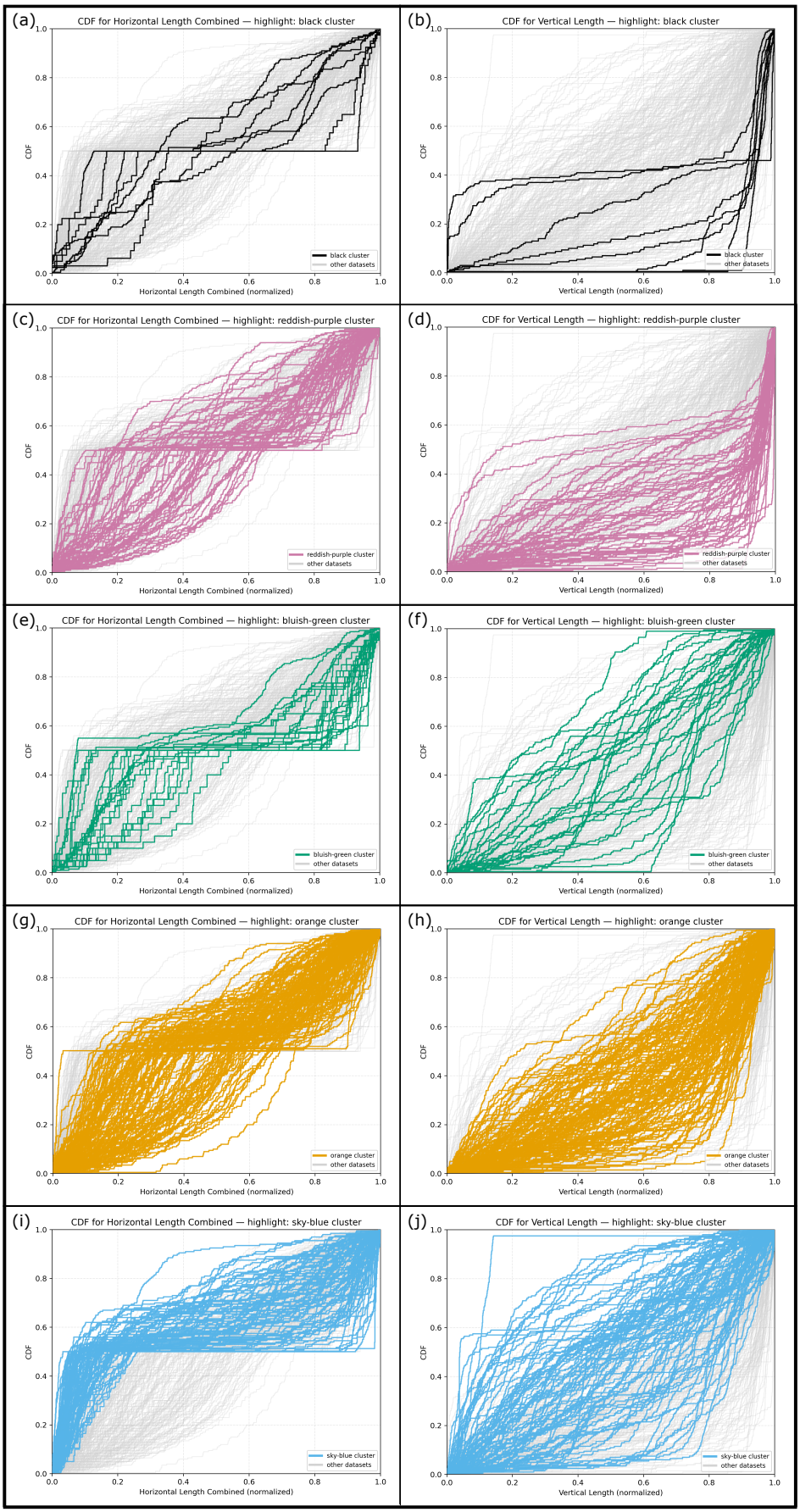


Figure A3.1: Combined cumulative distribution functions of all irregular input meshes of the database colorized according to the results of the second cluster approach, separated per cluster.

SCIENTIFIC CONTRIBUTIONS

The following lists present all scientific contributions, including peer-reviewed journal articles and conference presentations, related to the work performed during the time of this dissertation.

Peer-reviewed articles

- **Carl, F.**, Yang, J., Colling Cassel, M., Wellmann, F., and Achtziger-Zupančič, P.: Quantitative comparison of subsurface structures: an application to salt domes and crystalline bodies, J. Struct. Geol., 205, 105633, https://doi.org/10.1016/j.jsg.2026.105633, 2026.
- **Carl, F.**, Yang, J., Colling Cassel, M., Wellmann, F., and Achtziger-Zupančič, P.: Quantitative comparison of three-dimensional bodies using geometrical properties to validate the dissimilarity of a standard collection of 3D geomodels, Solid Earth, 17, 155–178, https://doi.org/10.5194/se-17-155-2026, 2026.
- Yang, J., **Carl, F.**, Achtziger-Zupančič, P., and Wellmann, F.: Flexible Geological Modeling with Radial Basis Functions Integrating External Drift, Math. Geosci., https://doi.org/10.1007/s11004-025-10250-0, 2025.

Conference contributions

- **Carl, F.**, Achtziger-Zupančič, P., Yang, J., Colling Cassel, M., Kukla, P. A., and Wellmann, F.: What's the top hat there? - A method for the quantification and comparison of subsurface bodies, poster presentation at the EGU General Assembly 2025 in Vienna, 2025.
- **Carl, F.**, Achtziger-Zupančič, P., Yang, J., Colling Cassel, M., Kukla, P. A., and Wellmann, F.: A methodology for the quantitative comparison of subsurface structures using geometrical parameters, poster presentation at the URS final meeting in Potsdam, 2025.

- **Carl, F.**, de los Angeles Gonzalez de Lucio, G., Achtziger-Zupančič, P., Yang, J., Kukla, P. A., Bense, F., and Wellmann, F.: GeoBlocks-Projekt: Überblick über Untergrundgeometrien der Wirtsgesteine und Eingangsdaten für die geologische Modellierung, presentation at the "Tage der Standortauswahl", 2024
- Yang, J., Colombo, C., **Carl, F.**, Gonzalez de Lucio, G., Achtziger-Zupančič, P., Kukla, P., and Wellmann, F.: (2023). Intelligent interpolation strategies in geological modelling for safe storage sites: comparison and uncertainty approach, conference paper, in: RING (S. 14), 2023
- **Carl, F.**, de los Angeles Gonzalez de Lucio, G., Yang, J., Achtziger-Zupančič, P., Kukla, P. A., Bense, F., and Wellmann, F.: Host rock analysis for the German nuclear waste disposal site-selection: review of subsurface geometries and input data for geological modelling, conference paper, in: RING, https://www.ring-team.org/ring_dl/public/publications/Carl_RM2023.pdf, 2023.

AI usage statement

Throughout the development of this thesis, I used OpenAI's ChatGPT in order to accelerate code generation, for debugging and to improve documentation. After the usage of the tool, I reviewed and edited the code as needed and take full responsibility for the final scripts and the resulting data and models.